UNIVERSITY OF CANTERBURY
Te Whare Wānanga o Waitaha
CHRISTCHURCH NEW ZEALAND

Size, Shape and Support Effects on the Catalytic Activity of Immobilized Nanoparticles

---

A thesis

submitted in partial fulfilment of the requirements for the Degree Of

Doctor of Philosophy in Chemistry

at the

University of Canterbury

by

Sedigheh Ghadamgahi

BS (Applied chemistry), MS (Analytical chemistry)

January, 2014

Dedication

To

My loving husband Amir Sadeghi

My ever brave son Sina Sadeghi

My brothers and sisters from Ghadamgahi's family

and

My parents Ali and Mehri Ghdamgahi

Declaration

I declare that this thesis is my own work. It is being submitted for the degree of Doctor of Philosophy in the University of Canterbury, Christchurch, New Zealand. It has not been submitted before for any degree or examination to any other university.

Ghadamgahi

09/02/2014

Acknowledgments

I would like to first thank God for His love and merciful grace upon my life. My deep gratitude is also expressed towards the following persons and institutions made this thesis possible:

- My supervisory team: Doctor Vladimir Golovko, Professor Bryce Williamson for their tremendous constant guidance, helpful discussions on this project, support and encouragements.
- My family, Amir and Sina Sadeghi for sharing with me joyful and difficult moments together.
- Mechanical and electrical workshops; Nick Oliver, Danny Leonard and Wayne Mackay for their constant technical assistance.
- NMR, HPLC & GC technicians; Dr. Marie Squire, Dr. Meike Holzenkaempfer and Dr. Matt Polson for their technical input in these projects.
- All the staff of the School of Chemistry for their assistance to issues related to these projects.
- My research group, in particular Baira Donoeva for synthesizing Au_8 nanoclusters , Nathaniel Gunby for synthesizing Au_9 nanoclusters, Au_1 precursor and $HAuCl_4$, Campbell McNicoll for measuring the surface area of Norit activated carbon, David Anderson for fabrication $HAuCl_4$ and ruthenium nanocatalysts, Jan-Yves Ruzicka for assistance in TEM software and also Faridah Abu Bakar for assistance of UV-Vis.
- Professor Antony Fairbanks's group, in particular Doctor Yusuke Tomabechi, Doctor Andrew Watson and David Lim.

- Professor Jim Johnston and Doctor Carla Francis from Victoria University of Wellington for palladium nanoparticles immobilized on wool.
- Associate Professor Richard Tilley and his group from Victoria University of Wellington for synthesizing ruthenium nanoparticles.
- Associate Professor Richard Hartshorn group's particularly Fatemeh Tavkoli Nia.
- Mike Flaws from Mechanical Engineering Department for his assistance with TEM images.
- Doctor Bezugla for modified granular activated carbon from National Taras Shevchenko University, Kyiv, Ukraine.
- Doctor Balaiah Kuppan and Professor Parasuraman Selvam for mesoporous carbon (CMK-3, CMK-8 and NCCR-41) from National Centre for Catalysis Research and Department of Chemistry (Indian institute of technology), Madras, India.
- My parents, brothers and sisters.
- All my friends and colleagues within the Schools of Chemistry.
- University of Canterbury for allowing me to undertake these projects.

Sedigheh Gahdamgahi

Abstract

A brief overview of this PhD thesis,

The emergence of nanotechnology has stimulated both fundamental and industrially relevant studies of the catalytic activity of noble metal nanoparticles. Palladium, ruthenium and gold are well known catalysts when used in nanoparticle-based systems. This body of work endeavoured to investigate the catalytic activity of these noble metal nanoparticles through three studies as a briefly overviewed below.

Study 1

Palladium is a well-known catalyst, even in bulk phases, but its high cost had driven industry towards its use in nanoparticle-based systems well before nanotechnology had attracted the attention of the media. Palladium nanoparticles often show remarkable catalytic activity and selectivity, particularly for the hydrogenation of some unsaturated hydrocarbons, such as alkenes, alkynes and unsaturated carbonyl compounds. The nature of supports can affect the catalytic activity and selectivity of metal-support interaction. Natural polymeric supports, such as wool, can be suitable for new generation of composite materials incorporating nanosized metal nanoparticles and have the added advantage of being "*environmentally friendly*".

Catalytic hydrogenation of cyclohexene to cyclohexane by palladium nanoparticles immobilized on wool was demonstrated by using a Parr high pressure hydrogenation set-up. The efficiency of the process was explored over loading rates from 1.6% to 2.6% of palladium nanoparticles (by weight) with a variety of particle sizes. Optimization of the reaction conditions including, stirring rate, amounts of reactants, gas pressure and target temperature, led to series of catalytic activity tests carried out for 5 or 24 hours (each) at 400

psi H_2 and 40 ^oC using a stirring rate 750 rpm. Product mixtures were analysed using gas chromatography (GC-FID) to determine conversions. Samples S_1 and S_2 proved to be the most active catalysts because the average Pd particle size was around ~5 nm and the particles were more accessible for the reactant (*i.e.* Pd particles were on the surface of wool). However, under the catalytic testing conditions studied, wool (Pd/wool) did not show advantages over commercially used palladium nanoparticles on activated carbon (Pd/C).

Study 2

Ruthenium fabricated as noble metal nanoparticles can be catalytically active for hydrogenation of organic compounds. However, a challenging issue for researchers is that Ru nanocatalysts can be spontaneously deactivated due to effects, such as sintering or leaching of active components, oxidation of noble metal nanoparticles, inactive metal or metal oxide deposition and impurities in solvents and reagents. Calcination of noble metal nanoparticles is one option for reactivation of Ru nanoparticles immobilized on SiO_2 (Ru/SiO_2) utilized as nanocatalysts in chemical reactions. In fact, the catalytic activity of noble metal nanoparticles is known to be proportional to the active part of the surface area. The effects of calcinations on catalytic activity of "*shape- specific*" 0.1 wt% Ru/SiO_2 for hydrogenation of cyclohexene to cyclohexane were investigated. Optimization of calcinations by varying temperature and time proved to be effective on the activity of nanocatalysts retaining the Ru nanocatalysts shapes for the hydrogenation of cyclohexene. Product mixtures were analysed using gas chromatography (GC-FID) to determine conversions. The Ru catalysts showed the highest activity (100%) when they were activated by calcination following protocol No.1 in a furnace under the mildest reductive conditions studied (temperature = 200 ^oC for 1 hour, which was the shortest calcination time). HRTEM study showed only minor deformation of the Ru nanoparticles and minimal aggregation for this type of activation.

Study 3

Supported gold nanoparticles have excited much interest owing to their unusual and somewhat unexpected catalytic activity particularly with the selective oxidation of organic compounds. Gold nanoparticles immobilized on Norit activated carbon (Au_{101}/C) *via* colloidal deposition gave high selectivity of benzyl alcohol oxidation. The presence of a base (K_2CO_3) increased the catalytic activity of gold nanocatalysts (which was negligible in the absence of base) through dehydrogenation of the alcohol *via* deprotonation of a primary OH groups, and helped overcome the rate-limitation step of the oxidation process. The interaction between the gold species and the support was investigated by measuring change in catalytic activity with different activation methods (*i.e.*, washing with a solvent at elevated temperature, and/or followed by calcinations). A mixture of benzyl alcohol as a reactant, methanol as a solvent, K_2CO_3 as a base and oxygen gas was studied by the activated gold nanocatalysts using a mini reactor set-up. The efficiency of the process was explored by varying the amounts of benzyl alcohol and the base, target temperature, metal loading of the gold catalysts rate and the solvent, between 3 and 24 hours at 73 psi O_2 and a stirring rate (750 rpm). The samples of the reaction mixture were centrifuged and analysed by high-performance liquid chromatography (HPLC) to determine conversions.

The effect of size on the catalytic activity was studied for different types of gold particles (Au_{101}, Au_{naked} and $Au_{citrate}$) and clusters (Au_8 and Au_9) immobilized on powder Norit activated carbon. The highest activity of benzyl alcohol oxidation was observed for activated 1.0 wt% Au_{101}/C catalysts (washed with toluene and followed by calcination under vacuum at 100 ^oC for 3 h) for ~3.5 nm gold particles. Additionally, the support effect was studied for gold particles immobilized on different types of carbons, such as Norit activated carbon (powder, granular and powdered) and mesoporous carbons (CMK-3, CMK-8 and NCCR-41), granular modified carbon (–SH and $–SO_3H$ groups) and Vulcan carbon. The highest activity

was observed by activated 1.0 wt% Au_{101}/C_8 catalysts (washed with toluene and followed by calcination under vacuum at 100 ^oC for 3 h). Activated 1% Au_{101}/C_{41} (washed with toluene followed by calcination under vacuum at 100 ^oC for 3 hours) with 2.6 ± 0.1 nm gold particle size showed the highest selectivity towards methyl benzoate as a main product (*S%*: 88%) after 3 hours reaction time. However, activated 1% Au_{101}/C (calcination in O_2 -H_2 at 100 ^oC for 3 hours) with 6.6 ± 0.3 nm gold particle size exhibited the highest selectivity towards benzoic acid as a main product (*S*: 86%) after 24 hours reaction time.Therefore, particle size and type of carbon support can be considered as playing crucial roles in defining the catalytic activity of gold nanocatalysts which were used for benzyl alcohol oxidation.

Table of Contents

List of Figures

List of Tables

List of Scheme

Chapter 1: General Introduction and Literature Survey

1.1 Introduction

The term "*catalysis"* was first used in the early 19th century by Davy,[1] who, along with Berzelius[2] and Faraday,[3] pioneered the first experimental observations and understandings of the crucial role of catalytic materials in chemical reactions. However, the first valid modern definition of *"catalysis"* was given in the early 20th century by Friedrich Wilhelm Ostwald (the Nobel Prize Winner of Chemistry in 1909).[4] Catalysis is the enhancement of the rate of a chemical reaction due to the participation of a substance called a catalyst. Unlike other participants in the chemical reaction; a catalyst is not itself consumed by the reaction. The reaction can proceed without the catalyst, but at a slower rate (see Figure 1.1).

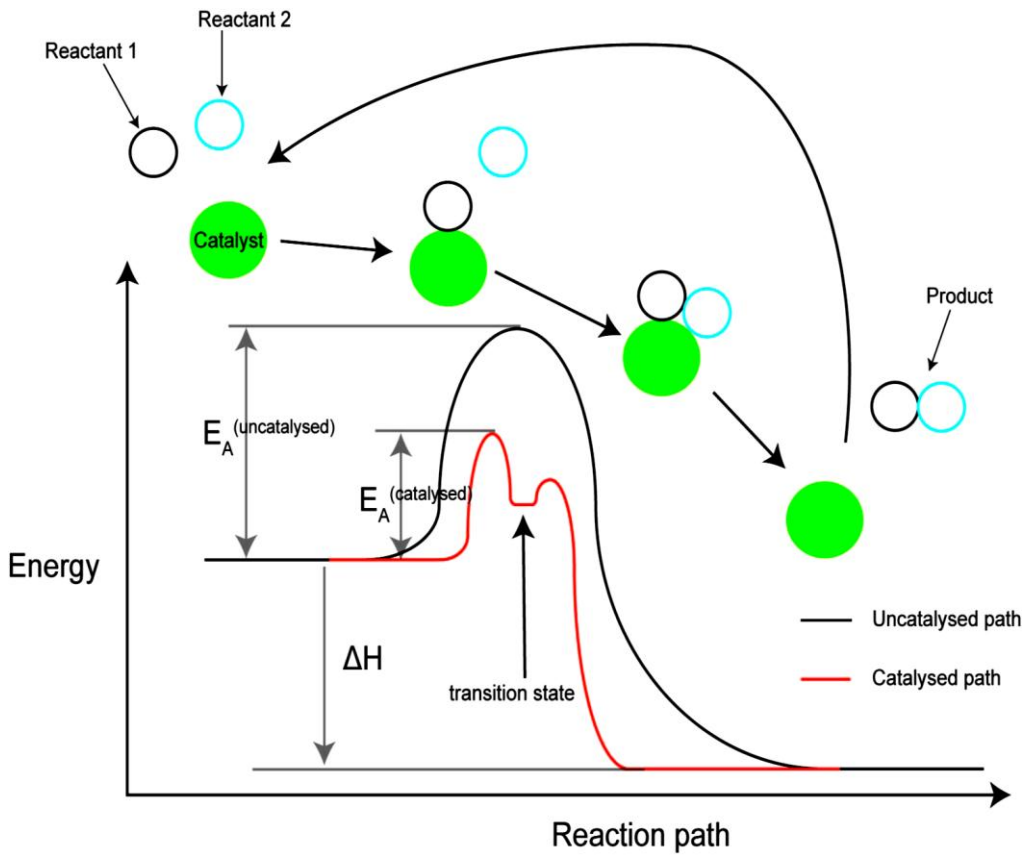

Figure 0.1: Comparison of the reaction pathways of reaction between reactants 1 and 2. The black curve shows the un- catalysed pathway with activation energy E_A (un- catalysed); the red curve is the pathway for the catalysed reaction with activation energy E_A (catalysed). ΔH is the overall enthalpy change and is independent of the reaction path. Reproduced from Kilmartin.[5]

There are three general types of catalysts; heterogeneous, homogeneous and enzymes. The last of these are biological catalysts and will not be considered further in this part.

Heterogeneous and homogeneous catalytic systems have both advantages and shortcomings. Homogeneous catalysts are mixed in the same phase as the reactants, generally a solution or gas, and often show higher activity than heterogeneous catalysts. However, they require separation as a final part of the. A heterogeneous catalyst is in a different phase from the reactants, usually solid with the substrates in either gas or liquid phases. Heterogeneous catalysts have the advantage of a simpler of recovery process, but often suffer from relatively low activity. There are two main sub-types of heterogeneous catalysts: bulk catalysts and supported catalysts.[5-6] It is supported heterogeneous catalysts that are of interest in this thesis.

A recent study of the economic contributions of catalysis noted that "one-third of material gross national product in the U.S. involves a catalytic process somewhere in the production chain".[7] Chlorine-free refrigerants, high-strength polymers, stain-resistant fibers, cancer-treatment drugs and many thousands of other products used by modern societies would not be possible without the existence of catalysts. These critical materials mediate the pathways by which chemical reactions occur, enabling the highly selective formation of desired products at rates that are commercially viable.

The development of industrial heterogeneous catalysts shows a trend towards small particle sizes, with the use of small nanoparticles common place in various applications for many years. Nanotechnology is an area of research aimed at the design, fabrication and application of functional structures of substances in the range between 1 and 100 nanometers (see Figure 1.2).[8] Nanomaterials fall into that intermediate state of matter between the molecular and the bulk and are of interest and utility because they can have significantly different properties from both bulk materials molecules.

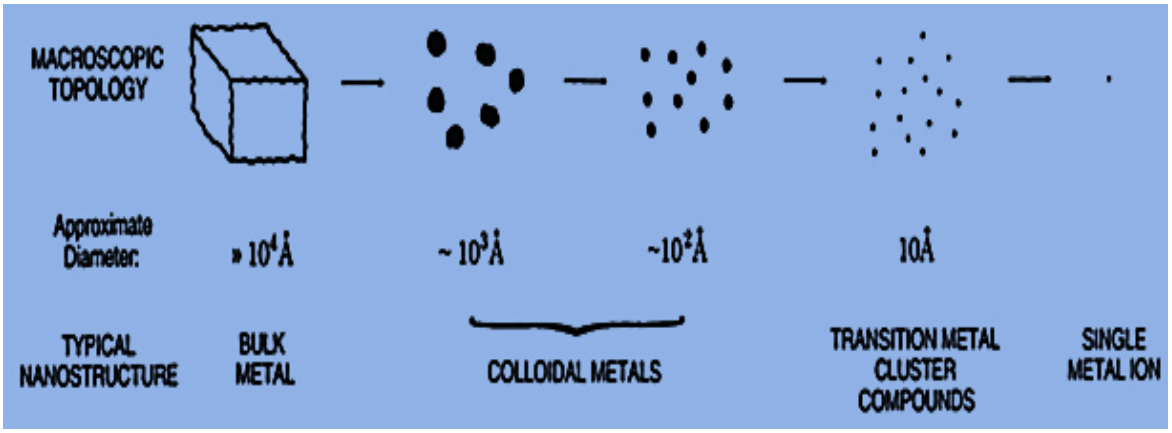

Figure 0.2: Nanomaterials and their scopes; the divided metals between single atom and bulk metal. See the text for more information (1 °A= 0.1 nm). Reproduced from Johnson.[9]

The physical and chemical properties of a material like gold can undergo remarkable transitions as the size of the material decreases and enters the nanosized domain.[10] Fabrication and application of nanostructured materials is an exciting area of research.[8] Recent advances in nanoscience have already contributed to scientific progress in many disciplines, such as physics, biology, medicine, engineering and chemistry. It has been proposed that nanostructures had a role on the origin of life.[8]

Nanostructure classification is based on the number of dimensions in the nanoscale domain as follow:[11]

I. one confined nanodimension gives *nanolayers* and *nanofilms*
II. two confined nanodimensions give *nanotubes* and *nanofilaments*
III. three confined nanodimensions give *nanopores* and *nanoparticles*.

Noble metal nanoparticles, are currently of considerable practical and theoretical interest because they frequently display unusual physical (*i.e.*, structural, electronic, magnetic and optical) and chemical (*i.e.*, catalytic) properties.[12,13] Nanoparticles made of various materials have been found to catalyze many chemical transformations in organic synthesis, pollutant

removal and energy production; and intense efforts are being made to characterize the structures and catalytic properties of such nanoparticles catalysts.[14]

Nanoscale, catalytically active noble metal particles/clusters supported on high surface area supports are one of the most important classes of heterogeneous catalysts.The catalytic activity of supported noble metal nanoparticles depends on the metal, particle size, particle shape, support, preparation method, type of reaction and catalyst activation. These areas will be briefly discussed in the following sections to provide further rationale for the studies undertaken in this thesis.

1.1.1 Type of noble metal nanoparticles

Noble metal nanoparticles have been attracted in scientific research and industrial applications due to their large surface-to-volume ratios and quantum size effects.[15] Catalytic properties of metal nanoparticles have been explored since the pioneering studies of Rampino and Nord in the early 1940s.[16] Design and fabrication of nanoparticles from noble metals such as palladium, ruthenium and gold are appealing because such nanostructured noble metals have shown unique catalytic behavior.[17] Ruthenium fabricated as nanoparticles has been shown to be catalytically active for hydrogenation of organic compounds.[18] Palladium nanoparticles have also been extensively studied for their remarkable catalytic properties. Additionally, metal nanoparticles have been recognized as a highly active and selective catalyst, particularly for the hydrogenation of some unsaturated hydrocarbons.[19] Overall, noble metal nanoparticles have created substantial interest because these metal particles are cost- effective particularly for industrial applications.

Gold used to be viewed as a poor catalyst is due to its small chemisorption ability compared to the platinum group metals. It has been often considered to be amongst the most inert

metals and its remarkable catalytic properties were not recognized until recently.[20,15a] The catalytic properties of nanogold were discovered in the 1970s,[21] but it did not raise much attention until Haruta and co-workers utilized it as a catalyst for CO oxidation late 1980s.[15a] The discovery of the catalytic efficiency of nanoparticulate gold led to a major motivation for new research in this field.[22] Gold nanoparticles have become important in catalyst applications owing to their unique physical and chemical properties. They are active catalysts for a number of important chemical reactions, including oxidation and hydrogenation of organic compounds.[23] Supported gold nanoparticles have excited much interest owing to their unusual and somewhat unexpected catalytic activity, particularly in the selective oxidation of organic compounds.[24] Haruta *et al.* argued that supported gold nanoparticles can be used at low temperature for aerobic oxidation of carbon monoxide.[25]

A major limitation in the synthesis of supported gold nanoparticles is the lack of control over the size of the particles. One approach towards this problem is to use nanoclusters as catalyst precursors.[26] Nanoclusters fall into a category between molecules and small mono-disperse nanoparticles. Nanoclusters are ensembles of bound atoms or molecules with intermediate size (< 2 nm) between molecules and a bulk solid (see Figure 1.3).

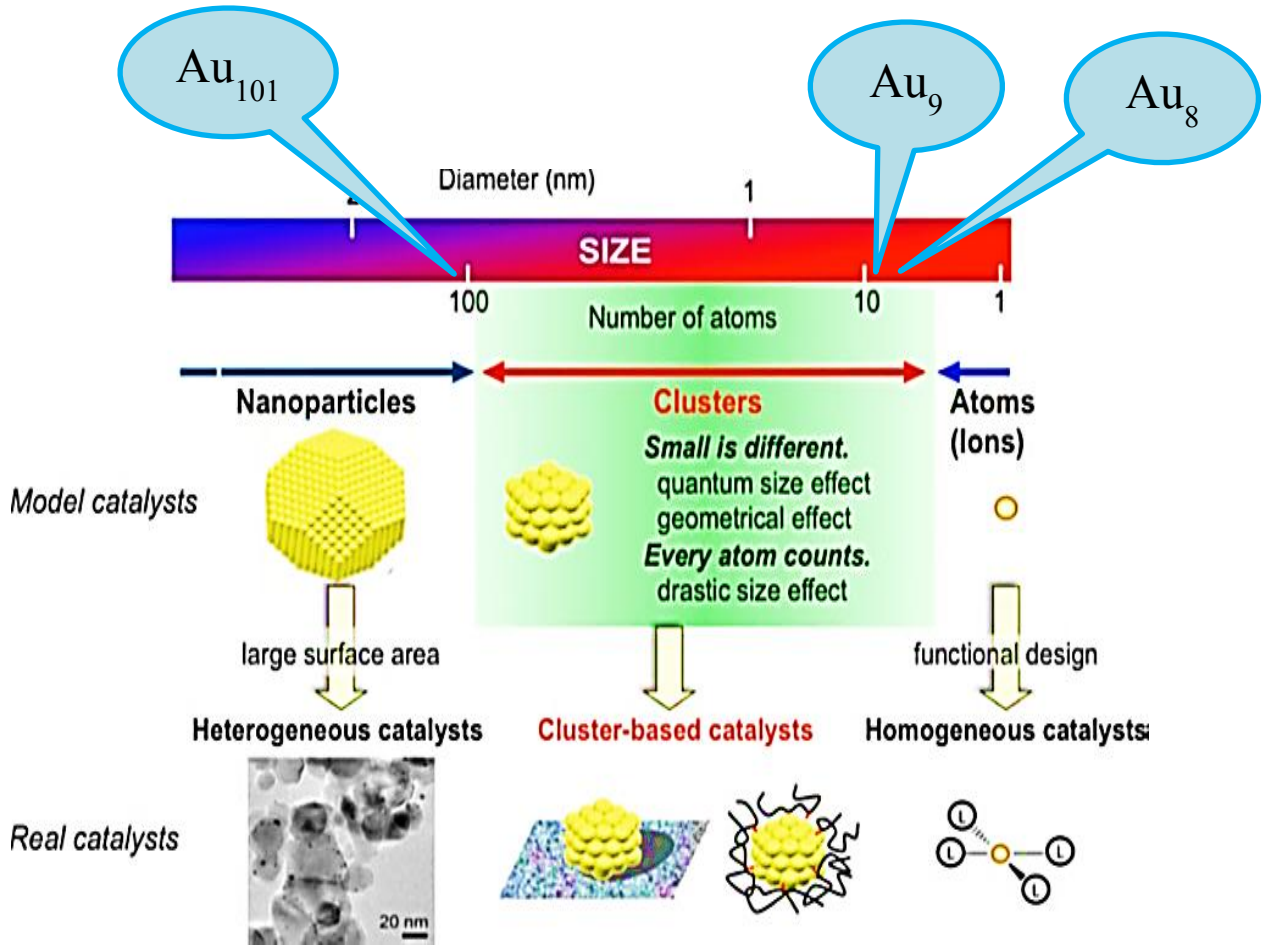

Figure 0.3: Particles and clusters based on catalysts. See the text for more information. Reproduced from Comotti.[27]

Water-soluble gold nanoclusters have been used as electron-dense biological labels in electron microscopy studies of proteins.[28] More recently, it has been found that gold nanoclusters can oxidize CO to CO_2 under low temperature conditions.[26]

Gold clusters can generally be classed into two different types: those that are protected by phosphine ligands and those that are protected by thiols or other ligands.[29] Gold phosphine complexes are known as a wide range of particle complexes, such as $Au_8(PPh_3)_8(NO_3)_2$ (abbreviated here as Au_8) and $Au_9(PPh_3)_8(NO_3)_3$ (abbreviated here as Au_9) (see Figure 1.4) which are active catalysts for organic compound oxidation.[30] One of the most widely studied clusters is Au_9. Wen *et al.* synthesized gold nanoclusters using $PPh_3Au(NO_3)$ and $NaBH_4$ (eq. 1.1).[31] The small nanoclusters were especially active for low temperature CO oxidation to CO_2.[30a]

$PPh_3Au(NO_3) + NaBH_4 \rightarrow [Au_9(PPh_3)_8](NO_3)_3$ (*eq.* 1.1)

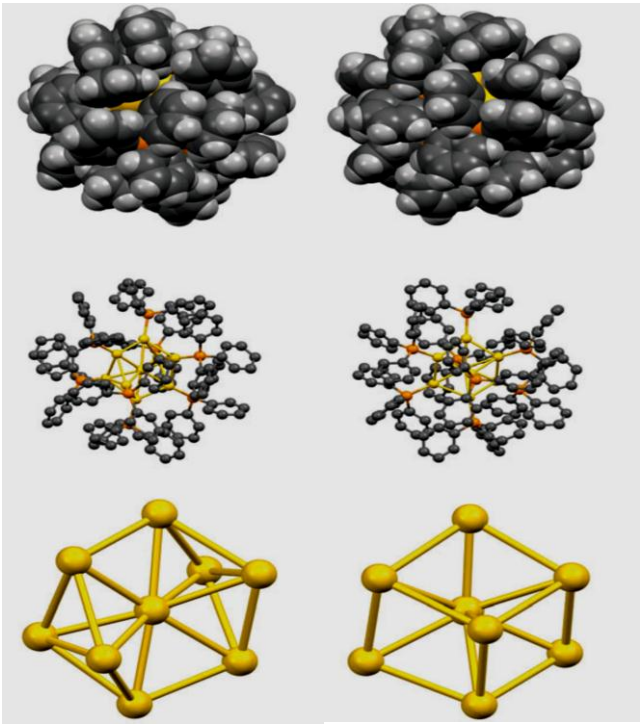

Figure 0.4: Crystal structures of right column: Au_8 nanoclusters ($Au_8(PPh_3)_8(NO_3)_2$) & left column: Au_9 nanoclusters ($Au_9(PPh_3)_8(NO_3)_3$). The atomic colour scheme is gold (Au), orange (P) and black (C). Rreproduced from Anderson *et al*.[32]

Iwasawa *et al.* demonstrated the use of gold-phosphine precursors to generate supported gold nanoparticles for low-temperature CO oxidation.[33] Turner and co-workers did the same using small gold nanoparticles (Au_{55}) to generate an active oxidation catalyst.[34] Schmid *et al.* synthesized clusters that they claimed as to be first well-defined ligand-stabilized gold nanoparticles. They formulated these as $Au_{55}(PPh_3)_{12}Cl_6$, (see Figure 1.5) which they abbreviated as Au_{55}.[35] However, in a report of an improved synthesis by Hutchison *et al*. (eq. 1.2 – 1.3) these nanoparticles were described as $Au_{101}(PPh_3)_{21}Cl_5$, abbreviated as Au_{101}, which is now understood to be the correct structure.[36]

$H_2O + HAuCl_4 + 2PPh_3 \rightarrow [AuClPPh_3] + O{=}PPh_3 + 3HCl$ (*eq.* 1.2)

$[AuClPPh_3] + NaBH_4 \rightarrow Au_{101}(PPh_3)_{21}Cl_5 + PPh_3 + NaCl + 3HCl$ (*eq.* 1.3)

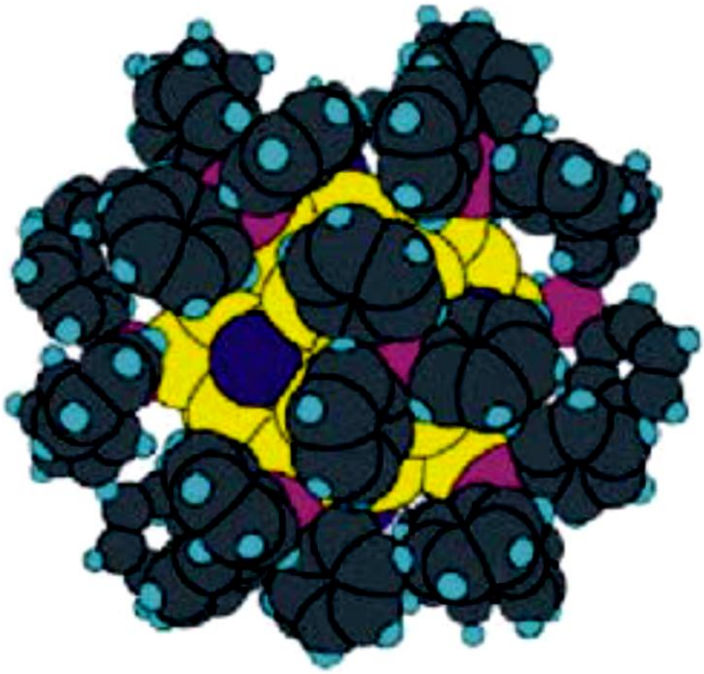

Figure 0.5: The reported structure of Au_{55} nanoparticles (formulated as $Au_{55}(PPh_3)_{12}Cl_6$). Reproduced from Schmid *et al*.[29a, 37]

1.1.2 Size effects of nanoparticles

Catalyst performance can be sensitive to particle size because the surface structure and electronic properties can change greatly in the nanoscale size range.[7] When the average particle size becomes smaller, the surface to volume ratio of the system increases (see Figure 1.6). Increasing the surface area leads to more of the metal atoms occupying positions close to the surface of the particle; thus more reaction sites are provided for a given total volume of catalytic material.[38] In addition, reducing the particle size leads to an increased proportion of under coordinated surface atoms with fewer inter-atomic bonds.[39] This causes the particle's constituent atoms to behave more as individual atoms rather than as parts of a metallic bulk.[40]

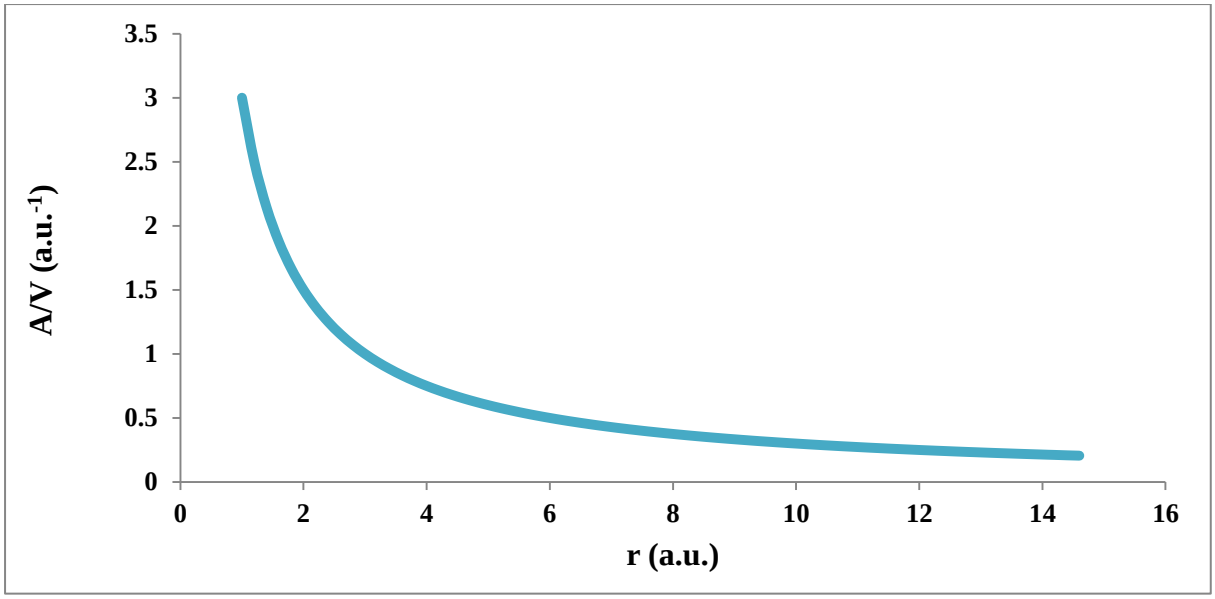

Figure 0.6: Surface to volume ratio as a function of particle size assuming a sphere ($A/V = 3/r$). The dimensions are arbitrary units.[41]

The majority of heterogeneous supported nanoparticle catalysts are high surface area solids onto which an active component is dispersed in the form of very small particles sizes. Reducing the individual particle size to nanometres, the total surface area available for a given volume (and cost) of metals catalysts are maximised. This reduction in size of the metallic particles is largely driven by economic motives, as catalysts are often made up of precious metals (*i.e.*, platinum, palladium *etc.*).

Much of the literature on noble metal nanoparticles exemplifies the impact of size on catalytic activity.[42] Studies of the catalytic activity of gold dispersed as small particles,[43] with dimensions from 1 to 20 nm,[7, 44,45] show that catalytic activity increases with decreasing size, in line with studies using solid-supported gold catalysts.[46] Larger gold particles (500 to 800 nm) are inactive for similar reactions.[47] Consequently, a correlation can be drawn between catalytic activity and average particle size when comparing the catalytic activity within the same type of gold catalyst.[46,48] This does not mean, however, that it can be predicted whether one type of catalyst is more active than another type based solely differences of their in particle sizes.[49]

1.1.3 Shape effects of nanoparticles

Noble metal nanoparticles are usually defined as materials with two or three dimensions below 100 nm.[30b, 50] In the last decade, shape control of noble metal nanoparticles attracted significant interest among synthetic chemists.[26,51] Recent investigations have exhibited how the shape of nanoparticles and the resulting arrangement of atoms on their surface can affect their catalytic activity.[52] To explain these effects, different models have been proposed. Irving Langmuir (the Chemistry Noble Prize Winner in 1932) established a simple model of the catalytic activity of materials.[4] This model depends on the particular facet exposed (*e.g.,* (111) *vs.*(100)).[53] This is because "*The atoms in the surface of crystal must tend to arrange themselves so that the total energy will be minimum*".[53] Later, Gerhard Ertl (the Chemistry Noble Prize Winner in 2007) introduced a modified model in terms of single crystal surfaces.[53-54] Single crystal metal surfaces are useful models by which to rationalize the role of surface defects and the mobility of reaction components in determining the activity and selectivity of a catalytic process.[55] In Ertl's model, surface defects and surface restructuring in the presence of reagents an intermediates play crucial roles.[53]

Ertl's model has provided convincing explications of the catalytic mechanisms in processes, such as ammonia synthesis, hydrogenation of ethylene to ethane, and carbon monoxide oxidation.[56] However, there is a big difference between a single crystal and a real-life nanostructured catalyst. Single-crystal models inherently lack the complexity need to uncover many of the factors important for catalytic turnover and selectivity.[56] Research on the catalytic activity of "*spherical*" nanoparticles has focused on size and composition effects, and has provided great deal of information that interrelate many properties, size, surface area, the percentage of surface atoms, defect types and densities to catalytic activity and selectivity. But there has been a lack of control over which facets are exposed in the nanostructured catalysts. The next step in extending the earlier models and knowledge about

catalytic mechanisms to nanoparticulate systems is to conduct studies using particles of controlled shape and size.

1.1.4 Roles of support

Immobilization of noble metal nanoparticles on a support plays a key role in defining catalytic activity and selectivity. Although noble metal nanoparticles can be used as homogeneous catalysts suspended in solvent,[57] it can lead to severe problems. Firstly, post-reaction separation of products from the nanoparticles (for recycling) may be very difficult. In addition, nanoparticles suspended in a solvent often exhibit poor long-term stability due to particle agglomeration.[58] Prevention of agglomeration for long periods can be achieved by coordination to ligands or anionic species, or by firm attachment of nanoparticles to a solid support surface.[58-59] For example, in the oxidation of CO using either pure gold nanoparticles or pure TiO_2 at 227 ^oC, no catalytic activity was observed. However, gold nanoparticles immobilized on TiO_2 displayed a reasonable catalytic performance at just 25 °C, clearly indicating the significant role of the support.[60]

In addition to preventing the aggregation of particles, the support can more directly affect catalytic activity via particle-support interactions.[61] As a consequence, the selection of the support material can critically affect catalytic activity even for the same reaction.[62] A recent remarkable finding in heterogeneous catalysis has shown different catalytic activity of gold nanoparticles dispersed on different types of support (*e.g.*, CeO_2, TiO_2, SiO_2 and C).[63] A particular exemplar for supported gold nanoparticles relates to different activity and selectivity for catalytic alcohol oxidation depending on the support.[64]

Support materials for metal nanoparticles are described as being either reducible (*e.g.*, TiO_2) or irreducible (*e.g.*, SiO_2 and carbon) based on the nature of the interaction between the

support and the nanoparticles.[63c] For reducible supports, a strong interaction between the support and the nanoparticles limits accessibility of reactants to the active sites of the nanoparticles. In contrast, irreducible supports are relatively inert towards interactions with the metal particles.[65] The catalytic activity of inert supports seems to depend critically on the diameter of the nanoparticles, and only extremely small particles ($\leq$ 3 nm) yield highly active catalytic systems.[20] There is a great deal of interest in using inert supports, such as SiO_2 and carbon;[66] firstly, because the shapes and morphologies of the nanoparticles are preserved during immobilization, and secondly, because the catalytic activity of the nanoparticles will be less strongly influenced by the weaker interaction that occur with this type of support.[6]

1.1.5 Catalysts preparation method

The morphologies of noble metal nanoparticles can be influenced by the catalyst preparation method.[65] Conversely, the preparation method can influence the catalytic activity and selectivity of the metal nanoparticles.[65, 67] For the preparation of highly dispersed noble metal nanoparticles on supports, several methods have been developed to obtain systems with high performance. The more common methods are listed in the following sections.

1.1.5.1 Colloidal deposition

The immobilization of a colloidal suspension involves deposition of pre-synthesized noble metal nanoparticles onto a support with consequent control of their mean size, size distribution and shape.[6, 68] This method involves a solid support being dipped into a colloidal dispersion of the particles, which become deposited onto the support surface with little change in the size of the metal particles. Parameters, such as the nature and concentration of the stabilizer-ligands, the stabilizer-ligands/gold ratio, and the nature of support, can be controlled.[69] A distinct advantage of this method is that it affords the possibility of tuning the

particle size with a high degree of mono-dispersity, something that is difficult to achieve with other approaches.[70]

Cluster deposition also can be considered as a colloidal method in which the pre-synthesised nanoclusters have no size variation – *i.e.*, the particles are perfectly mono-dispersed.[71] It has been used for immobilizing pre-synthesized Au_8 and Au_9 clusters on SiO_2.[72]

1.1.5.2 Impregnation

Impregnation is the simplest immobilization method. Metal nanoparticles or, more usually, a precursor, such as $HAuCl_4$ is dissolved in an organic solvent and stirred with a support until the solvent evaporates.[73-78] This method cannot be generally used for catalyst preparation because it usually leads to large gold particles (bigger than 10 nm). In the case of $HAuCl_4$, it has been suggested that the large particles form because Cl^- facilitates gold mobility and hence agglomeration during heating because this can also inhibit catalyst reactions. The Cl^- can be removed through reduction with hydrogen or washing.[74]

1.1.5.3 Co – precipitation

Whereas impregnation deposits the active precursor on to a pre-formed support, co-precipitation involves the simultaneous precipitation of both the support and the active phase from of a precursor solution by adjustment of the solutions pH;[75] for example, sodium carbonate added to an aqueous solution containing $HAuCl_4$ and the nitrate of the metal. This method results a dispersion of metal particles throughout the support. This method usually leads to high gold dispersions with small particles size (< 10 nm) to oxide surface area of the support.[59d] Despite the benefits of this method, it has been used only for certain metal oxides, such as TiO_2, Fe_2O_3 and ZnO.[76] Nanoscaled gold on iron oxide is one of the most studied catalysts prepared by this method, because of the many possible structures that the support can adopt.[77]

1.1.5.4 Deposition – precipitation

Deposition– precipitation (DP) is one of the most widely used methods for preparation of gold-based catalysts[78] because it produces very small gold particles.[79] It is a process whereby hydroxides or hydrated oxides are deposited onto the surface of the support as a result of gradually raising the pH of the solution in which the support is suspended. The precipitation may be nucleated by the support surface, and, when properly performed, the entire amount of the active- phase material may attach to the support.[80] The pH may be adjusting by adding Na_2CO_3/NaOH to the precursor solution with final addition of the support, or by slowly increasing the pH of the solution in the presence of the support.[81]

1.1.5.5 Chemical vapour deposition

In chemical vapour deposition (CVD), a volatile gold precursor compound (*i.e.,* gold nanoparticles suspensions or gold precursors) reacts is deposited from the vapour phase on to the surface of a support where it decomposes to form metallic particles or a coherent film.[82] When particles are formed they generally have a broad size distribution.[69a] CVD is one of the most successful methods for obtaining small gold particles on metal oxide supports, such as silica, with the further advantage of absence of chloride ions.[82b]

1.1.5.6 Co – sputtering

This method can be used to produce catalytically active gold films and requires magnetron sputtering equipment.[83] This process requires an atmosphere containing oxygen in which a gold plate and a metal oxide target like Co_3O_4 are sputter deposited simultaneously onto a substrate to form a thin film, which is then annealed in air.[5]

1.1.6 Type of reaction

Supported metal nanoparticles can be highly active catalysts for many reactions, especially involving hydrogenation and/or oxidation of organic compounds. This section aims to illustrate some of these reactions.

1.1.6.1 Oxidation

It has been generally reported that palladium and platinum nanoparticles are effective catalysts for oxidising organic compounds but that they do not offer good selectivity with complex substrates.[84] Gold has been recently found to be more active and, particularly, more selective for reactions such as CO oxidation at room temperature.[78] Abed *et al.* discovered that supported gold nanoparticles can oxidise alcohols to aldehydes and ketones and further, converting the aldehydes to acids under mild conditions.[85] The reactant conversions (~99%) proved to be higher than any reported for palladium catalyst for the same process.[85] Cyclohexane can be catalytically convert to nylon-6 or/and nylon-6, 6 by using palladium but only with very low activity (*C*% = ~ 4%). However, supported gold nanoparticles exhibited high activity (*C*% = ~ 90%) and selectivity for the same reaction process.[86]

Oxidation reactions are of enormous industrial importance, especially in the synthesis of fine chemicals. One of the most highly researched areas of gold catalysis during the past two decades has been that of carbon monoxide oxidation.[58, 87] In the 1980s Haruta and Goodman found that that if the particles of gold were small enough, conversion of carbon monoxide to carbon dioxide proceeds, even at temperatures well below 0 ^{o}C.[30b, 42a] The discovery of the remarkable catalytic effectiveness of gold for selective oxidation of hydrocarbons was a surprise comparable with its ability in CO oxidation at low temperature.[15a] It was first demonstrated in 1998 when supported gold nanoparticles were used to oxidise propene to propene oxide by Haruta *et al.*[88] Overall, gold is an incredibly active catalyst in the oxidation

of both unsaturated and saturated hydrocarbons, such as alkenes, alkanes, aldehydes, poloyls and alcohols.[17a, 17c, 17d, 89]

1.1.6.2 Hydrogenation

Over the last two decades, the uses of platinum, ruthenium and palladium nanoparticles has burgeoned and they have become established as active and selective catalysts for a large number of reactions.[18a, 73, 90] Platinum group metals, particularly palladium and platinum itself, have been extensively studied as key components of many highly active and selective catalysts particularly for hydrogenation of unsaturated hydrocarbons.[19-20, 91] Studies of palladium have been particularly extensive.[20, 73, 92] As an example, Ma *et al.* utilized palladium nanoparticles dispersed in polyethylene glycols (PEGs) as a catalyst for hydrogenation of olefins. The results showed that hydrogenation occurred entirely and exclusively (*C*% and *S*% = ~100%) on the double-bond carbons.[91]

Recently, ruthenium nanoparticles have been shown to be catalytically active and selective for hydrogenation of organic compounds.[18a, 18c, 18d] As an example, ruthenium nanocatalysts immobilized on supports, such as TiO_2 or SiO_2 have been reported as highly active (*C*% = 98.5%) and selective catalyst for hydrogenation of 3-hydroxypropanal to 1, 3-propanediol at 200 ^{o}C over 24 hours.[93]

The use of gold metal nanoparticles for hydrogenation of cyclohexene was the starting point of research investigating gold as a hydrogenation catalyst. In the 1970s, it was reported that both gold foil and gold powder catalyse the convers of cyclohexene was to cyclohexane and benzene at high temperatures. Bond and Sermon reported some interesting results on the hydrogenation of alkenes and alkynes over gold nanoparticles immobilized on silica (Au/SiO_2).[94] Later, Hutchings *et al.* utilized supported gold particles for α,β – unsaturated aldehydes hydrogenation.[95]

1.1.7 Catalyst activation

Catalyst activation is an established method for preparing highly dispersed supported metal nanoparticles. The catalyst activation helps to determine both the physical and chemical nature of the active species and plays an important role in controlling the activity, as well as the selectivity, of the catalyst.

Recent advances in nanoscience have led to the development of numerous methodologies for controlled synthesis of mono dispersed nanoparticles via surface stabilization by organic capping ligands.[96] The application of these nanoparticles in catalysis and other fields often requires the removal of organic ligands.[49] It is known that the removal of organic capping agents or organic residues on gold nanoparticles is necessary for achieving high activity of the catalyst and should ensure the particle remains isolated on the surface without agglomeration.[97] The nanoparticles are deposited on a support and the stabilizing ligands-capped metal particles are then thermally removed to activate the catalyst.[68, 71-72] In surface chemistry, clean metal surfaces are more active than *"dirty"* surfaces, which are passivated by organic fragments.[98] However, activation procedures depend on the nature of the reaction and the type of catalyst. In this section, the more common techniques used for activation of supported metal nanoparticles will be explain.

1.1.7.1 Washing procedures

Washing procedures are used to remove organic ligands (*e.g.*, PPh_3 and PVA) or impurities from supported metal nanocatalysts.[32, 68] Two terms are used in this thesis for what essentially amount to washing procedures: "*washing*" involves a solvent used at a (sometimes elevated) temperature substantially below its boiling point; and "refluxing" involves a solvent used at a temperature near to or at its boiling point.

The most effective washing procedures appear to depend on the type of the solvent. Lopez-Sanchez *et al.* investigated the effects of different solvents, including water, tetrahydrofuran (THF) and ethanol for washing active gold catalyst for the oxidation of CO oxidation to CO_2. They found that only water washing led to a change the activity, and that reflux treatment at 90 ^oC for 1 hour led to a high conversion (~100%).[68] Anderson *et al.* used toluene as a solvent to wash supported gold particles/clusters. They removed PPh_3 ligands to improve gold particles/clusters interaction with the support (TiO_2).[32]

1.1.7.2 Calcinations

Calcination is catch-all term for thermal process used to remove impurities and/or ligands to achieve a better contact between gold particles and the underlying support or reactants. Often, calcination is taken to mean oxidation in an atmosphere of air, but in this thesis it refers to any thermal treatment applied under air or oxygen (oxidative treatments), hydrogen (reductive treatment), vacuum, dry nitrogen or/and helium (inert treatments).

Calcination often improves the activity of gold catalysts that demonstrate low activity in their untreated form.[72] By calcination procedure, the stabilizer ligands are removed from the gold clusters/particles and are deposited on supports surface, while the gold clusters/particles cores are either partially or fully agglomerated.[72] Strong contact between gold and the underlying support may sometimes be achieved via calcination, normally at temperatures below the melting point of the reactants and products.[50, 78] Overall, calcination of catalysts under different atmospheres (*i.e.*, in H_2, O_2, $O_2 – H_2$ or air) can significantly affect the catalytic activity.[63e] In this section, calcination under different atmospheres (*i.e.*, in static air, O_2, H_2, vacuum, inert gas or $O_2 – H_2$) will be discussed:

1.1.7.2.1 Calcination under static air

A thermal treatment in oxidative atmospheres, such as air, can remarkably improve the catalytic activity of supported gold particles.[30a, 63e] Haruta *et al.* demonstrated enhanced activity, after high-temperatures air calcination, for a mixture of colloidal gold particles with TiO_2 powder as a support, which they attributed to a stronger metal-support interaction.[69b] Air calcination can also rid the surface of contaminant from the support or precursor materials.[99] However, it invariably leads to the substantial particle size growth following ligand removal.[100]

1.1.7.2.2 Calcination under oxygen

Calcination performed in an oxygen- rich atmosphere facilitates ligand removal by partial or complete oxidation.[84a,72] Overall, it can be substantially more effective at removing ligands than reductive or inert processes even at high temperatures.[101] But it can also improve the catalytic activity by surface restructuring and formation of subsurface oxygen species providing an oxygen-enriched interface with an enhanced metal-support synergy.[102] Reaction steps involving oxygen can be more effective on gold sites present on larger and smoother gold particles.[97a] This proposal agrees well with the observed higher initial activity of oxidatively activated gold nanocatalysts with fewer surface- stabilizing ligands due to ligand decomposition.[73]

1.1.7.2.3 Calcination under hydrogen gas

Hydrogen gas treatment can reductively detach stabilizer ligands from the gold particles/clusters with subsequent re-deposition onto the support surface.[102a] However, it can lead to the formation of metallic gold.[102b] For hydrogen treatment, the temperature is crucial to the catalytic performance in organic compounds oxidation[103] because of its influence on the size and structure of resulting metal particles.[102a]

Lopez-Sanchez *et al.* investigated the effect of calcination under hydrogen at 200 ^{o}C on the catalytic activity of supported gold nanoparticles for CO oxidation.[68] The result confirmed very low activity of the calcined catalysts,[68] because the reductive treatment processing led to large particles sizes in comparison with the oxidative treatment.[73] However, Bulushev *et al.* found that the supported gold nanoparticles can be active catalysts for CO oxidation if the hydrogen calcination is performed at high temperatures in the range 400–500 ^{o}C.[104]

1.1.7.2.4 Calcination under vacuum

Calcination under vacuum can lead to oxidation of the gold clusters/particles, most likely via interaction with the support surface after removal of ligands.[71] The stabilizer ligands are removed from the gold particles/clusters but remain in an oxidised form on the surface and their removal leads slightly to agglomeration of the gold particles/clusters.[71] Supported gold clusters exhibit Au–O bonds, coincident with the loss of phosphine ligands and formation of oxidised phosphorous species.[72]

The effect of vacuum calcination at 200 ^{o}C was investigated by Turner *et al.* as an effective activation procedure for removing PPh_3 from Au_{55} nanoparticles immobilized on silica.[34] They showed that this type of calcination permitted better exposure of the gold nanocatalysts to reactants.[34] Anderson *et al.* investigated calcination, under vacuum at 200 ^{o}C, of gold nanoparticles and nanoclusters including Au_8, Au_9, Au_{11} and Au_{101} immobilized on TiO_2. They confirmed that PPh_3 was partially removed from the gold catalysts causing improvement of the catalytic activity.[32]

1.1.7.2.5 Calcination under inert gas

Calcination under inert atmospheres, such as dry nitrogen, argon and helium can exert influence on the final structure and activity of the supported gold catalysts because the metal particles do not induce additional growth after calcination.[102b, 105] However, in catalysed

reactions by some supported metal particles, like gold particles immobilized on titanium dioxide, it is necessary to increase slightly the gold particles size to be an active catalyst because of better contact between the metal particles and the support.[69b] More recently, researchers have shown that calcination under an inert gas cannot improve the catalytic activity of gold nanocatalysts. Negligible or even no conversion for organic compounds using activated gold nanocatalysts by an inert gas has been reported; supported gold nanoparticles calcined under dry nitrogen demonstrated low activity for CO oxidation to CO_2.[68]

1.1.7.2.6 Calcinations under oxygen gas followed by hydrogen gas

Combinations of oxygen and hydrogen calcinations can in integrate the advantages of both treatments.[63e] Hydrogen reduction following oxygen treatment can induce dispersion of metal particles and form partly reduced oxygen- containing particles, which would be active sites for oxidation of organic compounds.[102a] Thermal treatments can reduce metal oxide to metallic particles which then readily disperse into the supports.[102a] However, this type of thermal treatment can lead to the complete detachment of the stabilizer ligands from the gold particles/clusters and their re-deposition onto the support surface, which causes the gold clusters/particles to fully aggregate.[72]

1.1.7.3 Washing procedure and followed by calcination

The surface exposure and the catalytic activity of gold nanocatalysts can be enhanced by removing weakly adsorbed stabilizers ligands by washing. Follow up calcination are then sometimes used to in order to integrate advantages of different activation treatments. Lopez-Sanchez *et al.* demonstrated successful removal of polyvinyl alcohol (PVA) as an organic ligand from gold nanoparticles immobilized on TiO_2 as a support.[68] They washed the catalyst by hot water (as a solvent) and then calcined the supported gold nanoparticles (under static air or 5% H_2/Ar at 200 ^oC for 3 hours) to get a high conversion for CO oxidation.[68]

1.1.7.4 Ozonolysis procedure

The removal of ligands via a reaction using a stronger oxidizer, like ozone, has been used as an effective treatment with less gold particles aggregation as well as better catalysts dispersion and thermal stability.[106] This type of treatment was conducted at a mild temperature (*i.e.*, 200 ^{o}C) to avoid the risk of catalyst sintering. The ozone- treated gold catalyst showed normal particle size distributions (*i.e.*, the metal particles did not induce additional growth) and high conversion for CO oxidation.[106] Ozone activation may produce partially oxidized states of gold,[107] which could reinforce the interactions between the gold nanoparticles and the support.[106] Even higher activity was achieved when ozonolysis was followed by calcination.[106] The exposure of ozone gas to activated carbon supports led to deposition on the carbon surface, transforming basic sites into acid sites. New acid sites were also generated by addition of ozone across double bonds of the carbon structure.

1.1.7.5 Plasma

Plasma is an ionized gas consisting of positive ions and free electrons in proportions resulting no overall electric charge, typically at low pressures (as in the upper atmosphere and in fluorescent lamps) or at very high temperatures (as in stars and nuclear fusion reactors).[108] Plasma treatments, such as corona discharges, spark discharges, and dielectric barrier discharge (DBD) are activation procedures that can be used remove the capping agents or organic ligands to enhance the catalytic activity of supported metal particles even at atmospheric pressure and ambient temperature.[109] They can achieve high metal dispersions and enhance metal- support interaction without the exposure of the material to a high temperature environment (see Figure 1.7).[109b, 110] They also provide unique ways to enhance metal support interactions while avoiding the formation of large nanoparticles because the temperature is too low overcome the activation energy for aggregation.[110-111] As an example,

supported gold particles were activated using O_2 plasma procedure for selective hydrogenation of acetylene at ambient temperature (~ 25 ^oC).[110]

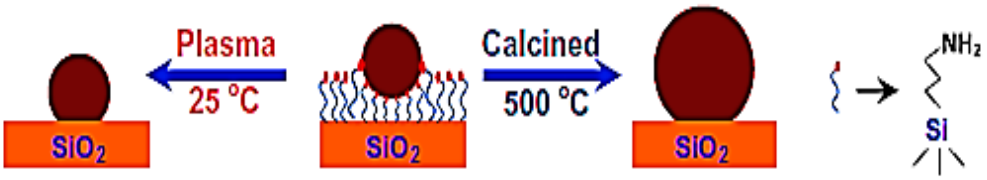

Figure 0.7: Schematic illustration of the gold particle size changes of Au/SiO_2 catalysts after activation by O_2 plasma treatment at ambient temperature (25 ^oC) or high temperature calcination (500 ^oC). Reproduced from Liu *et al.*[110]

1.1.7.6 Permanganate or potassium manganite procedures

Permanganate or manganite can activate supported gold particles by partially oxidizing residual organic ligands,[49] followed by thermal treatment at high temperature (at least 300 ^oC).[112] $KMnO_4$ or K_2MnO_4 treatment can make the gold catalysts more active under certain conditions, regardless of the support chosen and the size of gold nanoparticle.[112] In addition, the treatment with $KMnO_4$ can remove the functional organic ligands with minimal sintering of particles.[49] However, $KMnO_4$ or K_2MnO_4 can react with supports, such as carbon.[113]

1.2 Scope of this thesis

The aims of this thesis are:

- To gain a better understanding of shape, size and support effects on the catalytic activity of supported noble metal nanoparticles.
- To study the effect of different types of activation procedure on the catalytic activity of supported metal nanoparticles.
- To investigate the efficacy of different types of noble metal nanoparticles for various types of reactions.

- To optimize conditions for the catalytic activity of supported noble metal nanoparticles.

The particles or clusters were used for synthesizing novel supported gold catalysts by depositing the metal particles or clusters like gold and ruthenium on the surface of different types of support like silica and carbon. The catalysts were then investigated for their activity in liquid- phase oxidation or hydrogenation reactions. In order to investigate the effect of gold particles size on catalytic activity, the steric effects of the stabilizing ligands on the particles size has been explored. Preparation methods were improved with the aim of obtaining high quality, mono-disperse, well ordered gold particles. These particles and clusters were characterized extensively to understand the effects of the size, size distributions and dispersion on the catalytic activity of supported noble metal particles or clusters.

References

1. Davy, H., *Trans. R. Soc. Lond.*, **1817,** *107*, 77.
2. Berzelius, J. J., *Ann. Chim. Phys* **1836,** *61*, 146.
3. F(araday), M., *Quart. J. Science* **1823,** *16*, 179.
4. The Nobel Prize in Chemistry 1932. http://www.nobelprize.org/nobel_prizes/chemistry/laureates/1932/ (accessed Oct 31, 2013).
5. Kilmartin, J. Molecular gold clusters as precursors to heterogeneous catalysts University College London, London, England, 2010.
6. Bond, C.; Louis, C.; Thompson, D. T., The phenomenon of catalysis. In *Catalysis by gold*, First ed.; Hutchings, G., Ed. Imperial College Press: London,UK, 2006; Vol. 6, pp 1-4.
7. Bell, A. T., The impact of nanoscience on heterogeneous catalysis. *Science* **2003,** *299* (5613), 1688-1691.
8. Poole, C. P.; Owens, F. J., Size dependence of properties. In *Introduction to nanotechnology*, John Wiley & Sons: Hoboken, New Jersey, 2003; p 8.
9. Johnson, B. F. G., From clusters to nanoparticles and catalysis. *Coord. Chem. Rev.* **1999,** *190-192*, 1269-1285.
10. Brydson, R. M.; Hammond, C., Generic methodologies for nanotechnology: Classification and fabrication. In *Nanoscale Scienece and Technology*, Kelsall, R.; Hamiley, I. W.; Geoghegan, M., Eds. Wiley: West Sussex, 2005; pp 1-55.
11. Bartlett, P. N.; Baumberg, J. J.; Coyle, S.; Abdelsalam, M. E., Optical properties of nanostructured metal films. *Faraday Discuss.* **2004,** *125*, 117-132.
12. (a) Brune, H.; Ernst, H.; Grunwald, A.; Grünwald, W.; Hofmann, H.; Krug, H.; Janich, P.; Mayor, M.; Rathgeber, W.; Schmid, G.; Simon, U.; Vogel, V.; Wyrwa, D., Nanotechnology and Philosophy of Science. In *Nanotechnology: Assessment and Perspectives*, Gethmann, F. C., Ed. Springer: Berlin, Germany, 2006; Vol. 27, pp 25-65; (b) Collier, P. J.; Iggo, J. A.; Whyman, R., Preparation and characterisation of solvent-stabilised nanoparticulate platinum and palladium and their catalytic behaviour towards the enantioselective hydrogenation of ethyl pyruvate. *J. Mol. Catal. A: Chem.* **1999,** *146* (1-2), 149-157.
13. Vohs, J. M., Understanding the competing factors that control the selectivity of alcohol oxidation on Au catalysts. *Surf. Sci.* **2012,** *606* (15), 1127-1128.
14. Xu, W.; Kong, J. S.; Yeh, Y. T. E.; Chen, P., Single-molecule nanocatalysis reveals heterogeneous reaction pathways and catalyticdynamics. *Nature Mater.* **2008,** *7* (12), 992-996.
15. (a) Haruta, M.; Yamada, N.; Kobayashi, T.; Iijima, S., Gold catalysts prepared by coprecipitation for low-temperature oxidation of hydrogen and of carbon monoxide. *J. Catal.* **1989,** *115* (2), 301-309; (b) Haruta, M.; Uphade, B. S.; Tsubota, S.; Miyamoto, A., Selective oxidation of propylene over gold deposited on titanium-based oxides. *Res. Chem. Intermed.* **1998,** *24* (3), 329-336.
16. (a) Rampino, L. D.; Nord, F. F., Applicability of palladium synthetic high polymer catalysts. *J. Am. Chem. Soc.* **1941,** *63* (12), 3268; (b) Rampino, L. D.; Nord, F. F., Preparation of palladium and platinum synthetic high polymer catalysts and the relationship between particle size and rate of hydrogenation. *J. Am. Chem. Soc.* **1941,** *63* (10), 2745-2749.
17. (a) Della Pina, C.; Falletta, E.; Prati, L.; Rossi, M., Selective oxidation using gold. *Chem. Soc. Rev.* **2008,** *37* (9), 2077-2095; (b) Lignier, P.; Morfin, F.; Mangematin, S.; Massin, L.; Rousset, J. L.; Caps, V., Stereoselective stilbene epoxidation over supported gold-based catalysts. *Chem. Commun.* **2007,** (2), 186-188; (c) Lignier, P.; Morfin, F.; Piccolo, L.; Rousset, J.-L.; Caps, V., Insight into the free-radical chain mechanism of gold-catalyzed hydrocarbon oxidation reactions in the liquid phase. *Catal. Today* **2007,** *122* (3-4), 284-291; (d) Ingold, K. U.; Snelgrove, D. W.; MacFaul, P. A.; Oldroyd, R. D.; Thomas, J. M., Hydrophobic/hydrophilic effects on the titanium(IV)-catalyzed epoxidation of cyclohexene by tert-alkyl hydroperoxides: 2-methyl-l-phenyl-2-propyl hydroperoxide (MPPH) versus tert-butyl hydroperoxide (TBHP). *Catal. Lett.* **1997,** *48* (1-2), 21-24; (e) Wakita, H.; Ukai, K.; Takeguchi, T.; Ueda, W., Deactivation of Ru/Al_2O_3 catalyst for preferential CO oxidation in the presence of low-concentration NH_3 by nitrosyl species. *Chem. Lett.* **2006,** *35* (7), 734-735; (f) Wakita, H.; Ukai, K.; Takeguchi, T.; Ueda, W., Mechanistic investigation of deactivation of Ru/Al_2O_3 catalyst for preferential CO oxidation in the presence of NH_3. *J. Phys. Chem. C* **2007,** *111* (5), 2205-2211.

18. (a) Vollmer, C.; Redel, E.; Abu-Shandi, K.; Thomann, R.; Manyar, H.; Hardacre, C.; Janiak, C., Microwave irradiation for the facile synthesis of transition-metal nanoparticles (NPs) in ionic liquids (ILs) from metal–carbonyl precursors and Ru-, Rh-, and Ir-NP/IL dispersions as biphasic liquid–liquid hydrogenation nanocatalysts for cyclohexene. *Chem. – Eur. J.* **2010,** *16* (12), 3849-3858; (b) Liu, S.; Liu, Z.; Wang, Z.; Zhao, S.; Wu, Y., A novel amorphous alloy Ru-La-B/ZrO_2 catalyst with high activity and selectivity for benzene selective hydrogenation. *Appl. Catal., A* **2006,** *313* (1), 49-57; (c) Silveira, E. T.; Umpierre, A. P.; Rossi, L. M.; Machado, G.; Morais, J.; Soares, G. V.; Baumvol, I. J. R.; Teixeira, S. R.; Fichtner, P. F. P.; Dupont, J., The partial hydrogenation of benzene to cyclohexene by nanoscale ruthenium catalysts in imidazolium ionic liquids. *Chem. - Eur. J.* **2004,** *10* (15), 3734-3740; (d) Nagahara, H.; Ono, M.; Konishi, M.; Fukuoka, Y., Partial hydrogenation of benzene to cyclohexene. *Appl. Surf. Sci.* **1997,** *121-122*, 448-451.
19. Figueras, F.; Coq, B., Hydrogenation and hydrogenolysis of nitro-, nitroso-, azo-, azoxy- and other nitrogen-containing compounds on palladium. *J. Mol. Catal. A: Chem.* **2001,** *173* (1-2), 223-230.
20. Astruc, D., Palladium nanoparticles as efficient green homogeneous and heterogeneous carbon-carbon coupling precatalysts: A unifying view. *Inorg. Chem.* **2007,** *46* (6), 1884-1894.
21. Y., C. D.; G., P., *J. Catal* **1970,** *18*, 200-211.
22. Liu, Y.; Tsunoyama, H.; Akita, T.; Tsukuda, T., Preparation of ∼1 nm gold clusters confined within mesoporous silica and microwave-assisted catalytic application for alcohol oxidation. *J. Phys. Chem. C* **2009,** *113* (31), 13457-13461.
23. (a) Schimpf, S.; Lucas, M.; Mohr, C.; Rodemerck, U.; Brückner, A.; Radnik, J.; Hofmeister, H.; Claus, P., Supported gold nanoparticles: in-depth catalyst characterization and application in hydrogenation and oxidation reactions. *Catal. Today* **2002,** *72* (1–2), 63-78; (b) Claus, P., Heterogeneously catalysed hydrogenation using gold catalysts. *Appl. Catal., A* **2005,** *291* (1–2), 222-229; (c) Kótai, L.; Kazinczy, B.; Keszler, Á.; Holly, S.; Gács, I.; Banerji, K. K., Three reagents in one: Ammonium permanganate in the oxidation of benzyl alcohol. *Z. Naturforsch., B: Chem. Sci.* **2001,** *56* (8), 823-825; (d) Pillai, U. R.; Deevi, S., Highly active gold-ceria catalyst for the room temperature oxidation of carbon monoxide. *App. Catal., A* **2006,** *299* (0), 266-273.
24. Miedziak, P.; Sankar, M.; Dimitratos, N.; Lopez-Sanchez, J. A.; Carley, A. F.; Knight, D. W.; Taylor, S. H.; Kiely, C. J.; Hutchings, G. J., Oxidation of benzyl alcohol using supported gold–palladium nanoparticles. *Catal. Today* **2011,** *164* (1), 315-319.
25. Haruta, M., Gold as a low-temperature oxidation catalyst: Factors controlling activity and selectivity. *Stud. Surf. Sci. Catal.* **1997,** *110*, 123-134.
26. Herzing, A. A.; Kiely, C. J.; Carley, A. F.; Landon, P.; Hutchings, G. J., Identification of active gold nanoclusters on iron oxide supports for CO oxidation. *Science* **2008,** *321* (5894), 1331-1335.
27. Comotti, M.; Della Pina, C.; Matarrese, R.; Rossi, M., The catalytic activity of "naked" gold particles. *Angew. Chem., Int. Ed.* **2004,** *43* (43), 5812-5815.
28. Safer, D.; Hainfeld, J.; Wall, J. S.; Reardon, J. E., Biospecific labeling with undecagold: Visualization of the biotin-binding site on avidin. *Science* **1982,** *218* (4569), 290-291.
29. (a) Schmid, G.; Corain, B., Nanoparticulated gold: Syntheses, structures, electronics, and reactivities. *Eur. J. Inorg. Chem.* **2003,** (17), 3081-3098; (b) Weare, W. W.; Reed, S. M.; Warner, M. G.; Hutchison, J. E., Improved synthesis of small (dCORE ≈ 1.5 nm) phosphine-stabilized gold nanoparticies *J. Am. Chem. Soc.* **2000,** *122* (51), 12890-12891.
30. (a) Yuan, Y.; Kozlova, A. P.; Asakura, K.; Wan, H.; Tsai, K.; Iwasawa, Y., Supported Au catalysts prepared from Au phosphine complexes and As-precipitated metal hydroxides: Characterization and low-temperature CO oxidation. *J. Catal.* **1997,** *170* (1), 191-199; (b) Valden, M.; Lai, X.; Goodman, D. W., Onset of catalytic activity of gold clusters on titania with the appearance of nonmetallic properties. *Science* **1998,** *281* (5383), 1647-1650.
31. Wen, F.; Englert, U.; Gutrath, B.; Simon, U., Crystal structure, electrochemical and optical properties of $[Au_9(PPh_3)_8](NO_3)_3$. *Eur. J. Inorg. Chem.* **2008,** *2008* (1), 106-111.
32. Anderson, D. P.; Alvino, J. F.; Gentleman, A.; Qahtani, H. A.; Thomsen, L.; Polson, M. I. J.; Metha, G. F.; Golovko, V. B.; Andersson, G. G., Chemically-synthesised, atomically-precise gold clusters deposited and activated on titania. *PCCP* **2013,** *15* (11), 3917-3929.

33. Kozlov, A. I.; Kozlova, A. P.; Liu, H.; Iwasawa, Y., A new approach to active supported Au catalysts. *Appl. Catal., A* **1999,** *182* (1), 9-28.
34. Turner, M.; Golovko, V. B.; Vaughan, O. P. H.; Abdulkin, P.; Berenguer-Murcia, A.; Tikhov, M. S.; Johnson, B. F. G.; Lambert, R. M., Selective oxidation with dioxygen by gold nanoparticle catalysts derived from 55-atom clusters. *Nature* **2008,** *454* (7207), 981-983.
35. Schmid, G.; Pfeil, R.; Boese, R.; Bandermann, F.; Meyer, S.; Calis, G. H. M.; Vandervelden, W. A., $AU_{55}[P(C_6H_5)_3]_{12}CL_6$ -A gold cluster of an exceptional size. *Chem. Ber. Recl.* **1981,** *114* (11), 3634-3642.
36. Hutchinson, J. E.; Foster, E. W.; Warner, M. G.; Reed, S. M.; Weare, W. W., Triphenylphosphine-stabilised gold nanoparticles. In *Inorganic synthsis*, Shapley, J. R., Ed. John Wiley & Sons: 2004; Vol. 34 pp 228-232.
37. Schmid, G., The relevance of shape and size of Au_{55} clusters. *Chem. Soc. Rev.* **2008,** *37* (9), 1909-1930.
38. Bond, G. C.; Thompson, D. T., Catalysis by Gold. *Catal. Rev.—Sci. Eng.* **2001,** *641* (3-4), 319-388.
39. Hutchings, G. J., New directions in gold catalysis. *Gold Bulletin* **2004,** *37* (1-2), 3-11.
40. Maeda, Y.; Okumura, M.; Tsubota, S.; Kohyama, M.; Haruta, M., Local barrier height of Au nanoparticles on a TiO_2(1 1 0)-(1×2) surface. *Appl. Surf. Sci.* **2004,** *222* (1-4), 409-414.
41. Walsh, M. J. Aberration corrected in-situ electron microscopy of nanoparticle catalysts. University of York, England, 2012.
42. (a) Bamwenda, G. R.; Tsubota, S.; Nakamura, T.; Haruta, M., The influence of the preparation methods on the catalytic activity of platinum and gold supported on TiO_2 for CO oxidation. *Catal. Lett.* **1997,** *44* (1-2), 83-87; (b) Henry, C. R., Catalytic activity of supported nanometer-sized metal clusters. *Appl. Surf. Sci.* **2000,** *164* (1-4), 252-259; (c) Hu, J.; Chen, L.; Zhu, K.; Suchopar, A.; Richards, R., Aerobic oxidation of alcohols catalyzed by gold nano-particles confined in the walls of mesoporous silica. *Catal. Today* **2007,** *122* (3-4), 277-283; (d) Tsunoyama, H.; Liu, Y. M.; Akita, T.; Ichikuni, N.; Sakurai, H.; Xie, S. H.; Tsukuda, T., Size-controlled synthesis of gold clusters as efficient catalysts for aerobic oxidation. *Catal. Surv. Asia* **2011,** *15* (4), 230-239; (e) Tsunoyama, H.; Sakurai, H.; Negishi, Y.; Tsukuda, T., Size-specific catalytic activity of polymer-stabilized gold nanoclusters for aerobic alcohol oxidation in water. *J. Am. Chem. Soc.* **2005,** *127* (26), 9374-9375.
43. Haruta, M., Size- and support-dependency in the catalysis of gold. *Catal. Today* **1997,** *36* (1), 153-166.
44. Boronat, M.; Corma, A.; Illas, F.; Radilla, J.; Ródenas, T.; Sabater, M. J., Mechanism of selective alcohol oxidation to aldehydes on gold catalysts: Influence of surface roughness on reactivity. *J. Catal.* **2011,** *278* (1), 50-58.
45. Narayanan, R.; El-Sayed, M. A., Effect of nanocatalysis in colloidal solution on the tetrahedral and cubic nanoparticle SHAPE: Electron-transfer reaction catalyzed by platinum nanoparticles. *J. Phys. Chem. B* **2004,** *108* (18), 5726-5733.
46. Mikami, Y.; Dhakshinamoorthy, A.; Alvaro, M.; Garcia, H., Catalytic activity of unsupported gold nanoparticles. *Catal. Sci. Technol.* **2013,** *3* (1), 58-69.
47. Ketchie, W. C.; Fang, Y. L.; Wong, M. S.; Murayama, M.; Davis, R. J., Influence of gold particle size on the aqueous-phase oxidation of carbon monoxide and glycerol. *J. Catal.* **2007,** *250* (1), 94-101.
48. Van Bokhoven, J. A., Catalysis by gold: Why size matters. *Chimia* **2009,** *63* (5), 257-260.
49. Yin, H.; Ma, Z.; Overbury, S. H.; Dai, S., Promotion of $Au(en)_2Cl_3$-Derived Au/Fumed SiO_2 by Treatment with $KMnO_4$. *J. Phys. Chem. C* **2008,** *112* (22), 8349-8358.
50. Abad, A.; Corma, A.; García, H., Catalyst parameters determining activity and selectivity of supported gold nanoparticles for the aerobic oxidation of alcohols: The molecular reaction mechanism. *Chem.- Eur. J.* **2008,** *14* (1), 212-222.
51. (a) Ren, J.; Tilley, R. D., Shape-controlled growth of platinum nanoparticles. *Small* **2007,** *3* (9), 1508-1512; (b) Lu, C. Y.; Wey, M. Y.; Fu, Y. H., The size, shape, and dispersion of active sites on AC-supported copper nanocatalysts with polyol process: The effect of precursors. *Appl. Catal., A* **2008,** *344* (1-2), 36-44; (c) Mandal, M.; Ghosh, S. K.; Kundu, S.; Esumi, K.; Pal, T., UV photoactivation for size and shape controlled synthesis and coalescence of gold nanoparticles in

micelles. *Langmuir* **2002,** *18* (21), 7792-7797; (d) Kundu, S.; Pal, A.; Ghosh, S. K.; Nath, S.; Panigrahi, S.; Praharaj, S.; Pal, T., A new route to obtain shape-controlled gold nanoparticles from Au(III)-β-diketonates. *Inorg. Chem.* **2004,** *43* (18), 5489-5491; (e) Herricks, T.; Chen, J.; Xia, Y., Polyol synthesis of platinum nanoparticles: Control of morphology with sodium nitrate. *Nano Lett.* **2004,** *4* (12), 2367-2371; (f) Cui, H.; Zayat, M.; Levy, D., A chemical strategy to control the shape of oxide nanoparticles. *J. Nanopart. Res.* **2009,** *11* (6), 1331-1338.
52. Tian, N.; Zhou, Z.-Y.; Sun, S.-G., Platinum metal catalysts of high-index surfaces: From single-crystal planes to electrochemically shape-controlled nanoparticles. *J. Phys. Chem. C* **2008,** *112* (50), 19801-19817.
53. Ertl, G., Reactions at surfaces: From atoms to complexity (Nobel lecture). *Angew. Chem., Int. Ed.* **2008,** *47* (19), 3524-3535.
54. The Nobel Prize in Chemistry 2007. http://www.nobelprize.org/nobel_prizes/chemistry/laureates/2007/ (accessed Oct 31, 2013).
55. Somorjai, G. A.; York, R. L.; Butcher, D.; Park, J. Y., The evolution of model catalytic systems; studies of structure, bonding and dynamics from single crystal metal surfaces to nanoparticles, and from low pressure (less than 10^{-3} Torr) to high pressure (more than 10^{-3} Torr) to liquid *Phys. Chem. Chem. Phys.* **2007,** *9* (27), 3500-3513.
56. Aliaga, C.; Park, J. Y.; Yamada, Y.; Lee, H. S.; Tsung, C. K.; Yang, P.; Somorjai, G. A., Sum frequency generation and catalytic reaction studies of the removal of organic capping agents from Pt nanoparticles by UV-Ozone treatment. *J. Phys. Chem. C* **2009,** *113* (15), 6150-6155.
57. Lu, P.; Teranishi, T.; Asakura, K.; Miyake, M.; Toshima, N., Polymer-protected Ni/Pd bimetallic nano-clusters: Preparation, characterization and catalysis for hydrogenation of nitrobenzene. *J. Phys. Chem. B* **1999,** *103* (44), 9673-9682.
58. Haruta, M.; Tsubota, S.; Kobayashi, T.; Kageyama, H.; Genet, M. J.; Delmon, B., Low-temperature oxidation of CO over gold supported on TiO_2, α-Fe_2O_3, and Co_3O_4. *J. Catal.* **1993,** *144* (1), 175-192.
59. (a) Caballero, C.; Valencia, J.; Barrera, M.; Gil, A., Selective hydrogenation of citral over gold nanoparticles on alumina. *Powder Technol.* **2010,** *203* (2), 412-414; (b) Hayek, K.; Fuchs, M.; Klötzer, B.; Reichl, W.; Rupprechter, G., Studies of metal-support interactions with "real" and "inverted" model systems: Reactions of CO and small hydrocarbons with hydrogen on noble metals in contact with oxides. *Top. Catal.* **2000,** *13* (1-2), 55-66; (c) Corma, A.; Garcia, H., Supported gold nanoparticles as catalysts for organic reactions. *Chem. Soc. Rev.* **2008,** *37* (9), 2096-2126; (d) Haruta, M.; Kobayashi, T.; Sano, H.; Yamada, N., Novel gold catalysts for the oxidation of carbon monoxide at a temperature far below 0 °C. *Chem. Lett.* **1987,** *16* (2), 405-408.
60. Haruta, M., Spiers memorial lecture role of perimeter interfaces in catalysis by gold nanoparticles. *Faraday Discuss.* **2011,** *152*, 11-32.
61. (a) Cárdenas-Lizana, F.; Gómez-Quero, S.; Perret, N.; Keane, M. A., Support effects in the selective gas phase hydrogenation of p-chloronitrobenzene over gold. *Gold Bull.* **2009,** *42* (2), 124-132; (b) Lin, S. D.; Bollinger, M.; Vannice, M. A., Low temperature CO oxidation over Au/TiO_2 and Au/SiO_2 catalysts. *Catal. Lett.* **1993,** *17* (3-4), 245-262; (c) Liotta, L. F.; Di Carlo, G.; Pantaleo, G.; Deganello, G.; Venezia, A. M., Gold catalysis in southern Italy. *Gold Bull.* **2009,** *42* (1), 66-73.
62. Riva, R.; Miessner, H.; Vitali, R.; Del Piero, G., Metal–support interaction in Co/SiO_2 and Co/TiO_2. *Appl. Catal. A,* **2000,** *196* (1), 111-123.
63. (a) Yan, Z.; Chinta, S.; Mohamed, A.; Fackler, J.; Goodman, D., CO oxidation over Au/TiO_2 prepared from metal-organic gold complexes. *Catal. Lett.* **2006,** *111* (1), 15-18; (b) Goodman, D., "Catalytically active Au on Titania:" yet another example of a strong metal support interaction (SMSI)? *Catal. Lett.* **2005,** *99* (1), 1-4; (c) Gajan, D.; Guillois, K.; Delichère, P.; Basset, J.-M.; Candy, J.-P.; Caps, V. r.; Copéret, C.; Lesage, A.; Emsley, L., Gold nanoparticles supported on passivated silica: Access to an efficient aerobic epoxidation catalyst and the intrinsic oxidation activity of gold. *J. Am. Chem. Soc.* **2009,** *131* (41), 14667-14669; (d) Daté, M.; Ichihashi, Y.; Yamashita, T.; Chiorino, A.; Boccuzzi, F.; Haruta, M., Performance of Au/TiO_2 catalyst under ambient conditions. *Catal. Today* **2002,** *72* (1-2), 89-94; (e) Zhang, R. R.; Ren, L. H.; Lu, A. H.; Li, W. C., Influence of pretreatment atmospheres on the activity of Au/CeO_2 catalyst for low-temperature CO oxidation. *Catal. Commu.* **2011,** *13* (1), 18-21.

64. Demirel, S.; Kern, P.; Lucas, M.; Claus, P., Oxidation of mono- and polyalcohols with gold: Comparison of carbon and ceria supported catalysts. *Catal. Today* **2007,** *122* (3-4), 292-300.
65. Chen, Y.; Qiu, J.; Wang, X.; Xiu, J., Preparation and application of highly dispersed gold nanoparticles supported on silica for catalytic hydrogenation of aromatic nitro compounds. *J. Catal.* **2006,** *242* (1), 227-230.
66. (a) Biella, S.; Castiglioni, G. L.; Fumagalli, C.; Prati, L.; Rossi, M., Application of gold catalysts to selective liquid phase oxidation. *Catal. Today* **2002,** *72* (1-2), 43-49; (b) Prati, L.; Rossi, M., Gold on carbon as a new catalyst for selective liquid phase oxidation of diols. *J. Catal.* **1998,** *176* (2), 552-560.
67. Belin, S.; Bracey, C. L.; Briois, V.; Ellis, P. R.; Hutchings, G. J.; Hyde, T. I.; Sankar, G., CuAu/SiO2 catalysts for the selective oxidation of propene to acrolein: the impact of catalyst preparation variables on material structure and catalytic performance. *Catal. Sci. Technol.* **2013,** *3* (11), 2944-2957.
68. Lopez-Sanchez, J. A.; Dimitratos, N.; Hammond, C.; Brett, G. L.; Kesavan, L.; White, S.; Miedziak, P.; Tiruvalam, R.; Jenkins, R. L.; Carley, A. F.; Knight, D.; Kiely, C. J.; Hutchings, G. J., Facile removal of stabilizer-ligands from supported gold nanoparticles. *Nat. Chem.* **2011,** *3* (7), 551-556.
69. (a) Okumura, M.; Tsubota, S.; Haruta, M., Preparation of supported gold catalysts by gas-phase grafting of gold acethylacetonate for low-temperature oxidation of CO and of H_2. *J. Mol. Catal. A: Chem.* **2003,** *199* (1–2), 73-84; (b) Tsubota, S.; Nakamura, T.; Tanaka, K.; Haruta, M., Effect of calcination temperature on the catalytic activity of Au colloids mechanically mixed with TiO_2 powder for CO oxidation. *Catal. Lett.* **1998,** *56* (3-4), 131-135.
70. Pritchard, J.; Piccinini, M.; Tiruvalam, R.; He, Q.; Dimitratos, N.; Lopez-Sanchez, J. A.; Morgan, D. J.; Carley, A. F.; Edwards, J. K.; Kiely, C. J.; Hutchings, G. J., Effect of heat treatment on Au-Pd catalysts synthesized by sol immobilisation for the direct synthesis of hydrogen peroxide and benzyl alcohol oxidation. *Catal. Sci. Technol.* **2013,** *3* (2), 308-317.
71. Ahmad, M. Z.; Golovko, V. B.; Adnan, R. H.; Abu Bakar, F.; Ruzicka, J.-Y.; Anderson, D. P.; Andersson, G. G.; Wlodarski, W., Hydrogen sensing using gold nanoclusters supported on tungsten trioxide thin films. *Int. J. Hydrogen Energy* **2013,** (0).
72. Anderson, D. P.; Adnan, R. H.; Alvino, J. F.; Shipper, O.; Donoeva, B.; Ruzicka, J. Y.; Al Qahtani, H.; Harris, H. H.; Cowie, B.; Aitken, J. B.; Golovko, V. B.; Metha, G. F.; Andersson, G. G., Chemically synthesised atomically precise gold clusters deposited and activated on titania. Part II. *PCCP* **2013,** *15* (35), 14806-14813.
73. Abd El-Moemen, A.; Karpenko, A.; Denkwitz, Y.; Behm, R. J., Activity, stability and deactivation behavior of Au/CeO_2 catalysts in the water gas shift reaction at increased reaction temperature (300 °C). *J. Power Sources* **2009,** *190* (1), 64-75.
74. Sermon, P. A.; Bond, G. C.; Wells, P. B., Hydrogenation of alkenes over supported gold. *J. Chem. Soc., Faraday Trans. 1* **1979,** *75*, 385-394.
75. Haruta, M., Gold as a novel catalyst in the 21st century: Preparation, working mechanism and applications. *Gold Bull.* **2004,** *37* (1), 27-36.
76. Sakurai, H.; Haruta, M., Carbon dioxide and carbon monoxide hydrogenation over gold supported on titanium, iron, and zinc oxides. *Appl. Catal., A* **1995,** *127* (1-2), 93-105.
77. Haruta, M.; Yamada, N.; Kobayashi, T.; Iijima, S., Gold catalysts prepared by coprecipitation for low-temperature oxidation of hydrogen and of carbon monoxide. *J. Catal.* **1989,** *115* (2), 301-309.
78. Haruta, M., Catalysis of gold nanoparticles deposited on metal oxides. *CATTECH* **2002,** *6* (3), 102-115.
79. Zanella, R.; Delannoy, L.; Louis, C., Mechanism of deposition of gold precursors onto TiO_2 during the preparation by cation adsorption and deposition-precipitation with NaOH and urea. *Appl. Catal., A* **2005,** *291* (1-2), 62-72.
80. Zanella, R.; Giorgio, S.; Henry, C. R.; Louis, C., Alternative methods for the preparation of gold nanoparticles supported on TiO_2. *J. Phys. Chem. B* **2002,** *106* (31), 7634-7642.
81. Gluhoi, A. C.; Dekkers, M. A. P.; Nieuwenhuys, B. E., Comparative studies of the N_2O/H_2, N_2O/CO, H_2/O_2 and CO/O_2 reactions on supported gold catalysts: Effect of the addition of various oxides. *J. Catal.* **2003,** *219* (1), 197-205.

82. (a) Sergio, N.; Roberto, M.; Mercedes, A.; Hermenegildo, G., Sunlight-assisted fenton reaction catalyzed by gold supported on idamond nanoparticles as pretreatment for biological dDegradation of aqueous phenol solutions. *ChemSusChem* **2011,** *4* (5), 650-657; (b) Okumura, M.; Tanaka, K.; Ueda, A.; Haruta, M., The reactivities of dimethylgold(III)β-diketone on the surface of TiO_2: A novel preparation method for Au catalysts. *Solid State Ionics* **1997,** *95* (1-2), 143-149; (c) Palgrave, R. G.; Parkin, I. P., Aerosol assisted chemical vapor deposition using nanoparticle precursors: A route to nanocomposite thin films. *J. Am. Chem. Soc.* **2006,** *128* (5), 1587-1597.
83. Kobayashi, T.; Haruta, M.; Tsubota, S.; Sano, H.; Delmon, B., Thin films of supported gold catalysts for CO detection. *Sensors and Actuators: B. Chemical* **1990,** *1* (1-6), 222-225.
84. Matsura, V. A.; Potekhin, V. V.; Platonov, V. V.; Tatsenko, O. M.; Ukraintsev, V. B.; Khokhryakov, K. A., Hydrogention and oxidation of allyl alcohol in the presence of colloid palladium in situ. *Russ. J. Gen. Chem.* **2003,** *73* (12), 1900-1903.
85. Abad, A.; Concepción, P.; Corma, A.; García, H., A collaborative effect between gold and a support induces the selective oxidation of alcohols. *Angew. Chem., Int. Ed.* **2005,** *44* (26), 4066-4069.
86. G. M. Lu, R. Z., G. Qian, Y. X. Qi, X. L. Wang, J. S. Suo,, *Catal Lett* **2004,** *97*, 115.
87. Joo, S. H.; Park, J. Y.; Renzas, J. R.; Butcher, D. R.; Huang, W.; Somorjai, G. A., Size effect of ruthenium nanoparticles in catalytic carbon monoxide oxidation. *Nano Lett.* **2010,** *10* (7), 2709-2713.
88. Hayashi, T.; Tanaka, K.; Haruta, M., Selective vapor-phase epoxidation of propylene over Au/TiO_2 catalysts in the presence of oxygen and hydrogen. *J. Catal.* **1998,** *178* (2), 566-575.
89. (a) Adam, W.; Roschmann, K. J.; Saha-Möller, C. R.; Seebach, D., cis-stilbene and (1α,2β,3α)-(2-ethenyl-3-methoxycyclopropyl) benzene as mechanistic probes in the MnIII (salen)-catalyzed epoxidation: Influence of the oxygen source and the counterion on the diastereoselectivity of the competitive concerted and radical-type oxygen transfer. *J. Am. Chem. Soc.* **2002,** *124* (18), 5068-5073; (b) Haruta, M., When gold is not noble: Catalysis by nanoparticles. *Chem. Rec.* **2003,** *3* (2), 75-87; (c) Haruta, M., Nanoparticles can open a new world of heterogeneous catalysis. *J. Nanopart. Res.* **2003,** *5* (1-2), 3-4.
90. Ahmadi, T. S.; Logunov, S. L.; El-Sayed, M. A., Picosecond dynamics of colloidal gold nanoparticles. *J. Phys. Chem.* **1996,** *100* (20), 8053-8056.
91. Ma, X.; Jiang, T.; Han, B.; Zhang, J.; Miao, S.; Ding, K.; An, G.; Xie, Y.; Zhou, Y.; Zhu, A., Palladium nanoparticles in polyethylene glycols: Efficient and recyclable catalyst system for hydrogenation of olefins. *Catal. Commun.* **2008,** *9* (1), 70-74.
92. (a) Gual, A.; Godard, C.; Philippot, K.; Chaudret, B.; Denicourt-Nowicki, A.; Roucoux, A.; Castillón, S.; Claver, C., Carbohydrate-derived 1,3-diphosphite ligands as chiral nanoparticle stabilizers: Promising catalytic systems for asymmetric hydrogenation. *ChemSusChem* **2009,** *2* (8), 769-779; (b) Cárdenas-Lizana, F.; de Pedro, Z. M.; Gómez-Quero, S.; Keane, M. A., Gas phase hydrogenation of nitroarenes: A comparison of the catalytic action of titania supported gold and silver. *J. Mol. Catal. A: Chem.* **2010,** *326* (1-2), 48-54; (c) Alshammari, H.; Miedziak, P. J.; Bawaked, S.; Knight, D. W.; Hutchings, G. J., Solvent-free Liquid-phase oxidation of 1-hexene using supported gold catalysts. *ChemCatChem* **2012,** *4* (10), 1565-1571; (d) Beal, J. H. L.; Etchegoin, P. G.; Tilley, R. D., Transition metal polysulfide complexes as single-source precursors for metal sulfide nanocrystals. *J. Phys. Chem. C* **2010,** *114* (9), 3817-3821.
93. Besson, M.; Gallezot, P., Selective oxidation of alcohols and aldehydes on metal catalysts. *Catal. Today* **2000,** *57* (1-2), 127-141.
94. (a) Bond, G. C.; Sermon, P. A., Gold catalysts for olefin hydrogenation-transmutation of catalytic properties. *Gold Bull.* **1973,** *6* (4), 102-105; (b) Bond, G. C.; Sermon, P. A.; Webb, G.; Buchanan, D. A.; Wells, P. B., Hydrogenation over supported gold catalysts. *J. Chem. Soc., Chem. Commun.* **1973,** (13), 444b-445.
95. Bailie, J. E.; Hutchings, G. J., Promotion by sulfur of gold catalysts for crotyl alcohol formation from crotonaldehyde hydrogenation. *Chem. Commun.* **1999,** (21), 2151-2152.
96. Astruc, D.; Lu, F.; Aranzaes, J. R., Nanoparticles as recyclable catalysts: The frontier between homogeneous and heterogeneous catalysis. *Angew. Chem., Int. Ed.* **2005,** *44* (48), 7852-7872.
97. (a) Martra, G.; Prati, L.; Manfredotti, C.; Biella, S.; Rossi, M.; Coluccia, S., Nanometer-sized gold particles supported on SiO_2 by deposition of gold sols from $Au(PPh_3)_3Cl$. *J. Phys. Chem. B* **2003,** *107* (23), 5453-5459; (b) Budroni, G.; Corma, A., Gold-organic-inorganic high-surface-area materials

as precursors of highly active catalysts. *Angew. Chem., Int. Ed.* **2006,** *45* (20), 3328-3331; (c) Alvino, J. F.; Bennett, T.; Anderson, D.; Donoeva, B.; Ovoshchnikov, D.; Adnan, R. H.; Appadoo, D.; Golovko, V.; Andersson, G.; Metha, G. F., Far-infrared absorption spectra of synthetically-prepared, ligated metal clusters with Au_6, Au_8, Au_9 and Au_6Pd metal cores. *RSC Adv.* **2013,** *3* (44), 22140-22149.
98. Ma, Z.; Zaera, F., Organic chemistry on solid surfaces. *Surf. Sci. Rep.* **2006,** *61* (5), 229-281.
99. Maciejewski, M.; Fabrizioli, P.; Grunwaldt, J.-D.; Sven, B. O.; Baiker, A., Supported gold catalysts for CO oxidation: Effect of calcination on structure, adsorption and catalytic behaviour. *Phys. Chem. Chem. Phys.* **2001,** *3* (17), 3846-3855.
100. Beck, A.; Horváth, A.; Schay, Z.; Stefler, G.; Koppány, Z.; Sajó, I.; Geszti, O.; Guczi, L., Sol derived gold-palladium bimetallic nanoparticles on TiO_2: Structure and catalytic activity in CO oxidation. *Top. Catal.* **2007,** *44* (1-2), 115-121.
101. Long, C. G.; Gilbertson, J. D.; Vijayaraghavan, G.; Stevenson, K. J.; Pursell, C. J.; Chandler, B. D., Kinetic evaluation of highly active supported gold catalysts prepared from monolayer-protected clusters: An experimental michaelis−menten approach for determining the oxygen binding constant during CO oxidation catalysis. *J. Am. Chem. Soc.* **2008,** *130* (31), 10103-10115.
102. (a) Zhang, X.; Qu, Z.; Li, X.; Wen, M.; Quan, X.; Ma, D.; Wu, J., Studies of silver species for low-temperature CO oxidation on Ag/SiO_2 catalysts. *Sep. Purif. Technol.* **2010,** *72* (3), 395-400; (b) Wang, L. C.; He, L.; Liu, Y. M.; Cao, Y.; He, H. Y.; Fan, K. N.; Zhuang, J. H., Effect of pretreatment atmosphere on CO oxidation over α-Mn_2O_3 supported gold catalysts. *J. Catal.* **2009,** *264* (2), 145-153.
103. Chen, L. M.; Ma, D.; Pietruszka, B.; Bao, X. H., *J. Nat. Gas Chem.* **2006**.
104. Bulushev, D. A.; Yuranov, I.; Suvorova, E. I.; Buffat, P. A.; Kiwi-Minsker, L., Highly dispersed gold on activated carbon fibers for low-temperature CO oxidation. *J. Catal.* **2004,** *224* (1), 8-17.
105. (a) Tsubota, S.; Cunningham, D. A. H.; Bando, Y.; Haruta, M., Preparation of nanometer gold strongly interacted with TiO_2 and the structure sensitivity in low-temperature oxidation of CO. *Stud. Surf. Sci. Catal.* **1995,** *91* (c), 227-235; (b) Zanella, R.; Louis, C., Influence of the conditions of thermal treatments and of storage on the size of the gold particles in Au/TiO_2 samples. *Catal.Today* **2005,** *107–108* (0), 768-777.
106. Ho, K. Y.; Yeung, K. L., Effects of ozone pretreatment on the performance of Au/TiO_2 catalyst for CO oxidation reaction. *J. Catal.* **2006,** *242* (1), 131-141.
107. Lin, Q.; An, L.; Chen, J.; Qin, H.; Qi, S.; Zou, X., Effect of $LaFeO_3$ Decoration and Ozone Treatment on Thermal Stability of Au/Al_2O_3 for CO Oxidation. *Chin. J. Catal.* **2008,** *29* (6), 506-508.
108. Parvulescu, V. I., Catalysts used in plasma-assisted catalytic processes: Preparation, activation, and regeneration. In *Plasma chemistry and catalysis in gases and liquids*, Vasile, I.; Parvulescu, M.; Magureanu, P. L., Eds. Wiley-VCH: 2012; pp 45-87.
109. (a) Kim, H. H.; Tsubota, S.; Daté, M.; Ogata, A.; Futamura, S., Catalyst regeneration and activity enhancement of Au/TiO_2 by atmospheric pressure nonthermal plasma. *Appl. Catal., A* **2007,** *329*, 93-98; (b) Indarto, A.; Choi, J. W.; Lee, H.; Song, H. K.; Palgunadi, J., Partial oxidation of methane with sol-gel Fe/Hf/YSZ catalyst in dielectric barrier discharge: Catalyst activation by plasma. *J. Rare Earths* **2006,** *24* (5), 513-518.
110. Liu, X.; Mou, C.-Y.; Lee, S.; Li, Y.; Secrest, J.; Jang, B. W. L., Room temperature O_2 plasma treatment of SiO_2 supported Au catalysts for selective hydrogenation of acetylene in the presence of large excess of ethylene. *J. Catal.* **2012,** *285* (1), 152-159.
111. Legrand, J. C.; Diamy, A. M.; Riahi, G.; Randriamanantenasoa, Z.; Polisset-Thfoin, M.; Fraissard, J., Application of a dihydrogen afterglow to the preparation of zeolite-supported metallic nanoparticles. *Catal. Today* **2004,** *89* (1–2), 177-182.
112. Yin, H.; Ma, Z.; Chi, M.; Dai, S., Activation of dodecanethiol-capped gold catalysts for CO oxidation by treatment with $KMnO_4$ or K_2MnO_4. *Catal. Lett.* **2010,** *136* (3-4), 209-221.
113. Ma, Z.; Brown, S.; Overbury, S. H.; Dai, S., $Au/PO_4^{3-}/TiO_2$ and $PO_4^{3-}/Au/TiO_2$ catalysts for CO oxidation: Effect of synthesis details on catalytic performance. *Appl.Catal., A* **2007,** *327* (2), 226-237.

Chapter 2: General Experimental-Materials, Synthesis and Analysis

2.1 Introduction

This chapter outlines general experimental methods and materials utilized for the experiments described in this thesis. More detailed information relevant to the specific work described in the following chapters can be found in the experimental section of other chapters.

2.2 Materials

This section presents details of the materials utilized in the various experiments carried out in the thesis. The reactants were analytical grade reagents used without further purification. The details of the materials are classified in three general categories, as described in section 2.1-2.3 of this chapter, according to supported noble metal nanoparticles used as catalysts for organic compounds oxidation or hydrogenation.

General reagents were sourced as follows. Dichloromethane (99.99%), sodium borohydride (99%), sodium citrate (99%), dichloromethane (99.99%), toluene (99.99%) and chloroform (99.99%) were purchased from Fisher Scientific. Toluene (99.9 %), tetraoctylammonium bromide (98%), triphenylphosphine (99%) acetonitrile (99.9%) and sodium hydroxide (99%) were purchased from Merck. Sulfuric acid (98.5%) was obtained from Orica. Benzyl alcohol (99%), anisole (99.7%), benzaldehyde (99%), methyl benzoate (99%), benzoic acid (99.5%), cyclohexane (99.5%), [*n*]-decane (99%) and silica were purchased from Sigma Aldrich. Methanol (99.99%) and ethanol (99.99 %) were purchased from Fisher Chemical and dried using activated alumina column. Butyl amine (98%) and ethyl benzoate (99%) were purchased from BDH. Cyclohexene (99%) was purchased from Fluka. Tetrahydrofuran (99.5%) was purchased from Scharlau. Research grade (99.98%) O_2, H_2 and N_2 gases were obtained from BOC.

2.2.1 Supported gold nanoparticles/nanoclusters for benzyl alcohol oxidation

Vulcan carbon (BET: 235 m^2/g) was purchased from the Cabot Corp. Powder (SX1G 8001-9, BET: 813 m^2/g) and granular (RX 3 EXTRA 570104, BET: 1227 m^2/g) activated carbon were kindly donated by Norit. Granular activated carbon, which was also modified with -SO_3H and –SH, was provided by Doctor Bezugla from National Taras Shevchenko University, Kyiv, Ukraine. Meso-pores carbon, including CMK-3 (BET: 997 m^2/g), CMK-8 (BET: 1905 m^2/g) and NCCR-41 (BET:1080 m^2/g), was provided by Doctor Balaiah Kuppan and Professor Parasuraman Selvam from National Centre for Catalysis Research and Department of Chemistry, Indian Institute of Technology, Madras, India.

Gold metal (99.99 %) was supplied by Regal Castings from which $HAuCl_4$ was made (by David Anderson and Nathaniel Gunby, members of the Golovko's research group at the University of Canterbury) using a previously reported protocol.[1] Precursors for Au_1 and Au_9 nanoclusters (described below) were made by Nathaniel Gunby and Au_8 nanoclusters were made by Baira Donoeva (also a member of the Golovko's research group).

2.2.2 Supported Ru nanocrystals for cyclohexene hydrogenation

Ruthenium nanocrystals (Ru_{52}) were provided by Associate Professor Richard Tilley and co-workers in Victoria University of Wellington.

2.2.3 Supported Pd particles for cyclohexene hydrogenation

Merino (fine-fibre) and crossbred (coarse-fibre) wool, used as the natural substrates for the synthesis of Pd nanoparticles on wool fibre, were provided by Ag Research Limited, New Zealand. Palladium on charcoal (Pd, 10% on dry charcoal as a palladium standard) was purchased from Alfa Aesar.

2.3 Experimental procedures for characterization of catalysts

The characterization of noble metal nanoparticles is somewhat complex because not only are the metal nanoparticles are very small but they can also have different shape, size distributions *etc.* Therefore, a single technique cannot give complete information on the properties of the particles under investigations. It is essential to characterize the particles using various techniques for gaining deeper insights on the structure, size and catalytic properties. Noble metal nanoparticles can be characterized by two methods: physical and chemical. Common examples of physical characterization methods are ultraviolet–visible (UV-Vis) spectroscopy, nuclear magnetic resonance (NMR), transmission electron microscopy (TEM), surface area (BET) and pore size analysis. Examples of chemical methods can be considered as X-ray photoelectron spectroscopy (XPS), temperature programmed desorption (TPD) and Fourier transform infrared spectroscopy (FTIR).

While characterization of supported gold nanoparticles and nanoclusters by XPS (at the Australian Synchrotron) was attempted, it was technically impossible to investigate gold catalysts by XPS. Pumping the gold nanocatalysts at the ultra-high vacuum (UHV) showed the gold nanocatalysts continued to desorb gas even after 24 hours due to the high surface area and pore volume of carbon support. In addition, XPS is suitable for distinguishing between cationic or ultra-small NMPs like Au_8 nanoclusters (*i.e.*, smaller than 1 nm) and large metallic ones.[2] Since most of the gold nanocatalysts used in this research work contained large MNPs, usefulness of XPS was considered limited. Additionally, there was no access to CO-TPD or *in situ* DRIFTS at all for more detailed chemical characterization. These can be considered as limitations of the study reported here. Therefore, based on the facilities available at the University of Canterbury (and other institutions in New Zealand) and consistent with similar published research in the literature, the noble metal (*i.e.* gold,

ruthenium and palladium) particles were characterized using UV-Vis spectroscopy, NMR and TEM. These methods are briefly described in the following section.

2.3.1 Ultraviolet – visible spectroscopy (UV-Vis)

Ultraviolet–visible spectroscopy (UV-Vis) was used for the quantitative identification of different gold species, which it is responsible for the nearly metal particles size.[3] The size of gold particles suspended in liquid samples was characterized using Shimadzu Cary 100 Bio spectrophotometer.

2.3.2 Nuclear magnetic resonance (NMR)

In this thesis, ^{1}H NMR measurements were made using Agilent MR 400 or Varian Anova 500 spectrometer to study PPh_3 groups in gold nanoparticles or nanoclusters.[4] A small amount of the sample was dissolved in an appropriate deuterated solvent ($CDCl_3$ or CD_2Cl_2).

2.3.3 Preparation of samples for transmission (TEM) and scanning electron microscopy (SEM)

2.3.3.1 Gold nanoparticles and ruthenium nanocrystals

The structures the noble metal nanoparticles, nanoclusters, nanocrystals and nanocatalysts have been investigated using bright-field high-resolution transmission electron microscopy (TEM). In addition, based on size distribution, average gold core diameter estimated using TEM images of the gold catalysts before and after activation can indirectly imply the removal of capping agents (PPh_3).[5] The TEM instrument was a Philips CM20, operating at 200 kV and equipped with energy-dispersive spectrometer (EDS) for electron probe microanalysis. Particular attention was paid to the size and size distributions of the metal nanoparticles.[6] TEM is one of the best direct-imaging techniques for obtaining size distributions data and, under favorable conditions, also the information on the metal particle shape. Samples for

TEM study were prepared by ultrasonically dispersing a sample in methanol and depositing a drop of suspension onto holey carbon copper (300 mesh) TEM grid. The methanol was evaporated under vacuum (approximately 2 hours). The average particles diameters were determined by counting at least 150 particles in the high magnification micrographs by using Image J software.[7]

2.3.3.2 Palladium nanoparticles and ruthenium nanocrystals

The palladium nanoparticles synthesized in the wool fibres were examined by using a JEOL 6500F field-emission gun scanning electron microscope (SEM) operating at an acceleration voltage 15 kV and a JEOL 2010 transmission electron microscope (TEM) operating at 200 keV. The presence of palladium was confirmed by EDS for SEM and scanning transmission electron microscope (STEM) for TEM. All samples were coated with carbon prior to analysis. In addition, the TEM samples were embedded in resin, cut into thin films and placed on a copper grid before coating. Several TEM images of Ru nanocrystals and Ru/SiO_2 nanocatalysts were also obtained by using a JEOL 2010 TEM operated at an acceleration voltage of 200 keV.

2.4 Synthesis of noble metal nanoparticles

In this thesis, three types of noble metal nanoparticles were fabricated. These will be further explained in this section.

2.4.1 Preparation for synthesis gold nanoparticles or nanoclusters

Prior to synthesis of gold nanoparticles, all glassware was washed with *aqua regia* (3:1, v/v mixture of concentrated HCl and HNO_3) soaked overnight in base (KOH in a 1:1 mixture of *n*-propanol and water) solutions followed by rinsing with MilliQ water.

2.4.1.1 $HAuCl_4 \cdot 3H_2O$

Hydrogen tetrachloroaura*t*e (III) hydrate ($HAuCl_4.3H_2O$) was synthesized by David Philip Anderson (Doctor Golovko's PhD student) according to previously published protocol by Braunstein *et al.*[1]

2.4.1.2 Au_{101} nanoparticles

Au_{101} nanoparticles (Au_{101} $(PPh_3)_{21}Cl_5$) were synthesized according to the previously published protocol by Hutchinson *et al.*[8] The following procedures were also used to improve the purity of gold particles (Au_{101}):

- The particles were washed twice using a procedure reported in the literature[8] for removing $AuClPPh_3$ impurity.
- The washing solvents were added drop-wise to the precipitate (Au_{101} particles) during washing procedures (see above I and II).
- The gold particles were collected from the synthesis funnel by using dichloromethane as a solvent. To remove any acidic chloroform may cause decomposition of Au_{101} particles; the solvent was also passed through a basic alumina column before use.

The metal core diameter of Au_{101} nanoparticles is 1.5 ± 0.1 nm, according to the TEM investigation of this colloid reported in Hutchinson *et al.*[8] and Weare *et al.*(see Figure 2.1)[4] published papers. My TEM images confirmed the size of gold nanoparticles to have an average diameter of 1.6 ± 0.1 nm (see Figure 2.2).

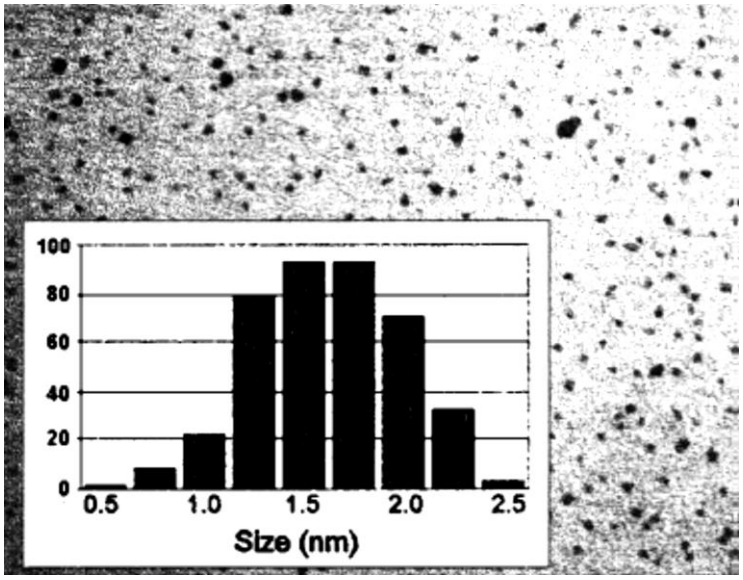

***Figure 0.1*:** A TEM image and particle size distributions histogram of Au_{101} nanoparticles. Reproduced from Weare *et al.*[4]

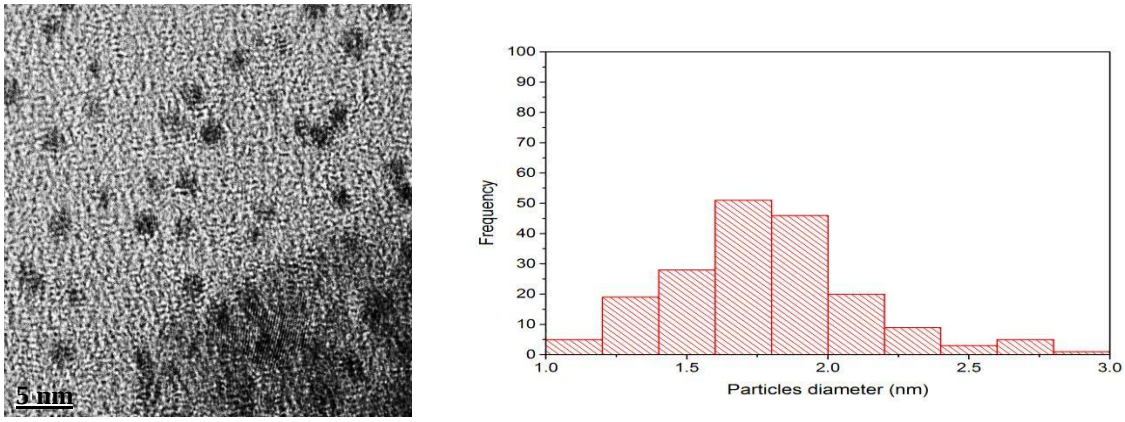

Figure 0.2: Left: a representative TEM image of Au_{101} nanoparticles deposited onto carbon film coated copper TEM grid; Right: Particle diameter frequency distribution histogram. The average particle diameter was determined to be 1.6 ± 0.1 nm (two standard deviations of the mean).

This gold colloid can also be characterised by ^{1}H NMR (as a solution in $CDCl_3$).

Tetraoctylammonium bromide resonance appear at δ ~ 3.5 ppm and a broad resonance at δ ~ 6 – 8 ppm is indicative of the PPh_3 bound to the Au core in Au_{101} with a weak multiplet at δ ~ 7.5 ppm (see Figure 2.3) due to residual (PPh_3AuCl).[4, 8] Figure 2.4 confirms the purity of particles made in this work because no resonance (due to tetraoctylammonium bromide) was observed at δ ~ 3.5 ppm. Additionally characteristic broad resonance at δ ~ 6 – 8 ppm confirmed presence of PPh_3 ligands bound to the Au core of Au_{101} with only a weak intensity multiplet at δ ~ 7.5 ppm corresponding to the impurity of PPh_3AuCl.

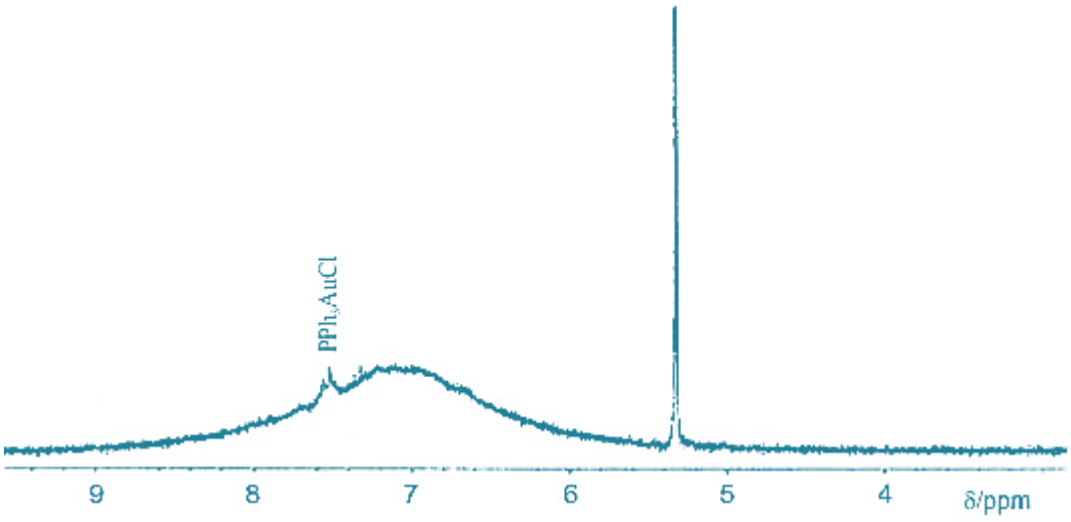

Figure 0.3: ^{1}H NMR of Au_{101} nanoparticles. Reproduced from Weare *et al.*[4]

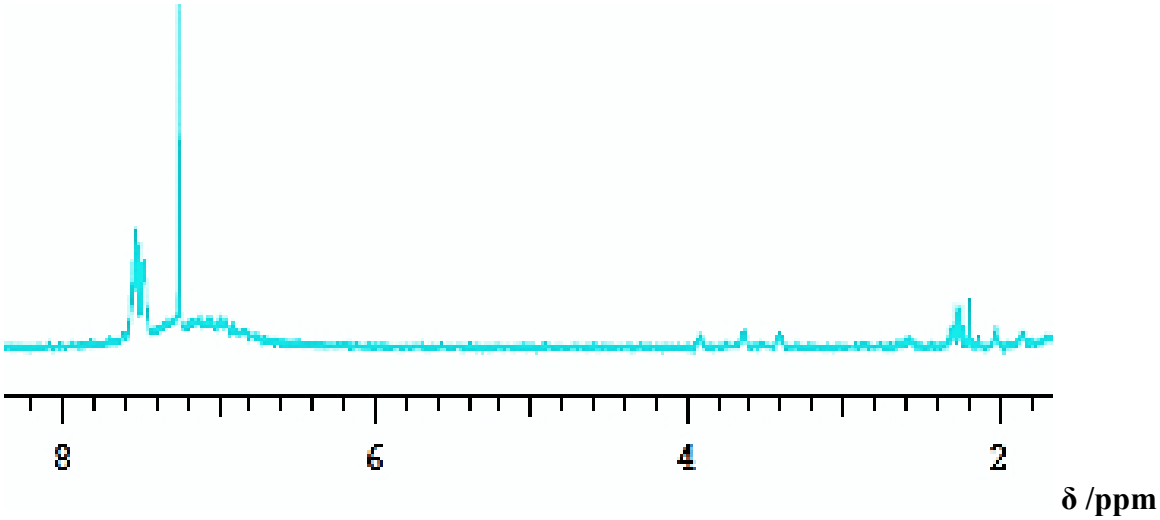

Figure 0.4: ^{1}H NMR of Au_{101} nanoparticles taken at 500 MHz; CD_2Cl_2 was used as a ^{1}H NMR solvent.

2.4.1.3 Au_9 nanoclusters

Au_9 nanoclusters ($Au_9(PPh_3)_8(NO_3)_3$) were synthesized by Nathaniel Gunby (Doctor Golovko's honours student) according to the previously published protocol by Wen *et al.*[9]

2.4.1.4 Au_8 nanoclusters

Au_8 nanoclusters ($Au_8(PPh_3)_8(NO_3)_2$) were synthesized by Baira Donoeva (Doctor Golovko's PhD student) according to the previously published protocol by Velden *et al.*[10]

2.4.1.5 Au_1 precursor

Au_1 precursor ($AuClPPh_3$) was synthesized by Nathaniel Gunby (Doctor Golovko's honours student) according to the previously published protocol by Malatesta *et al*.[11]

2.4.1.6 Gold citrate colloids

Citrate-capped gold colloids (*i.e.*, colloids are homogeneous non-crystalline substances consisting large molecules or ultramicroscopic particles dispersed in solution. Colloids include gels, sols, and emulsions with particles that are suspended in solution, and cannot be separated by ordinary filtering or centrifuging). They were prepared using a previously reported procedure by Turkevich *et al*.[12] Hydrogen tetrachloroaurate (III) hydrate ($HAuCl_4.3H_2O$) (42.5 mg, 0.11 mmol) solution was added to the 450 ml of MilliQ water. The solution was stirred (750 rpm) and heated to 70 ^oC, at which point a solution of sodium citrate (211.7 mg, 0.99 mmol) was added with stirring. The solution was stirred (750 rpm) at 70 ± 2 ^oC until the colour of solution turned from light yellow to purple and finally to red. The solution was cooled to room temperature (over approximately one hour) in an ice bath. The gold colloid solution was stored in a clean flask in a dark place and wrapped in aluminium foil to avoid exposure to light. This was done to prevent aggregation of the gold colloids upon exposure to light.

The average gold-particle diameter was determined by TEM to be 12.6 ± 0.2 nm (see Figure 2.5). Complementary to the TEM particle size estimate, UV-Vis spectrum of this colloid (see Figure 2.6) showed a surface Plasmon resonance absorption maximum at 521 nm, which, in comparison with the earlier reported data presented in Figure 2.7,[13] implied the gold particle average diameters of ~12-18 nm).

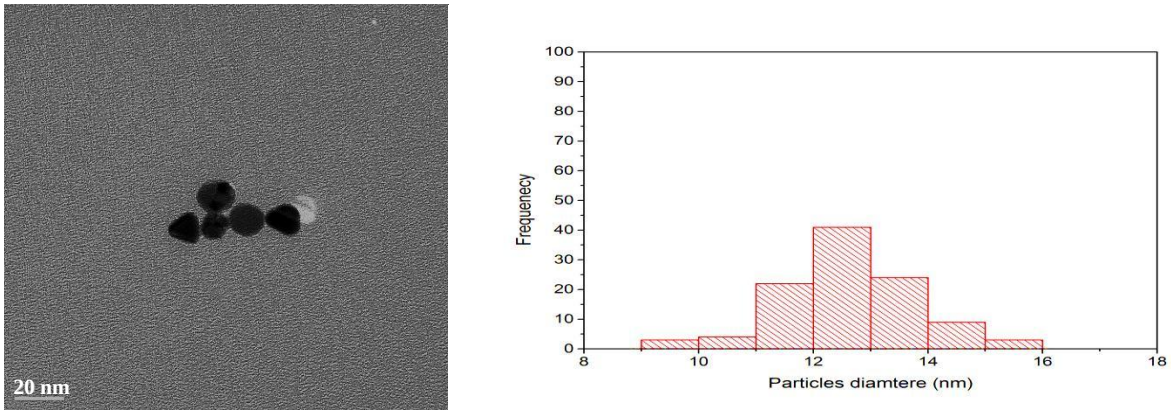

Figure 0.5: Left: a representative TEM image of gold citrate nanoparticles deposited onto carbon film coated copper TEM grid; Right: Particle size distribution histogram. The average particle size of gold particle was determined to be 12.6± 0.2 nm (two standard deviations of the mean).

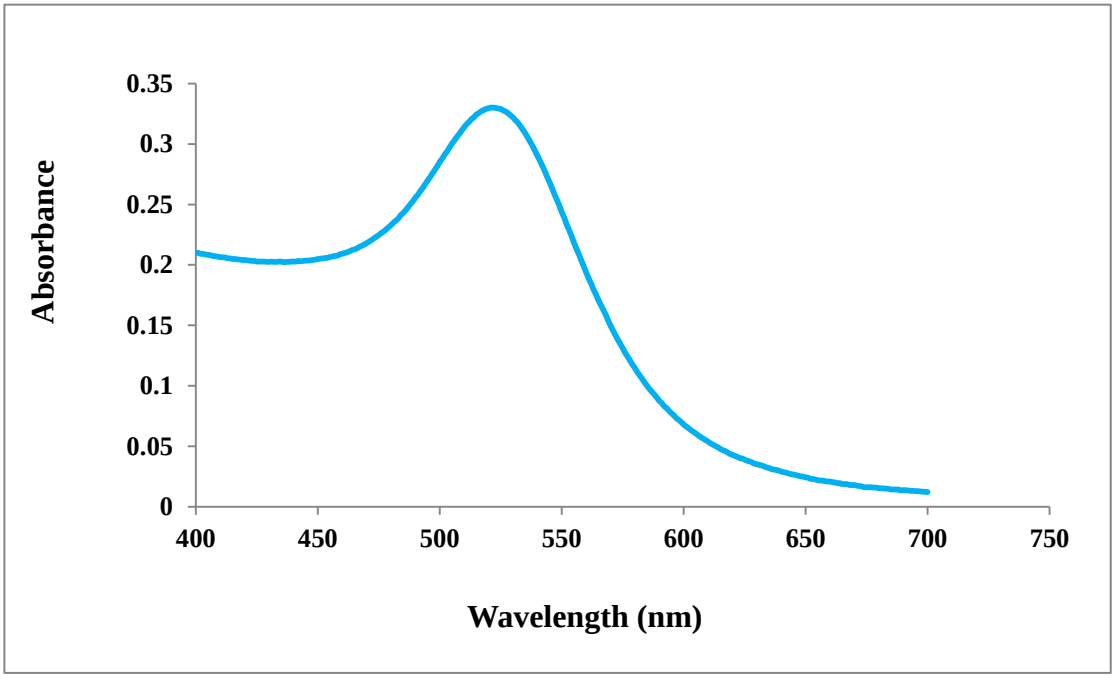

Figure 0.6: UV-Vis spectra of gold citrate nanoparticles.

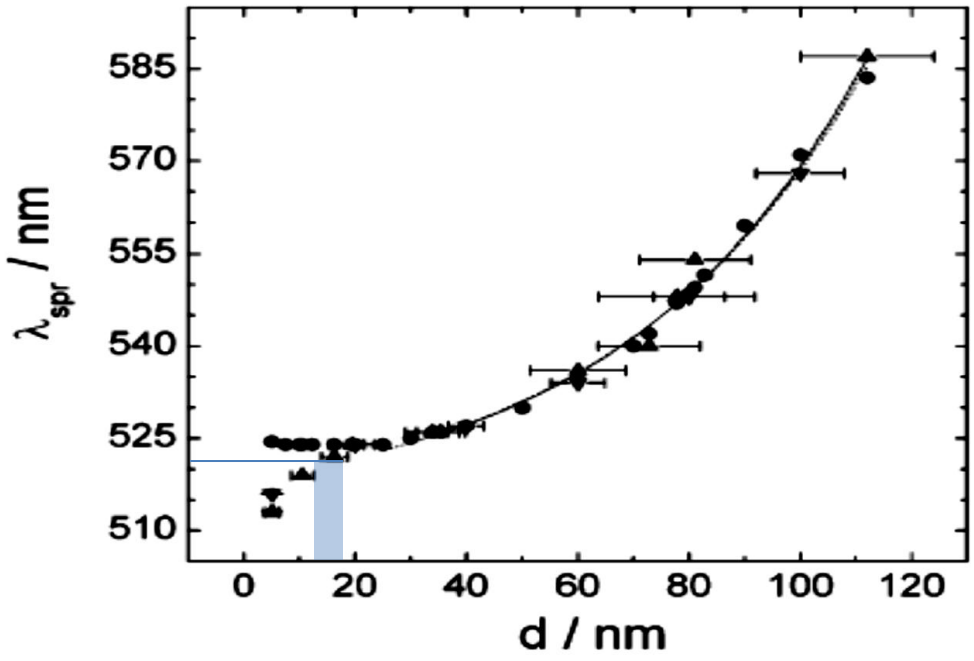

Figure 0.7: Position of the surface plasmon resonance (spr) band-maximum wavelength as a function of the particle diameter for gold nanoparticles (GNPs) in water: calculated (circles); experimentally measured (down ward pointing triangles, commercial GNPs; upward-pointing triangles, in-house synthesized GNPs). An exponential fit to the theoretical (experimental) data for d > 25 nm is shown as a dotted (dashed) line. Reproduced from Haiss *et al.*[13] The shaded bars at bottom left shows that a spr band at ~521 nm corresponds to average particles diameter in the range 12–18 nm.

2.4.1.7 "*Naked*" gold nanoparticles

Naked gold particles were synthesized according to the previously published protocol by Martin *et al.*[3a] Those authors proposed that these colloidal particles do not contain strongly bound stabilizing agents and hence named them "*naked*" to highlight this characteristic. A solution of 50 mM gold chloride in a glass vial was made by dissolving $HAuCl_4 \cdot 3H_2O$ at HCl (50 mM). Meanwhile, a base solution of 50 mM of borohydride anions in a glass beaker was made by dissolving $NaBH_4$ (189 mg, 5.00 mmol) at NaOH (50 mM). Then, 96 mL of MilliQ water was added to a round bottom flask and let the solution stir for the following procedure:

I. 1 mL of the $HAuCl_4$ solution was added to the flask and stirred for several minutes.

II. 3 mL of BH_4^-/OH^- solution was added and the mixture was stirred until the colour of solution was changed from light yellow to light red.

III. The gold solution was kept in a dark place.

The average size of gold particles was investigated by TEM (see Figure 2.8) and found to be 3.2 ± 0.2 nm. In comparison earlier researcher reported an average diameter of was 3.2 ± 0.1 nm (see Figure 2.9).[3a] Complementary to the TEM particles size estimate, UV-Vis spectrum of these gold particles shows a surface-Plasmon resonance absorption maximum at around 510 nm (see Figure 2.10) which, compared with earlier reported data, (see Figure 2.11) implies an average particle diameter of ~3.2– 4.8 nm.[3a]

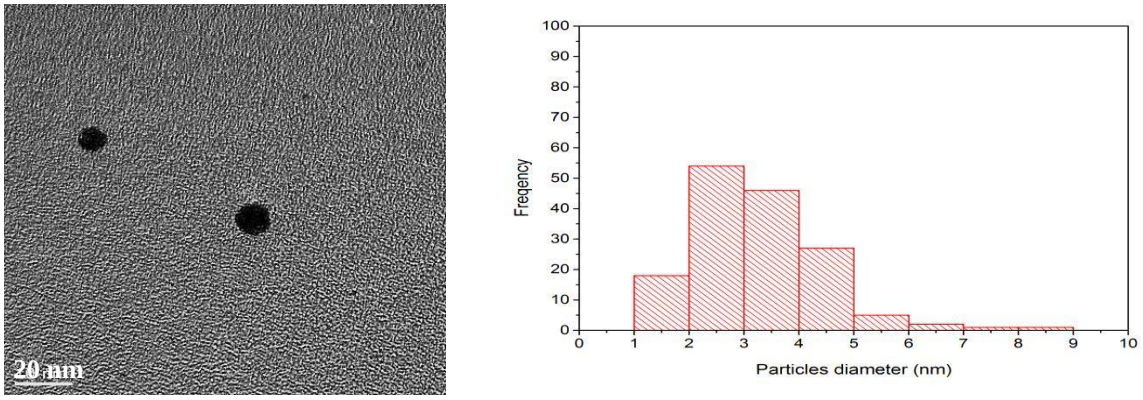

Figure 0.8: Left: a representative TEM image of naked gold nanoparticles deposited onto a carbon-film coated copper TEM grid; Right: Particle size distribution histogram. The average particle size of gold particles was determined to be 3.2 ± 0.2 nm (two standard deviations of the mean).

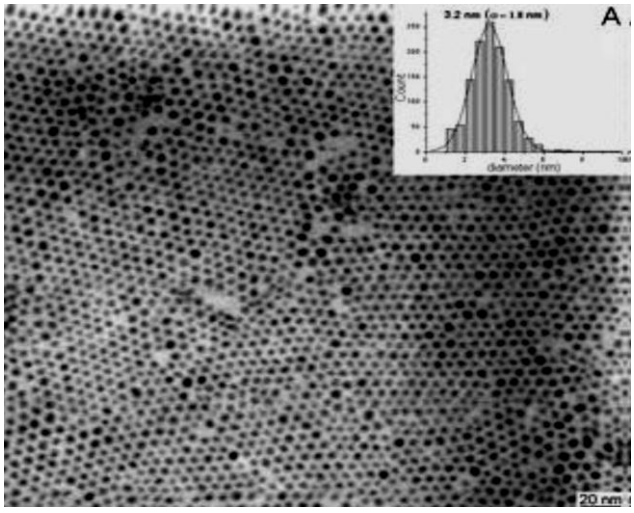

Figure 0.9: A FE-SEM micrograph of gold naked nanoparticles with insets showing size distribution. The average particle size of the particles was determined to be 3.2 ± 1.0 nm. Reproduced from Martin *et al.*[3a]

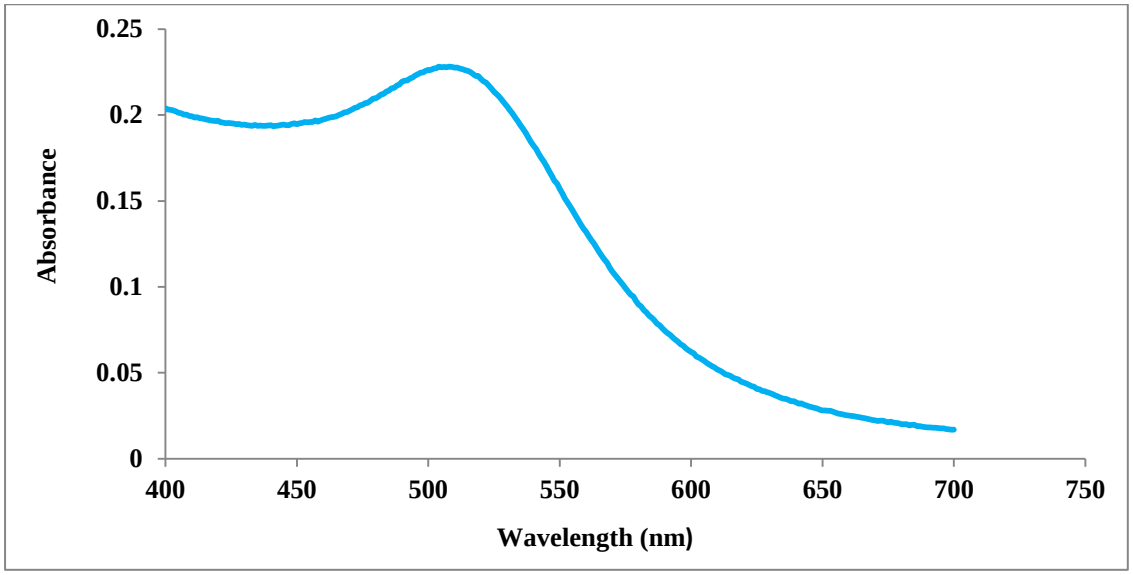

Figure 0.10: UV-Vis spectra of gold naked nanoparticles.

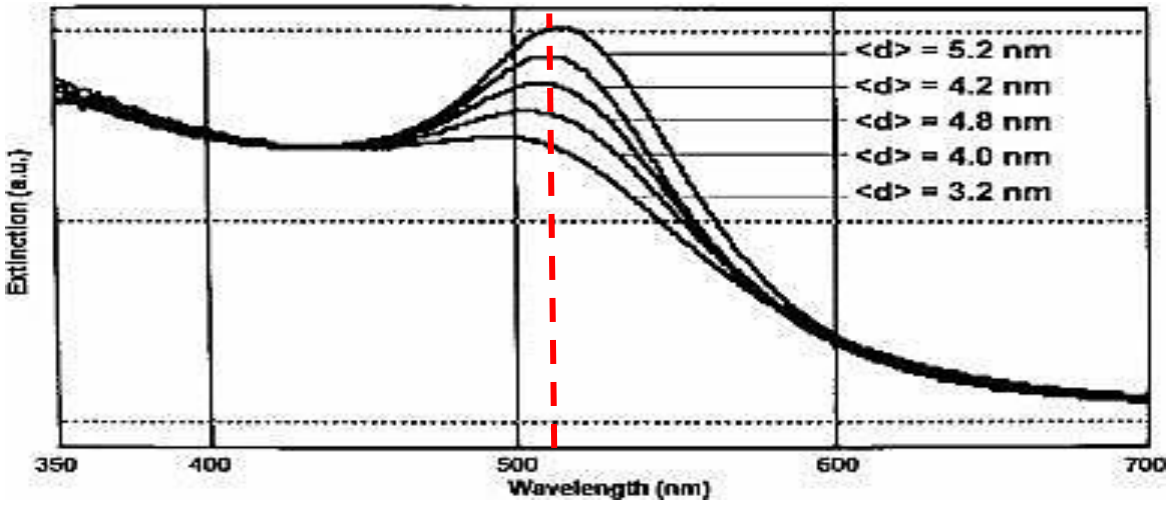

Figure 0.11: UV-Vis absorption spectra of five aqueous solutions of gold naked nanoparticles. Reproduced from Martin *et al*.[3a] The vertical line shows wavelength at ~513 nm corresponds to average particles diameter in the range 3.2–5.2 nm.

2.4.2 Preparation of ruthenium nanocrystals

Ruthenium nanocrystals were made in the laboratory of Associate Professor Richard Tilley at Victoria University of Wellington (see Figure 2.12). [14]

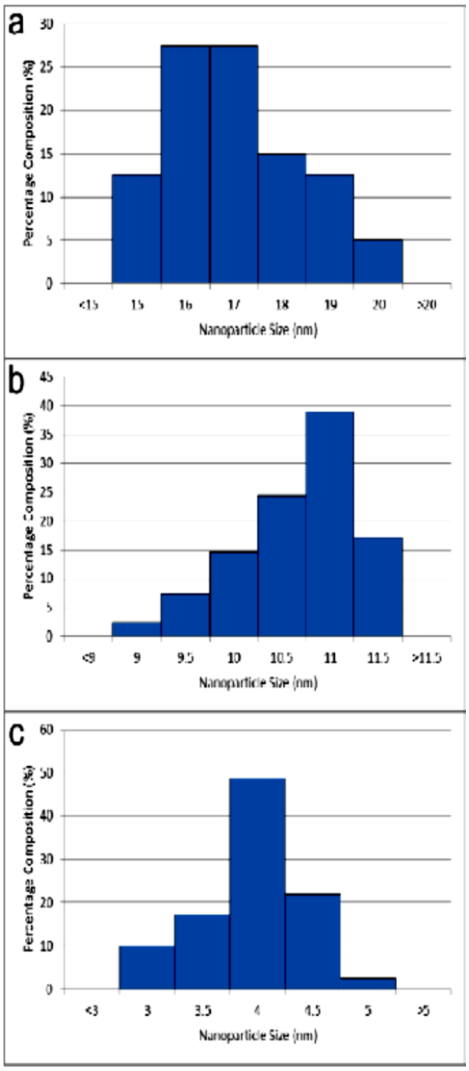

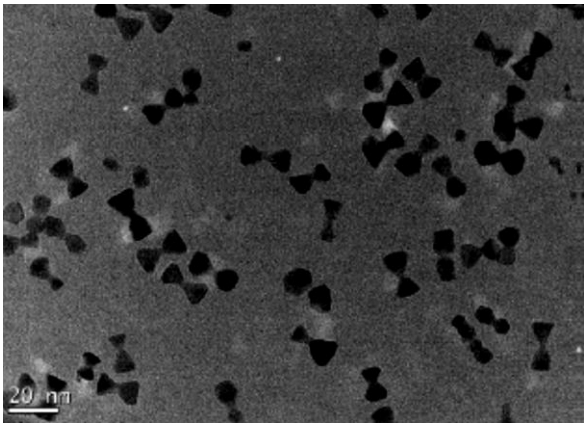

Figure 0.12: A TEM image and size distributions analysis of the ruthenium hourglass nanocrystals (a, b & c). a) Length of hourglass nanocrystals (18 ± 3 nm). b) Width of hourglass nanocrystals (11± 2 nm). c) Width of the hourglass nanocrystals 'necks' (4 ± 1 nm). Reproduced from Tilley *et al.*[14b]

2.5 Fabrication of nanocatalysts

2.5.1 Support immobilization of pre-synthesised particles/crystals

Immobilization of noble metal nanoparticles on supports plays a key role in defining the catalytic activity and selectivity.[15] This section presents preparation of different types of noble metal nanocatalysts used in this thesis.

2.5.1.1 Preparation of catalysts using gold nanoparticles/nanoclusters

The preparation method is crucial to the genesis of catalytic activity and selectivity, which argues for certain methods to bring about a strong interaction between gold particles/clusters

and supports to produce gold catalysts with a high performance.[16] In this work, colloidal suspension was used as a starting materials of nanocatalysts preparation.[17]

2.5.1.1.1 1.0 wt% Au_{101}/C

The $Au_{101}(PPh_3)_{21}Cl_5$: C gold/carbon nanocatalysts materials utilized in this thesis were fabricated using the following general procedure: the Norit activated carbon (5 g) to be used as a support was mixed with an appropriate amount of Au_{101} (see Table 2.1) in 200 mL of dichloromethane.[18] The mixture was stirred at 750 rpm until the solvent became colourless (about 2 hours for 1.0 wt% Au_{101}/C), indicating complete deposition of nanoparticles on to the support. Then nanocatalysts were centrifuged, washed several times with fresh CH_2Cl_2 (100 mL), and dried under vacuum for one day. Representative TEM and size-distribution data are given 1.0 wt% Au_{101}/C in Figure 2.13.

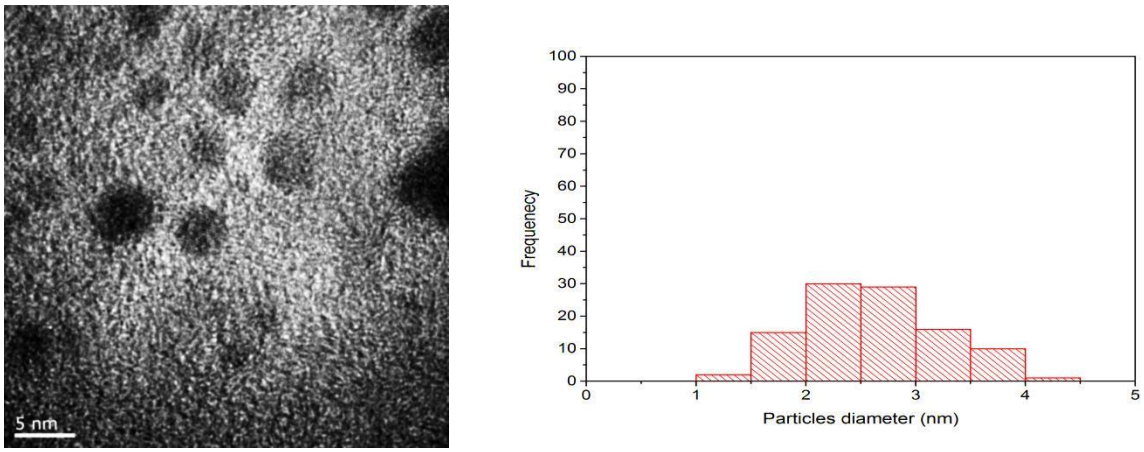

***Figure 0.13**:* Left: a representative TEM image of 1.0 wt% gold nanoparticles (Au_{101}) immobilized on Norit activated (as synthesised) deposited onto carbon film coated copper TEM grid; Right: Particle size distribution histogram. The average particle size of gold particles was determined to be 2.6 ± 0.1 nm (two standard deviations of the mean).

2.5.1.1.2 0.5 wt% Au_{101}/C

Catalyst 0.5 wt% Au_{101}/C was made using the procedure described in section 2.5.1.1.1 (1 wt% Au_{101}/C). This time, 25 mg of Au_{101} and 5.00 g powder activated carbon (Norit) were used.

2.5.1.1.3 0.2 wt% Au_{101}/C

Catalyst 0.2 wt% Au_{101}/C was made using the procedure described in section 2.5.1.1.1 (1 wt% Au_{101}/C). This time, 10 mg of Au_{101} and 5.00 g powder activated carbon (Norit) were used.

2.5.1.1.4 1.0 wt% Au_8/C

Catalyst 1 wt% Au_8/C was made using the procedure described section 2.5.1.1.1 (1 wt% Au_{101}/C). This time, 92 mg of Au_8 and 5.00 g powder activated carbon were (Norit) used.

2.5.1.1.5 1.0 wt% Au_9/C

Catalyst 1 wt% Au_9/C was made using the procedure described in section 2.5.1.1.1 (1 wt% Au_{101}/C). This time, 90 mg of Au_9 and 5.00 g powder activated carbon (Norit) were used.

2.5.1.1.6 1.0 wt% Au_1/C

Catalysts 1 wt% Au_1/C was made using the procedure described in section 2.5.1.1.1 (1 wt% Au_{101}/C). This time, 15.47 mg of Au_1 and 5.00 g powder activated carbon (Norit) were used.

2.5.1.1.7 1.0 wt% Au_{101}/C_g

Catalysts 0.2 wt% Au_{101}/C_g was made using the procedure described in section 2.5.1.1.1 (1 wt% Au_{101}/C). This time, granular activated carbon (Norit) was utilized as a support for $Au_{101.}$

2.5.1.1.8 1.0 wt% $Au_{101}/C_{g.p}$

Granular activated carbon (Norit) was powdered and then 1 wt% $Au_{101}/C_{g.p}$ was made using the procedure described in section 2.5.1.1.1 (1 wt% Au_{101}/C).

2.5.1.1.9 1.0 wt% Au_{101}/C_{-SO3H}

Catalyst 1 wt% Au_{101}/C_{-SO3H} was made using the procedure described in section 2.5.1.1.1 (1 wt% Au_{101}/C). The granular activated carbon was modified with $-SO_3H$ utilized as a support for Au_{101} for this procedure.

2.5.1.1.10 1.0 wt% Au_{101}/C_{-SH}

Catalyst 1wt% Au_{101}/C_{-SH} was made using the procedure described in section 2.5.1.1.1 (1 wt% Au_{101}/C). The granular activated carbon was modified with -SH utilized as a support for Au_{101} for this procedure.

2.5.1.1.11 1.0 wt% Au_{101}/C_3

Catalyst 1 wt% Au_{101}/C_3 was made using the procedure described in section 2.5.1.1.1 (1 wt% Au_{101}/C). Mesopores carbon (CMK-3) was utilized as a support for Au_{101} for this procedure.

2.5.1.1.12 1.0 wt% Au_{101}/C_8

Catalyst1 wt% Au_{101}/C_8 was made using the procedure described in section 2.5.1.1.1 (1 wt% Au_{101}/C). Mesopores carbon (CMK-8) was utilized as a support for Au_{101} for this procedure.

2.5.1.1.13 1.0 wt% Au_{101}/C_{41}

Catalyst 1 wt% Au_{101}/C_{41} was made using the procedure described in section 2.5.1.1.1 (1 wt% Au_{101}/C). Mesopores carbon (NCCR-41) was utilized as a support for Au_{101} for this procedure.

2.5.1.1.14 1.0 wt% Au_{101}/C_{Vulcan}

Catalyst 1 wt% Au_{101}/C_{Vulcan} was made using the procedure described in section 2.5.1.1.1 (1 wt% Au_{101}/C). Modified carbon (Vulcan) was utilized as a support for Au_{101} for this procedure.

Table 2.1 presents a summary of sections 2.5.1.1.1–2.5.1.1.14 of Au_{101} immobilized on different types of carbon with various loading rates.

Table 0.1: Summary of fabricated gold nanocatalysts.

Catalysts code	Types of carbons	Gold particles (mg)
1.0 wt% Au_{101}/C	Powder-Norit	50
0.5 wt% Au_{101}/C	Powder-Norit	25
0.2 wt% Au_{101}/C	Powder-Norit	10
1.0 wt% Au_8/C	Powder-Norit	92
1.0 wt% Au_9/C	Powder-Norit	90
1.0 wt% Au_1/C	Powder-Norit	15.47
1.0 wt% Au_{101}/C_g	granular -Norit	50
1.0 wt% $Au_{101}/C_{g.p}$	Powdered granular-Norit	50
1.0 wt% $Au_{101}/C_{g.SO3H}$	Granular –Norit modified with $–SO_3H$	50
1.0 wt% $Au_{101}/C_{g.SH}$	Granular –Norit modified with –SH	50
1.0 wt% Au_{101}/C_3	Mesopores (CMK-3)	50
1.0 wt% Au_{101}/C_8	Mesopores (CMK-8)	50
1.0 wt% Au_{101}/C_{41}	Mesopores (NCCR-41)	50
1.0 wt% Au_{101}/C_V	Vulcan	50

2.5.1.1.2 1.0 wt% $Au_{citrate}$/C

The catalytic materials with a target loading of 1.0 wt% $Au_{citrate}$ /C were prepared by mixing Norit activated carbon (powder) or Vulcan carbon (2.11 g) as a support with 2.4×10^{-4} M of gold citrate nanoparticles (47.27 mg/mL) in around bottom flask. The mixture was stirred at 750 rpm for 2 hours at which point the solvent became colourless, indicating complete deposition of nanoparticles on to the support. Then nanocatalysts were centrifuged and washed several times with of water (100 mL) and methanol (100 mL). Then, the catalysts were dried under vacuum for one day. Representative TEM and size-distribution data are given in Figure 2.14 for the material prepared on Norit carbon. The average diameters of the particles are listed in Table 2.2.

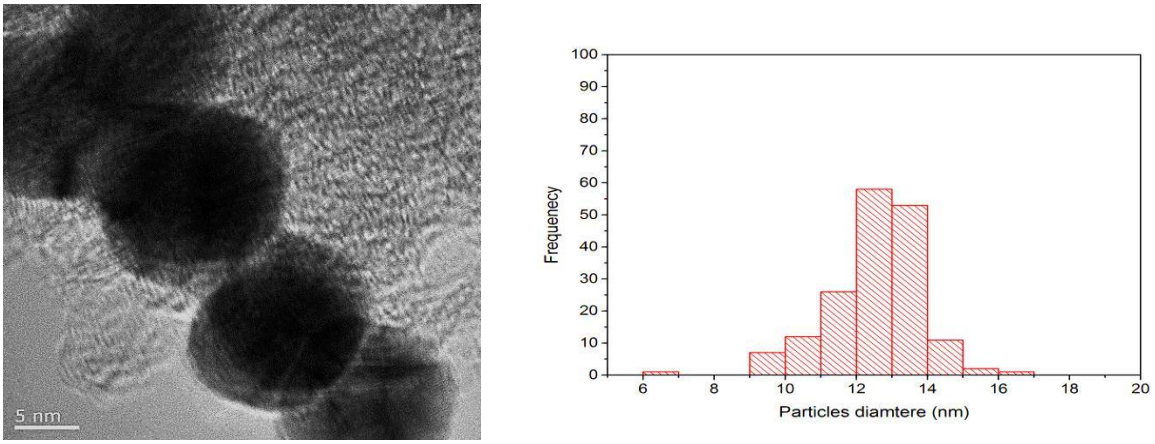

Figure 0.14: Left: a representative TEM image of 1.0 wt% gold citrate immobilized on Norit activated carbon (as synthesised – *i.e.* before catalytic reaction) deposited onto carbon film coated copper TEM grid; Right: Particle size distribution histogram. The average particle diameter of the gold particles was determined to be 12.5 ± 0.2 nm (two standard deviations of the mean).

2.5.1.1.3 1.0 wt% Au_{naked} /C

1.0 wt% Au_{naked} /C was made using the procedure as described in section 5.1.2 (for 1.0 wt% $Au_{citrate}$/C), but using 9.84 mg/mL of naked gold nanoparticles immobilized on 3.85 g of Norit activated carbon (powder) or Vulcan carbon. Representative TEM and size-distribution data are given in Figure 2.15 for the material prepared on Norit Carbon. The average diameters of the particles are given in Table 2.2.

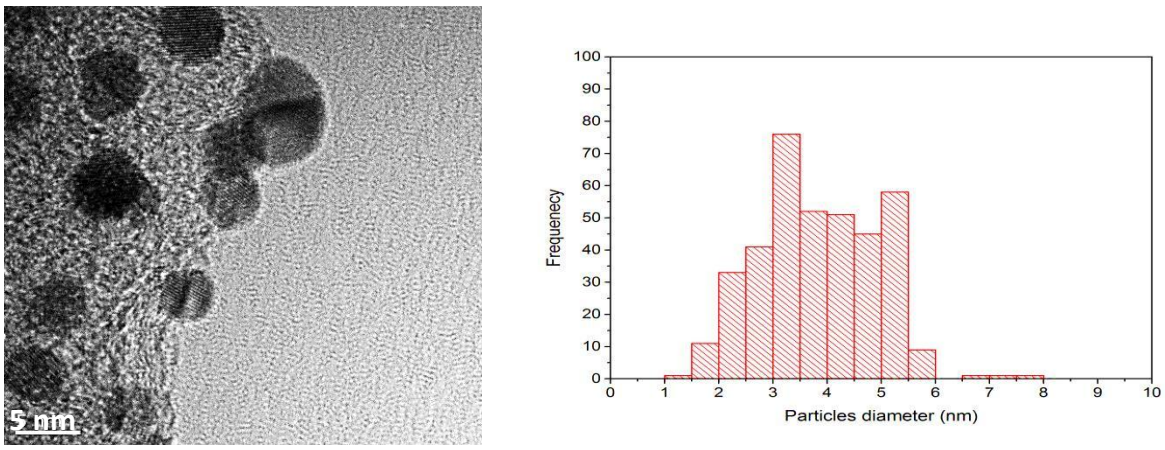

Figure 0.15: Left: a representative TEM image of 1.0 wt% naked gold nanoparticles immobilized on Norit activated carbon (as synthesised, *i.e.* before catalytic reaction) deposited onto carbon film coated copper TEM grid; Right: Particle size distribution histogram. The average particle diameter was determined to be 3.8 ± 0.1 nm (two standard deviations of the mean).

2.5.1.1.17 1.0 wt% Au_{naked}/C_{Vulcan}

Catalyst 1 wt% Au_{naked}/C_{Vulcan} was made using the procedure described in section 2.5.1.1.16 (1 wt% Au_{naked}/C). Modified carbon (Vulcan) was utilized as a support for Au_{naked} for this procedure.

2.5.1.1.18 1.0 wt% $Au_{citrate}/C_{Vulcan}$

Catalyst 1 wt% $Au_{citrate}/C_{Vulcan}$ was made using the same procedure described in section 2.5.1.1.15 (1 wt% $Au_{citrate}$/C). Modified carbon (Vulcan) was utilized as a support for $Au_{citrate}$ for this procedure.

Table 2.2 presents a summary of sections 2.5.1.1.15–2.5.1.1.18 of gold colloids, such as $Au_{citrate}$ and Au_{naked} immobilized on powder Norit activated carbon and Vulcan carbon.

Table 0.2: Summary of catalysts fabricated using naked and citrate-stabilized gold colloids.

Catalysts code	Carbon (g)	Gold (mg/mL)
1.0% $Au_{citrate}/C$	2.11	47.27
1.0% Au_{naked}/C	3.85	9.85
1.0% $Au_{citrate}/C_V$	2.11	47.27
1.0% Au_{naked}/C_V	3.84	9.85

2.5.1.2 Preparation of catalysts using shape-specific Ru nanocrystals

The shape-specific ruthenium nanoparticles (6 mg) were suspended in toluene (20 mL) with butylamine (100 µL) under dry nitrogen. Silica (6.07 g) was degassed at 200 ± 2 °C in a Schlenk tube for 3 hours, suspended in dry toluene (20 mL) and stored under dry nitrogen. The suspension of shape-specific ruthenium nanoparticles was added to the silica suspension rapidly under nitrogen gas and stirred overnight at 700 rpm. The silica containing immobilized ruthenium nanoparticles was allowed to settle and the supernatant layer of toluene was removed by a syringe. The toluene layer was clear whereas the (previously white) silica was grey, which indicated that the ruthenium nanoparticles had been successfully deposited on the support. Removal of residual toluene was accomplished under

vacuum. (Ru nanoparticles were immobilized on silica by David Anderson, a member of the Golovko research group at the University of Canterbury. Materials obtained in this way were used as catalysts either as made (un-activated) or after activation (described later).

2.5.2 Embedded palladium nanoparticles on wool fibres

Palladium nanocatalysts were made in the laboratory of Professor Jim Johnston at Victoria University of Wellington, by chemical reduction of a palladium chloride ($PdCl_2$) solution in the presence of wool fibres. By varying the reaction conditions, the size and shape of the nanoparticles and their distributions on and within the wool fibres can be controlled. This work was performed by Doctor Carla Fonseca-Paris in the Johnston research group under conditions that constitute a trade secret and have not been disclosed further.

2.6 Activation of nanocatalysts

The noble metal nanocatalysts (*i.e.*, ruthenium nanocrystals and gold nanoparticles or nanoclusters) were activated as described in in the following.

2.6.1 Activation of gold nanocatalysts

As described in the first chapter of this thesis, the properties of supported gold nanocatalysts have been found to depend on the fabrication and activation procedures. In this work, the stabilizing PPh_3 ligands were removed from the support-immobilized gold-containing nanoparticles or nanoclusters to expose the gold cores by using three methods:

I. Washing with a solvent at an elevated temperature[2b]

II. Calcinations in various atmospheres[2a, 19]

III. Washing with solvent at elevated temperature followed by calcinations in different atmospheres (the combination of I and II)[20]

2.6.1.1 Washing with a solvent at elevated temperature

The washing procedure was adopted from Anderson *et al.* who demonstrated removal of PPh_3 stabilizing ligands by refluxing supported gold nanoclusters in toluene.[2b] The gold particles were washed with 200 mL of toluene or, in the case of gold-citrate- or naked-based catalysts with 0.1 M of NaOH dissolved in 200 ml MilliQ water, placed into a 500 mL round-bottom flask fitted with a reflux condenser (see Figure 2.16).

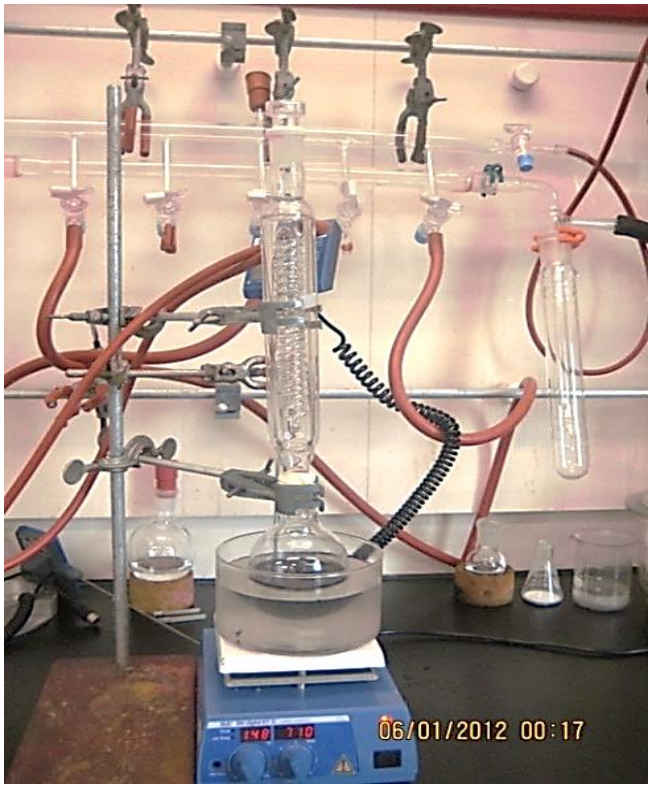

Figure 0.16 : A picture of washing procedure of gold nanocatalysts.

The mixture was heated to 100 ± 2 °C in an oil bath for 2 hours while stirring at 750 rpm. The mixture was allowed to cool to room temperature and the catalyst was separated by centrifugation (5000 rpm, 15 min), washed three times with fresh toluene and dried under vacuum for one day. After the washing procedure, the catalyst was kept in a freezer below - 4 ^{o}C. Thermal gravimetric analysis (TGA) can be considered for future work in estimating completeness of solvent removal (*i.e.*, toluene was used as a solvent used for washing procedure). However, even if traces of the solvent were present after this stage of activation

following treatments at the elevated temperature would have ensured complete removal of the solvent.

2.6.1.2 Calcinations under different controlled atmospheres

The activation of gold catalysts was performed by calcinations in Schlenk tubes attached to a Schlenk line (see Figure 2.17) that allowed control of the gas atmosphere (*i.e.* O_2–H_2, O_2, H_2, under vacuum or in static air). The solid powder gold catalyst to be calcined was placed in a Schlenk tube, and calcined by using different types of calcination conditions and a pre-heated aluminium heating block (200 ± 2 ^oC) or oil bath (100 ± 2 ^oC) for 3 hours. After the thermal treatment, the catalyst was cooled to room temperature and kept in a freezer below -4 ^oC.

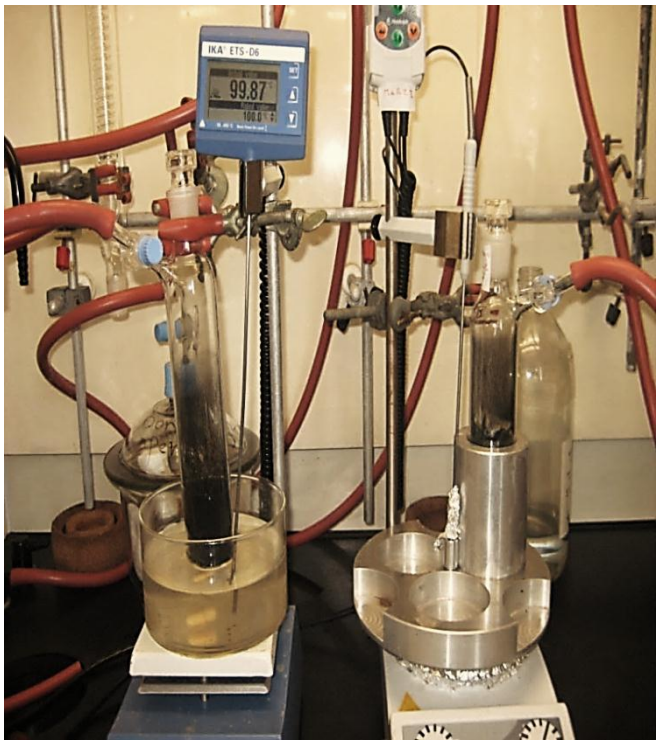

Figure 0.17: A picture of calcination procedure of gold nanocatalysts right: in an aluminium heating block and left: in an oil bath.

2.6.1.3 Washing with solvent at elevated temperature followed by calcinations under controlled atmospheres

A sample of gold catalysts was washed as described in Section 6.1.1, followed by calcinations as described in Section 6.1.2 under different atmospheres to integrate both advantages of washing and calcinations thermal treatments.

2.6.2 Activation of Ruthenium nanocatalysts

Ruthenium nanocatalysts thermal treatment was performed to remove O_2 and/or surfactants from the catalysts in either a vacuum (a Schlenk tube) or at atmospheric pressure in a furnace in the following manners.

2.6.2.1 Calcinations in vacuum by using a Schlenk tube

Ru/SiO_2 (~ 250 mg) was placed in a Schlenk tube attached to a Schlenk line and heated at 200± 2 ^oC in an aluminium block while stirring at 500 rpm under vacuum for 2 hours. The ruthenium catalysts was removed and cooled to room temperature under dry nitrogen gas.

2.6.2.2 Calcinations in a furnace (atmospheric pressure)

Ruthenium nanocatalysts were calcined[21] in a dual-zone split furnace (OTF-1200X (4") by MTI Corporation, see Figure 2.18) with the following general specifications:

- Maximum temperature: 1200 ^oC
- Continuous temperature: 1100 ^oC
- Maximum heating rate: ≤ 10 ^oC /min
- Tube size and materials: quartz; OD 40 mm; ID 38 mm; length 400 mm
- Heating zone length: 440 mm (single zone)

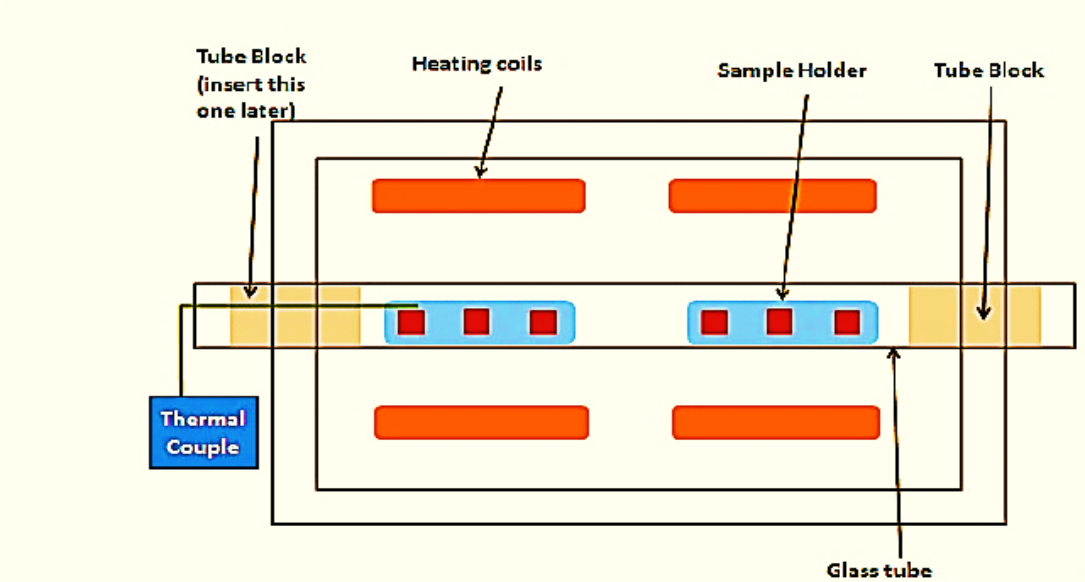

Figure 0.18: Schematic illustration of calcination furnace (OTF-1200X (4") by MTI Corporation).

The Ru catalyst (~ 250 mg) was loaded on to a quartz boat, which was placed quartz reaction tube purged with nitrogen gas for 30 minutes before starting. The furnace was programmed for different temperatures and lengths of time according to five protocols presented in Chapter 7.

2.7 Catalytic testing of noble metal nanocatalysts

In this section of the thesis, catalytic testing of different types of nanocatalysts is explained.

2.7.1 Catalytic testing of supported gold nanocatalysts

Benzyl alcohol oxidation was carried out in a stainless steel "mini-reactor" with internal volume of 50 mL fitted with a 50 mL Teflon liner (see Figure 2.19).

a)

b)

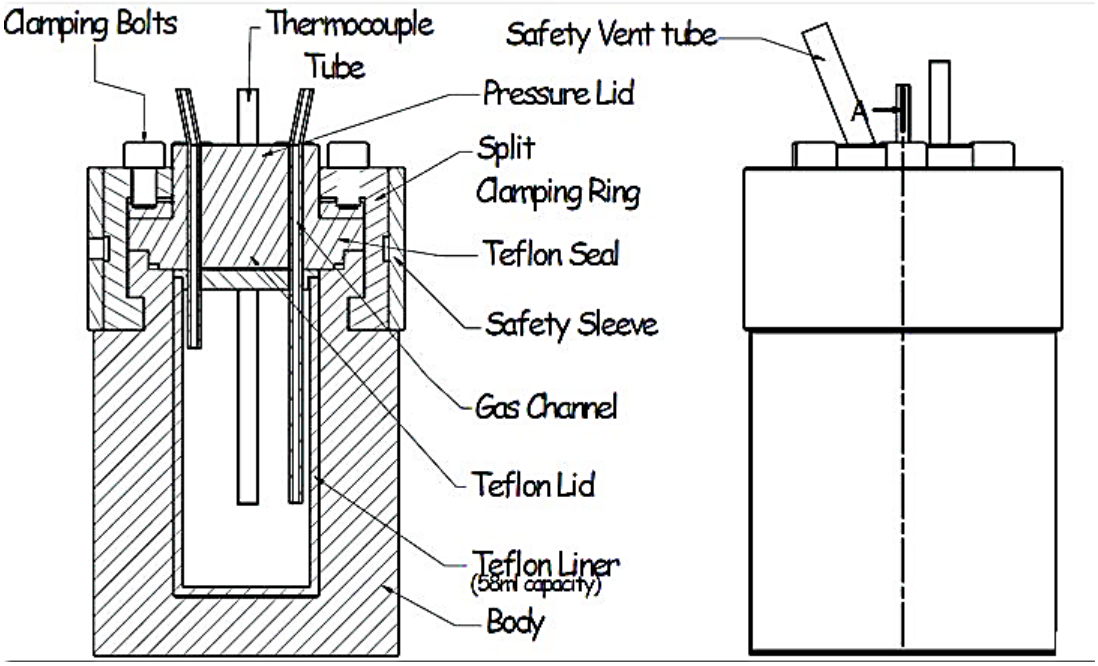

Figure 0.19: a) A picture & b) Schematic illustration of the pressurized mini-reactor apparatus.

The head (top removable part) of the reactor was fitted with an over-pressure relief valve, a long hollow thermocouple holder tube and two inlet/outlet lines of different lengths (*i.e.*, long and short) fitted with valves. The long line was utilized for pressurizing the reactor with a gas (*e.g.*, oxygen) that bubbled through the reactant mixture; the short line was used for venting

the gas from the headspace above the mixture during purging and after completion of the reaction.

Before being placed into the reactor, the Teflon liner was charged with reactant, internal standard, solvent, nanocatalysts and a magnetic stirring bar. The reactor was then assembled, connected to the gas line and purged five times with the gas leaving the desired reactor pressure and it placed onto a pre-heated magnetic stirring hotplate. A thermocouple was inserted into the thermocouple holder and the stirring rate was set at 750 rpm. The assembly was heated over ~20 minutes from ambient temperature (typically 20 ± 2 ^{o}C) to the target temperature of (normally 80 ^{o}C) at which point temperature was controlled (*via* a thermocouple control loop) to ± 2 ^{o}C for the remaining period of time of the reaction test. The mini-reactor was cooled in an ice bath for approximately 1 hour until temperature reached approximately 1 ± 0.2 ^{o}C to assure that most of volatiles present(*i.e.*, methanol) within the headspace were condensed, after which any remaining the gas (*i.e.*, oxygen) was vented. Samples of the reaction mixture were centrifuged (5000 rpm, 15 minutes) to separate out the catalyst, and product mixtures were analysed by a Dionex high-performance liquid chromatography (HPLC) system fitted with a Luna 5µ C18 reverse-phase column and UV detector.

Following several similar literature reports,[22] anisole was chosen as an internal standard for most benzyl alcohol oxidation experiments. [*n*]–Decane, which was used initially, was rejected because it could not be detected by the HPLC detector (UV). Benzene was disregarded being poisonous. Bi-phenyl was rejected because it changed from liquid to solid when the reactor was cooled in an ice bath.

Calibration curves were prepared by analysing standard samples whose concentrations were prepared across the range expected in the unknown sample. A typical example is shown for ethyl benzoate in Figure 2.20.

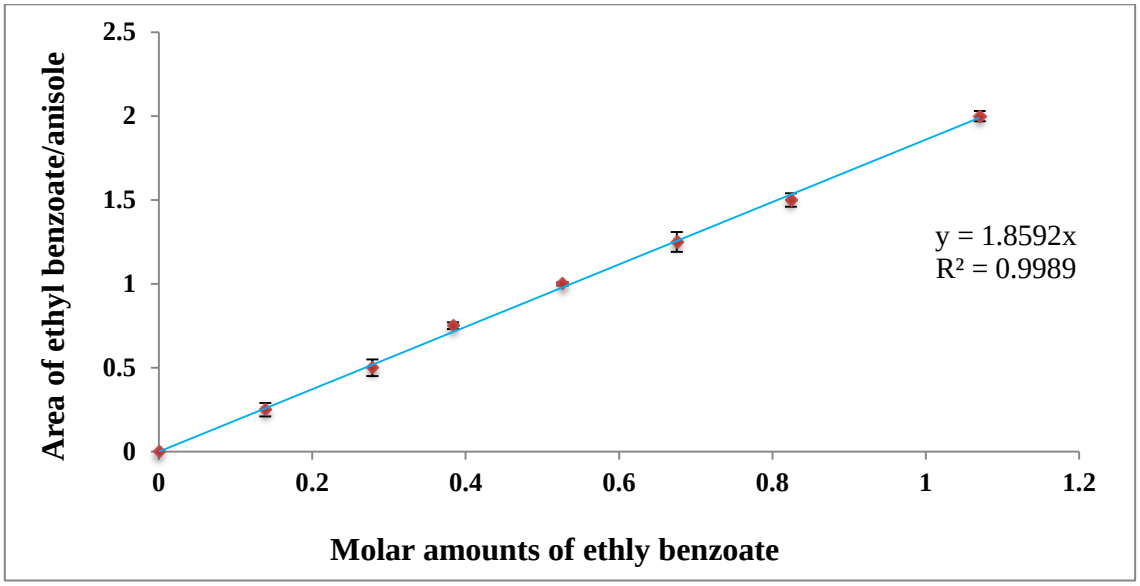

Figure 0.20: A calibration curve of ethyl benzoate.

For analysing the products mixture the following HPLC method was used (see Figure 2.21).

- The column-oven temperature was kept constant at 40 ^{o}C.
- The mixture of products was eluted using various v/v% mixtures of two solvents referred to as "A" (0.05 M of THF +MilliQ water) and "C" (acetonitrile). See Figure 2.21 for details of the eluent composition programme. (The HPLC system permits four solvents (A-D), but only two of them were used here.)
- The combined eluent flow rate was 1 mL/min.
- The total time required to analyse one sample was approximately 26 minutes.

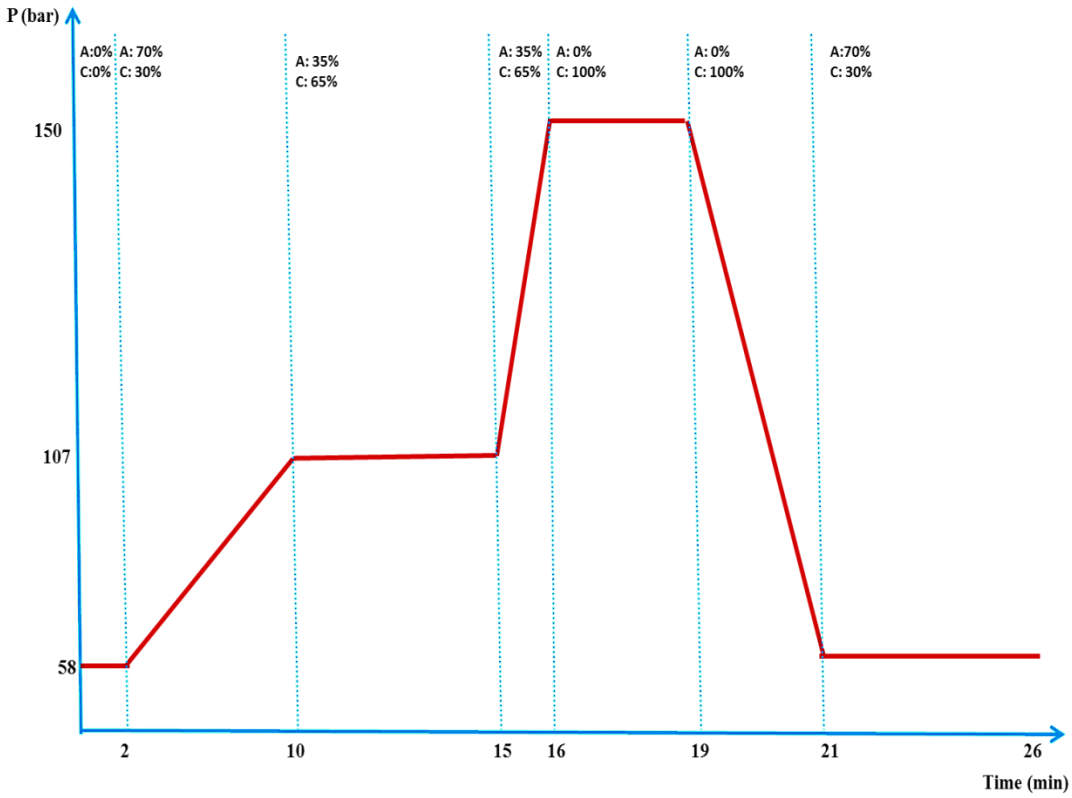

Figure 0.21: HPLC method for analysing benzyl alcohol oxidation products (A: MQ water + 0.05% THF and C: acetonitrile).

For each reaction, the conversion (*C*) and selectivity (*S*) for the products were calculated by these formulas:

$$\boldsymbol{C} = [(n_{react})_i - (n_{react})_f]/(n_{react})_i \times 100\%$$

$$\boldsymbol{S_{prod}} = (n_{prod})_f/[(n_{react})_i - (n_{react})_f] \times 100\%$$

Where n_{react} and n_{prod} represent to the molar amounts of reactants and products and the subscripts i and f indicate the initial and final states of the reaction, respectively.

2.7.2 Catalytic testing of supported ruthenium nanocatalysts

The catalytic activity of 0.1 wt% Ru/SiO_2 was studied using hydrogenation of cyclohexene to cyclohexane as a model reaction for alkene hydrogenation. A Parr high-pressure hydrogenation apparatus was used in this experiment. It was equipped with Teflon liner and a control unit to control the target temperature, gas pressure and stirring rate (see Figure 2.22).

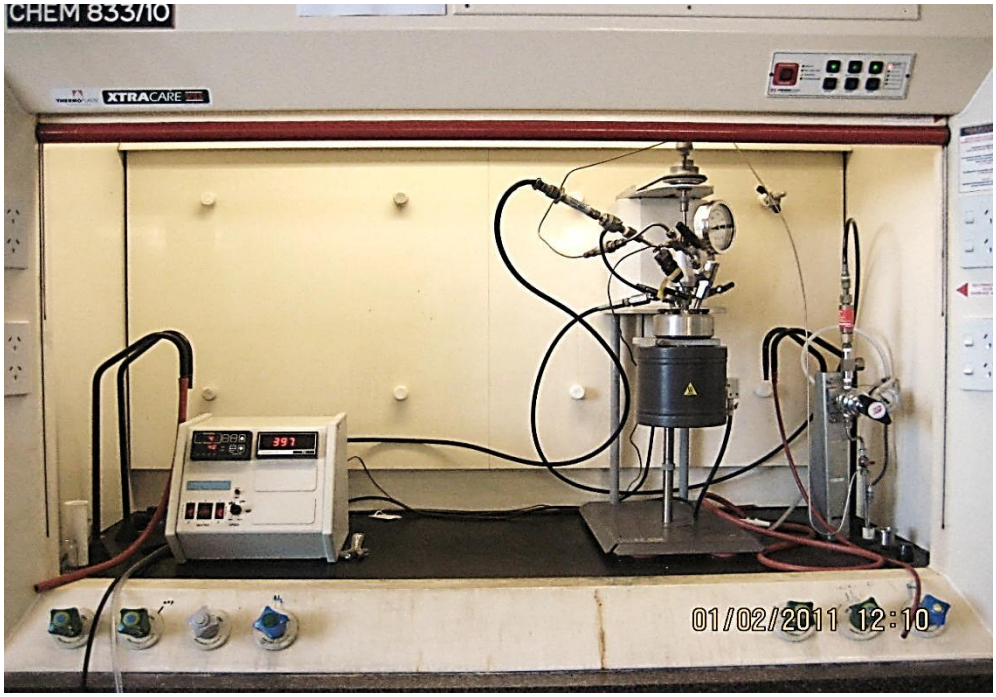

Figure 0.22: A Parr high-pressure hydrogenation apparatus.

The reaction conditions were optimized by carrying out series of preliminary experiments described below. For each test, approximately 10 g each of cyclohexene and cyclohexane (exact amounts were measured to 1 mg) were charged with 200 mg of 0.1 wt% Ru/SiO_2 into the reactor. The reactor was flushed with H_2 gas three times to remove air, and then pressurized to 400 psi of H_2 gas. The reactions were conducted under continuous stirring at 1200 rpm. Each sample was heated over ~15 minutes from ambient temperature (typically 20 ± 2 ^oC) to the target temperature (normally75 ^oC), at which point temperature was controlled to ± 1 ^oC for the remaining period of time of the reaction test. Progress of the reaction was monitored by recording the pressure inside the Parr reactor by using an Ashcroft model A2 heavy industrial pressure transducer. At the end of each catalytic run, the reactor was cooled to the room temperature and the remaining H_2 was vented. The composition of the liquid product mixture was analysed by using a Shimadzu gas chromatograph (GC–2010) fitted with a Restek RTX-5SIL-MS (30.0 m × 0.25 mm × 0.25 µm) capillary column and a flame

ionization detector (FID, 280 ^{o}C). The column oven temperature was programmed according to Table 2.3 with a total GC–FID run time of approximately 17 minutes for every sample.

Table 0.3: Column oven temperature program. The first column indicates the rate at which the temperature was increased to that indicated by the second column (the temperature prior to injection was 60 °C). The hold time (third column) indicates the period for which the stated temperature was maintained.

Step #	Rate (^{o}C/min)	Temperature (^{o}C)	Hold Time (min)
1	-----	60.0	0.0
2	2.0	74.0	0.0
3	35.0	174.0	0.0
4	50.0	280.0	5.0

Helium was used as a carrier gas. The injection inlet temperature was 220 ^{o}C and a split ratio of 100:1 was used with a purge flow of 7.0 mL/min. [*n*]–Decane was used as an internal standard.

For analysing the products mixture, calibration curves (see Figure 2.23) were used as a general method for determining the molar amounts of reactant (*i.e.,* cyclohexene as a reactant) and product (*i.e.,* cyclohexane as a product) as unknown samples by comparing them to a set of standard samples whose molar amounts were known. A series of standards were prepared and a typical example is shown for cyclohexane in Figure 2.23.

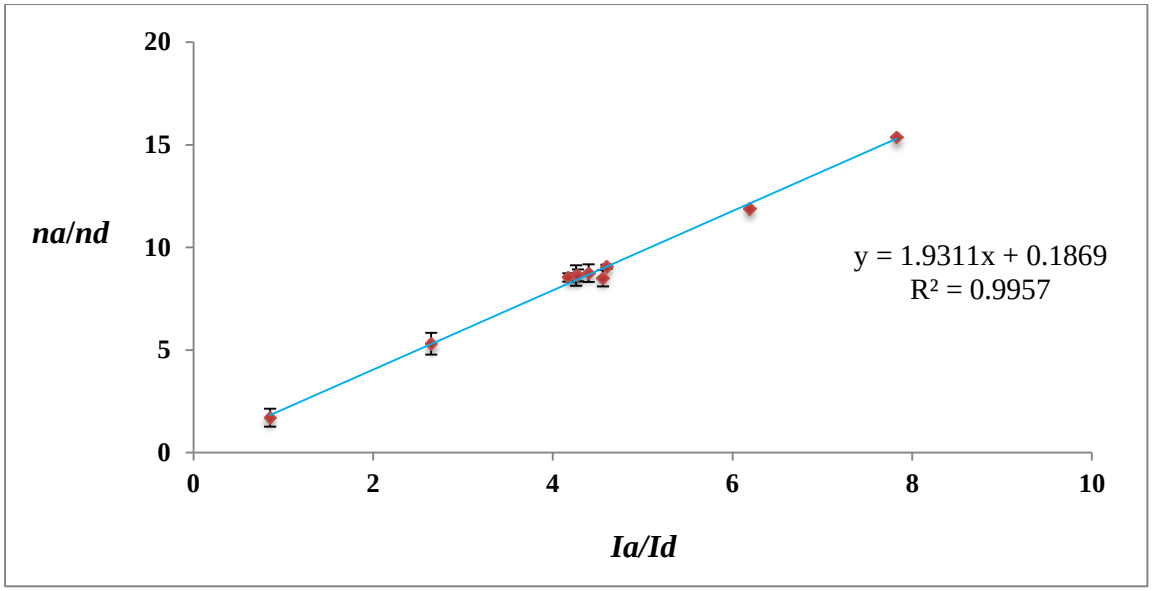

Figure 2.1: A calibration curve of cyclohexane (n_a and n_d represent the molar amounts of cyclohexane and decane, and I_a and I_d the peaks area of cyclohexene and decane, respectively).

In all of the experiments, cyclohexene was present in excess and H_2 gas was the limiting reagent. The conversion was calculated relative to the amount of cyclohexene initially available:

$$C = \frac{(n_e)_i - (n_e)_f}{(n_e)_i} \times 100\%$$

Where $(n_e)_i$ and $(n_e)_f$ represent the initial and final molar amounts of cyclohexene, determined by the GC–FID, respectively.

2.7.3 Catalytic testing of supported palladium nanocatalysts

The Pd/wool samples were labelled S$n_{.b}$ where *n* and *b* are the sample and batch numbers, respectively. Samples S_1 to S_4 were each provided in two batches, which are distinguished by appending *1* or *2* to the S_n descriptors. $S_{n,1}$ catalysts were provided in the first batch, *"the first batch"* received (27 January, 2010), whereas $S_{n,2}$ catalysts were received as the *"the second batch"* batch (18 December, 2010), S_5 and S_6 catalysts were received only as *"the second batch"* batches.

Table 0.4: Samples of Pd/wool with corresponding metal loadings as a percentage of the total Pd/wool mass and the total masses of Pd/wool loaded into the reactor for each test.

Sample code # (Pd/wool)	Mass % of Pd	Mass of nanocatalysts (mg)
$\mathbf{S_1}$	2.6	50
$\mathbf{S_2}$	2.6	50
$\mathbf{S_3}$	2.3	55
$\mathbf{S_4}$	1.6	80
$\mathbf{S_5}$	6.4	20
$\mathbf{S_6}$	6.4	20

2.7.3.1 Apparatus for hydrogenation reaction

The catalytic activity of Pd/wool was studied through hydrogenation of cyclohexene to cyclohexane by using a Parr high-pressure hydrogenation apparatus described earlier in this chapter. The reactor was charged with the Pd/wool catalyst and ~20 g mixtures of cyclohexene, flushed three times with H_2 gas and then pressurized to 400 psi with H_2 gas. The mass of the catalyst used (see third column of Table 2.4) was calculated to keep the mass of Pd nanoparticles constant, at about 1.3 mg, across the series of experiments. Apart from preliminary work on optimization of conditions, all reactions were conducted under continuous stirring at 750 rpm for approximately 5 or 24 hours at a target temperature of 40 ± 1 ^{o}C. During each catalytic test run, the mixture of reagents and catalysts was heated over a period (approximately 15 minutes) from ambient temperature to the target temperature, where it was held for the remainder of the reaction. At the end of each test, the reactor was cooled to room temperature before venting of any remaining H_2 gas. The composition of the liquid product mixture was analysed by using a gas chromatograph.

The conversions were calculated using the GC-FID as described above (in Section 2.7.2).The ~95% (two standard deviation) confidence interval for all values of conversion is ± 6%, which is determined essentially entirely by the uncertainly of the volume of gas. This uncertainty constitutes a systematic error and so substantially smaller (than 6%) differences between conversion values may be statistically significant.

References

1. Braunstein, P.; Kormann, H. P.; Meyer-Zaika, W.; Pugin, R.; Schmid, G., *Chem.-Eur. J.* **2000,** *6*, 4637.
2. (a) Anderson, D. P.; Adnan, R. H.; Alvino, J. F.; Shipper, O.; Donoeva, B.; Ruzicka, J. Y.; Al Qahtani, H.; Harris, H. H.; Cowie, B.; Aitken, J. B.; Golovko, V. B.; Metha, G. F.; Andersson, G. G., Chemically synthesised atomically precise gold clusters deposited and activated on titania. Part II. *PCCP* **2013,** *15* (35), 14806-14813; (b) Anderson, D. P.; Alvino, J. F.; Gentleman, A.; Qahtani, H. A.; Thomsen, L.; Polson, M. I. J.; Metha, G. F.; Golovko, V. B.; Andersson, G. G., Chemically-synthesised, atomically-precise gold clusters deposited and activated on titania. *PCCP* **2013,** *15* (11), 3917-3929.
3. (a) Martin, M. N.; Basham, J. I.; Chando, P.; Eah, S.-K., Charged gold nanoparticles in non-polar solvents: 10-min synthesis and 2D self-assembly. *Langmuir* **2010,** *26* (10), 7410-7417; (b) Link, S.; El-Sayed, M. A., Size and temperature dependence of the plasmon absorption of colloidal gold nanoparticles. *J. Phys. Chem. B* **1999,** *103* (21), 4212-4217.
4. Weare, W. W.; Reed, S. M.; Warner, M. G.; Hutchison, J. E., Improved synthesis of small (dCORE ≈ 1.5 nm) phosphine-stabilized gold nanoparticies *J. Am. Chem. Soc.* **2000,** *122* (51), 12890-12891.
5. Donoeva, B. G.; Ovoshchnikov, D. S.; Golovko, V. B., Establishing a Au nanoparticle size effect in the oxidation of cyclohexene using gradually changing Au catalysts. *ACS Catalysis* **2013,** *3* (12), 2986-2991.
6. (a) Bond, G. C.; Thompson, D. T., Catalysis by Gold. *Catal. Rev.—Sci. Eng.* **2001,** *641* (3-4), 319-388; (b) Horváth, A.; Beck, A.; Sárkány, A.; Stefler, G.; Varga, Z.; Geszti, O.; Tóth, L.; Guczi, L., Silica-supported Au nanoparticles decorated by TiO_2: Formation, morphology, and CO oxidation activity. *J. Phys. Chem. B* **2006,** *110* (31), 15417-15425.
7. ImageJ (Image processing and analysis in Java). http://rsb.info.nih.gov/ij/download.html (accessed Nov 17,2010).
8. Hutchinson, J. E.; Foster, E. W.; Warner, M. G.; Reed, S. M.; Weare, W. W., Triphenylphosphine-stabilised gold nanoparticles. In *Inorganic synthsis*, Shapley, J. R., Ed. John Wiley & Sons: 2004; Vol. 34 pp 228-232.
9. Wen, F.; Englert, U.; Gutrath, B.; Simon, U., Crystal structure, electrochemical and optical properties of $[Au_9(PPh_3)_8](NO_3)_3$. *Eur. J. Inorg. Chem.* **2008,** *2008* (1), 106-111.
10. Van der Velden, J. W. A.; Bour, J. J.; Bosman, W. P.; Noordik, J. H., Reactions of cationic gold clusters with Lewis bases. Preparation and x-ray structure investigation of $[Au_8(PPh_3)_7](NO_3)_{2.2}CH_2Cl_2$ and $Au_6(PPh_3)_4[Co(CO)_4]_2$. *Inorg. Chem.* **1983,** *22* (13), 1913-1918.
11. Malatesta, L.; Naldini, L.; Simonetta, G.; Cariati, F., Triphenylphosphine-gold(0)/gold(I) compounds. *Coord. Chem. Rev.* **1966,** *1* (1-2), 255-262.
12. Turkevich, J.; Stevenson, P. C.; Hillier, J., A study of the nucleation and growth processes in the synthesis of colloidal gold. *Disc. Faraday Soc.* **1951,** *11*, 55-75.
13. Haiss, W.; Thanh, N. T. K.; Aveyard, J.; Fernig, D. G., Determination of size and concentration of gold nanoparticles from UV-Vis spectra. *Anal. Chem.* **2007,** *79* (11), 4215-4221.
14. (a) Shiohara, A.; Hanada, S.; Prabakar, S.; Fujioka, K.; Lim, T. H.; Yamamoto, K.; Northcote, P. T.; Tilley, R. D., Chemical reactions on surface molecules attached to silicon quantum dots. *J. Am. Chem. Soc.* **2010,** *132* (1), 248-253; (b) Watt, J.; Yu, C.; Chang, S. L. Y.; Cheong, S.; Tilley, R. D., Shape control from thermodynamic growth conditions: The case of HCP ruthenium hourglass nanocrystals. *J. Am. Chem. Soc.* **2013,** *135* (2), 606-609; (c) LaGrow, A. P.; Cheong, S.; Watt, J.; Ingham, B.; Toney, M. F.; Jefferson, D. A.; Tilley, R. D., Can polymorphism be ued to form banched mtal nnostructures? *Adv. Mater.* **2013,** *25* (11), 1552-1556.
15. (a) Prati, L.; Rossi, M., Gold on carbon as a new catalyst for selective liquid phase oxidation of diols. *J. Catal.* **1998,** *176* (2), 552-560; (b) Okumura, M.; Nakamura, S.; Tsubota, S.; Nakamura, T.; Azuma, M.; Haruta, M., Chemical vapor deposition of gold on Al_2O_3, SiO_2, and TiO_2 for the oxidation of CO and of H_2. *Catal. Lett.* **1998,** *51* (3-4), 53-58.
16. Haruta, M., Novel catalysis of gold deposited on metal oxides. *Catal. Surv. Jpn.* **1997,** *1* (1), 61-73.

17. Lopez-Sanchez, J. A.; Dimitratos, N.; Hammond, C.; Brett, G. L.; Kesavan, L.; White, S.; Miedziak, P.; Tiruvalam, R.; Jenkins, R. L.; Carley, A. F.; Knight, D.; Kiely, C. J.; Hutchings, G. J., Facile removal of stabilizer-ligands from supported gold nanoparticles. *Nat. Chem.* **2011,** *3* (7), 551-556.
18. Raghuveer, V.; Manthiram, A., Mesoporous carbons with controlled porosity as an electrocatalytic support for methanol oxidation. *J. Electrochem. Soc.* **2005,** *152* (8), A1504-A1510.
19. Turner, M.; Golovko, V. B.; Vaughan, O. P. H.; Abdulkin, P.; Berenguer-Murcia, A.; Tikhov, M. S.; Johnson, B. F. G.; Lambert, R. M., Selective oxidation with dioxygen by gold nanoparticle catalysts derived from 55-atom clusters. *Nature* **2008,** *454* (7207), 981-983.
20. Dimitratos, N.; Lopez-Sanchez, J. A.; Morgan, D.; Carley, A.; Prati, L.; Hutchings, G. J., Solvent free liquid phase oxidation of benzyl alcohol using Au supported catalysts prepared using a sol immobilization technique. *Catal. Today* **2007,** *122* (3–4), 317-324.
21. Vollmer, C.; Redel, E.; Abu-Shandi, K.; Thomann, R.; Manyar, H.; Hardacre, C.; Janiak, C., Microwave irradiation for the facile synthesis of transition-metal nanoparticles (NPs) in ionic liquids (ILs) from metal–carbonyl precursors and Ru-, Rh-, and Ir-NP/IL dispersions as biphasic liquid–liquid hydrogenation nanocatalysts for cyclohexene. *Chem. – Eur. J.* **2010,** *16* (12), 3849-3858.
22. Morales-Valle, H.; Silva, L. C.; Paterson, R. R. M.; Oliveira, J. M.; Venâncio, A.; Lima, N., Microextraction and Gas Chromatography/Mass Spectrometry for improved analysis of geosmin and other fungal "off" volatiles in grape juice. *J. Microbiol. Methods* **2010,** *83* (1), 48-52.

Chapter 3: Optimization of Conditions for Benzyl Alcohol Oxidation by Au_{101}/C Catalysts

3.1 Introduction

Gold nanoparticles have become an active subject of research lately because of the discovery of their remarkable catalytic properties and potential applications. Gold is known to have a remarkable and genuine "nanosize effect". These properties were discovered in the 1970s but were not exploited until the late 1980s, when Haruta and co-workers verified their utility in the aerobic oxidation of carbon monoxide.[1] Since then, many studies conducted on selective CO oxidation catalysed by supported gold nanoparticles have shown activity and selectivity that are highly dependent upon the gold particle size.[2]

Previous studies have shown that the catalytic activity of gold nanoparticles can be greatly affected by a number of factors, but mainly by their size,[3] with the greatest activity being associated with very small gold clusters, containing just a few atoms.[4] Chemically made phosphine-stabilized gold complexes (*i.e.*, clusters and colloids) over a wide range of particle sizes, from Au_8 and Au_9 to Au_{101}, are active catalysts for oxidation of organic compounds.[5] Among these, Au_9 ($Au_9(PPh_3)_8(NO_3)_3$) is the most widely studied, and is active for low-temperature CO oxidation.[5b] Another example is a gold phosphine colloid with metal core size of *ca*. 1.5 nm, introduced initially as Au_{55} by Schmid *et al.*,[6] but later described by Hutchison *et al*.[7] as Au_{101} ($Au_{101}(PPh_3)_{12}Cl_6$). Au_{101} was the first type of well-defined ligand-stabilized nanoparticle. Turner *et al.* used Au_{101} for styrene oxidation and demonstrated its high activity and selectivity towards benzaldehyde formation.[5a] Pei *et al.* also studied the nature of active sites on the Au_{101} nanoparticles and a mechanism underlying its high selectivity in styrene oxidation.[3b]

One of the fundamental factors for catalytic activity of gold catalysts is the choice of an appropriate support for the gold nanoparticles because the catalytic activity depends on particle sizes, which are often defined by their interaction with supports.[5b] The nature of

supports can affect the morphology and dispersion of noble metal nanoparticles via so-called metal-support interactions (described in Chapter 6, Section 6.1).[8] Carbon is an environmentally friendly support that has other benefits, such as high surface area,[9] good Au particles dispersion,[10] possibility to achieve high metal loading,[11] availability of various types of support on a large scale,[10, 12] good recyclability,[11] and potential for tuning of the surface *via* modification and tethering.[13] Among the many types of carbon used to prepare supported catalysts, high-surface-area activated carbon is considered to be one of the best.[14] Its high porosity and well-developed internal pore structure, as well as a wide spectrum of surface functional groups, make this type of carbon a very versatile support material (as described in Chapter 5, Section 5.1).[15] Gold nanoparticles exhibit high activity and selectivity in alcohol oxidation when immobilized on this type of carbon.[11]

The method of preparation can also influence the activity and selectivity of noble metal nanoparticles.[11,16] Preparation methods include impregnation, deposition-precipitation, chemical vapour deposition, photochemical/sono-chemical activation and deposition of colloidal gold onto the support. The immobilization of a colloidal suspension is an important method by which pre-synthesized metal particles can be immobilized on a support with good control of their size and size distribution.[17] It involves a solid support being mixed with a colloidal dispersion of the active phase, resulting in adsorption of the colloidal particles onto the support surface. When carried out successfully, there should be little increase in the size of the metal particles due to undesirable aggregation. Apart from good control over particle size, this approach offers other benefits, such as control of the nature and concentration of the stabilizer, the stabilizer/gold ratio, and the nature of the support.[18]

Alcohols, being stable compounds (*e.g.* easy to handle and store), play a central role as intermediates in the fine-chemical synthesis of many compounds with various functional groups.[19] They are also involved as intermediates in many conventional C– C bond-forming

reactions, such as the Grignard reaction, in which organometallic alkyl- or aryl-magnesium halides (Grignard reagents) add to a carbonyl group in an aldehyde or ketone.[20] Alcohols are also recognized as having high potential for large-scale industrial applications, *e.g.*, energy from bio-feedstocks. Biodiesel production *via* trans-esterification affords large amounts of alcohols as by-products.[21] As the simplest and lightest alcohol, methanol has received major attention in terms of partial oxidation and steam reforming to an auto-thermal reforming process.[22] Glycerol, as a heavy alcohol, is an attractive feedstock for alcohol oxidation because of its ability to be transformed to a large number of higher-value products by gold catalysts.[23]

Highly selective alcohol oxidation to useful chemical intermediates and fine chemicals represents an attractive but demanding target in green chemistry.[24] However, comprehensive studies of the effects of numerous parameters in this catalytic reaction are scarce.[25] Benzyl alcohol oxidation has been often reported as a model reaction for alcohol oxidation.[26] Importantly, benzyl alcohol oxidation proceeds with negligible conversion (4%) in the absence of a catalyst,[27] but can be performed with high conversion and selectivity using supported gold catalysts. It has been demonstrated that gold catalysts can convert benzyl alcohol and its analogues to benzaldehyde, benzoic acid and methyl benzoate derivatives with high activity and selectivity that depends on substituents on the aromatic ring.[26-28]

Appropriate selection of key reaction conditions helps to improve the performance of gold nanoparticles in catalytic aerobic oxidation of alcohols,[24] as demonstrated by numerous investigations of the role of one or several specific parameters. The roles of temperature, nature of solvent, type of support, presence type and concentration of a base have been previously investigated in respect to selectivity of gold catalysts for benzyl alcohol oxidation.[25c] The effects of the base, alcohol concentration and metal/substrate ratio for benzyl alcohol oxidation have also been explored.[25a] Ishida *et al.* investigated catalytic

activity of supported gold nanoparticles for benzyl alcohol oxidation by changing conditions such as reactant concentrations, base, O_2 gas pressure, reaction temperature and solvent.[29] However, holistic optimization of these conditions has scarcely been studied.

The use of a base is essential when a using a monometallic gold catalyst alcohol oxidations.[25a, 30] Base aids the initial dehydrogenation of the alcohol *via* deprotonation of a primary OH groups (see Figure 3.1),[29, 31] and helps to overcome the rate-limitation step of the oxidation process.[32] Enhancement of the gold catalyst activity by using the base depends on the type of alcohol[25a] and/or a solvent.[30a] The products typically formed in the presence of the base are primarily intermediate aldehydes and ketones rather than acids.[30c] However, in the case of benzyl alcohol, methyl benzoate is the main product in the presence of the base.[29] Table 3.1 provides selected examples illustrating the use of a base in various types of reactions.

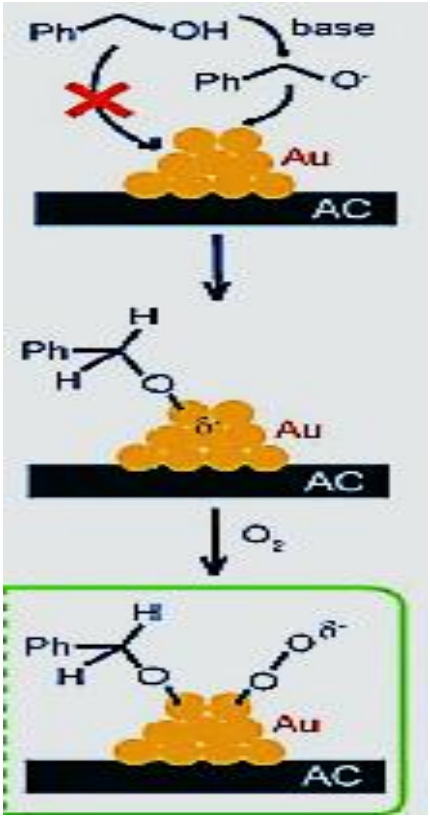

Figure 0.1: The effect of a base on benzyl alcohol oxidation by gold particles immobilized on activated carbon. Reproduced from Ishida *et al*.[29]

Table 0.1: Example of reactions catalysed by supported metal particles in the presence of a base.

Catalyst code	Base (substrate: base)	Reaction	*C* (%)	TOF (h^{-1})	*T* (^oC)	time (h)	Ref.
Au/C	NaOH (1:1)	Phenylethanediol oxidation	96	-	70	4	[33]
Au/C	NaOH	Benzyl alcohol oxidation	-	78	60	1/4	[25a]
Au/C	NaOH	Cinnamyl alcohol oxidation	-	470	60	1/4	[25a]
Au/C	K_2CO_3 (1:0.5)	1-phenylethanol oxidation	99	-	80	1	[29]
Au–Pd/C	NaOH	*n*-octanol oxidation	50	-	60	8	[30c]
Au/C	NaOH (1:2)	Glycerol oxidation	6.8	6.1	60	1/2	[34]
Au/TiO_2	$NaOCH_3$	Benzyl alcohol oxidation	99	-	130	10	[35]
Au/TiO_2	K_2CO_3 (2.5:0.4)	Benzyl alcohol oxidation	100	-	130	4	[31]
Au/SiO_2	K_2CO_3 (1:1)	Benzyl alcohol oxidation	99	-	80	2	[26a]

Previous studies confirm that reactions performed without base showed negligible conversion so, using a base is obligatory to approach full conversion.[25a, 30] Gold catalysts have shown a strong dependence on the nature of the acid/base, supports and substrates, and exhibited unique reactivity when basic conditions were used. Adding a base to a reaction mixture may accelerate a reaction dramatically which is essential to proceed to high conversion.[25a, 29-30, 31] Bases that have been used include $Co(CH_3COO)_2$, $K_2B_4O_7$, $NaCH_3COO$, KCH_3COO, $Na_2B_4O_7$ and K_2CO_3 and the highest conversion of benzyl alcohol (77%) with reasonable selectivity towards benzaldehyde (51%) was achieved with K_2CO_3.[36]

The catalytic activity and, especially, selectivity of gold catalysts may also depend on the reaction temperature.[9, 19, 29] Choudhary *et al.* demonstrated that increasing the temperature from 70 to 130 ^oC improved benzyl alcohol conversion from 0 to 100%.[24a] It was suggested earlier that molecular oxygen can be activated by gold nanoparticles at mild temperatures (*i.e.*, ~80 ^oC).[37] In fact, a higher reaction temperature may lead to reduced dissolved oxygen concentrations, retarding oxidation.[29, 38] Hutchings *et al.* showed that gold nanoparticles can help to activate molecular oxygen under mild temperatures (*i.e.*, from 60 to 80 ^oC) speeding

up oxidation reactions.[39] Table 3.2 provides selected examples illustrating the effect of reaction temperature on the catalytic activity of metal catalysts in benzyl alcohol oxidation.

Table 0.2: Examples of benzyl alcohol oxidation catalysed by supported metal particles as a function of temperature.

Catalysts code	*C* (%)	T (^{o}C)	Time (h)	Ref.
Au/TiO_2	100	130	4	[31]
$Au\text{-}Pd/TiO_2$	28	140	1.15	[40]
Au/MgO	55.5	120	5	[27]
Au–Pd/MgO	50	80	4	[40]
$Au/K_2Ti_6O_{13}$	99	25	10	[30a]
Au/TiO_2	99	25	10	[30a]
Au/MgO	95	120	9	[41]
Au/SiO_2	99	80	2	[26a]

Ideally, the liquid phase oxidation processes should be carried out in the absence of solvent to make them more environmentally friendly. Although, benzyl alcohol oxidation over supported gold catalysts under solvent-free conditions had been demonstrated with excellent selectivity towards benzaldehyde, the low activity (conversion of only 48%) and long reaction time (6 hours) needed under these conditions undermine the effectiveness of this method.[42]

The choice of a solvent is important for optimal catalytic activity and selectivity of gold catalysts.[43] A range of solvents from nonpolar to polar, including water, has been utilized for benzyl alcohol oxidations. The surface of the activated carbon is hydrophobic, which may cause the catalyst to be poorly dispersed in water;[44] but hydrophilic supports (like silica-based MCM-41) have proved to be appropriate in catalysing reactions in water.[38, 45] Methyl benzoate, one of the main products of benzyl alcohol oxidation, is poorly soluble in water,[46] so in aqueous solvent the main product can be either an acid or an ester.[32] There are some circumstances in which an organic solvent is required owing to the limited solubility in water or (for research purposes) the need to use a water-insoluble internal standard for accurate quantification of reaction products.[25c] High conversion of benzyl alcohol has been

demonstrated using polar organic solvents like methanol.[30a, 47] Methanol is a polar solvent that can adequately enhance the reaction rate of the benzyl alcohol oxidation using gold particles immobilized on activated carbon.[29]

The gold loading of the support plays an important role determining the catalytic activity,[22b, 48] and has been investigated to evaluate its influence.[22b, 46, 49] Recent studies have shown that appropriate gold loading can improve gold catalysts performance.[22b, 50] Gold deposition can increase almost linearly with the amount of gold available in the solution (see Figure 3.2). However, investigations of styrene epoxidation over a range from 0.9 to 6.6 wt% Au on Yb_2O_3 support showed the best conversion to be 58% at 1.0 wt% gold loading.[51] The variation of the gold loadings on $MnO_x - CeO_2$ between 0.5 wt% and 5.0 wt% also showed that the highest CO conversion (90%) and selectivity when the gold loading was adjusted to 1.0 wt%.[52] Choudhary *et al.* found that benzyl alcohol conversion increased with increasing Au loading in Au/U_3O_8 catalyst from 18% at 1 wt% to 50% at 8 wt% [53] Pojanavaraphan *et al.* investigated the effect of gold loading in steam reforming of methanol. They studied 1.0, 3.0 and 5.0 wt %t gold loadings and found that 3.0 wt% promoted the greatest dispersion and gave the optimum gold particle size for this reaction.[50] An invariant particle size indicated that the deposited Au particles did not agglomerate during preparation.[22b] Table 3.3 provides selected examples illustrating the effect of gold loadings on the catalytic activity of gold catalysts and average gold diameter (nm) in various reactions.

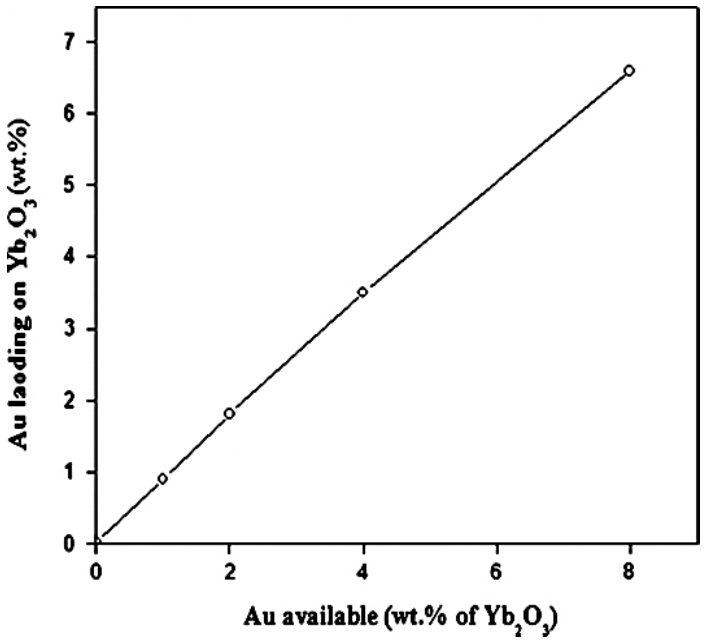

Figure 0.2: Dependence of gold loading in Au/Yb_2O_3 catalyst upon the initial amount of gold available in the solution for the gold deposition on the support. Reproduced from Choudhary *et al*.[48]

It is well known that long-term stability of a catalyst is no less important than its activity, especially in the context of possible industrial applications.[1, 54] Gold catalysts can lose their catalytic activity due to factors such as poisoning of active sites by accumulation of by-products, contamination of the catalytic surface by reaction products and agglomeration of gold particles.[25c, 26a, 55] To investigate the long-term stability of gold catalysts, a series of batches from the same catalyst (fresh *vs*. restored catalysts) is required;[56] If the interaction between metal particles and supports is weak, the gold particles could move on the surface of the support leading to sintering (*e.g*. formation of enlarged gold particles), which could result in loss of their catalytic activity.[25c, 57]

Table 0.3: Examples of reactions catalysed by supported gold particles as a function of gold loadings rate.

Catalysts code	Reactions	Loading (%)	Particle size (nm)	*C* (%)	TOF (h^{-1})	Ref.
Au/TiO_2	CO oxidation	1	4.6 ± 1.5	-	9.6×10^{-6}	[58]
		1.8	2.7 ± 0.6	-	1.2×10^{-1}	
$Au/Ti\text{-}SiO_2$	Propylene epoxidation	16	-	61	-	[49]
		8	-	57	-	
Au/Yb_2O_3	Styrene epoxidation	1	-	58.1	-	[51]
		6.6	-	63.5	-	
Au/MgO	Benzyl alcohol oxidation	0.4	1.9	-	113	[59]
		0.8	3.3	-	324	
		1.5	4.1	-	74	
$Au/CeO_2\text{-}Fe_2O_3$	Steam reforming of methanol	1	23.53	70	-	[50]
		3	43.07	100	-	
		5	62.57	80	-	
$Au/MnO_x\text{-}CeO_2$	CO oxidation	0.5	-	80	-	[52]
		1	-	90	-	

Benzyl alcohol can be catalytically oxidized into its corresponding aldehyde, acid or esters by using oxidising reagents such as ammonium permanganate,[60] hydrogen peroxide[61] or oxygen.[23, 62] However, some of these oxidants have serious drawbacks of being expensive and/or toxic, and producing a large amounts of waste, requiring treatment.[61] Stringent ecological standards have forced researchers to develop new, environmentally benign methods.[28b] Recently, molecular oxygen has received more attention as an oxidising reagent for alcohol oxidation because it is the most "*environmentally friendly*" choice.[23, 62]

Aerobic oxidation of benzyl alcohol depends on oxygen gas pressure. It is evident that oxygen has a substantial promotional effect on the deprotonation of benzyl alcohol[40, 63] It has been reported that benzyl alcohol disproportionation is promoted when O_2 pressure is increased up to 1.0 barg (barg is the pressure in bars above ambient pressure or atmospheric pressure) but reduced when the O_2 pressure further increased.[40] Oliveira *et al.* showed that

benzyl alcohol conversion increased from 45% to 90% when oxygen gas pressure was increased from 1 to 6 atm.[35]

Nanoparticle protection ligands such as PPh_3 impede catalysis by shielding the gold cores.[64] Thermal treatments can remove such ligands, permitting better interactions between the gold particles and the support, which, in turn, change the catalytic activity of gold catalysts.[65] Various approaches to catalyst activation are discussed in detail in Chapter 1 (Section 1.1.7). For the purpose of this thesis, various washing and calcination procedures were used (as described in Chapter 4) as treatments for removal of PPh_3 from gold nanocatalysts.

An overview of various reactions in which supported Au particles have been used as catalysts was presented Chapter 1 (Sections 1.1.6). The current chapter and the following two chapters will focus on oxidation of alcohols and, more specifically, benzyl alcohol as a model catalytic test reaction. In this chapter, I sought to investigate the effects of systematic alterations of the reaction conditions on the activity and selectivity of activated Au_{101} ($Au_{101}(PPh_3)_{21}Cl_5$) nanoparticles (washed with toluene followed by calcination under static air at 100 ^oC for 3 hours) immobilized on powder Norit activated carbon support in the aerobic oxidation of benzyl alcohol (see more details in Chapter 2, Section 2.5.1.1.1 and Chapter 4, Section 4.2.3.1). I investigated the effects of a base (K_2CO_3) and its mole ratio to substrate, reaction temperature and reaction time, solvent and gold loading on the long-term stability of the catalysts using oxygen as a low-cost and green oxidant. The effects of changes in these reaction parameters provided a guideline for the optimal conditions for further tests using a wider range of catalysts, as reported in Chapters 4 and 5.

3.2 Results and discussion

3.2.1 Initial tests (blank, control and stability of standard)

In this study, benzyl alcohol was utilized as a model aromatic alcohol reagent for testing the catalytic activity of gold nanoparticle-based catalysts in partial oxidation in the liquid phase. Performance of gold nanocatalysts was investigated systematically in the following manner:

a. The reactivity of the benzyl alcohol in the absence of catalysts, but in the presence of the base under typical reactions conditions (see footnotes to Table 3.4) was investigated as a '*blank*' reaction to establish the efficiency of non-catalytic benzyl alcohol oxidation.[22b, 27]
b. The catalytic activity of Au-free Norit activated carbon support was investigated with reactants in the presence of the base under typical conditions (as above (a)). These '*control*' reactions were to used examine whether the support can catalyse benzyl alcohol oxidation without gold particles.[29, 66]
c. The reactivity of the internal standard (anisole) was investigated without benzyl alcohol but in the presence of the base and Au-free Norit activated carbon under typical conditions to examine the ability of anisole to undergo oxidation by activated carbon.[37]
d. The reactivity of an internal standard (anisole) was investigated in the presence of the gold nanocatalysts and base under typical conditions to examine the ability of anisole to undergo oxidation by the gold catalysts.[37]
e. The catalytic activity of gold nanocatalysts in oxidation of benzyl alcohol using anisole as an internal standard was investigated under various conditions. These experiments are referred to as '*catalytic tests'* in further discussion.

Table 3.4 summarizes the results of the initial tests listed above.

Table 0.4: Summary of the initial catalytic tests.

	Conversion%	Selectivity%		
		Benzaldehyde	**Benzoic acid**	**Methyl benzoate**
[a] **Blank**	0	0	0	0
[b] **Control**	0	0	0	0
[c] **Anisole**	0	0	0	0
[d] **Anisole**	0	0	0	0
[e] **Catalytic test**	100	0	22	78

Reaction Conditions: Benzyl alcohol: 2.5 mmol, Anisole: 1.25 mmol, Base: 2.5 mmol, Methanol: 25 mL, Pressure: 73 psi, Temperature: 80 ^{o}C, Stirring: 750 rpm and Reaction time: 24 hours, *a*: Without gold catalysts, *b-c*: 50 mg Norit activated carbon and *d-e*: 50 mg activated 1.0% Au_{101}/C.

3.2.2 Amount of oxidant

Economically and environmentally, there is an urgent demand for industrially relevant green oxidation agents.[47, 67] Oxygen is an efficient and clean oxidant since it produces water as the main by-product and avoids producing highly toxic organic residues.[47, 68] In the current work, oxygen gas was used at a pressure of 73 ± 1 psi (5.03 ± 0.07 bar). This pressure was determined according to the volume of the mini rector and to ensure that maximum possible conversion was not limited by the amount of gas. The volume of the Teflon liner was 50 mL, of which 25 mL was filled with the reactant, solvent and internal standard. At ~5 bar and 80 ^{o}C the 25 mL head space of the liner corresponds to ~43 mmol at O_2, which is in excess of the 25 mmol of benzyl alcohol initially. This O_2 pressure was used in all experiments and no attempt was made to investigate effects of different gas pressures.

3.2.3 Mechanism of reaction

Under the conditions investigated in this work, the predominant products of catalytic oxidation of benzyl alcohol were methyl benzoate and benzoic acid, with much smaller amounts of benzaldehyde sometimes produced.[25a, 26a, 41] The chemical reaction mechanism suggested in earlier studies[25a, 28, 30, 37] involves an oxidative esterification reaction between

methanol solvent and benzaldehyde, an intermediate, in the presence of a base (K_2CO_3) and the gold catalysts (see Scheme 3.1).

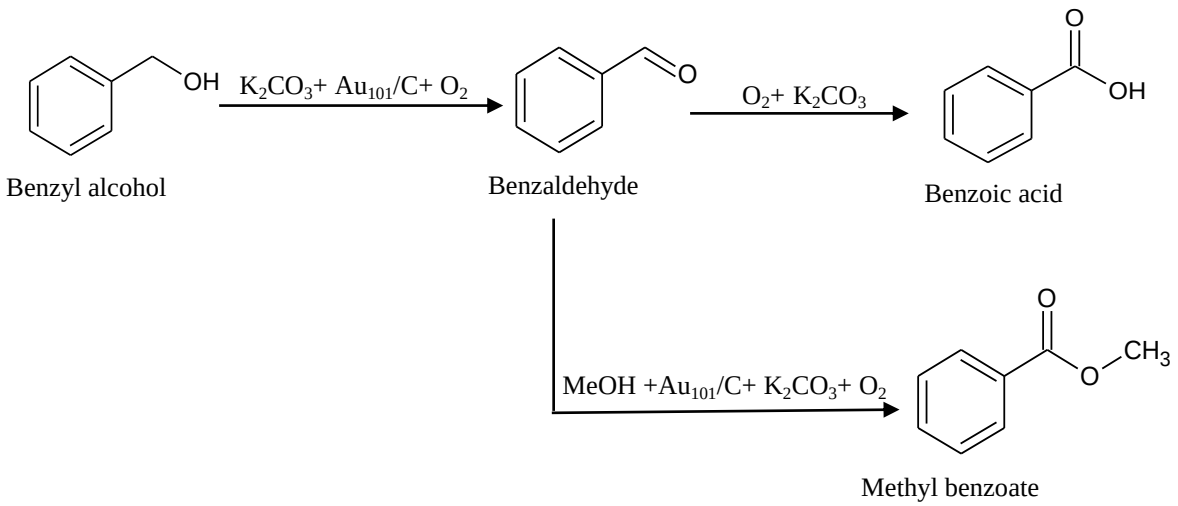

Scheme 0.1: Reaction pathway of benzyl alcohol oxidation in the presence of the base and methanol by activated 1.0 wt% Au_{101}/C catalysts.

This mechanism relies on benzyl alcohol being oxidized to benzaldehyde with further oxidization to benzoic acid and also to methyl benzoate in the presence of the base, the solvent (methanol) and gold catalysts.[25a, 29, 37, 41] Feasibility of oxidative esterification of benzaldehyde in the presence of gold catalysts, methanol and the base were investigated and formation of ester was confirmed (see Table 3.5).[30a, 69]

Table 0.5: Results of the control experiment using benzoic acid and benzaldehyde as starting materials.

	Conversion%	**Selectivity%**		
		Benzaldehyde	**Benzoic acid**	**Methyl benzoate**
[a] **Benzoic acid**	0	0	100	0
[b] **Benzoic acid**	0	0	100	0
Benzaldehyde	100	0	37	63

Conditions: Reactant: 2.5 mmol, Anisole: 1.25 mmol, Methanol: 25 mL, Temperature: 80 ^oC, Pressure: 73 psi, Time: 24 h, Stirring: 750 rpm, activated 1.0% Au_{101}/C: 50 mg, *a*: 2.5 & *b*: 1.25 mmol of K_2CO_3.

To test this mechanism, we performed catalytic reactions using benzaldehyde or benzoic acid as the starting materials. Table 3.5 presents the results showing no reaction of benzoic acid,

but full conversion of benzaldehyde to methyl benzoate (the major product) and benzoic acid.[31, 47] To avoid the possibility of misinterpretation due to any significant change in the pH, two ratios (1 and 2) of benzoic acid to the base were considered, but no benzoic acid conversion was observed (see Table 3.5, footnotes *a* & *b*). Hence, it can be concluded that benzyl alcohol in methanol oxidizes to methyl benzoate *via* benzaldehyde.[30a] The formation of methyl benzoate indicates that methanol is not merely an inert solvent, but participates as a reactant,[29, 47] which is consistent with previous research.[29-30, 47] The involvement of the solvent suggests that changing the solvent to ethanol should produce ethyl benzoate.[70] Indeed, this prediction was confirmed (see Table 3.7), but benzoic acid is not converted to an ester as efficiently in ethanol under similar conditions.[26a, 37]

3.2.4 Effect of a base (K_2CO_3)

Carbonates have been widely applied as weak bases in many organic synthesis reactions, particularly those involving deprotonation. In most of these syntheses, a stoichiometric excess of a carbonate is required to achieve high reaction efficiencies.[71] In addition, carbonates are soluble in alcohol and they are cheap.[31] As seen in Table 3.6 and Figure 3.3, the base plays an important role in the Au_{101}/C-catalysed oxidation of benzoic acid, both in terms of conversion and selectivity. In the experiments discussed below, all parameters were constant with amounts of benzyl alcohol and the base (mmol) modified to reach the best catalytic performance. The ratio of benzyl alcohol to the base (k_2CO_3) was abbreviated as following: A): 2.5 mmol of benzyl alcohol to 2.5 mmol of the base, B): 2.5 mmol of benzyl alcohol to 1.25 mmol of the base, C): 1.25 mmol of benzyl alcohol to 2.5 mmol of the base, and D): 1.25 mmol of benzyl alcohol to 1.25 mmol of the base. There is no conversion in the absence of base, which accords with previous reports.[29] However, conversion improved with addition of K_2CO_3, reaching C = 100% at a 1:1 mole ratio of the base to benzyl alcohol (*i.e.*, A and D) after 24 hours of reaction at 80 ^oC (see Figure 3.3).[26a, 32-33]

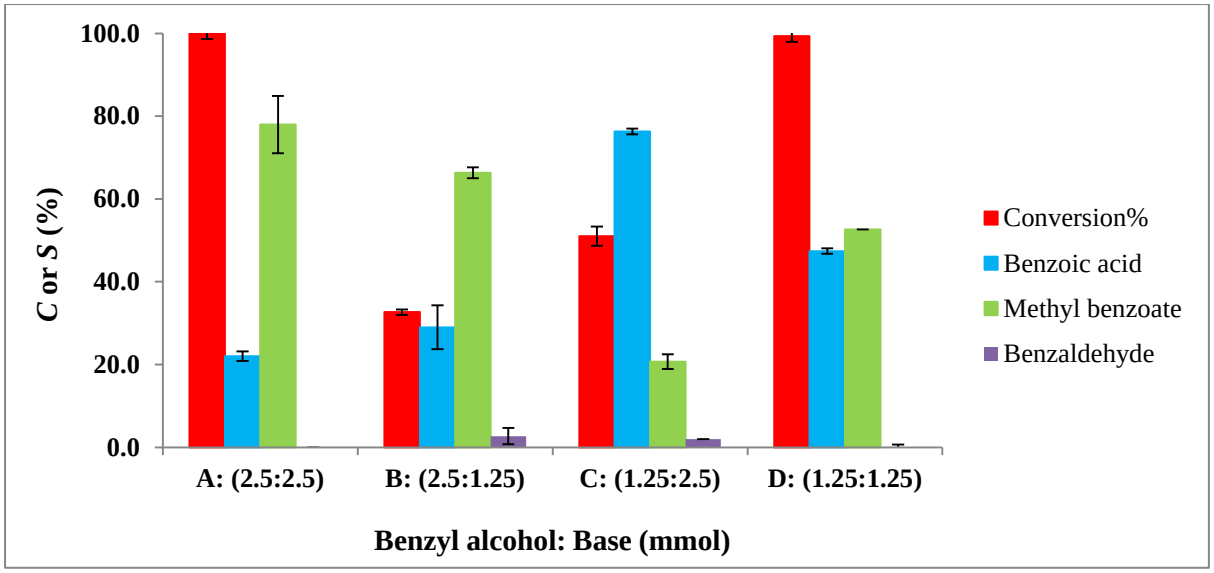

Figure 0.3: Ratio of benzyl alcohol to the base on conversion (*C%*) and selectivity (*S%*) of activated 1.0 wt% Au_{101}/C catalysts. A, B, C and D were mmol of benzyl alcohol to mmol of the base.

Changes in the base concentration affect the selectivity, too. An equimolar, 2.5 mmol: 2.5 mmol, mixture gives 100% conversion of benzyl alcohol with selectivity of ~78% towards methyl benzoate (A in Figure 3.3). Decreasing the amount of K_2CO_3 led to a decrease of conversion to 33% but with the no significant change in selectivity (B in Figure 3.3).[3a, 33] However, decreasing the amount of benzyl alcohol to 1.25 mmol led to a decrease in the alcohol conversion to 51% towards benzoic acid as the main product (~76%) with methyl benzoate (~20 %) and benzaldehyde (~2%) when the amount of base is 100% greater than the amount of the reactant (*i.e., C*).[32-33] Clearly, the base not only facilitates the catalytic reaction,[72] but also accelerates the oxidation of benzaldehyde to methyl ester and benzoic acid.

Table 0.6: The effect of 2.5 mmol of K_2CO_3 as a base on the catalytic activity of activated 1.0 wt% Au_{101}/C catalysts on 2.5 mmol of benzyl alcohol oxidation.

Base	**Conversion%**	**Selectivity%**		
		Benzaldehyde	**Benzoic acid**	**Methyl benzoate**
With base	100	0	22	78
Without base	0	0	0	0

The results showed that the ratio of benzyl alcohol to the base plays a crucial role in the catalytic activity and selectivity of benzyl alcohol oxidation. The highest activity of gold catalysts (100%) occurred when this ratio was adjusted to 1 (*i.e.*, A and D) regardless of actual reagent concentrations.[26a, 32] At this concentration the main product was methyl benzoate;[30c] but whereas, in the case of D, where the amounts are lower (1.25 mmol), the product branching ratio (methyl benzoate to benzoic acid) was near 1:1, changing to 4:1 in case A, where the amounts were larger (2.5 mmol). In case of B (2.5 mmol: 1.25 mmol), the product branching ratio was 3:1 (methyl benzoate to benzoic acid), but in case C (1.25 mmol: 2.5 mmol), the main product was benzoic acid with a product ratio of ~1:3 (the ester to acid). Benzaldehyde appeared as the minor product (less than 3%) only when the conversion was low(~50%).[53] Since both the highest conversion (100%) and the highest selectivity towards one of the products (the ester: 78%) was observed when the amounts of benzyl alcohol and K_2CO_3 were both 2.5 mmol, these conditions were chosen for further experiments.[73]

3.2.5 Reaction temperature

To achieve full conversion in the oxidation of alcohols, an elevated reaction temperature is usually needed.[30a] Figure 3.4 shows conversion and selectivity as functions of reaction temperature up to 100 ^{o}C over a reaction period of 24 hours with an initial benzyl alcohol to base ratio of 2.5 mmol: 2.5mmol. Below ~ 40 ^{o}C, conversion (the red line in Figure 3.4) is less than 10% but then it increases rather dramatically to 86% at ~ 60 ^{o}C, ~100% at ~80 ^{o}C and slightly decreased to 96% at 100 ^{o}C. At lower temperatures, methyl benzoate is the strongly favoured product, with a small amount of benzaldehyde being produced. Earlier studies indicate that the methyl benzoate reaction competes more favourably at mild temperature.[24a, 36, 74] Here, we observed that the methyl benzoate to benzoic acid product ratio levels off at *ca*. 2:1 over the range ~ 60–100 ^{o}C. The weak selectivity for benzaldehyde decreases to essentially zero, while that for the acid product increases with increasing

temperature from 40 to 100 °C.[24a, 41] The 80 °C point appears to represent the low-temperature end of a range of catalytic activity above which conversion is 100% and the product ratio is relatively temperature independent. Therefore, this temperature was selected for our follow-up experiments. Methyl benzoate was also found by Haruta *et al.* to be the favoured product at 80 °C, but the conversion they reported was only 86%.[29]

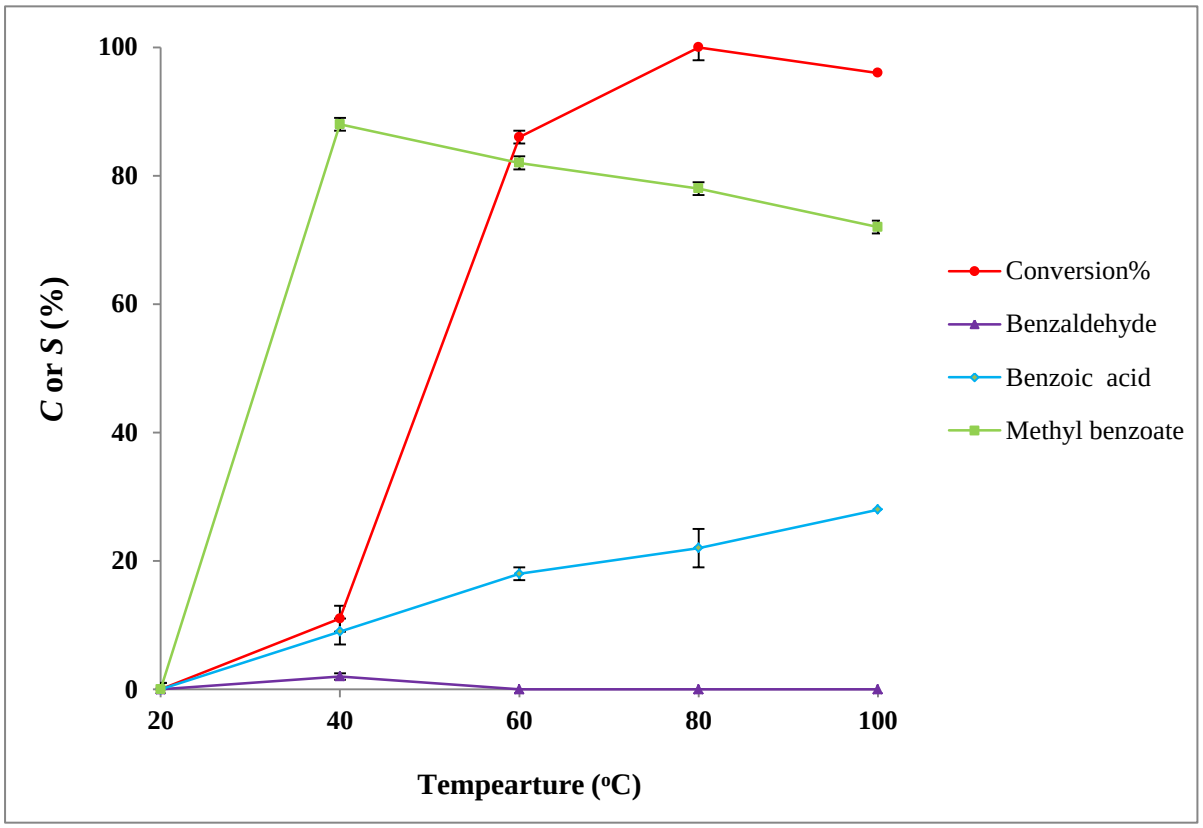

Figure 0.4: The effect of temperature on the catalytic activity (*C%*) and selectivity (*S%*) of activated 1.0 wt% Au_{101}/C catalysts.

3.2.6 Choice of solvent

For industrially relevant catalysis, the use of a starting material with no solvent would help to minimize costs and the need of separation, and would also diminish environmental risks. However, in the case of these reactions there are practical limitations relating to gas pressure and the head space of reactor that require the use of a solvent (as described above). In this section, toluene (as a non-polar solvent), ethanol and methanol (as polar solvents) were

utilized to study the effect of solvents on conversion and selectivity in benzyl alcohol oxidation. Despite some published reports indicating conversion with toluene as a solvent,[26a, 66] Dimitratos *et al.* found no conversion by supported gold catalysts under reaction conditions where benzyl alcohol: 0.3 M, benzyl alcohol/metal 1/500 (mol/mol), T: 333 K, t: 3 h, pO_2: 1.5 atm.[30c] In our study, no conversion was observed when toluene was utilized as a solvent.

As described above, methanol is an appropriate solvent for this reaction, giving high conversion and selectivity towards of methyl benzoate under appropriate conditions.[26a, 29, 37] However, with ethanol as a solvent, conversion dropped to ~34%, with selectivity to ethyl benzoate of ~11% towards and ~80% production of other materials (see Table 3.7).[37, 74] Ethanol may undergo oxidative self-esterification leading to formation of appreciable amounts of products, such as ethyl acetate.[36, 75] Although, methanol can also be oxidized directly to methyl esters in high yields at mild condition,[22b, 35, 37] other primary alcohols oxidize much more rapidly.[30a]

Table 0.7: The effect of solvents on conversion and selectivity of benzyl alcohol oxidation using activated 1.0 wt% Au_{101}/C.

Solvent	**Conversion%**	**Selectivity%**				
		Benzaldehyde	**Benzoic acid**	**Methyl benzoate**	**Ethyl benzoate**	**Others**
Methanol	100	0	22	78	0	0
Ethanol	34	1	8	0	11	80
Toluene	0	0	0	0	0	0

These results showed that activity and selectivity of products depend on the types of solvents used. For benzyl alcohol oxidation, methanol was the best of the solvents considered, showing the highest conversion and selectivity. For further experiments methanol was selected as a solvent of choice.

3.2.7 Gold loading

All catalytic materials used in this part of the research were freshly made (on the same day as the tests) using the same fresh batch of Au_{101} to avoid potential aggregation during storage. Table 3.8 presents the effect of gold loadings on the catalytic activity of the catalyst for benzyl alcohol oxidation. The highest conversion (100% over 24 hours) occurred for 1.0 wt% gold loading. The conversion decreased to 51% when the gold loading was decreased to 0.5 wt% with the same, 50 mg, total mass of the catalyst used. No conversion was observed for 0.2 wt% gold loading. In similar vein, Boronat *et al.* studied the effect of gold loadings on benzyl alcohol oxidation and found that the highest turnover frequency (TOF) occurred at 0.8 wt% loading among 0.4, 0.8 and 1.5 wt%.[59]

The effect of the total *amount* of gold used in the reaction was studied by carrying out a test using a five-fold scale-up (250 mg) of the catalyst with 0.2 wt% (indicated as 5×0.2 in the bottom row of Table 3.9). If catalytic efficiency were dependent on only the amount of gold, this last test should give the same results as that using 50 mg of the catalyst with 1.0 wt%. However, the result confirmed negligible activity (2%) for 250 mg of gold catalyst. A change in the amount of carbon (*i.e.*, five times more for 5×0.2 wt% than for 1.0 wt%) may cause a relatively modest increase in the amount of solid in the reaction vessel which has a negative impact on stirring/mass transfer.

Table 0.8: Gold nanoparticles size and conversion values for benzyl alcohol oxidation using activated Au_{101}/C catalysts with different gold loading rates.

Gold loading (wt%)	Average particle diameter (nm)	Au_{101}/C (g)	*C*%	*S*%		
				Benzaldehyde	Benzoic acid	Methyl benzoate
[a]**1**	3.0 ± 0.1	0.05/5	100	0	22	78
[b]**0.5**	3.6 ± 0.1	0.025/5	51	1	61	38
[c]**0.2**	4.1 ± 0.2	0.01/5	0	0	0	0
[d]**(5×0.2)**	4.1 ± 0.2	0.01/5	2	0	100	0

Reaction conditions: Benzyl alcohol: 2.5 mmol, Anisole: 1.25 mmol, Base: 2.5 mmol, Solvent: 25 mL, Temperature: 80 °C, Pressure: 73 psi, Stirring: 750 rpm, Time: 24 h, *a-c*: Activated 1.0, 0.5 and 0.2 wt % Au_{101}/C: 50 mg & *d*: (5×0.2 wt %) Au_{101}/C: 250 mg.

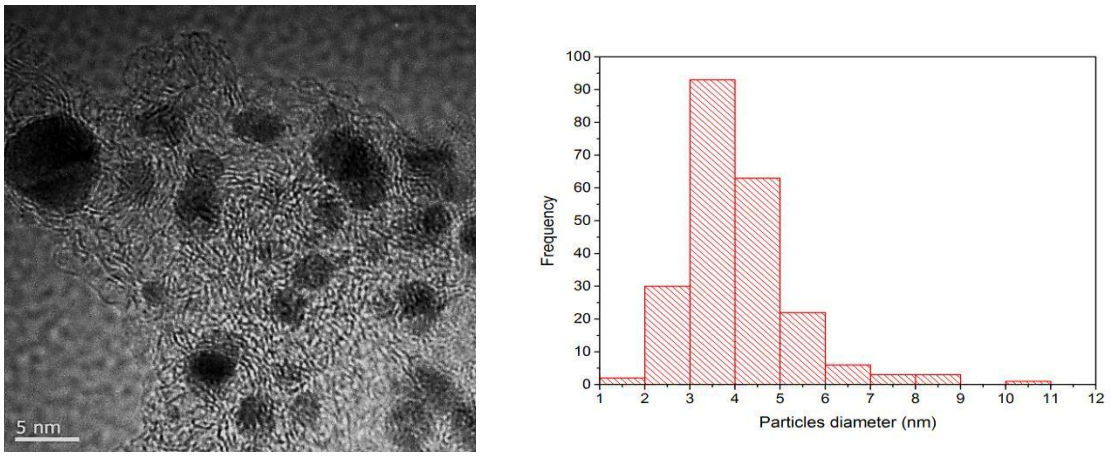

Figure 0.5: Left: a representative TEM image of activated 0.2 wt% Au_{101}/C deposited onto carbon film coated Cu TEM grid; Right: Particle size distribution histogram. The average particle size of gold particles was determined to be 4.1 ± 0.2 nm (two standard deviations of the mean).

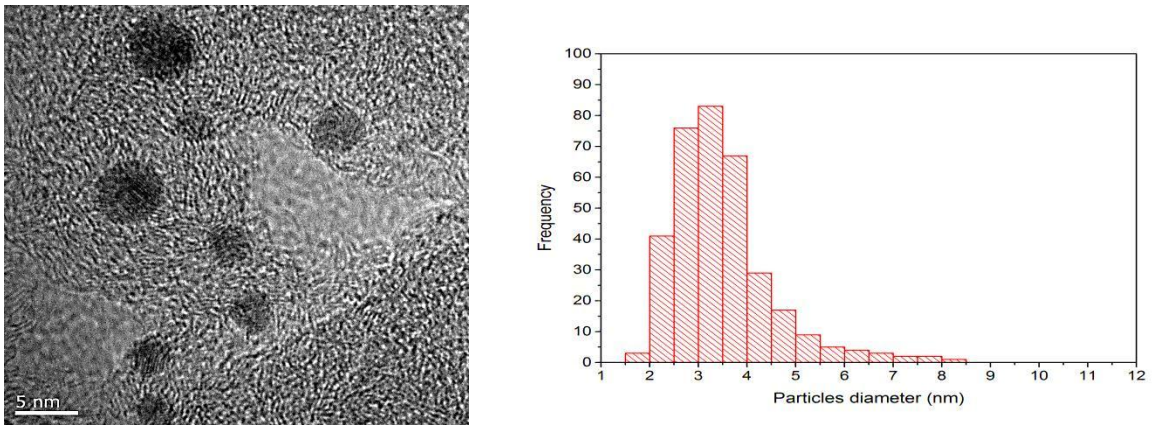

Figure 0.6: Left: a representative TEM image of activated 0.5 wt% Au_{101}/C deposited onto carbon film coated Cu TEM grid; Right: Particle size distribution histogram. The average particle size of gold particles was determined to be 3.6 ± 0.1 nm (two standard deviations of the mean)

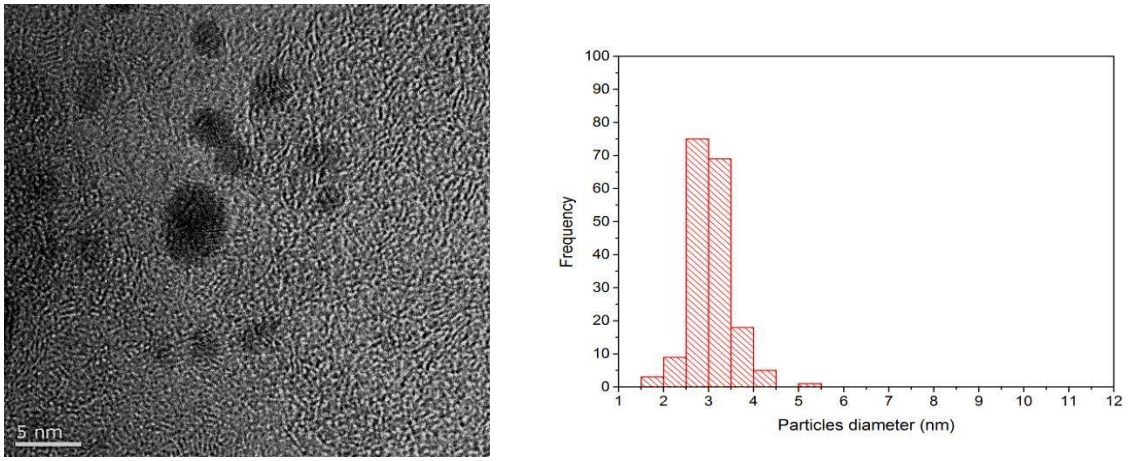

Figure 0.7: Left: a representative TEM image of activated 1.0 wt% Au_{101}/C deposited onto carbon film coated Cu TEM grid; Right: Particle size distribution histogram. The average particle size of gold particles was determined to be 3.0 ± 0.1 nm (two standard deviations of the mean).

To investigate the last possibility, we carried out a study of the particle sizes and size distributions for three representative activated samples (washed with toluene followed by calcination under static air at 100 ^{o}C for 3 hours), with 1.0, 0.5 and 0.2 wt% loadings, by means of transmission electron microscopy (TEM) (see Figures 3.5–3.7 and Table 3.9). The results showed that the smallest average particles diameter (3.0 ± 0.1 nm) belonged to the sample with 1.0 wt% gold loading. Those with 0.5 and 0.2 wt% gold loadings showed progressively bigger average particles diameters of 4.1 ± 0.2 and 3.6 ± 0.1 nm, respectively.[76] The finding that the particle size decreases at higher loading is counter-intuitive as an increase in particle size would be normally expected with increase in metal loading. Yet, obtained result is consistent with results reported by Rodrı´guez-Gonza´lez *et al.* in that gold particle diameters decreased from 3.1 to 2.4 nm when the gold loading increased from 1.0 to 6.7 or 12.3 wt%. However, the authors did not provide further explanation why the average gold particle size decreased when the gold loading increased. Further research is required to provide better understanding on the effect of gold loading on the average gold particle size in both cases (the case reported here and that reported by Rodrı´guez-Gonza´lez *et al.*).

It is all very well to recognise a correlation between loading and particles size, but a reasonable explanation is needed to rationalise both this observation and its causal effect (if any) on the very large differences in activity between gold catalysts that were otherwise prepared following the same method. The activity of a gold catalyst is closely associated with the number of Au active sites and the size of gold particles.[50] In these experiments the largest gold particles were obtained at the lowest gold loading (0.2 wt%) and resulted in the least active catalyst. This suggests that the smaller (3.0 ± 0.1 nm) gold particles size were responsible for the much greater activity of the 1.0 wt% gold catalysts. Similarly, Boronat *et al.* found that particles with *ca*. 3.3 nm diameter in a gold catalyst with 0.8 wt % resulted in the most efficient oxidation of benzyl alcohol among 0.4, 0.8 and 1.5 wt% samples, which had particles with sizes of 1.9, 3.3 and 4.1 nm, respectively.[59]

Since 1.0 wt% Au catalyst demonstrated much better catalytic performance than the other loadings, it was determined to be the most suitable for benzyl alcohol oxidation. TEM images indicated that a 1.0 wt % gold catalyst possesses the gold particles with a narrow size distribution of Au species, which may correlate with the largest number of surface-bound activated oxygen species that facilitate benzyl alcohol oxidation. For further experiments 1.0 wt% gold loading was selected as an optimal metal loading.

3.2.8 Long-term stability of gold catalysts and reactant/products mixtures

Gold nanoparticles supported on certain support materials, such as TiO_2 and CeO_2, can aggregate spontaneously upon storage at room temperature, with light-induced aggregation often having been reported.[24a, 26a, 77] The stability depends on both the support's structure and its specific interaction between gold particles and the support.[53, 78] Heidkamp *et al.* investigated deactivation of the catalytic activity of gold nanoparticles supported on ceria

during storage in a dark place at room temperature, finding that fresh samples were four times more active than stored ones.[79] The Au_{101}/C catalysts used in this project were normally stored in a freezer, at or below - 4 ^{o}C, under N_2 and in the dark, because gold catalysts can be aggregated by heat and/or light during storage.[15, 80] Investigations into the stability of gold on the carbon support under these storage conditions were one of the novelties of the current study, as to the best of my knowledge such studies were not reported in the literature.

In this section, comparisons of the catalytic activity and selectivity between freshly made and stored catalysts (*i.e.*, kept in a freezer for 6 months) proved that the gold catalysts used in this study have very good long-term stability of catalytic activity (see Table 3.9). TEM images of freshly made and stored gold samples showed average particle diameters of ~3 nm for both samples (see Figure 3.8). This long-term stability is an excellent result if these were ever considered for industrial application.[80c]

Table 0.9: The effect of storage on the catalytic activity of activated 1.0 wt% Au_{101}/C catalysts.

	Conversion%	**Selectivity%**		
		Benzaldehyde	**Benzoic acid**	**Methyl benzoate**
Fresh Au_{101}/C	75	0	22	78
Stored Au_{101}/C	74	0	24	74

Conditions: Benzyl alcohol: 2.5 mmol, Anisole: 1.25 mmol, Methanol: 25 mL, Base: 2.5 mmol, Temperature: 80 ^{o}C, Pressure: 73 psi, Time: 24 h, Stirring: 750 rpm and 50 mg of activated 1.0 wt % Au_{101}/C (washed with toluene followed by calcination under static air at 100 ^{o}C for 3 h).

a) 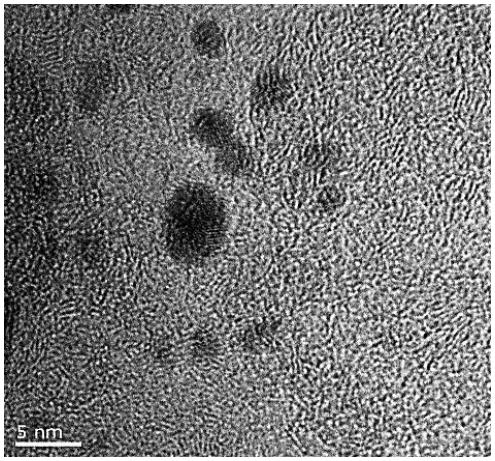

b) 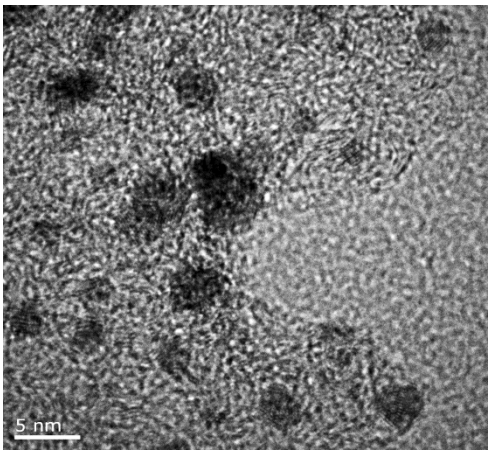

Figure 0.8: TEM images of a) fresh & b) restored activated 1.0 wt% Au_{101}/C catalysts (washed with toluene followed by calcination under static air at 100 ^{o}C for 3 h) deposited onto carbon film coated copper TEM grid.

In addition to the stability of gold catalysts as previously examined in details, it was important to establish the stability of the reactants/product mixtures due to limited access to the HPLC instrument. I often had to store product mixtures over short (a day) to medium (a week) times. Hence, it was important to establish the stability of the product mixtures. A range of samples including benzyl alcohol, anisole, benzaldehyde, methyl benzoate and benzoic acid were studied, with and without base, at room temperature and after refrigerator and freezer storage. Samples stored in a freezer were quite stable with or without the base (K_2CO_3). Interestingly, the results demonstrated that base can stabilize the product mixtures, which were stable even at room temperature in the presence of the base.[30a]

3.3 Conclusions

The present study shows that activated 1.0 wt% Au_{101}/C can be employed as a catalyst for liquid-phase oxidation of benzyl alcohol under mild conditions. The selectivity of the catalyst was towards was methyl benzoate and benzoic acid as the main products. Based on the results discussed in this chapter, the following catalytic test conditions were selected for further studies: oxygen gas pressure of 73 psi; reaction temperature of 80 ^{o}C; methanol as a solvent,

2.5 mmol of K_2CO_3 as a base in an equimolar proportion to benzyl alcohol, a gold loading of 1.0 wt% and a reaction time of 24 hours. Anisole (1.25 mmol) was established as an appropriate internal standard. Under these conditions, the gold catalysts showed high conversions, as well as good long-term stability.

References

1. Haruta, M.; Yamada, N.; Kobayashi, T.; Iijima, S., Gold catalysts prepared by coprecipitation for low-temperature oxidation of hydrogen and of carbon monoxide. *J. Catal.* **1989,** *115* (2), 301-309.
2. (a) Bamwenda, G. R.; Tsubota, S.; Nakamura, T.; Haruta, M., The influence of the preparation methods on the catalytic activity of platinum and gold supported on TiO_2 for CO oxidation. *Catal. Lett.* **1997,** *44* (1-2), 83-87; (b) Valden, M.; Lai, X.; Goodman, D. W., Onset of catalytic activity of gold clusters on titania with the appearance of nonmetallic properties. *Science* **1998,** *281* (5383), 1647-1650; (c) Haruta, M., Gold as a low-temperature oxidation catalyst: Factors controlling activity and selectivity. *Stud. Surf. Sci. Catal.* **1997,** *110*, 123-134.
3. (a) Chang, C. M.; Cheng, C.; Wei, C. M., CO oxidation on unsupported Au_{55}, Ag_{55}, and $Au_{25}Ag_{30}$ nanoclusters. *J. Chem. Phys.* **2008,** *128* (12), 124710/1-124710/4; (b) Pei, Y.; Shao, N.; Gao, Y.; Zeng, X. C., Investigating active site of gold nanoparticle $Au_{55}(PPh_3)_{12}Cl_6$ in selective oxidation. *ACS Nano* **2010,** *4* (4), 2009-2020.
4. (a) Chi, L. F.; Rakers, S.; Hartig, M.; Gleiche, M.; Fuchs, H.; Schmid, G., Monolayers of nanosized Au_{55}-clusters: Preparation and characterization. *Colloids Surf., A* **2000,** *171* (1-3), 241-248; (b) Zhang, H.; Mautes, D.; Hartmann, U., Negative differential resistance and nonclassical capacitive behaviour in networks of metal clusters. *Nanotechnology* **2007,** *18* (6), 065202.
5. (a) Turner, M.; Golovko, V. B.; Vaughan, O. P. H.; Abdulkin, P.; Berenguer-Murcia, A.; Tikhov, M. S.; Johnson, B. F. G.; Lambert, R. M., Selective oxidation with dioxygen by gold nanoparticle catalysts derived from 55-atom clusters. *Nature* **2008,** *454* (7207), 981-983; (b) Yuan, Y.; Kozlova, A. P.; Asakura, K.; Wan, H.; Tsai, K.; Iwasawa, Y., Supported Au catalysts prepared from Au phosphine complexes and As-precipitated metal hydroxides: Characterization and low-temperature CO oxidation. *J. Catal.* **1997,** *170* (1), 191-199.
6. Schmid, G.; Pfeil, R.; Boese, R.; Bandermann, F.; Meyer, S.; Calis, G. H. M.; Vandervelden, W. A., $AU_{55}[P(C_6H_5)_3]_{12}CL_6$ -A gold cluster of an exceptional size. *Chem. Ber. Recl.* **1981,** *114* (11), 3634-3642.
7. Hutchinson, J. E.; Foster, E. W.; Warner, M. G.; Reed, S. M.; Weare, W. W., Triphenylphosphine-stabilised gold nanoparticles. In *Inorganic synthsis*, Shapley, J. R., Ed. John Wiley & Sons: 2004; Vol. 34 pp 228-232.
8. Cárdenas-Lizana, F.; Gómez-Quero, S.; Perret, N.; Keane, M. A., Support effects in the selective gas phase hydrogenation of p-chloronitrobenzene over gold. *Gold Bull.* **2009,** *42* (2), 124-132.
9. Bulushev, D. A.; Yuranov, I.; Suvorova, E. I.; Buffat, P. A.; Kiwi-Minsker, L., Highly dispersed gold on activated carbon fibers for low-temperature CO oxidation. *J. Catal.* **2004,** *224* (1), 8-17.
10. Raghuveer, V.; Manthiram, A., Mesoporous carbons with controlled porosity as an electrocatalytic support for methanol oxidation. *J. Electrochem. Soc.* **2005,** *152* (8), A1504-A1510.
11. Prati, L.; Rossi, M., Gold on carbon as a new catalyst for selective liquid phase oxidation of diols. *J. Catal.* **1998,** *176* (2), 552-560.
12. J. Branton, P.; S. W. Sing, K.; W. White, J., Adsorption of carbon tetrachloride and nitrogen by 3.4 nm pore diameter siliceous MCM-41. *J. Chem. Soc., Faraday Trans.* **1997,** *93* (13), 2337-2340.
13. Schmidt, W., Calculation of XRD patterns of simulated FDU-15, CMK-5, and CMK-3 carbon structures. *Microporous Mesoporous Mater.* **2009,** *117* (1–2), 372-379.
14. Kauffman, D. R.; Alfonso, D.; Matranga, C.; Li, G.; Jin, R. C., Photomediated oidation of atomically precise $Au_{25}(SC_2H_4Ph)_{18}^-$ nanoclusters. *J. Phys. Chem. Lett.* **2013,** *4* (1), 195-202.
15. Anderson, D. P.; Adnan, R. H.; Alvino, J. F.; Shipper, O.; Donoeva, B.; Ruzicka, J. Y.; Al Qahtani, H.; Harris, H. H.; Cowie, B.; Aitken, J. B.; Golovko, V. B.; Metha, G. F.; Andersson, G. G., Chemically synthesised atomically precise gold clusters deposited and activated on titania. Part II. *PCCP* **2013,** *15* (35), 14806-14813.
16. Chen, Y.; Qiu, J.; Wang, X.; Xiu, J., Preparation and application of highly dispersed gold nanoparticles supported on silica for catalytic hydrogenation of aromatic nitro compounds. *J. Catal.* **2006,** *242* (1), 227-230.

17. (a) Bond, C.; Louis, C.; Thompson, D. T., The phenomenon of catalysis. In *Catalysis by gold*, First ed.; Hutchings, G., Ed. Imperial College Press: London,UK, 2006; Vol. 6, pp 1-4; (b) Lopez-Sanchez, J. A.; Dimitratos, N.; Hammond, C.; Brett, G. L.; Kesavan, L.; White, S.; Miedziak, P.; Tiruvalam, R.; Jenkins, R. L.; Carley, A. F.; Knight, D.; Kiely, C. J.; Hutchings, G. J., Facile removal of stabilizer-ligands from supported gold nanoparticles. *Nat. Chem.* **2011,** *3* (7), 551-556.
18. (a) Okumura, M.; Tsubota, S.; Haruta, M., Preparation of supported gold catalysts by gas-phase grafting of gold acethylacetonate for low-temperature oxidation of CO and of H_2. *J. Mol. Catal. A: Chem.* **2003,** *199* (1–2), 73-84; (b) Tsubota, S.; Nakamura, T.; Tanaka, K.; Haruta, M., Effect of calcination temperature on the catalytic activity of Au colloids mechanically mixed with TiO_2 powder for CO oxidation. *Catal. Lett.* **1998,** *56* (3-4), 131-135.
19. Haruta, M., Catalysis: Gold rush. *Nature* **2005,** *437* (7062), 1098-1099.
20. Abad, A.; Corma, A.; García, H., Supported gold nanoparticles for aerobic, solventless oxidation of allylic alcohols. *Pure Appl. Chem.* **2007,** *79* (11), 1847-1854.
21. Suramanee, P.; Poompradub, S.; Rojanathanes, R.; Thamyongkit, P., Effects of reaction parameters in catalysis of glycerol oxidation by citrate-stabilized gold nanoparticles. *Catal. Lett.* **2011,** *141* (11), 1677-1684.
22. (a) Hereijgers, B. P. C.; Weckhuysen, B. M., Selective oxidation of methanol to hydrogen over gold catalysts promoted by alkaline-earth-metal and lanthanum oxides. *ChemSusChem* **2009,** *2* (8), 743-748; (b) Kähler, K.; Holz, M. C.; Rohe, M.; van Veen, A. C.; Muhler, M., Methanol oxidation as probe reaction for active sites in Au/ZnO and Au/TiO_2 catalysts. *J. Catal.* **2013,** *299* (0), 162-170.
23. Carrettin, S.; McMorn, P.; Johnston, P.; Griffin, K.; Hutchings, G. J., Selective oxidation of glycerol to glyceric acid using a gold catalyst in aqueous sodium hydroxide. *Chem. Commun.* **2002,** (7), 696-697.
24. (a) Choudhary, V. R.; Jha, R.; Jana, P., Solvent-free selective oxidation of benzyl alcohol by molecular oxygen over uranium oxide supported nano-gold catalyst for the production of chlorine-free benzaldehyde. *Green Chem.* **2007,** *9* (3), 267-272; (b) Tsunoyama, H.; Tsukuda, T.; Sakurai, H., Synthetic application of PVP-stabilized Au nanocluster catalyst to aerobic oxidation of alcohols in aqueous solution under ambient conditions. *Chem. Lett.* **2007,** *36* (2), 212-213.
25. (a) Villa, A.; Janjic, N.; Spontoni, P.; Wang, D.; Su, D. S.; Prati, L., Au-Pd/AC as catalysts for alcohol oxidation: Effect of reaction parameters on catalytic activity and selectivity. *Appl. Catal., A* **2009,** *364* (Copyright (C) 2012 American Chemical Society (ACS). All Rights Reserved.), 221-228; (b) Miedziak, P. J.; Kondrat, S. A.; Sajjad, N.; King, G. M.; Douthwaite, M.; Shaw, G.; Brett, G. L.; Edwards, J. K.; Morgan, D. J.; Hussain, G.; Hutchings, G. J., Physical mixing of metal acetates: Optimisation of catalyst parameters to produce highly active bimetallic catalysts. *Catal. Sci. Technol.* **2013,** *3* (11), 2910-2917; (c) Abad, A.; Corma, A.; García, H., Catalyst parameters determining activity and selectivity of supported gold nanoparticles for the aerobic oxidation of alcohols: The molecular reaction mechanism. *Chem.- Eur. J.* **2008,** *14* (1), 212-222.
26. (a) Hu, J.; Chen, L.; Zhu, K.; Suchopar, A.; Richards, R., Aerobic oxidation of alcohols catalyzed by gold nano-particles confined in the walls of mesoporous silica. *Catal. Today* **2007,** *122* (3-4), 277-283; (b) Pina, C. D.; Falletta, E.; Rossi, M., Update on selective oxidation using gold. *Chem. Soc. Rev.* **2011**.
27. Choudhary, V. R.; Dhar, A.; Jana, P.; Jha, R.; Uphade, B. S., A green process for chlorine-free benzaldehyde from the solvent-free oxidation of benzyl alcohol with molecular oxygen over a supported nano-size gold catalyst. *Green Chem.* **2005,** *7* (11), 768-770.
28. (a) Meenakshisundaram, S.; Nowicka, E.; Miedziak, P. J.; Brett, G. L.; Jenkins, R. L.; Dimitratos, N.; Taylor, S. H.; Knight, D. W.; Bethell, D.; Hutchings, G. J., Oxidation of alcohols using supported gold and gold-palladium nanoparticles. *Faraday Discuss.* **2010,** *145*, 341-356; (b) Ma, C. Y.; Dou, B. J.; Li, J. J.; Cheng, J.; Hu, Q.; Hao, Z. P.; Qiao, S. Z., Catalytic oxidation of benzyl alcohol on Au or Au-Pd nanoparticles confined in mesoporous silica. *Appl. Catal., B* **2009,** *92* (Copyright (C) 2012 American Chemical Society (ACS). All Rights Reserved.), 202-208.
29. Ishida, T.; Nagaoka, M.; Akita, T.; Haruta, M., Deposition of gold clusters on porous coordination polymers by solid grinding and their catalytic activity in aerobic oxidation of alcohols. *Chem.- Eur. J.* **2008,** *14* (28), 8456-8460.

30. (a) Klitgaard, S. K.; Dela Riva, A. T.; Helveg, S.; Werchmeister, R. M.; Christensen, C. H., Aerobic oxidation of alcohols over gold catalysts: Role of acid and base. *Catal. Lett.* **2008,** *126* (3-4), 213-217; (b) Fristrup, P.; Johansen, L. B.; Christensen, C. H., Mechanistic investigation of the gold-catalyzed aerobic oxidation of alcohols. *Catal. Lett.* **2008,** *120* (3-4), 184-190; (c) Dimitratos, N.; Villa, A.; Wang, D.; Porta, F.; Su, D.; Prati, L., Pd and Pt catalysts modified by alloying with Au in the selective oxidation of alcohols. *J. Catal.* **2006,** *244* (1), 113-121.
31. Li, F.; Zhang, Q.; Wang, Y., Size dependence in solvent-free aerobic oxidation of alcohols catalyzed by zeolite-supported palladium nanoparticles. *A. Appl. Catal., B* **2008,** *334* (1–2), 217-226.
32. Carrettin, S.; McMorn, P.; Johnston, P.; Griffin, K.; Kiely, C. J.; Hutchings, G. J., Oxidation of glycerol using supported Pt, Pd and Au catalysts. *PCCP* **2003,** *5* (6), 1329-1336.
33. Biella, S.; Castiglioni, G. L.; Fumagalli, C.; Prati, L.; Rossi, M., Application of gold catalysts to selective liquid phase oxidation. *Catal. Today* **2002,** *72* (1-2), 43-49.
34. Zope, B. N.; Hibbitts, D. D.; Neurock, M.; Davis, R. J., Reactivity of the gold/water interface during selective oxidation catalysis. *Science* **2010,** *330* (6000), 74-78.
35. Oliveira, R. L.; Kiyohara, P. K.; Rossi, L. M., Clean preparation of methyl esters in one-step oxidative esterification of primary alcohols catalyzed by supported gold nanoparticles. *Green Chem.* **2009,** *11* (9), 1366-1370.
36. Zheng, N.; Stucky, G. D., Promoting gold nanocatalysts in solvent-free selective aerobic oxidation of alcohols. *Chem. Commun.* **2007,** (37), 3862-3864.
37. Choudhary, V. R.; Dumbre, D. K., Magnesium oxide supported nano-gold: A highly active catalyst for solvent-free oxidation of benzyl alcohol to benzaldehyde by TBHP. *Catal. Commun.* **2009,** *10* (13), 1738-1742.
38. Hou, W.; Dehm, N. A.; Scott, R. W. J., Alcohol oxidations in aqueous solutions using Au, Pd, and bimetallic AuPd nanoparticle catalysts. *J. Catal.* **2008,** *253* (1), 22-27.
39. Hughes, M. D.; Xu, Y. J.; Jenkins, P.; McMorn, P.; Landon, P.; Enache, D. I.; Carley, A. F.; Attard, G. A.; Hutchings, G. J.; King, F.; Stitt, E. H.; Johnston, P.; Griffin, K.; Kiely, C. J., Tunable gold catalysts for selective hydrocarbon oxidation under mild conditions. *Nature* **2005,** *437* (7062), 1132-1135.
40. Choudhary, V.; Dumbre, D., Supported Nano-Gold Catalysts for Epoxidation of Styrene and Oxidation of Benzyl Alcohol to Benzaldehyde. *Top. Catal.* **2009,** *52* (12), 1677-1687.
41. Guan, B.; Xing, D.; Cai, G.; Wan, X.; Yu, N.; Fang, Z.; Yang, L.; Shi, Z., Highly selective aerobic oxidation of alcohol catalyzed by a gold(I) complex with an anionic ligand. *J. Am. Chem. Soc.* **2005,** *127* (51), 18004-18005.
42. Dimitratos, N.; Lopez-Sanchez, J. A.; Morgan, D.; Carley, A.; Prati, L.; Hutchings, G. J., Solvent free liquid phase oxidation of benzyl alcohol using Au supported catalysts prepared using a sol immobilization technique. *Catal. Today* **2007,** *122* (3-4), 317-324.
43. (a) Abd El-Moemen, A.; Karpenko, A.; Denkwitz, Y.; Behm, R. J., Activity, stability and deactivation behavior of Au/CeO_2 catalysts in the water gas shift reaction at increased reaction temperature (300 °C). *J. Power Sources* **2009,** *190* (1), 64-75; (b) Xu, Y. J.; Landon, P.; Enache, D.; Carley, A. F.; Roberts, M. W.; Hutchings, G. J., Selective conversion of cyclohexane to cyclohexanol and cyclohexanone using a gold catalyst under mild conditions. *Catal. Lett.* **2005,** *101* (3-4), 175-179.
44. Choudhary, T. V.; Sivadinarayana, C.; Chusuei, C. C.; Datye, A. K.; Fackler Jr, J. P.; Goodman, D. W., CO oxidation on supported nano-Au catalysts synthesized from a $[Au_6(PPh_3)_6](BF_4)_2$ complex. *J. Catal.* **2002,** *207* (2), 247-255.
45. Tsunoyama, H.; Sakurai, H.; Negishi, Y.; Tsukuda, T., Size-specific catalytic activity of polymer-stabilized gold nanoclusters for aerobic alcohol oxidation in water. *J. Am. Chem. Soc.* **2005,** *127* (26), 9374-9375.
46. Choudhary, T. V.; Goodman, D. W., Oxidation catalysis by supported gold nano-clusters. *Top. Catal.* **2002,** *21* (1), 25-34.
47. Nielsen, I. S.; Taarning, E.; Egeblad, K.; Madsen, R.; Christensen, C. H., Direct aerobic oxidation of primary alcohols to methyl esters catalyzed by a heterogeneous gold catalyst. *Catal. Lett.* **2007,** *116* (1-2), 35-40.
48. Choudhary, T. V.; Sivadinarayana, C.; Datye, A. K.; Kumar, D.; Goodman, D. W., Acetylene hydrogenation on Au-based catalysts. *Catal. Lett.* **2003,** *86* (1-3), 1-8.

49. Qi, C.; Okumura, M.; Akita, T.; Haruta, M., Vapor-phase epoxidation of propylene using H_2/O_2 mixture over gold catalysts supported on non-porous and mesoporous titania-silica: effect of preparation conditions and pretreatments prior to reaction. *Appl. Catal., A.* **2004,** *263* (1), 19-26.
50. Pojanavaraphan, C.; Luengnaruemitchai, A.; Gulari, E., Effect of support composition and metal loading on Au catalyst activity in steam reforming of methanol. *Int. J. Hydrogen Energy* **2012,** *37* (19), 14072-14084.
51. Zhu, Y.; Wu, Z.; Gayathri, C.; Qian, H.; Gil, R. R.; Jin, R., Exploring stereoselectivity of Au_{25} nanoparticle catalyst for hydrogenation of cyclic ketone. *J. Catal.* **2010,** *271* (2), 155-160.
52. Meng, M.; Tu, Y.; Ding, T.; Sun, Z.; Zhang, L., Effect of synthesis pH and Au loading on the CO preferential oxidation performance of Au/MnOx-CeO_2 catalysts prepared with ultrasonic assistance. *Int. J. Hydrogen Energy* **2011,** *36* (15), 9139-9150.
53. Choudhary, V. R.; Dumbre, D. K., Solvent-free selective oxidation of benzyl alcohol to benzaldehyde by tert-butyl hydroperoxide over U_3O_8-supported nano-gold catalysts. *Appl. Catal., A* **2010,** *375* (2), 252-257.
54. Horváth, D.; Toth, L.; Guczi, L., Gold nanoparticles: effect of treatment on structure and catalytic activity of Au/Fe2O3 catalyst prepared by co-precipitation. *Catal. Lett.* **2000,** *67* (2-4), 117-128.
55. (a) Besson, M.; Gallezot, P., Deactivation of metal catalysts in liquid phase organic reactions. *Catal. Today* **2003,** *81* (4), 547-559; (b) Donoeva, B. G.; Ovoshchnikov, D. S.; Golovko, V. B., Establishing a Au nanoparticle size effect in the oxidation of cyclohexene using gradually changing Au catalysts. *ACS Catalysis* **2013,** *3* (12), 2986-2991.
56. Auten, B. J.; Lang, H.; Chandler, B. D., Dendrimer templates for heterogeneous catalysts: Bimetallic Pt–Au nanoparticles on oxide supports. *Appl. Catal., B* **2008,** *81* (3–4), 225-235.
57. (a) Astruc, D.; Lu, F.; Aranzaes, J. R., Nanoparticles as recyclable catalysts: The frontier between homogeneous and heterogeneous catalysis. *Angew. Chem., Int. Ed.* **2005,** *44* (48), 7852-7872; (b) Wang, L.-C.; He, L.; Liu, Y.-M.; Cao, Y.; He, H.-Y.; Fan, K.-N.; Zhuang, J.-H., Effect of pretreatment atmosphere on CO oxidation over α-Mn_2O_3 supported gold catalysts. *J. Catal.* **2009,** *264* (2), 145-153.
58. Haruta, M., Gold as a novel catalyst in the 21st century: Preparation, working mechanism and applications. *Gold Bull.* **2004,** *37* (1), 27-36.
59. Boronat, M.; Corma, A.; Illas, F.; Radilla, J.; Ródenas, T.; Sabater, M. J., Mechanism of selective alcohol oxidation to aldehydes on gold catalysts: Influence of surface roughness on reactivity. *J. Catal.* **2011,** *278* (1), 50-58.
60. Kótai, L.; Kazinczy, B.; Keszler, Á.; Holly, S.; Gács, I.; Banerji, K. K., Three reagents in one: Ammonium permanganate in the oxidation of benzyl alcohol. *Z. Naturforsch., B: Chem. Sci.* **2001,** *56* (8), 823-825.
61. Li, H.; Guan, B.; Wang, W.; Xing, D.; Fang, Z.; Wan, X.; Yang, L.; Shi, Z., Aerobic oxidation of alcohol in aqueous solution catalyzed by gold. *Tetrahedron* **2007,** *63* (Copyright (C) 2012 American Chemical Society (ACS). All Rights Reserved.), 8430-8434.
62. Dimitratos, N.; Lopez-Sanchez, J. A.; Lennon, D.; Porta, F.; Prati, L.; Villa, A., Effect of particle size on monometallic and bimetallic (Au,Pd)/C on the liquid phase oxidation of glycerol. *Catal. Lett.* **2006,** *108* (3-4), 147-153.
63. Sankar, M.; Nowicka, E.; Tiruvalam, R.; He, Q.; Taylor, S. H.; Kiely, C. J.; Bethell, D.; Knight, D. W.; Hutchings, G. J., Controlling the duality of the mechanism in liquid-phase oxidation of benzyl alcohol catalysed by supported Au–Pd nanoparticles. *Chem.-Eur. J.* **2011,** *17* (23), 6524-6532.
64. Schmid, G., The relevance of shape and size of Au_{55} clusters. *Chem. Soc. Rev.* **2008,** *37* (9), 1909-1930.
65. (a) Zou, X.; Qi, S.; Suo, Z.; An, L.; Duan, X., Effects of pretreatment conditions on catalytic performance of Au/Al_2O_3 for CO oxidation. *Chin. J. Catal.* **2004,** *25* (2), 153-157; (b) Zhang, R. R.; Ren, L. H.; Lu, A. H.; Li, W. C., Influence of pretreatment atmospheres on the activity of Au/CeO_2 catalyst for low-temperature CO oxidation. *Catal. Commu.* **2011,** *13* (1), 18-21.
66. Tsukamoto, D.; Shiraishi, Y.; Sugano, Y.; Ichikawa, S.; Tanaka, S.; Hirai, T., Gold nanoparticles located at the interface of anatase/rutile TiO_2 particles as active plasmonic photocatalysts for aerobic oxidation. *J. Am. Chem. Soc.* **2012,** *134* (14), 6309-6315.

67. Sheldon, R. A.; Arends, I. W. C. E.; Brink, G. J. T.; Dijksman, A., Green, catalytic oxidations of alcohols. *Acc. Chem. Res.* **2002,** *35* (9), 774-781.
68. Bond, G., Gold: A relatively new catalyst. *Gold Bulletin* **2001,** *34* (4), 117-119.
69. Mori, N.; Togo, H., Facile oxidative conversion of alcohols to esters using molecular iodine. *Tetrahedron* **2005,** *61* (24), 5915-5925.
70. (a) Bond, G.; Thompson, D., Gold-catalysed oxidation of carbon monoxide. *Gold Bull.* **2000,** *33* (2), 41-50; (b) Qi, C.; Huang, J.; Bao, S.; Su, H.; Akita, T.; Haruta, M., Switching of reactions between hydrogenation and epoxidation of propene over Au/Ti-based oxides in the presence of H_2 and O_2. *J. Catal.* **2011,** *281* (1), 12-20.
71. Zhu, J.; Faria, J. L.; Figueiredo, J. L.; Thomas, A., Reaction mechanism of aerobic oxidation of alcohols conducted on activated-carbon-supported cobalt oxide catalysts. *Chem.-Eur. J.* **2011,** *17* (25), 7112-7117.
72. Shang, C.; Liu, Z. P., Origin and activity of gold nanoparticles as aerobic oxidation catalysts in aqueous solution. *J. Am. Chem. Soc.* **2011,** *133* (25), 9938-9947.
73. Guo, H.; Al-Hunaiti, A.; Kemell, M.; Rautiainen, S.; Leskelä, M.; Repo, T., Gold catalysis outside nanoscale: Bulk gold catalyzes the aerobic oxidation of π-activated alcohols. *ChemCatChem* **2011,** *3* (12), 1872-1875.
74. Su, F.-Z.; Ni, J.; Sun, H.; Cao, Y.; He, H.-Y.; Fan, K.-N., Gold supported on nanocrystalline β-Ga_2O_3 as a versatile bifunctional catalyst for facile oxidative transformation of alcohols, aldehydes, and acetals into esters. *Chem. Eur. J.* **2008,** *14* (24), 7131-7135.
75. Hayashi, T.; Inagaki, T.; Itayama, N.; Baba, H., Selective oxidation of alcohol over supported gold catalysts: methyl glycolate formation from ethylene glycol and methanol. *Catal. Today* **2006,** *117* (1-3), 210-213.
76. Haruta, M., Spiers Memorial Lecture Role of perimeter interfaces in catalysis by gold nanoparticles. *Faraday Discuss.* **2011,** *152* (0), 11-32.
77. Miedziak, P. J.; Tang, Z.; Davies, T. E.; Enache, D. I.; Bartley, J. K.; Carley, A. F.; Herzing, A. A.; Kiely, C. J.; Taylor, S. H.; Hutchings, G. J., Ceria prepared using supercritical antisolvent precipitation: A green support for gold-palladium nanoparticles for the selective catalytic oxidation of alcohols. *J. Mater. Chem.* **2009,** *19* (45), 8619-8627.
78. Choudhary, V. R.; Dumbre, D. K.; Bhargava, S. K., Oxidation of benzyl alcohol to benzaldehyde by tert-butyl hydroperoxide over nanogold supported on TiO_2 and other transition and rare-earth metal oxides. *Ind. Eng. Chem. Res.* **2009,** *48* (21), 9471-9478.
79. Heidkamp, K.; Aytemir, M.; Vorlop, K.-D.; Pru, Ceria supported gold-platinum catalysts for the selective oxidation of alkyl ethoxylates. *Catal. Sci. Technol.* **2013,** *3* (11), 2984-2992.
80. (a) Anderson, D. P.; Alvino, J. F.; Gentleman, A.; Qahtani, H. A.; Thomsen, L.; Polson, M. I. J.; Metha, G. F.; Golovko, V. B.; Andersson, G. G., Chemically-synthesised, atomically-precise gold clusters deposited and activated on titania. *PCCP* **2013,** *15* (11), 3917-3929; (b) Kulkarni, A.; Lobo-Lapidus, R. J.; Gates, B. C., Metal clusters on supports: Synthesis, structure, reactivity, and catalytic properties. *Chem. Commun.* **2010,** *46* (33), 5997-6015; (c) Liu, H.; Jiang, T.; Han, B.; Liang, S.; Zhou, Y., Selective phenol hydrogenation to cyclohexanone over a dual supported Pd-Lewis acid catalyst. *Science* **2009,** *326* (5957), 1250-1252.

Chapter 4: Effects of Activation Treatments on the Catalytic Activity of Au_{101} Immobilized on Carbon

4.1 Introduction

Ligands are commonly used to protect metal nanoparticles during synthesis, but their presence can be detrimental to catalytic activity[1] because they shield the gold cores from the reactants.[2] However, recent researchers have found that the presence of ligands is essential for catalytic activity of some metal particle systems. Jin *et al*. demonstrated that the core/shell nature of the thiolated gold clusters is primarily responsible for their catalytic activity,[3] and that calcination should be avoided because it can decompose the gold catalyst structure.[3] As-made clusters and colloids could, in principle, be used as homogeneous catalysts even without ligand removal; such systems would suffer from problems with aggregation due to exposed active sites and recyclability due to their homogeneous nature. Immobilization of chemically made nanoparticle precursors onto truly heterogeneous supports opens pathways toward fabrication of better catalysts, as discussed in more detail in Chapter 2 (see Section 2.5).

Many factors affect the catalytic activity of gold nanocatalysts, and several key studies have demonstrated the importance of better understanding the effects of catalyst activation treatment conditions.[4] Although, thermal treatments can be used to remove organic residues from gold particles, they can also cause an increase in particle sizes.[5] Key problems that may emerge from the removal of the stabilizing ligand include the loss of stability and sintering of the particles on the support. Lopez-Sanchez *et al.* improved catalytic activity for benzyl alcohol oxidation of gold catalysts by removing polyvinyl alcohol (PVA) ligands. However, TEM images showed that the gold particles aggregated after the catalysts activation, increasing from 3.0 to 4.8 nm diameter.[1]

An overview of various methods used to activate heterogeneous catalysts made by support-immobilization of chemically pre-synthesised particles, clusters and colloids was presented in

Chapter 1 (see Section 1.1.7). In this Section, I will discuss recent literature relating to removal of ligands by washing procedures and thermal treatments, since these activation methods were the ones ultimately selected for the research presented in this thesis.[1, 6] Catalytic enhancement of gold catalysts arises from the interplay of several factors: a) removal of the stabilizing ligands, permitting access of reagents to the active sites at the surface of supported gold particles; b) establishment of a direct interaction between metal nanoparticle and support; and c) changes in size of the particles following ligand removal.[1, 6-7]

Solvents can be used to remove ligands establishing equilibrium between free (solvated) and coordinated ligands. Previous researchers have studied the effects on the catalytic activity of gold particles of time, temperature and the solvents used in ligand-removing washing procedures.[1, 8] Lopez-Sanchez *et al.* investigated the efficacy of water, tetrahydrofuran (THF) and ethanol in removing PVA from supported gold catalysts by reflux at 90 ^{o}C for 60 minutes.[1] They used Raman spectroscopy to demonstrate the removal of PVA and TEM images to monitor changes in the particle sizes. Treatment with water changed the average particle diameters from 3.0 to 4.8 nm and led to the formation of an active gold catalyst that demonstrated high conversion (100%) in CO oxidation. However, no conversion was observed when the gold catalyst was refluxed in THF or ethanol.[1] Anderson *et al.* used a toluene reflux procedure (at 100 ^{o}C for 2 hours) to remove PPh_3 ligands from gold particles/clusters, to improve interactions with TiO_2 support.[6] Qi *et al.* investigated the effect of washing procedures on the stability of gold particles deposited on Ti-doped nonporous silica. Non-washed catalyst was less stable and more inclined to particle coagulation than washed catalyst. Additionally, the activity and selectivity of the washed catalysts after storage in air at room temperature for 4–6 months was comparable with that of freshly washed catalyst.[9]

Thermal treatments of gold nanocatalysts can result in better interaction between the gold species and the support, and thus change the catalytic activity of gold catalysts.[10] For example, Turner *et al.* reported that the removal of ligands by a heat treatment can significantly increase the activity and selectivity of gold nanoparticles with diameters of around 1.5 nm or smaller.[11] Those authors used calcination at 200 ^{o}C under vacuum for 2 hours to remove PPh_3 stabilizing ligands from Au particles immobilized on SiO_2 and BN. Diminution in the intensity of the phosphorus signal in the EDS was used to confirm the success of ligand removal. In the case of low loadings (0.6 wt%), only minor aggregation occurred, but high loadings (6.0 wt%) resulted in pronounced aggregation to larger (3.0 nm) catalytically inactive particles. These results show that this type of calcination is promising for better exposure of some gold catalysts to reactants.[11] Calcination under vacuum at 200 ^{o}C of Au_{101} particles immobilized on TiO_2 was investigated by Anderson *et al.* using a synchrotron-based XPS study.[6] Their result confirmed that PPh_3 moved from the nanoparticle and became bonded (possibly in oxidised form) to the support surface, resulting in an increase in the phosphorous high-binding energy peak (P-HBP) signal in the XPS. This ligand removal improved the interaction of the gold particles with the support.[6]

Calcination processes in the presence of a specific chemical atmosphere (*cf.* vacuum as discussed above), have also been applied to remove impurities or ligands from gold nanocatalysts (as described in Chapter 1, Section 1.1.7)[1, 5b] and to improve the strength of the contact often deemed necessary between the gold nanoparticles and underlying support.[8b, 12] Untreated Au/TiO_2 demonstrated no conversion in benzyl alcohol oxidation; but conversion improved from 0% to 43% when the catalysts were calcined under hydrogen gas at 300 ^{o}C for 3 hours.[13] It was proposed that better contact was established with partial removal of PVC ligands, an idea that was supported by laser Raman spectroscopy and TEM images. The TEM

images also showed an increase of gold particle diameters from 3.0 to 6.1 nm after the calcination.[1]

It has been reported that the chemical nature of the atmosphere used during calcination can exert an influence on the final structure and catalytic activity of the supported gold particles.[13-14] Calcinations in oxidative atmospheres, such as air, can remarkably improve the catalytic activity of gold catalysts.[10, 15] Yuan *et al.* calcined supported $[Au(PPh_3)(NO_3)]$ and $[Au_9(PPh_3)_8]_3$ under air flow and tested the resultant materials as catalysts for low-temperature CO oxidation, with PPh_3 ligand removal confirmed by a Fourier-transform extended X-ray absorption fine structure (EXAFS) oscillations technique.[15] Based on X-ray diffraction (XRD) and TEM, they proposed that better contact was established between the gold catalysts and reactants. However, the air treatment invariably led to substantial particle growth, from ~1 to 25 nm diameter, following ligand removal.[16]

Variations in calcination temperature permit a range of conditions for removal of the ligands from the catalyst surfaces,[17] and may have a pronounced effect on the properties of the final material.[5b] High-temperature calcination has been widely used to remove organic ligands, but its main drawback is the facile sintering of metal particles.[18] Yin *et al.* showed that the size of gold particles supported on silica (Au/SiO_2) increased from 2.1 nm (as-synthesized) to 3.3, 4.5 and 4.8 nm after calcination in an H_2 reducing atmosphere at 300, 500 and 600 ^oC, respectively. The catalysts calcined at 300 °C showed CO oxidation with 100% conversion.[18] Hence, a significant decrease in the gold catalyst activity can be related to the gold particles sintering at high calcination temperature.[19] Chang *et al.* reported a detailed investigation into the effect of calcination at temperatures from 100 to 475 ^oC on 2.0 wt% gold catalysts supported on Mg_2AlO, made by a co-precipitation method.[20] They showed that catalysts calcined at 100 ^oC are the most active in CO oxidation.[20]

Calcination at mild temperature is preferred for fabrication of structure-sensitive gold catalysts because higher temperatures generally lead to more particle agglomeration.[14a, 21] The improvement in catalytic activity of gold catalysts, as discussed above, demonstrates that low-temperature heat treatment is beneficial for gold particles immobilized on a support. Wang *et al.* studied the effect of calcination temperature on the catalytic activity of supported Au particles for benzyl alcohol oxidation. They showed that the mean particle diameters increased from 2.5 ± 0.7 to 2.6 ± 0.7, 2.7 ± 0.8, 3.9 ± 1.2 and 7.9±2.7 nm when the catalyst was calcined at 100, 200, 300, 400 and 500 ^{o}C; the corresponding benzyl alcohol conversions were 92%, 92%, 94%, 84% and 54%, respectively.[22] Pritchard *et al.* studied the effect of (air) calcination temperature on the catalytic activity of carbon-immobilised Pd-Au particles in benzyl alcohol oxidation. The mean particle diameters increased from 2.7 (as synthesized) to 5.3, 9.4 and 27 nm when the catalysts were calcined at 200, 300 and 400 ^{o}C, respectively. Treatment at 200 ^{o}C significantly improved the catalytic activity (see Table 4.1), but further increases in the calcination temperature, especially over 300 ^{o}C, led to a very significant decrease in catalytic activity.[23] The challenge remains in selecting an effective calcination temperature for good contact between the gold particles and the support, without inducing significant sintering.

Table 0.1: The effect calcination temperature (in air) on mean particle diameters of 1.0 wt % Pd–Au/C the catalyst and benzyl alcohol oxidation conversion (*C%*). Reproduced from Pritchard *et al.*[23]

Catalyst code	Calcination temperature (^{o}C)	Mean particle diameter (nm)	*C* (%)
1.0% Pd–Au/C	200	5.3	85
1.0% Pd–Au/C	300	9.4	12
1.0% Pd–Au/C	400	27	6

Reaction conditions: Benzyl alcohol: 40 mL, 1.0 wt% Au-Pd/C: 0.1 g, Temperature: 120 ^{o}C and pO_2: 150 psi.

It is generally assumed that ligand removal is relatively crucial for good control of particles size of gold supported on carbon.[24] Consequently, the activity of the gold nanoparticles

immobilized on activated carbon is likely to depend on the type of treatment.[25] The present chapter focuses on the effects of different types of treatments on catalytic activity for benzyl alcohol oxidation under the mild conditions established in Chapter 3 (*i.e.,* benzyl alcohol: 2.5 mmol, base: 2.5 mmol, anisole: 1.25 mmol, methanol: 25 mL, temperature: 80 ^{o}C, oxygen gas pressure: 73 psi, stirring: 750 rpm, time: 24 h and Au_{101}/C: 50 mg). A gold catalyst immobilized on Norit activated carbon (1.0 wt% Au_{101}/C) was activated in three ways:[23, 26]

a. washed with toluene;
b. calcined under vacuum or in air, O_2, H_2 or O_2 followed by H_2 at 100 or 200 ^{o}C for 3 hours;
c. a sequence of (a) followed by (b).

Evidence from the relevant earlier research demonstrates that alcohol oxidation can be forced to completion with an overall yield or conversion as a function of reaction time.[27] Fristrup *et al.* confirmed that the activation of benzyl alcohol involves breakage of the C–H bond in the benzylic position to generate a partial positive charge in the benzylic position (*i.e.*, hydride abstraction).[28] Catalytic results showed that yield of methyl benzoate in the presence of a base depends on the reaction time.[28] Table 3.4 provides some selected examples illustrating the effect of reaction time on benzyl alcohol oxidation.

Table 0.2: Examples of benzyl alcohol oxidation catalysed by supported gold nanoparticles as a function of time.

Catalyst code	*time$_1$ (h) → C_1 (%)	*time$_2$ (h) → C_2 (%)	T (^{o}C)	Ref.
Au/TiO_2	0.5→0.6	8→15.3	100	[27b]
Au-Pd/TiO_2	0.5→12	4→25	100	[27a]
Au/TiO_2	0.5→16	24→99	130	[28]
Au/TiO_2	1→4	150→85	100	[29]
Au/C	1→0	24→5	100	[30]
Au/TiO_2	1→8	10→75	25	[31]
Au/$K_2Ti_6O_{13}$	1→24	10→85	25	[31]

*Time$_1$: Initial reaction time, C_1: Initial conversion, time$_2$: Final reaction time and C_2: Final conversion.

Experiments should be repeated several times in order to ascertain reproducibility.[32] Particularly, in the case of gold catalysts, reproducibility of catalytic results is rarely reported, probably due to the sensitivity of the catalyst surface to activation and reaction conditions, along with the difficulty in exercising effective control over particle size and sensitivity to the many experimental variables that play a significant role during catalytic testing.[5a, 21a, 33]

These treatments could conceivably activate the gold nanoparticles without causing excessive particle sintering, which would be detrimental to the efficiency of benzyl alcohol oxidation.[23] The important and novel contribution of this chapter is in screening over a wide range of mild activations, including combinations, aimed to activate Au nanocatalysts through the removal of the ligands (PPh_3). The performance of each catalyst was investigated under exactly the same test conditions, making it possible to pinpoint the most efficient activation protocol. HPLC was used to analyse the products and TEM was used to study the effect of activation treatments on the gold nanocatalysts size.

4.2 Results and discussion

In this chapter, the effects of various types of activation processes were investigated with the main focus on the catalytic activity and selectivity of gold catalysts for benzyl alcohol oxidation. Specific details of catalyst preparation and activation procedures were reported in Chapter 2 (see Sections 2.5-2.6).

4.2.1 Un-treated "as-made" gold nanocatalysts

The catalytic activity of 1.0 wt% Au_{101}/C nanocatalysts was investigated "as-made", without treatment while controlling the stirring rate (750 rpm), pressure (73 psi) and target temperature (80 ^{o}C) for 24 hours. The catalysts can be activated *in situ* during rather long (24 hours) catalytic tests (see Table 4.3).

Table 0.3: Conversion and selectivity achieved using un-treated 1.0 wt% Au_{101}/C catalysts.

Catalyst code	Conversion%	Selectivity%		
		Benzaldehyde	Benzoic acid	Methyl benzoate
1.0% Au_{101}/C	70	1	45	54
1.0% Au_{101}/C	68	1	44	55
1.0% Au_{101}/C	71	1	45	54

The effects of immobilization on the size and size distribution of the gold nanoparticles were studied using HRTEM (see Figure 4.1). The gold particles showed some agglomeration during immobilization resulting in an increase of the average particle diameters from 1.6 ± 0.1 nm (for "as-made" $Au_{101,}$ see Chapter 2, Section 2.4.1.2 and Figure 2.2) to 2.6 ± 0.1 nm for the gold particles immobilized on activated carbon. This could be because gold particles could not be fully maintained on the carbon support and they were slightly agglomerated during immobilization.[34]

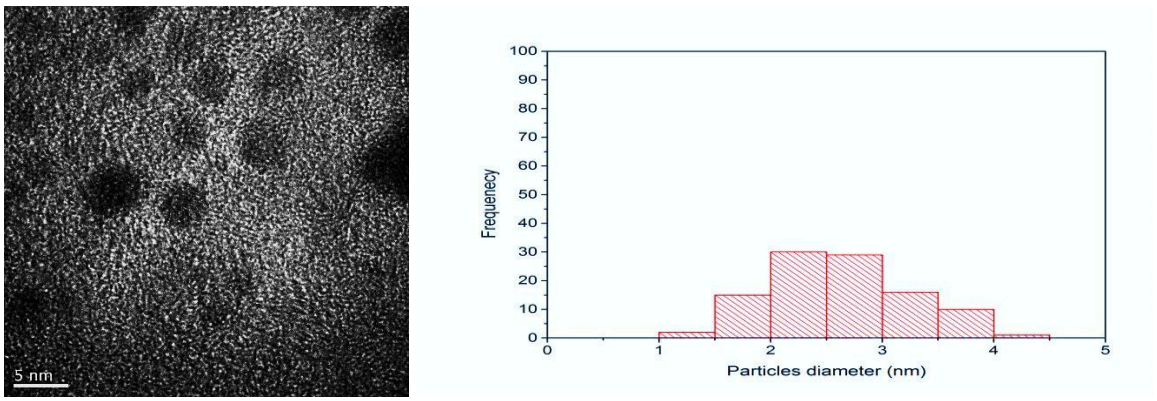

Figure 0.1: Left: a representative TEM image of as-made (un-treated) 1.0 wt% Au_{101}/C deposited onto carbon film coated copper TEM grid; Right: Particle size distribution histogram. The average particle size of gold particles was determined to be 2.6 ± 0.1 nm (two standard deviations of the mean).

The as-made gold nanocatalysts showed ~70% conversion with ~55:45 selectivity slightly in favour of methyl benzoate over benzoic acid as the only detectable products. This result contrasts with the findings of Lopez-Sanchez *et al*. who reported no conversion for as-made Au/TiO_2,[1] so one can appreciate that we have reached a relatively high conversion in this study, even without treatment of the gold catalyst.

There are several factors that could explain the difference in reactivity reported here and by Lopez-Sanchez *et al*. First, the supports (carbon and TiO_2) are quite different in terms of interactions with the Au MNPs. Second, Lopez-Sanchez *et al*. fabricated their catalysts using colloidal Au protected by PVA, while we used a PPh_3-protected precursor. Loss of PPh_3 (and hence catalytic activation) *during* catalytic testing conditions is likely to be more facile for mono-dentate PPh_3 than for a polymeric surfactant; and the oxidized form of ligand (phosphine oxide) is also soluble in methanol.[35] One should also consider effect of particles size. Previously published papers on benzyl alcohol oxidation indicate that the highest activity is attained by Au nanoparticles with diameters greater than ~3 nm (as discussed in Chapter 5, Section 5.1). One possible explanation for the activity of un-treated Au_{101}/C in our study is that some gold particles have diameters near or in excess of approximately 3 nm, making them active enough to play a major role in obtaining the relatively high ~70% observed conversion.[36] However, the TEM images reported by Lopez-Sanchez *et al*. showed that they used larger gold particles (average diameter ~3.0 nm compared with 2.6 ± 0.1 nm for the catalyst used here) with a significantly wider distribution. On this basis, one would expect their catalyst to be more active than mine, which contradicts earlier studies and makes a size-only explanation unlikely.

There are two other possible explanations for the observed activity: a) homogeneous catalysis by Au_{101} particles that have leached off the support during the catalytic test and b) in-situ aggregation of particles, coincident with the loss of ligands and resulting in the formation of larger, more active particles during the catalytic tests. The first of these explanations relates to studies of thiolate-capped Au nanoclusters (denoted as Au-SRx clusters) as homogeneous catalysts performed by Jin *et al*., who claimed that such unsupported catalysts could outperform their supported analogues.[3] Leaching of gold-phosphine species from as-made Au_{101}/TiO_2, as evidenced by a synchrotron-XPS study, was previously reported by Anderson

et al.[7b] Such leaching is plausible because the interaction between Au_{101} and its support is the weakest in a series of studies reported for the same gold particles (Au_{101}) in the literature due to the fact that the metal core is almost fully enclosed by phosphine ligands, which reduce gold-support interactions while possibly improving solubility in the solvent and thereby promoting leaching.[7] For leaching tests, our results, even for the same sample, were not consistent in this part for no apparent reason. Future work is necessary to further determine the gold loadings of the catalyst materials before and after catalytic tests which should allow confirmation of the leaching; also control tests using a solution of unsupported Au_{101} are suggested to establishment of the possibility of homogeneous catalytic activity. Explanation (b) is plausible based on Anderson *et al*.'s synchrotron-XPS observation of aggregation of phosphine-protected gold clusters supported on TiO_2 induced by washing in hot toluene,[7b] and my HRTEM study of the effect of such washing on particle sizes in a Au_{101}/C system (see Section 4.2.2.1 (below)). Detailed HRTEM of the catalyst material recovered after the test could have been conducted to prove that aggregation occurred *in situ*. However, the priority of determining whether either of the explanations (*i.e.*, explanation a, or b, as given above) were likely was judged to be low and given the lack of time, it was decided not to pursue further detailed investigations of this system.

4.2.2 Activation of gold nanocatalysts

Activation to remove PPh_3 from gold nanocatalysts and enhance the catalytic activity of Au_{101}/C was achieved by combinations of washing with a solvent (toluene or NaOH in MilliQ water (0.1 M), and/or calcinations.[1, 6] The activity of all catalysts discussed in this Chapter was investigated while keeping all catalytic test reaction parameters constant, as described in Section 4.1.

4.2.2.1 Washing with toluene at elevated temperature

The procedure of washing with toluene at 100 ^{o}C was adopted from Anderson *et al.* who demonstrated its successful use in removing PPh_3 ligands from gold nanoparticles or nanoclusters deposited onto TiO_2.[6] The results presented in Tables 4.3 and 4.4 shows that this process improves the catalytic activity of 1.0 wt% Au_{101}/C from ~70% to ~100%, while the selectivity in favour of methyl benzoate *vs* benzoic acid increases from ~55:45 to ~ 67:33. These observations are consistent with earlier research,[1] in which gold catalysts washed with a solvent (like water) demonstrated 100% conversion and 100% selectivity towards methyl benzoate (see Table 4.4). The improvement of catalytic activity after washing with toluene could be due to the ability of toluene to remove PPh_3 from the gold particles.[6]

Table 0.4: The effect of washing (with toluene) at elevated temperature on conversion and selectivity of activated 1.0 wt% Au_{101}/C catalysts.

Catalyst code	Conversion%	Selectivity%		
		Benzaldehyde	Benzoic acid	Methyl benzoate
1.0% Au_{101}/C	100	0	33	67
1.0% Au_{101}/C	100	0	32	68
1.0% Au_{101}/C	98	0	34	66

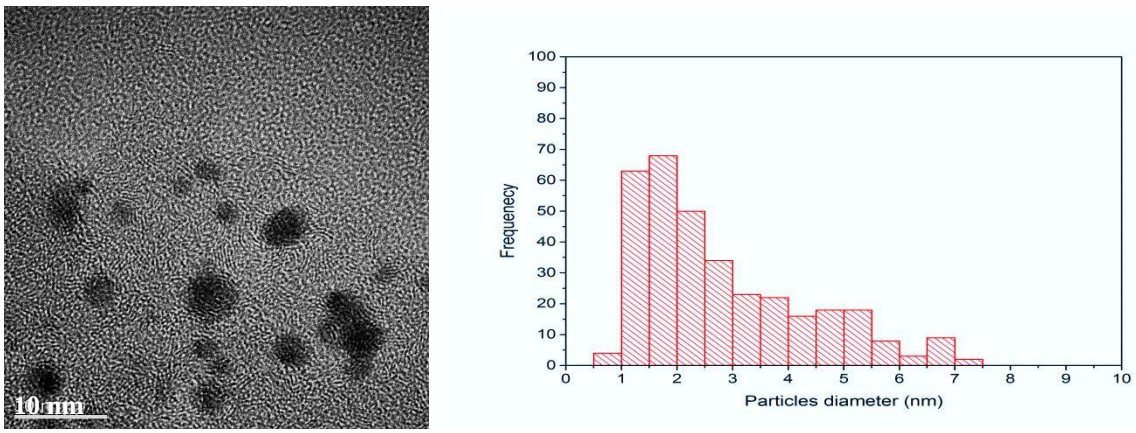

Figure 0.2: Left: a representative TEM image of activated 1.0 wt% Au_{101}/C (washed with toluene at 100 ^{o}C for 2 hours) deposited onto carbon film coated copper TEM grid; Right: Particle size distribution histogram. The average particle size of the gold particles was determined to be 2.8 ± 0.2 nm (two standard deviations of the mean).

TEM (see Figures 4.1- 4.2) shows that the average gold particles diameter increases very slightly (and perhaps statistically insignificantly) from 2.6 ± 0.1 nm for the "as-made" 1.0 wt% Au_{101}/C to 2.8 ± 0.2 nm after washing, so aggregation is only very slight if it occurs at all. Slight aggregation upon washing was previously reported for PPh_3-protected gold clusters and colloids immobilized on TiO_2,[6] but the catalytic activity of theses gold catalysts was attributed to some gold particles of approximately 3 nm diameter.[36]

4.2.2.2 Effect of heat treatments

In this Section of the thesis, heat treatments of gold catalysts were investigated using various atmospheres (*i.e.*, static air, vacuum, O_2, H_2 or O_2 then H_2 sequentially) at 100 or 200 ^oC for 3 hours to remove the phosphine ligands from the gold particles (see Tables 4.5-4.9). A trapping experiment (*e.g*. Staudinger reaction of the 1-azido-2, 4-dinitrobenzene with PPh_3) can be used to quantitatively determine amount of free PPh_3; when the ligands leave the gold core, free PPh_3 can rapidly react with trapping reagent.[37] However, such study was not undertaken due to the time limitations.

The mean diameter of detectable particles is different before and after activation due to the ligand removal. Donoeva *et al.* demonstrated that gold clusters cannot agglomerate when the ligands are still bound to the gold cores of the clusters.[7a] The change in the average gold particle diameter was monitored using transmission electron microscopy (TEM). The ligand removal may be inferred using comparison of the TEM images with the focus on size distribution and the average gold core diameter before and after activation. The average gold core diameter increased after activation of the catalysts made using phosphine-stabilized gold clusters probably due to the removal of PPh_3 from gold core particles.

4.2.2.2.1 Calcinations in static air

High conversions of 96% and 100% were achieved by gold catalysts calcined for 3 hours at 100 and 200 ^{o}C, respectively, under static air. Methyl benzoate was the major product with selectivity in the 60-70% range, while benzoic acid was the only other product. The performance of catalysts activated in this manner was quite similar, despite different activation temperatures. The results confirmed that high activity and selectivity can be induced in gold catalysts by using static air calcination.[8b] They are also consistent with research reported in the literature that, of 0.45 wt% Au/CeO_2 samples calcined in static air at 100, 200 and 400 ^{o}C of gold catalysts, that calcined at 100 ^{o}C showed the highest activity for cinnamyl alcohol oxidation.[8b]

Table 0.5: The effect of static air calcination on conversion and selectivity of 1.0 wt% Au_{101}/C catalysts.

Catalyst code	Temperature (^{o}C)	Conversion%	Selectivity%		
			Benzaldehyde	Benzoic acid	Methyl benzoate
1.0% Au_{101}/C	200	96	0	34	66
1.0% Au_{101}/C	100	100	0	40	60

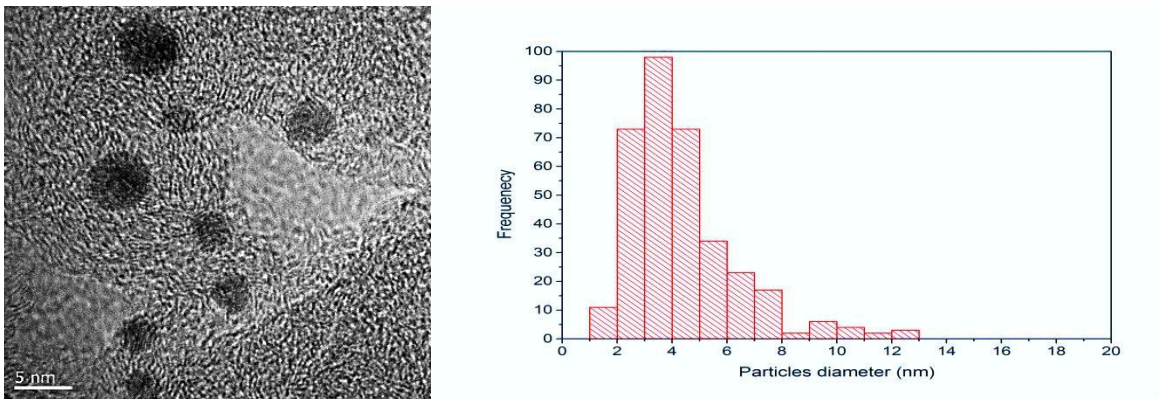

Figure 0.3: Left: a representative TEM image of activated 1.0 wt% Au_{101}/C (calcined under static air at 100 ^{o}C for 3 hours) deposited onto carbon film coated copper TEM grid; Right: Particle size distribution histogram. The average particle size of the gold particles was determined to be 4.4 ± 0.2 nm (two standard deviations).

Figure 4.3 shows that aggregation during calcination under static air at 100 ^{o}C for 3 hours increased the average gold particle diameter from 2.6 ± 0.1 nm ("as-made") to 4.4 ± 0.2 nm and led to a wider range size distribution. The activity of gold catalysts reportedly can be related to the number of gold particles with *ca*. ≥3 nm particles size.[36] Importantly, the observed activity and selectivity is similar to the case of washed catalysts discussed above, which is to be expected since both methods are thought to partially remove the PPh_3 ligands. However, the washed catalysts showed less aggregation (smaller particles ~2.8 nm) compared to calcined catalysts under static air.

4.2.2.2.2 Calcination in vacuum

The 1.0 wt% Au_{101}/C nanocatalysts calcined under vacuum also demonstrated relatively temperature independent high conversion of benzyl alcohol (~ 100%), along with higher selectivity (~73%) than observed in the earlier experiments towards methyl benzoate (see Table 4.6).

Table 0.6: The effect of vacuum calcination on conversion and selectivity of 1.0 wt% Au_{101}/C catalysts.

Catalyst code	**Temperature (^{o}C)**	**Conversion%**	**Selectivity%**		
			Benzaldehyde	**Benzoic acid**	**Methyl benzoate**
1.0% Au_{101}/C	200	99	0	26	73
1.0% Au_{101}/C	100	98	0	24	74

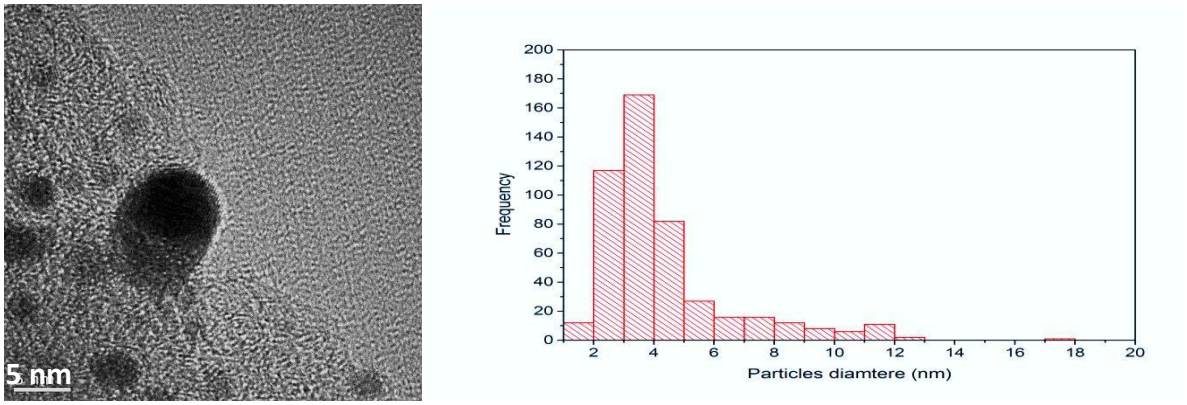

Figure 0.4: Left: a representative TEM image of activated 1.0 wt% Au_{101}/C (calcined under vacuum at 100 ^{o}C for 3 hours) deposited onto carbon film coated copper TEM grid; Right: Particle size distribution histogram. The average particle size of the gold particles was determined to be 4.3 ± 0.2 nm (two standard deviations of the mean).

Figure 4.4 shows that the average particle diameter increased from the "as-made" value of 2.6 ± 0.1 to 4.3± 0.2 nm, and that the distribution broadened. These changes indicate particle aggregation associated with partially removal of the PPh_3 ligands.[6] In addition, this could be due to the nature of carbon as a support, which may drastically influence the gold particles' size after thermal treatments.[34] The high activity of gold catalysts can be related to numerous gold particles of approximately 3 nm size,[36] but it is harder to explain a small but noticeable shift in selectivity towards the formation of methyl benzoate.

4.2.2.2.3 Calcination under oxygen atmosphere

The Au_{101}/C catalysts calcined under oxygen also showed high conversion (> 95%) and selectivity towards methyl benzoate and benzoic acid (see Table 4.7) similar to those observed in the case of washed and air-calcined catalysts. Notably, the selectivity as a function of activation temperature for catalysts calcined in air and under pure oxygen (which might be expected to exhibit a close correspondence, because both involve O_2) changes in opposite directions – for air, methyl benzoate selectivity increases with higher calcination temperature, while for oxygen it decreases. Activation at higher temperature should lead to a

more effective removal of phosphine ligands, but could also result in more pronounced aggregation.[18]

Table 0.7: The effect of oxygen gas calcination on conversion and selectivity of activated 1.0 wt% Au_{101}/C catalysts.

Catalyst code	Temperature (^{o}C)	Conversion%	Selectivity%		
			Benzaldehyde	Benzoic acid	Methyl benzoate
1.0% Au_{101}/C	200	95	0	40	60
1.0% Au_{101}/C	100	98	0	32	68

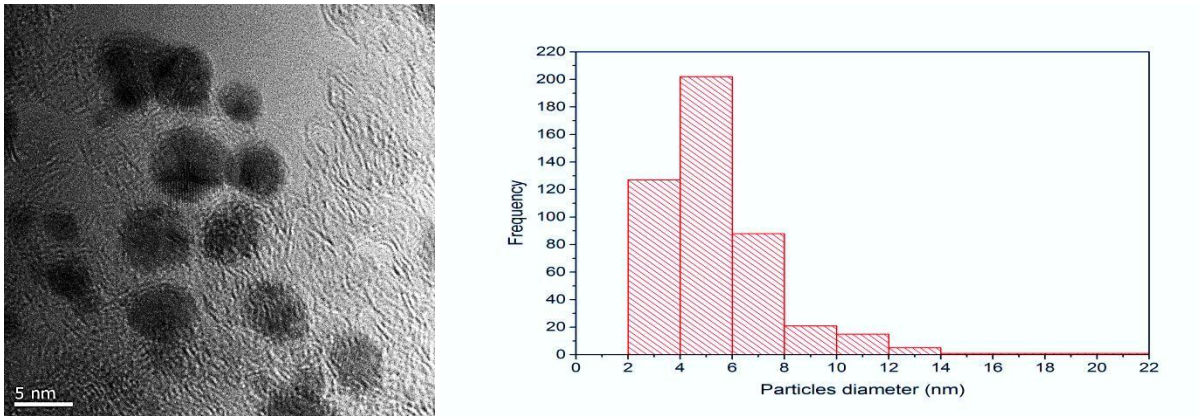

Figure 0.5: Left: a representative TEM image of activated 1.0 wt% Au_{101}/C (calcined under oxygen gas at 100 ^{o}C for 3 hours) deposited onto carbon film coated copper TEM grid; Right: Particle size distribution histogram. The average particle size of the gold particles was determined to be 5.4 ± 0.2 nm (two standard deviations of the mean).

Figure 4.5 shows that the average particles size increased from 2.6 ± 0.1 for the as-made material to 5.4 ± 0.2 nm after calcination under oxygen at 100 ^{o}C for 3 hours. The gold particles aggregated, which led to a wide size distribution. The phosphorous ligands were removed from the gold particles and deposited on the carbon surface while the gold cluster cores either partially or fully agglomerate.[7b, 38] The activity of the gold catalysts can be related to many gold particles bigger than 3 nm.[36, 39]

4.2.2.2.4 Calcination under hydrogen atmosphere

The 1.0 wt% Au_{101}/C catalysts calcined under hydrogen atmosphere at 100 or 200 ^{o}C demonstrated (see Table 4.8) much lower conversions of benzyl alcohol ($\lesssim$ 20%),[24] and

benzaldehyde was detected as a significant product (selectivity ~11%), which is similar to results reported in Chapter 3 when low conversions of benzyl alcohol were observed. Another very significant difference in comparison with the cases earlier in this Chapter is that the major product was benzoic acid, with ~55% selectivity. In the temperature-effect study illustrated in Figure 3.4, at 40 ^{o}C, the selectivity towards methyl benzoate was very significant (~87%) at approximately the same degree of conversion.

The very low activity of presented in Table 4.8 for 1.0 wt% Au_{101}/C nanocatalysts calcined under hydrogen gas may be due to the relatively low calcination temperature (100 and 200 ^{o}C) utilized in this study.[1] Other researchers found high activity for gold catalysts calcined under hydrogen gas at higher temperatures of ≥300 ^{o}C.[1, 8b]

Table 0.8: The effect of hydrogen gas calcination on conversion and selectivity of activated 1.0 wt% Au_{101}/C catalysts.

Catalyst code	Temperature (^{o}C)	Conversion%	Selectivity%		
			Benzaldehyde	Benzoic acid	Methyl benzoate
1.0% Au_{101}/C	200	14	11	55	27
1.0% Au_{101}/C	100	20	11	54	27

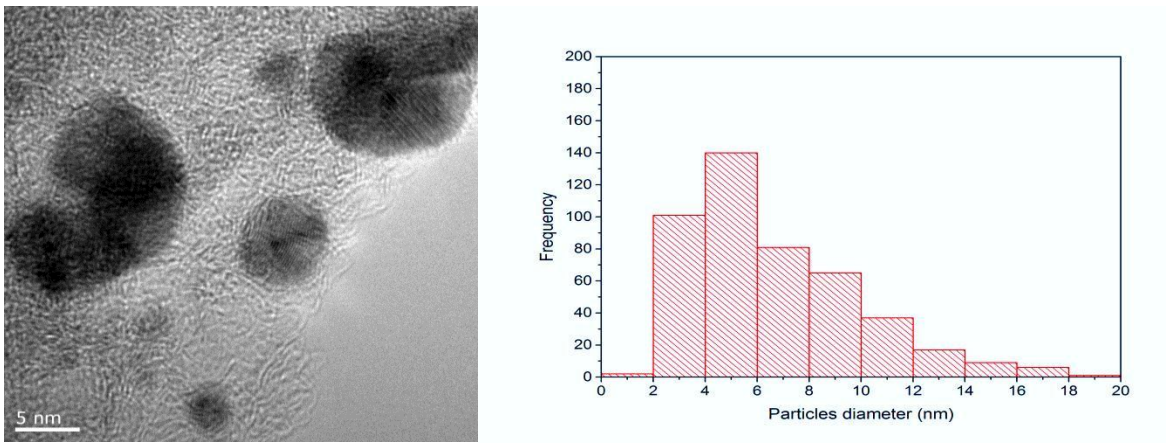

Figure 0.6: Left: a representative TEM image of 1.0 wt% Au_{101} treated under hydrogen gas at 100 ^{o}C for 3 hours, deposited onto carbon film coated copper TEM grid; Right: Particle size distribution histogram. The average particle size of the gold particles was determined to be 5.6 ± 0.3 nm (two standard deviations of the mean).

Figure 4.6 shows that the average gold particle size increased from 2.6 ± 0.1 to 5.6 ± 0.3 nm after calcination under hydrogen at 100 ^{o}C for 3 hours. Again, the gold particles' aggregation led to a wide size distribution. The activity of activated gold catalyst was not substantially changed by this thermal treatment.[1] It seems that numerous small (~3 nm) and big particles (≥ 8 nm) caused to drop the conversion of benzyl alcohol by the gold nanocatalysts.[36, 39-40]

4.2.2.2.5 Calcinations under oxygen and followed by hydrogen gases

In this section, the gold nanocatalysts were calcined first in oxygen and then in hydrogen in order to integrate the potential advantages of both treatments.[10] This combined calcination, denoted here as O_2-H_2, has been shown to completely remove phosphorous-based ligands gold and re-deposits the ligand residues onto a support surface; but at the same time it caused the gold particle cores to become highly agglomerated.[7b, 8b, 24]

The activity of 1.0 wt% Au_{101}/C nanocatalysts calcined in O_2-H_2 at 100 and 200 ^{o}C for 3 hours, was investigated under the same standard conditions as above. The highest conversion (96%) was achieved using catalysts activated at the lower temperature, with a significant drop to only 58% conversion when heated at 200 ^{o}C (see Table 4.9). This was the first time in the series of studies reported here that such a significant difference was observed between the performances of catalysts activated at different temperature. Furthermore, both results are in stark contrast to the very much lower conversions obtained using catalysts activated under hydrogen atmosphere alone, despite the fact that in both cases the last treatment before the catalytic test was under a hydrogen atmosphere and the gold particles sizes are quite similar. Based on the results discussed in 2.2.2.4 one might have expected low conversions in the case of O_2-H_2 treatment as well. Hence, one could hypothesise that the treatment under O_2 prior to H_2 is crucial in preventing deterioration of catalytic performance; yet at higher temperature this effect is diminished.[7b]

As shown in Table 4.8, the reaction products are essentially entirely benzoic acid and methyl benzoate for both calcination temperatures. However, there is a pronounced reversal in the ratios of selectivity: 2:1 in favour of methyl benzoate acid at 100 ^{o}C while at 200 ^{o}C the ratio was 1:2 in favour of benzoic acid. Along with activation under hydrogen gas, this is the second time within the series studied here that such a significant reversal has occurred in the selectivity of gold catalysts.

Table 0.9: The effect of O_2 –H_2 calcination on conversion and selectivity of activated 1.0 wt% Au_{101}/C catalysts.

Catalyst code	Temperature (^{o}C)	Conversion%	Selectivity%		
			Benzaldehyde	Benzoic acid	Methyl benzoate
1.0% Au_{101}/C	200	58	1	66	33
1.0% Au_{101}/C	100	96	0	33	67

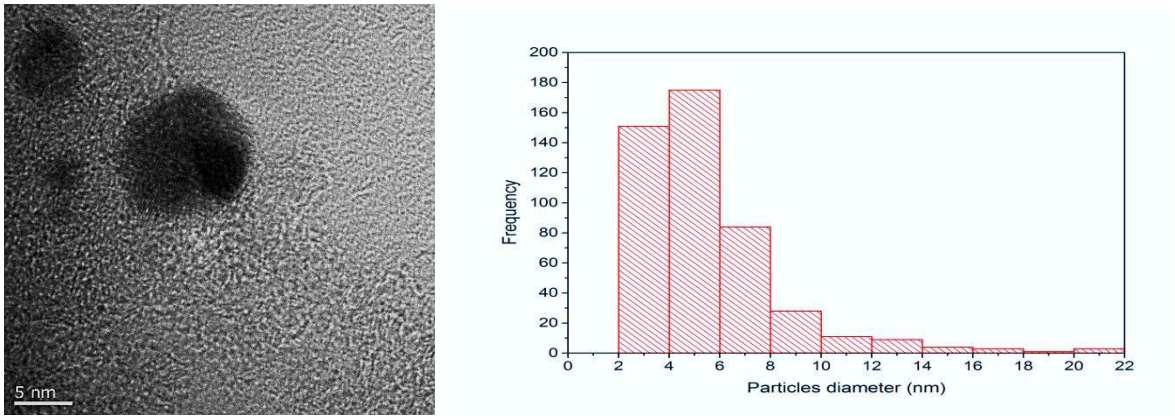

Figure 0.7: Left: a representative TEM image of activated 1.0 wt% Au_{101}/C (calcinated under O_2–H_2 gases at 100 ^{o}C for 3 hours) deposited onto carbon film coated copper TEM grid; Right: Particle size distribution histogram. The average particle size of the gold particles was determined to be 6.6 ± 0.3 nm (two standard deviations of the mean).

Figure 4.7 shows that the average particles size increased from 2.6 ± 0.1 to 6.6 ± 0.3 nm after calcination under O_2–H_2 gases at 100 ^{o}C for 3 hours; the gold particles also aggregated to broaden the size distribution. The combination of two types of calcinations (O_2 and H_2) may lead to the phosphorous ligands completely detaching from the gold and re-deposition onto the support surface, but the gold particle cores may also agglomerate substantially.[7b] The

activity of the gold catalysts could be related to the proportion of gold particles larger than 3 nm.[36, 39]

4.2.3 Washing with a solvent at elevated temperature followed by calcinations

This section concerns procedures that integrate advantages of both washing and calcination to more effectively remove weakly adsorbed PPh_3 from gold particle surfaces, to enhance the surface exposure of the particles and hence the catalytic activity.[6] A washing procedure and follow-up calcinations were undertaken according to a protocol similar to that described by Lopez-Sanchez *et al.*, who demonstrated removal of PVA from gold particles immobilized on TiO_2.[1] The result of benzyl alcohol oxidation by gold catalysts treated in this manner confirmed an improvement of activity as compared with the un-treated, or simply washed or calcined catalyst. Un-washed gold catalyst particles are inclined to coagulate more readily than washed catalyst, meaning that they are less stable.[9]

4.2.3.1 Washing followed by calcination in static air

The method here was adapted from Lopez-Sanchez *et al.*[1] 1.0 wt% Au_{101}/C was washed with toluene and then calcined for 3 hours under static air at 100 or 200 ^{o}C. The activity of the treated nanocatalysts was tested under the standard conditions used above. The gold catalysts showed high conversion (~100%) and high total selectivity, producing methyl benzoate and benzoic acid. The product ratios were approximately 2:1 (the ester to acid for both temperatures) in favour of latter (see Table 4.10). Treatment at the higher temperature resulted in a slight shift towards benzoic acid, as observed in several other high conversion tests discussed earlier (4.2.2.2.4).

Table 0.10: The effect of washing and calcination (under static air) on conversion and selectivity of activated 1.0 wt% Au_{101}/C catalysts.

Catalyst code	Temperature (^{o}C)	Conversion%	Selectivity%		
			Benzaldehyde	Benzoic acid	Methyl benzoate
1.0% Au_{101}/C	200	100	0	34	66
1.0% Au_{101}/C	100	100	0	21	78

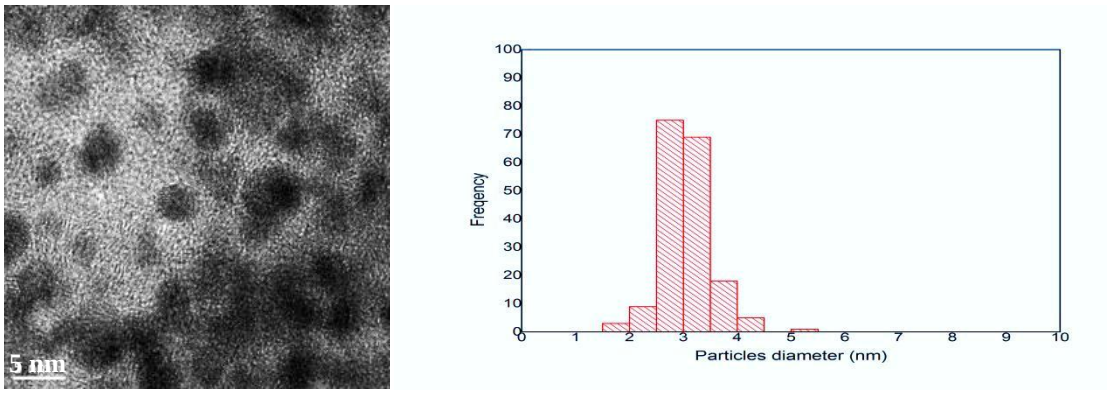

Figure 0.8: Left: a representative TEM image of treated 1.0 wt%Au_{101} (washed with toluene and followed by calcination under static air at 100 ^{o}C for 3 hours) deposited onto carbon film coated copper TEM grid; Right: Particle size distribution histogram. The average particle size of the gold particles was determined to be 3.0 ± 0.1 nm (two standard deviations of the mean).

The size and size distribution of the gold particles resulting from the 100 °C treatment are depicted in Figure 4.8. The treatment led to a small increase in the gold particle diameters from 2.6 ± 0.1 (un-treated) to 3.0 ± 0.1 nm, which is only slightly (and hardly significantly) bigger than that obtained using washing alone (2.8 ± 0.1 nm). In comparison, in the case of calcination under static air alone, the average gold particle diameters increased to 4.4 ± 0.2 nm. It appears that washing substantially stabilizes the gold particles and makes them less prone to aggregation. It is also noticeable that the sample showed high activity, presumably as a consequence of more particles with sizes bigger than 3 nm.[36, 39]

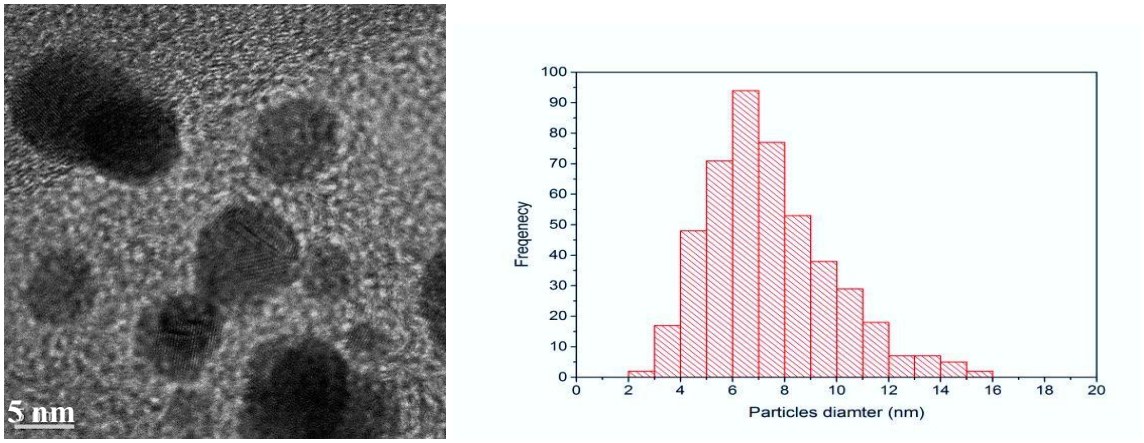

Figure 0.9: Left: a representative TEM image of activated 1.0 wt% Au_{101}/C (washed with toluene and followed by calcination under static air at 200 ^{o}C for 3 hours) deposited onto carbon film coated copper TEM grid; Right: Particle size distribution histogram. The average particle size of gold particles was determined to be 7.4 ± 0.2 nm (two standard deviations of the mean).

The resulting particles size and size distribution of the 1.0 wt% Au_{101}/C nanocatalysts after the 200 °C treatment are depicted in Figure 4.9. These results clearly demonstrate that the treatment at higher temperature led to a much larger gold particles sizes with a mean diameter of 7.4 ± 0.2 nm and a very broad distribution. It is also noticeable that the sample showed high activity, presumably as a consequence of a higher proportion of particles bigger than 3 nm.[36, 39] But this result is in contradiction with the low conversions obtained using catalysts treated under hydrogen, despite the fact that particle sizes are large in both cases (7.4 ± 0.2 nm here *vs*. 6.6 ± 0.3 nm in the case of catalysts treated under H_2).

4.2.3.2 Washing followed by calcination in vacuum

The activity of 1.0 wt% Au_{101}/C washed with toluene and then calcined under vacuum was investigated under standard conditions. The observed conversion of benzyl alcohol was essentially 100% for both calcination temperatures. For a catalyst treated using the 100 ^{o}C procedure a ~1:3 product ratio of benzoic acid to methyl benzoate was obtained, similar to that observed earlier in the case of a catalyst heat treated under vacuum without prewashing. The selectivity ratio shifted closer to ~1:2 for calcination at 200 ^{o}C (see Table 4.11).

Table 0.11: The effect of washing and following by calcination under vacuum on conversion and selectivity of activated 1.0 wt% Au_{101}/C catalysts.

Catalyst code	Temperature (^{o}C)	Conversion%	Selectivity%		
			Benzaldehyde	Benzoic acid	Methyl benzoate
1.0% Au_{101}/C	200	100	0	29	71
1.0% Au_{101}/C	100	99	0	24	74

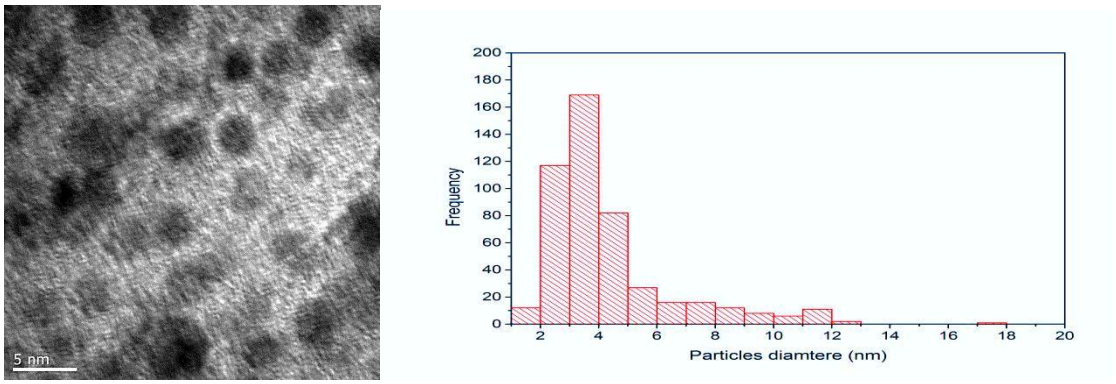

Figure 0.10: Left: a representative TEM image of activated 1.0 wt% Au_{101}/C (washed with toluene and followed by calcination under vacuum at 100 ^{o}C for 3 hours) deposited onto carbon film coated copper TEM grid; Right: Particle size distribution histogram. The average particle size of the gold particles was determined to be 3.5 ± 0.1 nm (two standard deviations of the mean).

The gold particle size and size distribution of 1.0 wt% Au_{101}/C nanocatalysts after treatment at 100 °C are depicted in Figure 4.10. The final average gold particle diameter was 3.5 ± 0.1 nm, which is larger than that obtained using washing alone (2.8 ± 0.1 nm), but smaller than obtained by calcination under vacuum alone (4.3 ± 0.2 nm). One can deduce that calcination under vacuum of the washed particles increases the size from 2.8 ± 0.1 to 3.5 ± 0.1 to nm.[9] In contrast, the unwashed particles would have aggregated under vacuum calcination to 4.3 ± 0.2 nm. Pre-washing the particles appears to convey on the particles partial protection against aggregation during calcination.[9]

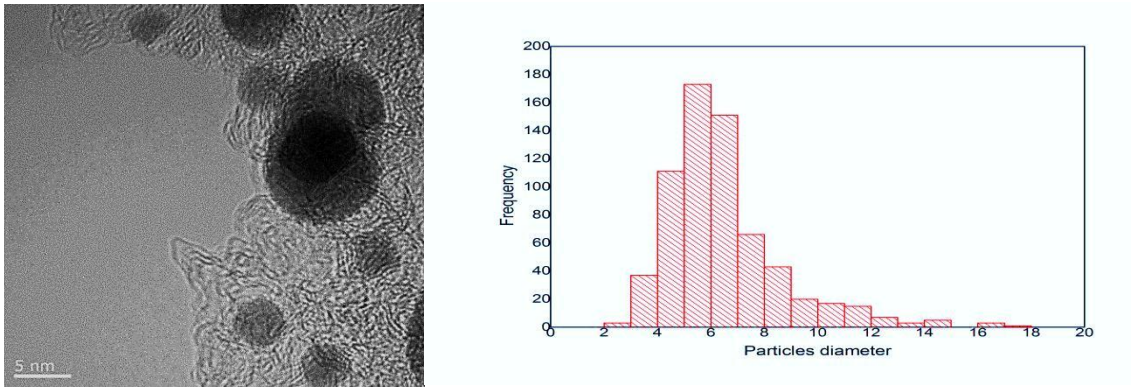

Figure 0.11: Left: a representative TEM image of activated 1.0 wt% Au_{101}/C (washed with toluene and followed by calcination under vacuum at 200 ^{o}C for 3 hours) deposited onto carbon film coated copper TEM grid; Right: Particle size distribution histogram. The average particle size of the gold particles was determined to be 6.5 ± 0.2 nm (two standard deviations of the mean).

The resulting particle size and size distribution of the 1.0 wt% Au_{101}/C nanocatalysts after the 200 °C treatment are depicted in Figure 4.11. The gold particle mean diameter has increased from 2.6 ± 0.1 (un-retreated) to 2.8 ± 0.1 nm (washing alone) and to 6.5 ± 0.2 nm after the combined activations. The final diameter is substantially greater than achieved by the 100 ^{o}C activation, as would be expected since higher calcination temperatures generally lead to greater aggregation.

The sample showed high activity, presumably as a consequence of the effect of the predominant particle population between 3 and 8 nm.[36, 39] Comparison of particle diameters and performance of catalysts activated at 100 ^{o}C and 200 ^{o}C implies that the size *before* catalytic testing has a very minor effect because these samples have distinctly different particle diameters of 3.5 ± 0.1 and 6.5 ± 0.2 nm, respectively. Clearly, *initial* particle size alone is insufficient to explain the catalyst's performance. Indeed, low conversions have been previously obtained using catalysts, treated under hydrogen, which contained particles with sizes nearly identical to those discussed here (6.5 ± 0.2 nm here *vs*. 6.6 ± 0.3 nm). Due to time and TEM access limitations, we were not able to perform a study of particle size evolution during catalytic testing.

4.2.3.3 Washing followed by calcination under oxygen gas

The 1.0 wt% Au_{101}/C catalysts washed with toluene and calcined under oxygen atmosphere showed ~100% conversion for material calcined at 100 ^{o}C, but only ~20% conversion for material calcined at 200 ^{o}C (see Table 4.12). A similar but less pronounced drop in conversion (from *ca*. 100% to 60%) for a catalyst treated at higher temperature was observed earlier after O_2–H_2 calcination (see Section 4.2.2.2.5). Unlike most other cases, benzoic acid is consistently the major product especially at the higher temperature, where the selectivity of 70% is close to that for the case of the catalyst activated by O_2–H_2 calcination at 200 ^{o}C (see Section 4.2.2.2.5). It is hard to explain this finding since, in the case of catalysts activated by washing alone (Table 4.4) or by calcination in static air (Table 4.4) or in oxygen (Table 4.6), methyl benzoate was obtained as the main product with selectivity of 60-70%. Interestingly, the results of the 100 ^{o}C treatment constitute the first example of significant (21%) selectivity towards benzaldehyde at a conversion close to 100% (see Table 4.12).

Table 0.12: The effect of washing with toluene and following by calcinations under oxygen gas on conversion and selectivity of activated 1.0 wt% Au_{101}/C catalysts.

Catalyst code	**Temperature (^{o}C)**	**Conversion%**	**Selectivity%**		
			Benzaldehyde	**Benzoic acid**	**Methyl benzoate**
1.0% Au_{101}/C	200	20	17	70	23
1.0% Au_{101}/C	100	94	21	44	35

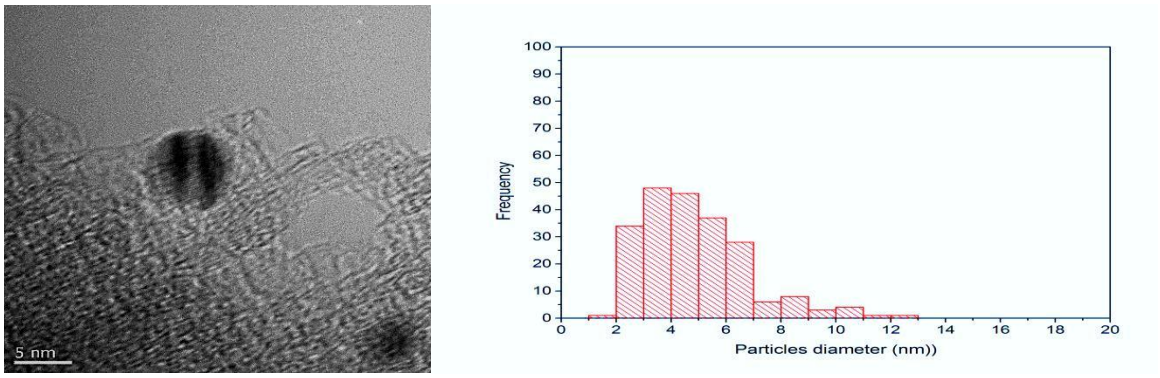

Figure 0.12: Left: a representative TEM image of activated 1.0 wt% Au_{101}/C (washed with toluene and followed by calcination under O_2 gas at 100 ^oC for 3 hours) deposited onto carbon film coated copper TEM grid; Right: Particle size distribution histogram. The average particle size of the gold particles was determined to be 4.4 ± 0.2 nm (two standard deviations of the mean).

Figure 4.12 shows that the gold particles s agglomerate under the 100 ^oC treatment to an average diameter of 4.4 ± 0.2 nm,[7b, 38] which is substantially larger than the 2.8 ± 0.1 nm diameter for the gold catalysts treated using washing alone, but still much smaller than 5.4 ± 0.2 nm obtained in the case of calcination under O_2 alone. These comparisons indicate that that gold particles may be stabilized by the washing procedure, and hence show lesser aggregation during calcination.

4.2.3.4 Washing followed by calcination under hydrogen gas

Table 4.13 displays results of catalytic tests with 1.0 wt% Au_{101}/C nanocatalysts washed with toluene and calcined under hydrogen gas. After the higher temperature (200 ^oC) activation, a pronounced drop in conversion to 53% and a typical product distribution ratio (similar to 4.2.2.2.4 – 4.2.2.2.5) was observed in the case of hydrogen treatment at 200 ^oC. However, a high conversion (95%) and reversal of the product distribution ratio was evident too, with benzoic acid becoming a major product with 61% selectivity at 100 ^oC activation. This is very similar to earlier observations after treatment under O_2 followed by H_2 at 100 ^oC (Section 4.2.2.2.5).

Table 0.13: The effect of washing with toluene followed by calcination under hydrogen gas on conversion and selectivity of activated 1.0 wt% Au_{101}/C catalysts.

Catalyst code	Temperature (°C)	Conversion%	Selectivity%		
			Benzaldehyde	Benzoic acid	Methyl benzoate
1.0% Au_{101}/C	200	53	11	60	29
1.0% Au_{101}/C	100	95	11	28	61

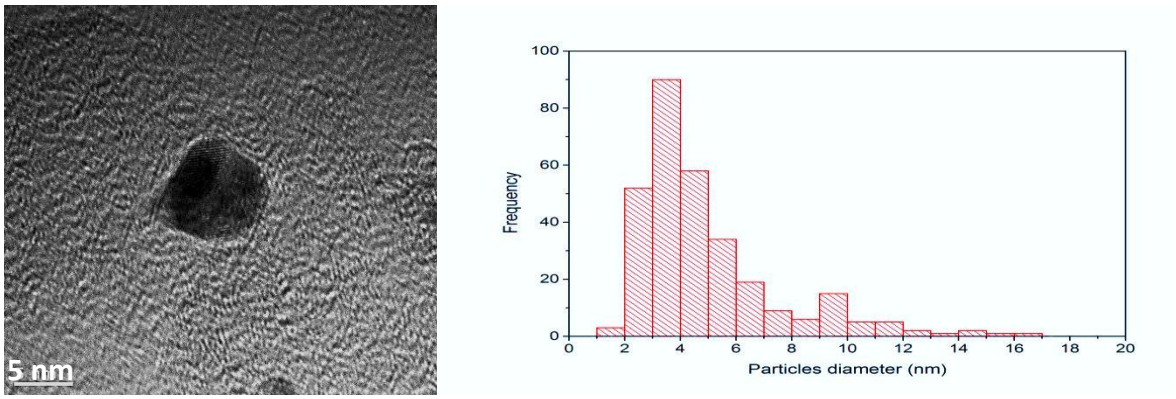

Figure 0.13: Left: a representative TEM image of activated 1.0 wt% Au_{101}/C (washed with toluene and followed by calcination under H_2 gas at 100 °C for 3 hours) deposited onto carbon film coated copper TEM grid; Right: Particle size distribution histogram. The average particle size of the gold particles was determined to be 4.9 ± 0.3 nm (two standard deviations of the mean).

Figure 4.13 shows a representative HRTEM image and the associated particles size and size distribution (histogram). The gold particles have grown to an average diameter of 4.9 ± 0.2 nm, which is bigger than that for catalysts that were treated by using washing alone (2.8 ± 0.1 nm), but smaller than that obtained by calcination only under hydrogen (5.6 ± 0.3 nm). As in many (4.2.3.1- 4.2.3.4) of the cases above, the average gold particle diameters falls between those obtained using washing alone or calcination alone. The observed drop in conversion and inverted selectivity is impossible to explain based on the gold particle diameters according to the results discussed in previous sections (including 4.2.2.2.4 above). The results show that selectivity towards the acid as the main product for catalyst particles spanning a wide range of particle sizes. The high activity of gold catalysts after calcination at 100 °C showed a significant population of small gold particles (*ca*. 3 nm).[36]

4.2.3.5 Washing followed by calcinations under oxygen and hydrogen

A sample of 1.0 wt% Au_{101}/C was firstly washed with toluene and then sequentially calcined in oxygen and hydrogen in order to integrate both advantages of the oxygen and hydrogen treatments (see Figure 4.14). Both temperatures showed high selectivity towards benzoic acid, with higher conversion (94%) observed for the lower calcination temperature (at100 ^{o}C).

Table 0.14: The effect of washing and following by calcination under O_2-H_2 gases on conversion and selectivity of activated 1.0 wt% Au_{101}/C catalysts.

Catalyst code	Temperature (^{o}C)	Conversion%	Selectivity%		
			Benzaldehyde	Benzoic acid	Methyl benzoate
1.0% Au_{101}/C	200	74	2	60	6
1.0% Au_{101}/C	100	94	4	86	10

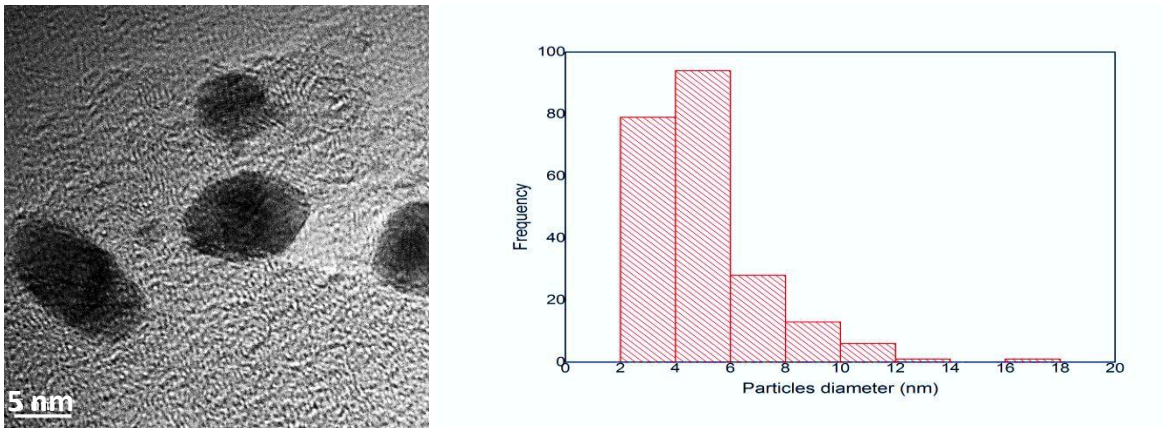

Figure 0.14: Left: a representative TEM image of activated 1.0 wt% Au_{101}/C (washed with toluene and followed by calcination under O_2 -H_2 gases at 100 ^{o}C at for 3 hours) deposited onto carbon film coated copper TEM grid; Right: Particle size distribution histogram. The average particle size of the gold particles was determined to be 5.0 ± 0.3 nm (two standard deviations).

A HRTEM image and associated particle size distributions taken from gold nanocatalysts which was washed with toluene and calcined under oxygen followed by hydrogen gas at 100 ^{o}C (see Figure 4.14) showed that the gold catalyst agglomeration gives rise to substantially enlarged particles with average particle diameters of 5.0± 0.3 nm. There were many smaller particles with diameters still bigger than 3 nm, which were presumably responsible for the activity of the treated nanocatalysts.[36, 39] It is hard to explain observed

high selectivity towards benzoic acid based on the *initial* particle sizes alone since the opposite product pattern, with methyl benzoate as the main product, was previously observed in reactions catalysed by materials containing particles in the 3.0±0.1 and 3.5±0.1 nm range (Sections 4.2.3.1 and 4.2.3.4), similar sizes to those discussed here (~5.0 nm, in Sections 4.2.2.1 and 4.2.3.4) and even larger (~7.4 nm, Section 4.2.3.1). The final average particle diameter of 5.0± 0.3 nm is bigger than that of the gold catalysts treated using washing alone (2.8 ± 0.1 nm) but smaller than the case of calcination under O_2-H_2 alone, (6.6 ± 0.3 nm).

4.2.4 Summary of results for 24 hour reaction time

For a 24 hours reaction time, the results of gold catalysts activations, including "as-made", washing, calcinations in different atmospheres and combinations of both, showed a range of conversions. However, many conversions close to 100% made it hard to pinpoint the best treatment. Some activated gold catalysts were clearly inferior, resulting in catalysts incapable of achieving full conversions after 24 hours of reaction. These included: calcinations under hydrogen (at 100 ^{o}C: 14% and 200 ^{o}C: 20%) or O_2-H_2 at 200 ^{o}C (58%); and washing with toluene followed by calcination under oxygen at 200 ^{o}C (20%), under hydrogen at 200 ^{o}C (53%), under oxygen at 200 ^{o}C (20%) or under oxygen-hydrogen at 200 ^{o}C (74%).

Most of the activated gold catalysts had selectivity in favour of methyl benzoate as the main product; those that favoured benzoic acid were calcined under hydrogen or oxygen-hydrogen, or washed with toluene followed of calcination under oxygen-hydrogen. Benzaldehyde appeared as the minor product for catalysts calcined under hydrogen (at 100 and 200 ^{o}C: 11%) or washed with toluene and then calcined under oxygen-hydrogen (at 100

^{o}C: 4% and 200 ^{o}C: 2%). When it was present, benzaldehyde occurred with higher selectivity when benzyl alcohol conversion was small.

It is difficult to explain the effect of average gold particle diameters on the benzyl alcohol conversion. Previous literature (see more details in Chapter 5, Section 5.1) indicates that gold particles bigger than 3 nm can be active gold nanoparticles for benzyl alcohol oxidation.[36b, 39] It seems clear that more than just the average gold particle size is important; the size distribution and gold dispersion should also be considered (see Chapter 5). In addition, calcination of gold particles on the surface of the carbon support invariably caused larger gold particles to be formed due to aggregation.[34] It seems that the interaction between gold particles and carbon is insufficient to prevent this.[4] However, washing before calcinations can stabilize the gold particles on the support and decrease the degree of aggregation.[9]

4.3 The effect of activation for three hours reaction time

In catalyst kinetics, it is customary to measure the initial rate of a reaction from a fixed, initial reactant concentration so as to minimize complications due to reversible reactions and the inhibition by products.[41] In this Section, the concentration of gold catalysts was held constant at 2.5 mmol, and the reaction time was reduced to 3 hours to ensure conversions significantly lower than 100%, so that the best catalysts could be distinguished. All other reaction parameters were kept the same as in the 24 hour tests discussed above.

Figure 4.15 shows conversion and selectivity of aerobic oxidation of benzyl alcohol at 80 °C as a function of time with K_2CO_3 (2.5 mmol: 2.5 mmol ratio with benzyl alcohol). After an induction period of ~1 hour (not shown in the figure), conversion increases rapidly to ~75% after 3 hours, ~96% after 6 hours and 100% after 12 hours. The main product was methyl

benzoate, with benzaldehyde present as a very minor product (~2%) until about 3 hours reaction time when it could be detected in only trace amounts. Immediately after the induction period, the ratio of methyl benzoate to benzoic acid was as high as ~9:1, but this ratio decreased monotonically to ~2.3:1 after 6 hours and then more gradually to an apparent asymptote of ~2:1 near 24 hours (as noted above in the investigation of temperature dependence).[27b] Other studies have demonstrated high conversion of benzyl alcohol by supported gold catalysts over more than 10 hours reaction time.[31, 42] As an example, Zheng and Stucky reported the effect of reaction time on catalytic activity and selectivity of Au/TiO_2 for benzyl alcohol oxidation with the highest conversion (80%) and selectivity (40%) towards benzaldehyde occurring at 80 hours.[43] In contrast, Ishida *et al.* confirmed high activity of gold catalysts for benzyl alcohol oxidation for 1 hour reaction time (the reaction conditions were benzyl alcohol:1 mmol, base: 0.5 mmol, 2.0 wt% Au/C: 99 mg, methanol: 3 mL, T: 80 ^{o}C); but used 99 mg of 2.0 wt% Au catalysts,[44] which is effectively 10 times more than we used (50 mg of 1.0 wt% Au_{101}/C) for 2.5 mmol of benzyl alcohol.

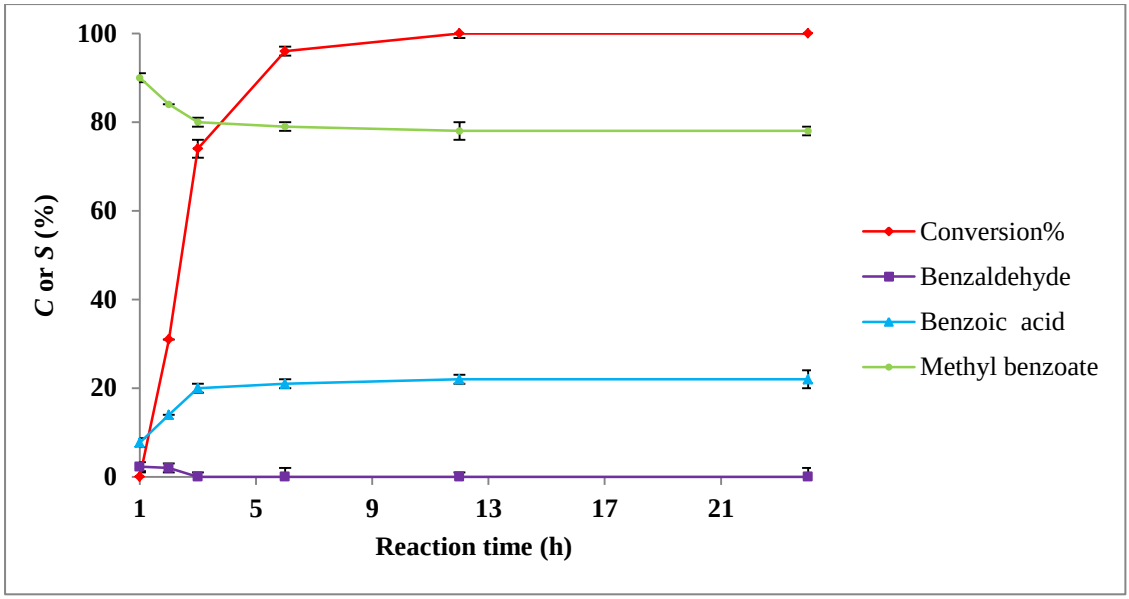

Figure 0.15: The effect of reaction time on conversion (*C*) and selectivity (*S*) of activated 1.0 wt% Au_{101}/C catalysts**.**

In order to be able to distinguish between the relative merits of different reactions, it is important that the reactions are reasonably well advanced without being "*saturated*" (*i.e.*, without having proceeded to 100% conversion). From the results presented here (3 hours), which corresponds to the time of near-maximum, TOF was considered to be a suitable reaction time and was selected for subsequent reactions.

Table 0.15: Examples of benzyl alcohol oxidation catalysed by activated (with different activations methods) 1.0 wt% Au_{101}/C for 3 hours reaction time.

*Activation method	Particle diameter (nm)	Calcine Temp. (^oC)	Initial rate (mol/h)	*C*%	*S* %		
					Benzaldehyde	Benzoic acid	Methyl benzoate
As-made	2.6±0.1	-	2.5×10^{-5}	3	68	-	32
W	2.8±0.2	-	2.5×10^{-5}	3	47	15	38
Static air	4.4±0.2	100	0	0	0	0	0
Static air	-	200	1.58×10^{-4}	19	1	16	83
Vacuum	4.3±0.2	100	0	0	0	0	0
Vacuum	-	200	4.16×10^{-5}	5	37	15	48
O_2	5.4±0.2	100	0	0	0	0	0
O_2	-	200	2.5×10^{-5}	3	35	13	53
H_2	5.6±0.3	100	0	0	0	0	0
H_2	-	200	4.16×10^{-5}	5	36	8	56
O_2-H_2	6.6±0.3	100	2.5×10^{-5}	3	31	19	55
O_2-H_2		200	1.0×10^{-4}	12	32	20	54
W+ Static air	3±0.1	100	6.3×10^{-4}	75	0	24	76
W+ Static air	7.4±0.1	200	1.16×10^{-4}	14	6	21	73
W+ Vacuum	3.5±0.1	100	7.58×10^{-4}	91	0	26	74
W+ Vacuum	6.5±0.1	200	3.66×10^{-4}	44	0	13	87
W+ O_2	4.4±0.2	100	0	0	0	0	0
W+ O_2	-	200	1.25×10^{-4}	15	4	12	84
W+ H_2	4.9±0.3	100	1.63×10^{-3}	5	16	15	69
W+ H_2	-	200	8.3×10^{-6}	1	42	11	47
W+ O_2-H_2	5±0.3	100	0	0	0	0	0
W+ O_2-H_2	-	200	1.75×10^{-4}	21	4	21	75

*W: Washed in toluene (as described in Section 4.2.2.1). Other entries indicate calcination atmosphere conditions (as described in Section 4.2.2.2). W+ indicates "washed in toluene followed by the corresponding calcination" (as described in Section 4.2.3). Initial rate calculated based for 3 hours reaction time.

Table 4.15 shows the initial rates of benzyl alcohol oxidation, conversions and selectivities towards detectable products after 3 hour reactions using catalysts from the same batches as used in 24 hour reactions discussed earlier. Negligible conversions (*ca*. 3%) were achieved in blank and control experiments. Samples with small (~ 2.6 nm) and large (~ 5.0 nm) average gold particle sizes had low activities over 3 hours of reaction, except for those washed with toluene then calcined under vacuum at 200 ^oC for 3 hours, which presented 44% conversion.

Low or moderate conversions were achieved within 3 hours using catalysts calcined under O_2, H_2, vacuum, O_2- H_2 or static air without prewashing with toluene. No conversion was

observed for samples treated by calcination alone at 100 ^{o}C in static air, vacuum, oxygen and hydrogen at lower temperature, while conversion was very low (5%) for a sample treated under O_2-H_2 alone. Of the samples calcined at 200 ^{o}C, a maximum conversion of 19% was observed for catalysts calcined under static air; 0%, 3%, 5% and 12% were achieved after calcination at 200 ^{o}C under vacuum, oxygen, hydrogen or O_2- H_2, respectively. The selectivity for reactions using all types of preparation favoured methyl benzoate over benzoic acid. In some cases, invariably where conversions were low, benzaldehyde was one of the major products. The product ratio was ~0:1:5 (aldehyde to acid to ester) when the catalyst calcined under static air at 200 ^{o}C without prewashing; it was ~2:1:3, 3:1:4, 5:1:7 and 2:1:3 (benzaldehyde and benzoic acid to methyl benzoate) when the gold catalyst was calcined under, vacuum, oxygen, hydrogen and O_2 - H_2 at 200 ^{o}C, respectively, without prewashing. Overall, the selectivity for benzaldehyde was much greater over 3 hours reaction than it was over 24 hours.

For catalysts that were prewashed in toluene, it is noteworthy that treated gold catalysts at the higher temperature (200 ^{o}C) showed systematically lower conversions except for R+O_2 (15%) or R+O_2 – H_2 (21%). The highest conversion of 91% was achieved using catalyst that was calcined in vacuum at 100 ^{o}C for 3 hours after washing in toluene. This catalyst had one of the smallest average particle sizes in series studied here (*ca*. 3.5±0.1 nm prior to reaction). The second best conversion (75%) was observed for a catalyst calcined in air at 100 ^{o}C after washing. It had the smallest average particle diameter of only 3.0 nm. The selectivity of gold catalysts for these two best-activated gold catalysts were both towards methyl benzoate, with product ratios of ~3:1 (methyl benzoate to benzoic acid), and no benzaldehyde. Of the methods investigated in this work, washing in hot toluene and mild calcination treatment conditions are both required to fabricate the most active catalysts. Interestingly, the third best conversion (44%) was achieved using a catalyst that was calcined in vacuum at 200 ^{o}C after

washing in toluene – a treatment that resulted in a large average particle size of 6.5 ± 0.2 nm with only *ca*. 3% of the particles being larger than *ca*. 3 nm. The selectivity of gold catalysts was towards methyl benzoate and the product ratio was ~7:1 (methyl benzoate to benzoic acid). Thus, interpretation based on particle sizes alone seems untenable.

Overall, activations of gold catalysts can be optimized to achieve high conversion of benzyl alcohol when the catalysts were washed with toluene and followed by calcinations in static air or vacuum at 100 ^{o}C for 3 hours. Although, thermal treatments are necessary to remove organic residues from gold particles, they cause an increase in the gold particle sizes.[5] One of the key problems that may emerge from the removal of the stabilizing ligand could be the loss of stability and sintering of the gold particles on the support due to the removal of the ligands.[1]

4.4 Reproducibility and stability of catalysts on storage

One important issue when testing a heterogeneous catalyst is to determine its reusability.[45] A common problem with gold catalysts is the lack of reproducibility of results obtained using freshly made catalysts and ones after storage, which may be because of catalyst preparation and/or (in) activation.[5a, 21a, 33a, 33b] To investigate this problem, we performed a comparative study on 1.0 wt% Au_{101}/C catalysts taken from the same batch and activated under the same conditions (washed with toluene followed by calcination under static air at 100 ^{o}C for 3 hours), but used either fresh or after stored in the refrigerator for 6 months. Each experiment was repeated several times in order to measure the reproducibility. Figure 4.16 presents the results for activated 1.0 wt% gold catalysts on conversion and selectivity, which show good reproducibility for benzyl alcohol oxidation.

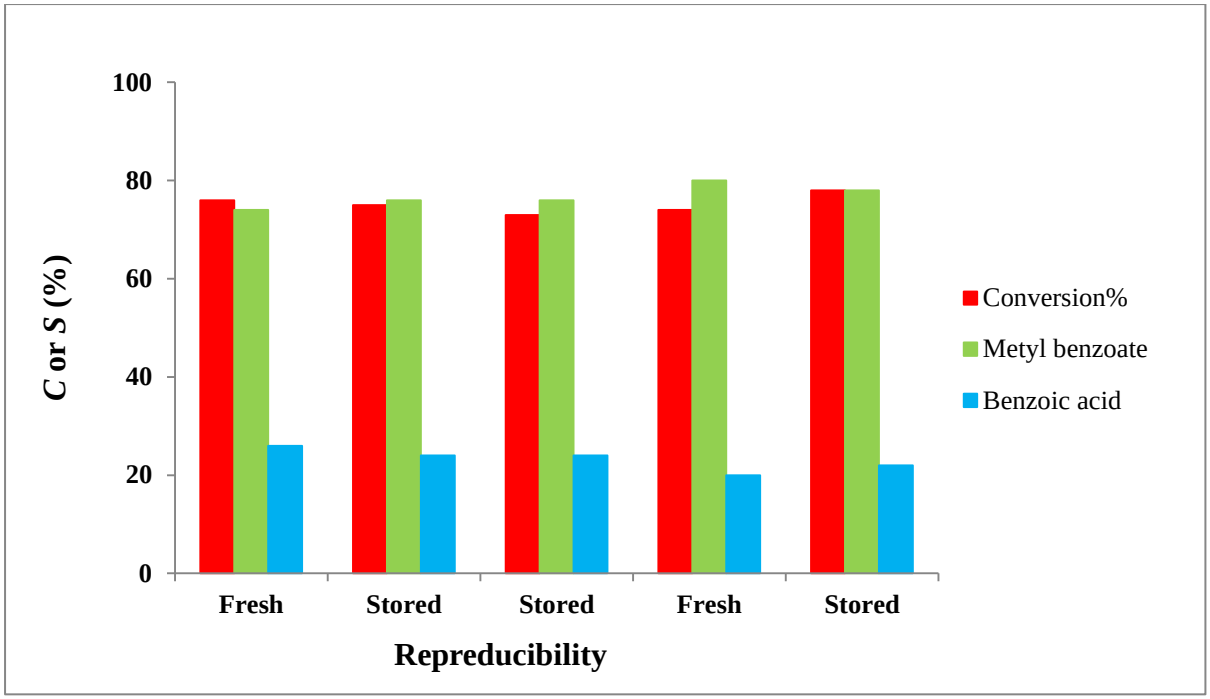

Figure 0.16: The reproducibility of conversion (*C%*) and selectivity (*S%*) of activated 1.0 wt% Au_{101}/C catalysts in the catalytic test under standard conditions with reaction time of 3 hours.

4.4 Conclusions

The data presented in this Chapter suggests that structural and catalytic properties of gold nanocatalysts for benzyl alcohol oxidation depend on the choice of the treatment and temperature. Activations including a toluene washing procedure and calcination under oxidising conditions mostly resulted in full conversions over 24 hour of reaction. However, some activation processes proved to be clearly inferior resulting in catalysts incapable of achieve full conversions after 24 hours of reaction.

Carbon-supported gold nanoparticles including un-treated, washed with toluene or calcined without prewashing, were inactive over 3 hours of reaction time. However, those treated by prewashing with toluene followed by calcination under mild conditions, led to a significant enhancement in the activity for benzyl alcohol. The conversion level displayed in this reaction is known to be affected by the gold nanoparticle size. The gold particles after

activation treatments were larger than the gold cores in the original clusters, meaning that sintering was occurring during treatment. One could conclude that catalysts containing small gold nanoparticles (≤ 2.6 nm) prior to treatment were less effective than slightly bigger particles (≤ 3.5 nm). For the best-performing gold catalysts, the highest catalytic activities and selectivities were achieved when the gold catalysts were pre-washed with toluene and calcined in static air (*C*%: 75%) or under vacuum at 100 ^{o}C for 3 hours (*C*%: 91%) with methyl benzoate as the main product. In comparison, treatments that did not involve prewashing were found to be relatively ineffective. The results of this study indicate that conversion of Au_{101} immobilized on activated gold can be remarkably influenced by the treatments conditions. For an inert support like carbon, the other important contributions are the type, temperature of calcinations and their combination with prewashing with toluene.

References

1. Lopez-Sanchez, J. A.; Dimitratos, N.; Hammond, C.; Brett, G. L.; Kesavan, L.; White, S.; Miedziak, P.; Tiruvalam, R.; Jenkins, R. L.; Carley, A. F.; Knight, D.; Kiely, C. J.; Hutchings, G. J., Facile removal of stabilizer-ligands from supported gold nanoparticles. *Nat. Chem.* **2011,** *3* (7), 551-556.
2. (a) Schmid, G.; Pugin, R.; Meyer-Zaika, W.; Simon, U., Clusters on clusters: Closo-dodecaborate as a ligand for Au_{55} clusters. *Eur. J. Inorg. Chem.* **1999,** *1999* (11), 2051-2055; (b) Schmid, G., The relevance of shape and size of Au_{55} clusters. *Chem. Soc. Rev.* **2008,** *37* (9), 1909-1930.
3. Zhu, Y.; Qian, H.; Jin, R., An atomic-level strategy for unraveling gold nanocatalysis from the perspective of Aun(SR)m nanoclusters. *Chem. Eur. J.* **2010,** *16* (37), 11455-11462.
4. Zou, X.; Qi, S.; Suo, Z.; An, L.; Duan, X., Effects of pretreatment conditions on catalytic performance of Au/Al_2O_3 for CO oxidation. *Chin. J. Catal.* **2004,** *25* (2), 153-157.
5. (a) Beck, A.; Horváth, A.; Schay, Z.; Stefler, G.; Koppány, Z.; Sajó, I.; Geszti, O.; Guczi, L., Sol derived gold-palladium bimetallic nanoparticles on TiO_2: Structure and catalytic activity in CO oxidation. *Top. Catal.* **2007,** *44* (1-2), 115-121; (b) Maciejewski, M.; Fabrizioli, P.; Grunwaldt, J.-D.; Sven, B. O.; Baiker, A., Supported gold catalysts for CO oxidation: Effect of calcination on structure, adsorption and catalytic behaviour. *Phys. Chem. Chem. Phys.* **2001,** *3* (17), 3846-3855.
6. Anderson, D. P.; Alvino, J. F.; Gentleman, A.; Qahtani, H. A.; Thomsen, L.; Polson, M. I. J.; Metha, G. F.; Golovko, V. B.; Andersson, G. G., Chemically-synthesised, atomically-precise gold clusters deposited and activated on titania. *PCCP* **2013,** *15* (11), 3917-3929.
7. (a) Donoeva, B. G.; Ovoshchnikov, D. S.; Golovko, V. B., Establishing a Au nanoparticle size effect in the oxidation of cyclohexene using gradually changing Au catalysts. *ACS Catalysis* **2013,** *3* (12), 2986-2991; (b) Anderson, D. P.; Adnan, R. H.; Alvino, J. F.; Shipper, O.; Donoeva, B.; Ruzicka, J. Y.; Al Qahtani, H.; Harris, H. H.; Cowie, B.; Aitken, J. B.; Golovko, V. B.; Metha, G. F.; Andersson, G. G., Chemically synthesised atomically precise gold clusters deposited and activated on titania. Part II. *PCCP* **2013,** *15* (35), 14806-14813.
8. (a) Yin, H.; Wang, C.; Zhu, H.; Overbury, S. H.; Sun, S.; Dai, S., Colloidal deposition synthesis of supported gold nanocatalysts based on Au-Fe3O4 dumbbell nanoparticles. *Chem. Commun.* **2008,** (36), 4357-4359; (b) Abad, A.; Corma, A.; García, H., Catalyst parameters determining activity and selectivity of supported gold nanoparticles for the aerobic oxidation of alcohols: The molecular reaction mechanism. *Chem.- Eur. J.* **2008,** *14* (1), 212-222.
9. Qi, C.; Okumura, M.; Akita, T.; Haruta, M., Vapor-phase epoxidation of propylene using H_2/O_2 mixture over gold catalysts supported on non-porous and mesoporous titania-silica: effect of preparation conditions and pretreatments prior to reaction. *Appl. Catal., A.* **2004,** *263* (1), 19-26.
10. Zhang, R. R.; Ren, L. H.; Lu, A. H.; Li, W. C., Influence of pretreatment atmospheres on the activity of Au/CeO_2 catalyst for low-temperature CO oxidation. *Catal. Commu.* **2011,** *13* (1), 18-21.
11. Turner, M.; Golovko, V. B.; Vaughan, O. P. H.; Abdulkin, P.; Berenguer-Murcia, A.; Tikhov, M. S.; Johnson, B. F. G.; Lambert, R. M., Selective oxidation with dioxygen by gold nanoparticle catalysts derived from 55-atom clusters. *Nature* **2008,** *454* (7207), 981-983.
12. Haruta, M., Catalysis of gold nanoparticles deposited on metal oxides. *CATTECH* **2002,** *6* (3), 102-115.
13. Tsubota, S.; Cunningham, D. A. H.; Bando, Y.; Haruta, M., Preparation of nanometer gold strongly interacted with TiO_2 and the structure sensitivity in low-temperature oxidation of CO. *Stud. Surf. Sci. Catal.* **1995,** *91*, 227-235.
14. (a) Park, E. D.; Lee, J. S., Effects of pretreatment conditions on CO oxidation over supported Au catalysts. *J. Catal.* **1999,** *186* (1), 1-11; (b) Ho, K. Y.; Yeung, K. L., Effects of ozone pretreatment on the performance of Au/TiO_2 catalyst for CO oxidation reaction. *J. Catal.* **2006,** *242* (1), 131-141.
15. Yuan, Y.; Kozlova, A. P.; Asakura, K.; Wan, H.; Tsai, K.; Iwasawa, Y., Supported Au catalysts prepared from Au phosphine complexes and As-precipitated metal hydroxides: Characterization and low-temperature CO oxidation. *J. Catal.* **1997,** *170* (1), 191-199.
16. Kilmartin, J. Molecular gold clusters as precursors to heterogeneous catalysts University College London, London, England, 2010.

17. (a) Gardner, S. D.; Hoflund, G. B.; Schryer, D. R.; Upchurch, B. T., Characterization study of silica-supported platinized tin oxide catalysts used for low-temperature carbon monoxide oxidation: Effect of pretreatment temperature. *J. Phys. Chem.* **1991,** *95* (2), 835-838; (b) Maciejewski, M.; Fabrizioli, P.; Grunwaldt, J. D.; Becker, O. S.; Baiker, A., Supported gold catalysts for CO oxidation: Effect of calcination on structure, adsorption and catalytic behaviour. *PCCP* **2001,** *3* (17), 3846-3855.
18. Yin, H.; Ma, Z.; Overbury, S. H.; Dai, S., Promotion of $Au(en)_2Cl_3$-Derived Au/Fumed SiO_2 by Treatment with $KMnO_4$. *J. Phys. Chem. C* **2008,** *112* (22), 8349-8358.
19. Dondur, V.; Lampa, S.; Vucelic, D., Thermal analysis of MnO-CuO catalysts. *J. Chem. Soc., Faraday Trans. 1* **1983,** *79* (7), 1633-1638.
20. Chang, C. T.; Liaw, B. J.; Chen, Y. P.; Chen, Y. Z., Characteristics of Au/Mg_xAlO hydrotalcite catalysts in CO selective oxidation. *J. Mol. Catal. A: Chem.* **2009,** *300* (1-2), 80-88.
21. (a) Abd El-Moemen, A.; Karpenko, A.; Denkwitz, Y.; Behm, R. J., Activity, stability and deactivation behavior of Au/CeO_2 catalysts in the water gas shift reaction at increased reaction temperature (300 °C). *J. Power Sources* **2009,** *190* (1), 64-75; (b) Minicò, S.; Scirè, S.; Crisafulli, C.; Galvagno, S., Influence of catalyst pretreatments on volatile organic compounds oxidation over gold/iron oxide. *Appl. Catal., B* **2001,** *34* (4), 277-285; (c) Kung, H. H.; Kung, M. C.; Costello, C. K., Supported Au catalysts for low temperature CO oxidation. *J. Catal. 216* (1-2), 425-432; (d) Lee, S. J.; Gavriilidis, A.; Pankhurst, Q. A.; Kyek, A.; Wagner, F. E.; Wong, P. C. L.; King, L. Y., Effect of drying conditions of AU-Mn co-precipitates for low-temperature CO oxidation. *J. Catal.* **2001,** *200* (2), 298-308.
22. Wang, X.; Kawanami, H.; Dapurkar, S. E.; Venkataramanan, N. S.; Chatterjee, M.; Yokoyama, T.; Ikushima, Y., Selective oxidation of alcohols to aldehydes and ketones over TiO_2-supported gold nanoparticles in supercritical carbon dioxide with molecular oxygen. *Appl. Catal., A.* **2008,** *349* (1–2), 86-90.
23. Pritchard, J.; Piccinini, M.; Tiruvalam, R.; He, Q.; Dimitratos, N.; Lopez-Sanchez, J. A.; Morgan, D. J.; Carley, A. F.; Edwards, J. K.; Kiely, C. J.; Hutchings, G. J., Effect of heat treatment on Au-Pd catalysts synthesized by sol immobilisation for the direct synthesis of hydrogen peroxide and benzyl alcohol oxidation. *Catal. Sci. Technol.* **2013,** *3* (2), 308-317.
24. Chiang, C.-W.; Wang, A.; Mou, C.-Y., CO oxidation catalyzed by gold nanoparticles confined in mesoporous aluminosilicate Al-SBA-15: Pretreatment methods. *Catal. Today* **2006,** *117* (1–3), 220-227.
25. Bulushev, D. A.; Yuranov, I.; Suvorova, E. I.; Buffat, P. A.; Kiwi-Minsker, L., Highly dispersed gold on activated carbon fibers for low-temperature CO oxidation. *J. Catal.* **2004,** *224* (1), 8-17.
26. Wang, L. C.; He, L.; Liu, Y. M.; Cao, Y.; He, H. Y.; Fan, K. N.; Zhuang, J. H., Effect of pretreatment atmosphere on CO oxidation over α-Mn_2O_3 supported gold catalysts. *J. Catal.* **2009,** *264* (2), 145-153.
27. (a) Miedziak, P.; Sankar, M.; Dimitratos, N.; Lopez-Sanchez, J. A.; Carley, A. F.; Knight, D. W.; Taylor, S. H.; Kiely, C. J.; Hutchings, G. J., Oxidation of benzyl alcohol using supported gold–palladium nanoparticles. *Catal. Today* **2011,** *164* (1), 315-319; (b) Villa, A.; Janjic, N.; Spontoni, P.; Wang, D.; Su, D. S.; Prati, L., Au-Pd/AC as catalysts for alcohol oxidation: Effect of reaction parameters on catalytic activity and selectivity. *Appl. Catal., A* **2009,** *364* (Copyright (C) 2012 American Chemical Society (ACS). All Rights Reserved.), 221-228.
28. Fristrup, P.; Johansen, L. B.; Christensen, C. H., Mechanistic investigation of the gold-catalyzed aerobic oxidation of alcohols. *Catal. Lett.* **2008,** *120* (3-4), 184-190.
29. Zhu, J.; Faria, J. L.; Figueiredo, J. L.; Thomas, A., Reaction mechanism of aerobic oxidation of alcohols conducted on activated-carbon-supported cobalt oxide catalysts. *Chem.-Eur. J.* **2011,** *17* (25), 7112-7117.
30. Enache, D. I.; Knight, D. W.; Hutchings, G. J., Solvent-free Oxidation of Primary Alcohols to Aldehydes using Supported Gold Catalysts. *Catal. Lett.* **2005,** *103* (1), 43-52.
31. Klitgaard, S. K.; Dela Riva, A. T.; Helveg, S.; Werchmeister, R. M.; Christensen, C. H., Aerobic oxidation of alcohols over gold catalysts: Role of acid and base. *Catal. Lett.* **2008,** *126* (3-4), 213-217.

32. Ma, Z.; Brown, S.; Overbury, S. H.; Dai, S., Au/PO_4^{3-}/TiO_2 and PO_4^{3-}/Au/TiO_2 catalysts for CO oxidation: Effect of synthesis details on catalytic performance. *Appl.Catal., A* **2007,** *327* (2), 226-237.
33. (a) Bus, E.; Prins, R.; van Bokhoven, J. A., Origin of the cluster-size effect in the hydrogenation of cinnamaldehyde over supported Au catalysts. *Catal. Commun.* **2007,** *8* (9), 1397-1402; (b) Haruta, M.; Yamada, N.; Kobayashi, T.; Iijima, S., Gold catalysts prepared by coprecipitation for low-temperature oxidation of hydrogen and of carbon monoxide. *J. Catal.* **1989,** *115* (2), 301-309; (c) Tsunoyama, H.; Sakurai, H.; Negishi, Y.; Tsukuda, T., Size-specific catalytic activity of polymer-stabilized gold nanoclusters for aerobic alcohol oxidation in water. *J. Am. Chem. Soc.* **2005,** *127* (26), 9374-9375.
34. Porta, F.; Prati, L.; Rossi, M.; Coluccia, S.; Martra, G., Metal sols as a useful tool for heterogeneous gold catalyst preparation: Reinvestigation of a liquid phase oxidation. *Catal. Today* **2000,** *61* (1-4), 165-172.
35. Zhu, J.; Carabineiro, S. A. C.; Shan, D.; Faria, J. L.; Zhu, Y.; Figueiredo, J. L., Oxygen activation sites in gold and iron catalysts supported on carbon nitride and activated carbon. *J. Catal.* **2010,** *274* (2), 207-214.
36. (a) Nielsen, I. S.; Taarning, E.; Egeblad, K.; Madsen, R.; Christensen, C. H., Direct aerobic oxidation of primary alcohols to methyl esters catalyzed by a heterogeneous gold catalyst. *Catal. Lett.* **2007,** *116* (1-2), 35-40; (b) Oliveira, R. L.; Kiyohara, P. K.; Rossi, L. M., Clean preparation of methyl esters in one-step oxidative esterification of primary alcohols catalyzed by supported gold nanoparticles. *Green Chem.* **2009,** *11* (9), 1366-1370.
37. Woehrle, G. H.; Brown, L. O.; Hutchison, J. E., Thiol-functionalized, 1.5-nm gold nanoparticles through ligand exchange reactions: Scope and mechanism of ligand exchange. *J. Am. Chem. Soc.* **2005,** *127* (7), 2172-2183.
38. Yuan, Y.; Asakura, K.; Wan, H.; Tsai, K.; Iwasawa, Y., Supported gold catalysts derived from gold complexes and as-precipitated metal hydroxides, highly active for low-temperature CO oxidation. *Chem. Lett.* **1996,** (9), 755-756.
39. Su, F.-Z.; Ni, J.; Sun, H.; Cao, Y.; He, H.-Y.; Fan, K.-N., Gold supported on nanocrystalline β-Ga_2O_3 as a versatile bifunctional catalyst for facile oxidative transformation of alcohols, aldehydes, and acetals into esters. *Chem. Eur. J.* **2008,** *14* (24), 7131-7135.
40. Dimitratos, N.; Lopez-Sanchez, J. A.; Morgan, D.; Carley, A. F.; Tiruvalam, R.; Kiely, C. J.; Bethell, D.; Hutchings, G. J., Solvent-free oxidation of benzyl alcohol using Au-Pd catalysts prepared by sol immobilisation. *PCCP* **2009,** *11* (25), 5142-5153.
41. (a) Sergio, N.; Roberto, M.; Mercedes, A.; Hermenegildo, G., Sunlight-assisted fenton reaction catalyzed by gold supported on idamond nanoparticles as pretreatment for biological dDegradation of aqueous phenol solutions. *ChemSusChem* **2011,** *4* (5), 650-657; (b) Wang, Z. J.; Brown, C. J.; Bergman, R. G.; Raymond, K. N.; Toste, F. D., Hydroalkoxylation catalyzed by a gold(I) complex encapsulated in a supramolecular host. *J. Am. Chem. Soc.* **2011,** *133* (19), 7358-7360.
42. (a) Allen, J.; Rosenberg, E.; Karakhanov, E.; Kardashev, S. V.; Maximov, A.; Zolotukhina, A., Catalytic properties of transition metal salts immobilized on nanoporous silica polyamine composites II: Hydrogenation. *Appl. Organomet. Chem.* **2011,** *25* (4), 245-254; (b) Choudhary, V. R.; Jha, R.; Jana, P., Solvent-free selective oxidation of benzyl alcohol by molecular oxygen over uranium oxide supported nano-gold catalyst for the production of chlorine-free benzaldehyde. *Green Chem.* **2007,** *9* (3), 267-272; (c) Bond, G.; Thompson, D., Gold-catalysed oxidation of carbon monoxide. *Gold Bull.* **2000,** *33* (2), 41-50.
43. Zheng, N.; Stucky, G. D., Promoting gold nanocatalysts in solvent-free selective aerobic oxidation of alcohols. *Chem. Commun.* **2007,** (37), 3862-3864.
44. Ishida, T.; Nagaoka, M.; Akita, T.; Haruta, M., Deposition of gold clusters on porous coordination polymers by solid grinding and their catalytic activity in aerobic oxidation of alcohols. *Chem.- Eur. J.* **2008,** *14* (28), 8456-8460.
45. Zhu, J.; Figueiredo, J. L.; Faria, J. L., Au/activated-carbon catalysts for selective oxidation of alcohols with molecular oxygen under atmospheric pressure: Role of basicity. *Catal. Commun.* **2008,** *9* (14), 2395-2397.

Chapter 5: Support and Size Effects on the Catalytic Activity of Gold Catalysts

5.1 Introduction

Gold is known to have the most remarkable and genuine "nanosize effect". In terms of catalytic activity, the small particles size means a larger number of the atoms are in contact with the support, and on the edge and vertex sites of the particles. In the case of CO oxidation, it is found that the catalytic activity depends on gold particle size (see Figure 5.1).[1] Hutching *et al.* found that small gold nanoclusters with diameters of ~0.5 nm are active catalysts for conversion of CO to CO_2 under low temperature conditions.[2] However, Haruta *et al.*[3] and later Goodman *et al.*[4] the best performance for CO oxidation is also exhibited by particles with diameters of approximately 3 nm.[5] The general observation that small particles are good catalysts was explained by taking into account that the number of low-coordinate atoms, which are considered to be active sites in many reactions, increases as the particle size decreases.

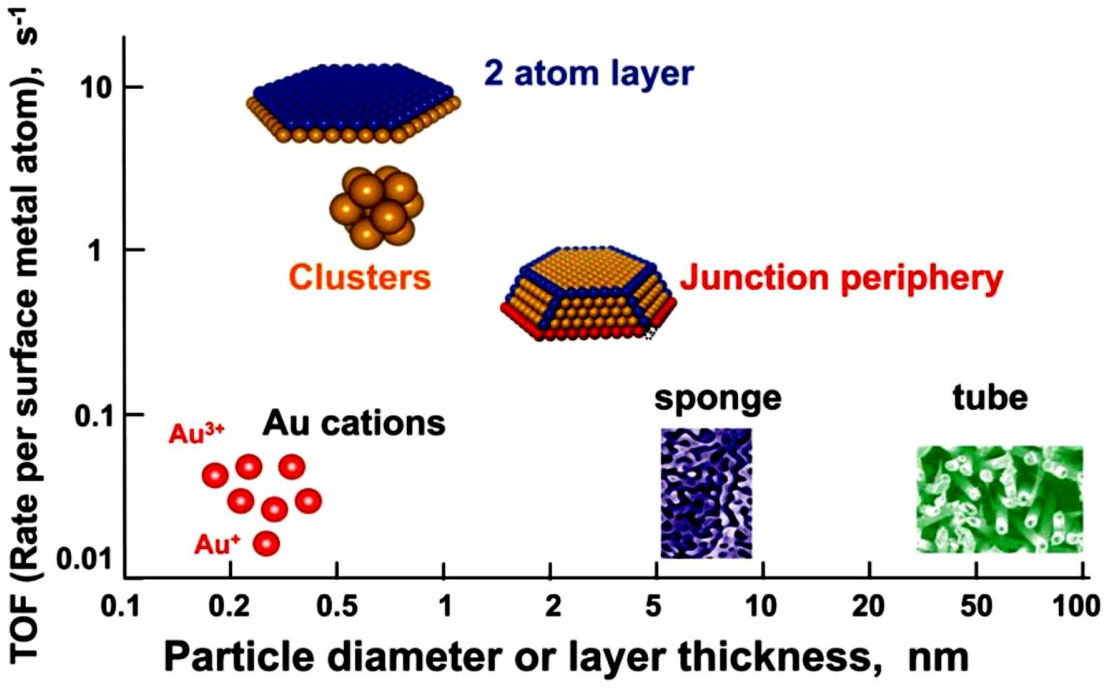

Figure 0.1: Turn over frequency (TOF) per surface metal atom for CO oxidation at room temperature for as a function of gold particle sizes (diameter of height of gold). Reproduced from Haruta.[6]

As the size of a metal particle decreases, a number of things occur as follows:

A. the fraction of surface atoms increases (see Figure 5.2) and, because these vibrate more freely, the melting temperature falls and surface atom mobility rises.[7]
B. Because the overlap of electron orbitals decreases as the average number of bonds between atoms becomes less, the band structure is weakened and surface atoms, in particular, start to behave more as individuals than as members of the bulk.
C. At the same time, a greater fraction of the atoms comes into contact with the support, and the length of the edge per unit mass rises.[6, 8]

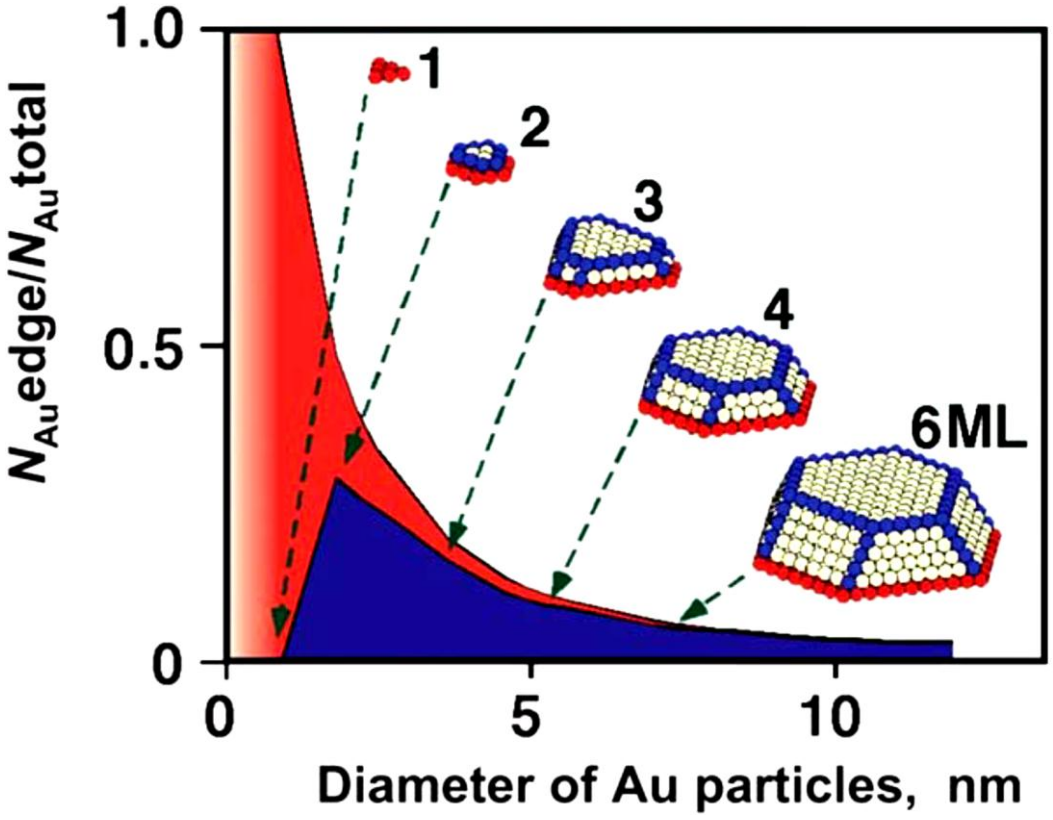

Figure 0.2: Fractions of edge and corner atoms and of perimeter atoms as a function of the diameter of pseudo-hemispherical gold nanoparticles. 'Red' and 'blue' colours correspond to the total and "free" step sites on the Au particles. "Free" are the step sites *not* in direct contact with the support. Reproduced from Mavrikakis *et al.*[7]

Ever since the potential catalytic applications of gold nanoparticles have been seriously considered, controlling the size of clusters has been one of the biggest challenges.[9] Early studies have shown that the activity of small gold clusters depends on the exact number of atoms.[10] Many researchers believe that the active species are very small gold particles, containing just a few atoms.[11] Gold clusters can be generally classified into two types: those stabilised by phosphine ligands and those stabilised by thiol or other ligands.[12] Of the gold clusters that have been investigated for heterogeneous catalysts, Au_9 (*i.e.*, $Au_9(PPh_3)_8(NO_3)_3$), is the most widely studied, especially for low-temperature CO oxidation.[13] A range of gold phosphine complexes have been synthesised with other particles sizes.[14]

Schmid *et al.* introduced Au_{55} nanoparticles as the first example of a well-defined phosphine ligand-stabilized nanoparticles in 1981.[14c] Their synthesis involved the reduction of $Au(PPh_3)Cl$ with diborane to yield gold particles that they formulated as $(Au_{55}(PPh_3)_{12}Cl_6)$, where the 55 gold atoms were believed to form a two-shell cuboctahedron with a ccp arrangement. Each of the 12 corner atoms was bound to a phosphine ligand, while the six chloride ligands were located at the central gold atom of six square planes (see Figure 5.3). However, this "model" assignment has never been confirmed by X-ray crystallography, while cryo-TEM study showed that this system has at least some degree of particle-size distribution (see more details in Chapter 1, Section 1.1.1).[14c]

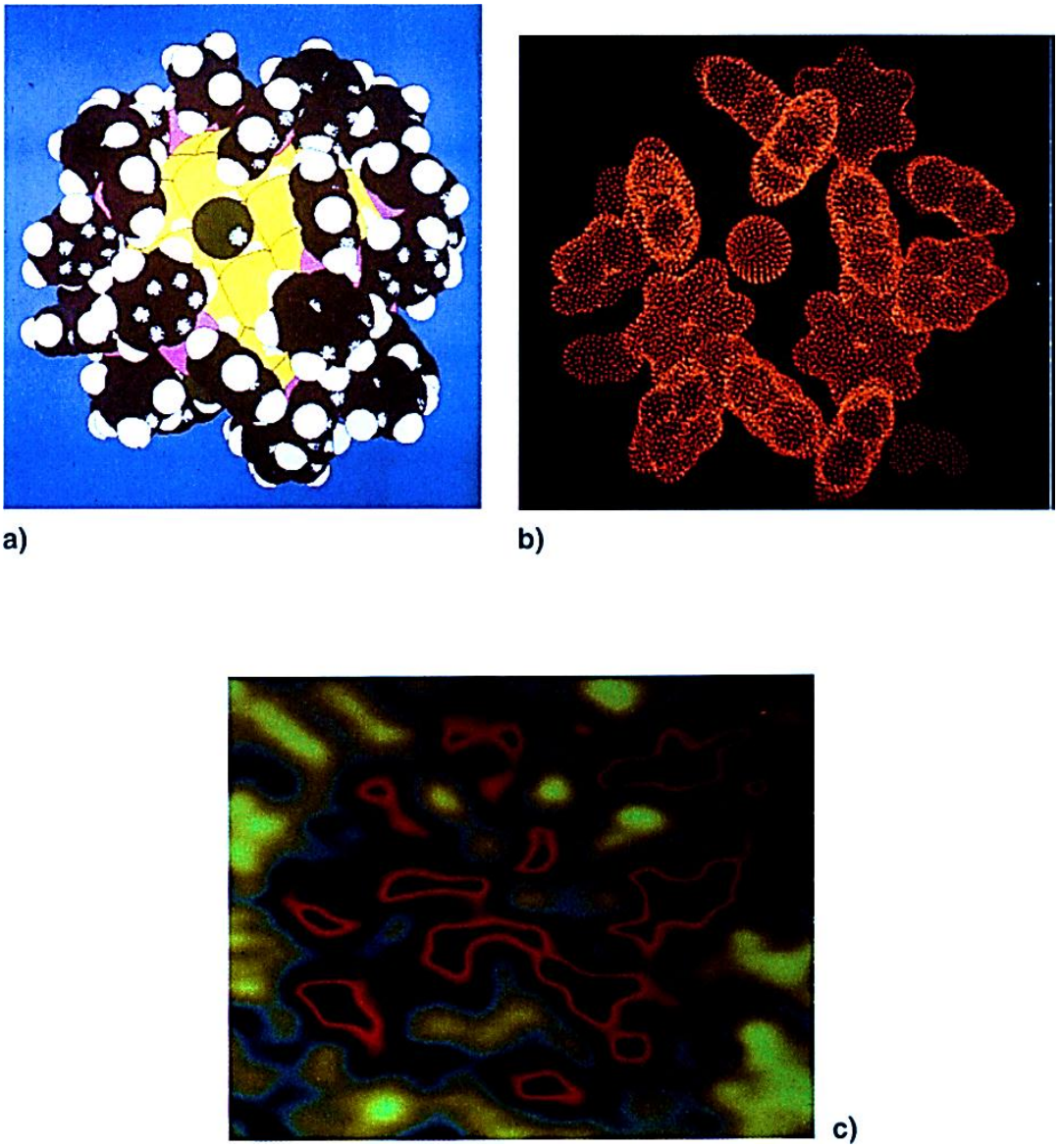

Figure 0.3: a) A computer simulated space filling model of Au_{55}. b) A computer simulated "two-dimensional" electron density image of Au_{55}. c) The STM image of the same cluster in probably the same orientation as in b). The similarities between images in b) and c) are evident. A chlorine atom is positioned in the centre of the images. Reproduced from Fenske *et al.*[15]

Au_{55} has been considered to be a model system for studies of the catalytic properties of very small metal particles. Turner *et al.* reported that supported Au_{55} exhibited the high activity of styrene oxidation with high selectivity towards benzaldehyde.[16] Later, Roldan *et al.* showed that catalytic activity of bare Au_{55} strongly depended on the gold particles' structure.[17] Pei *et al.* found, by using computational methods, that the catalytic activity and selectivity of Au_{55} can be attributed to a combination of factors, including the shape and the core-and-ligands structural arrangement.[18] Particular attention has been placed on determining the active site

on the Au_{55} core and the mechanism underlying the high selectivity of the nanocatalysts in styrene oxidation.[18]

In the field of alcohol oxidation, recent studies have shown that in the case of unsupported gold particles that smaller gold particles are more active,[19] whereas for supported gold somewhat larger particles were found to have higher activity.[20] "*Naked*" gold with small particle sizes (< 4 nm) proved to be an active catalyst for organic compounds, such as alcohol oxidation and olefin epoxidation, especially when immobilized on a support.[21] For example, Comotti *et al.* found that ~3.6 nm naked gold nanoparticles immobilized on carbon can act as an active catalyst for aerobic oxidation of glucose to gluconate under mild conditions.[21b]

Many experimental studies have focused on the catalytic activity of gold nanoparticles with small (~3 nm) gold particles.[4] However, CO oxidation catalysed by larger ~4 nm nanoparticles has been scarcely studied, [21b] and the effect of the particle size on the catalytic oxidation of organic compounds by gold catalysts containing larger particles is still not well understood.[22] Gold colloids with particle diameters bigger than 10 nm have been utilized,[23] and when immobilized on carbon showed high activity in the liquid phase oxidation of ethane-1,2-diol.[23b] Although, small gold clusters are generally more active as hydrogenation catalysts,[24] supported gold particles with a diameters from 10 to 20 nm have been found (possibly as an exception) to be more active than the smaller ones for selective hydrogenation of but-2-enal.[25]

In the case of benzyl alcohol oxidation, Haider *et al.* investigated the effect of the gold particle size on the catalytic activity of Au colloids, prepared by reduction of $HAuCl_4$ by tetrakis (hydroxymethyl) phosphonium chloride (THPC) in alkaline solution and immobilized on TiO_2, with four different mean particle diameters: 1.3 ± 0.5, 2.1 ± 0.7, 6.9 ± 3.61, and 11.3 ± 5.95 nm. The highest (25%) conversion of benzyl alcohol oxidation in mesitylene solution

occurred when the average particle diameters was ~6.9 nm. However, when the solvent changed to toluene the conversion decreased to 10% for ~6.9 nm gold particles.[26] Liu *et al.* studied the size effect of silica-supported gold clusters on benzyl alcohol oxidation in the presence of H_2O_2 and microwave radiation. They immobilized gold clusters with average diameters of 0.8 ± 0.3, 1.5 ± 0.6, and 1.9 ± 1 nm on mesopores silica (SBA-15) , and found that the activity decreased monotonically with the increase in size.[27]

Boronat *et al.* studied the reaction pathway for the selective oxidation of alcohols to aldehydes by using periodic density functional theory (DFT) calculations on a series of catalyst models. They showed that small (~3 nm) gold nanoclusters can act as effective nanocatalysts for alcohol oxidation.[5] By combining their theoretical results with experimental results reported in the literature, they concluded that the presence of low-coordinate gold atoms enhances alcohol adsorption on the gold catalyst thereby decreasing the activation barrier for dehydrogenation. This suggests a compelling explanation for the influence of particle size on the oxidation activity of gold nanocatalysts.[5] However, previous research clearly demonstrated that aerobic oxidation of benzyl alcohol in methanol solution can be catalysed by 2–8 nm gold particles immobilized on various types of support.[28] Table 5.1 provides selected examples illustrating the size effect on catalytic activity of supported gold particles in benzyl alcohol oxidation.

Table 0.1: Examples of benzyl alcohol oxidation catalysed using supported gold particles.

Catalyst code	Size	Solvent	Oxidant	BzOH (mmol)	Au (mg)	*Method	Temp. (^{o}C)	*C*%	Ref.
Au/SiO_2	5.7	MeOH	O_2	2.5	24	IG	70	3	[28b]
							110	96	
							130	100	
Au/C	2	MeOH	O_2	1	99	SG	80	>99	[28d]
Au/TiO_2	2-5	MeOH	O_2	1.1	0.33	-	-	>99	[28a]
Au/Ga_2O_3	7-8	MeOH	O_2	3.5	56.1	GP	90	98	[28c]

*Method abbreviations: IG= impregnation, SG= solid grinding and GP= gel precipitation.

To prevent particle aggregation, catalytic nanoparticles can be immobilized on solid supports (*e.g.*, carbon, metal oxides, zeolites *etc.*) or stabilized by capping ligands ranging from small organic molecules to large polymers.[1a, 29] The interaction of nanoparticles with stabilizer or a capping agent is one of the pivotal factors determining the catalytic performance.[30] Generally, catalytic activity is low if the interactions are very strong due to blocking of surface sites, while interaction that are too weak fail to stabilize the system and lead to nanoparticle agglomeration.[1a, 29b, 31] The cluster geometry may play an important role in the interaction of the clusters with the support.[30]

Supports are typically catalytically inert and are used as surface area promoters, to ensure a high surface area of un-aggregated metal nanoparticles.[32] Pores materials have internal surface areas up to hundreds of square metres per gram, and micro-pores materials have even higher internal surface areas.[30] Supported metals typically have high dispersions so that large fractions of the atoms are accessible to reactants.[30] Many industrial catalysts incorporate additional components[30] that can provide a combination of large specific surface area with appropriate size particles for better connection with reactants.[33]

Carbon is a low cost, high surface area and environmentally friendly material that is increasing in popularity as a support for the catalytically active phases.[34] Activated carbon is

a common term used to describe commercially available carbon-based materials that contain well-developed internal pore structures.[19] The surface area and pore structures of carbon play important roles in the dispersion and hence their catalytic activity of nanoparticles.[35] Moreover, supported metals catalysts can be recovered by simply burning off the catalyst support.[34b]

Activated carbon surfaces are known to include acidic or basic functional groups, such as carboxyl, carbonyl and phenol groups,[25] which can be derived from activation process, precursors, thermal treatments and/or post chemical treatments.[19, 36] These functional groups can act as anchors to which metal complexes could be attached and as nucleation centres, limiting the particle growth, improving their dispersion, and enhancing their stability.[37] Activated carbon exhibits a strong surface interaction with oxygen through the functional groups.[38] A wide variety of activated carbons bearing such functional groups allow the use of various immobilization procedures.[26] The amount of oxygen containing functional groups on a carbon surface can be characterized by using temperature programmed desorption (TPD) profiles, which can be analysed by a simple deconvolution method.[39] Functional groups can be influenced by types of activation and activation temperatures.[38a]

The relationship between different types of activated carbons and catalytic activity mainly depends on the total active surface area,[40] which can be measured using the Brunauer–Emmett – Teller (BET) method based on the adsorption of nitrogen gas.[41] The high surface areas (251 to 2204 m^2/g) typically possessed by activated carbons leads to better dispersion of gold particles which generally enhances catalytic activity.[42]

The structural and dynamical properties of pores carbon materials depend on variables, such as pore size.[40] Pore size not only determines the available surface area but also controls access of substrate molecules to the immobilized gold particles.[43] A wide range of possible

porosity types (micro-, meso- and macro-pores) and well-developed internal pore structures make activated carbon a versatile material with numerous potential applications in catalysis.[19] Micropores carbon has pores smaller than 2 nm that give rise to poor catalytic activity.[44] Larger pore diameters (greater than 2 nm) and larger pore volumes are more suitable for catalysis since they increase the surface area and facilitate transport of reactants and products.[45]

Vulcan carbon is composed of extensively agglomerated nanosized carbon particles with a significant volume of micropores material in addition to a minority of mesopores material and a total pore volume of 0.67 $cm^3. g^{-1}$ (see Figure 5.4).[45b, 46] Its utilization as an inert support for noble metal nanoparticles results in poor catalytic activity due to the low surface area (235 $m^2. g^{-1}$) and the presence of many microspores (0.25 $m^3.g^{-1}$).[45b, 47]

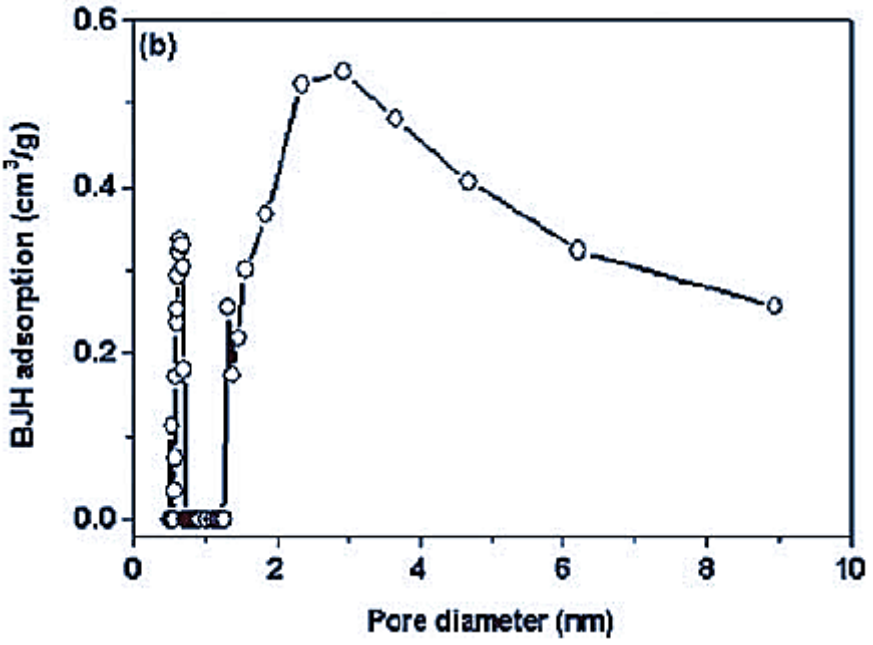

Figure 0.4: Pore size analyses from the adsorption branch of the isotherms of Vulcan XC 72R carbon. Reproduced from Raghuveer and Manthiram.[46]

Mesopores carbons have an interconnected pore network, tuneable high surface area with tailor-made surface properties, a large pore volume with a tuneable pore size and a narrow pore-size distribution. These features make such supports an attractive choice for fabrication of catalysts with uniform dispersion of metal particles that are active in various processes.[37a, 48] These types of materials can be of natural origin or be synthesised by carbonization of carbon-containing substances followed by activation of the samples.[49]

CMK-3 is a type of synthetic mesopores carbon composed of carbon nanorods arranged in a two-dimensional (2-D) hexagonal pattern (see Figure 5.5) and formed by using a silica sieve SBA-15 as a template.[50] The size distribution of metal nanoparticles on CMK-3 strongly depends on the carbon support properties.[37a] Kuppan and Selvam investigated the activities of platinum particles immobilized on CMK-3 (Pt/CMK-3) and activated carbon (Pt/C) for the catalytic oxidation of methanol. They found that Pt/CMK-3 showed higher activity (95%), which they attributed to a higher surface area (997 m^2/g), larger pore size (4 nm) and more appropriate pore volume (1.3 cm^3/g).[37a] Garcı´a *et al.* compared the catalytic activity of bimetallic Au-Pd/C and Au-Pd/CMK-3 in the direct synthesis of H_2O_2, finding a slightly higher catalytic activity of 37% for the former compared with 34% for the latter.[51]

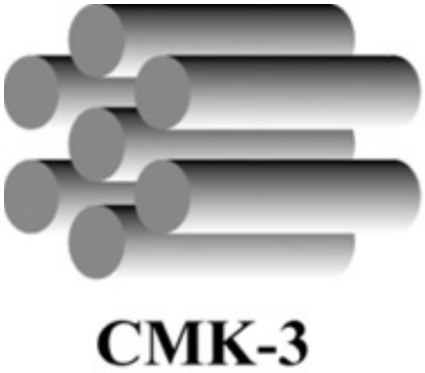

Figure 0.5*:* A framework of mesopores carbon CMK-3. Reproduced from Kawase *et al.*[52]

Another type of meso-pores carbon is CMK-8 with an ordered three-dimensional (3-D) cubic arrangement of continuous but interpenetrating networks of chiral channels prepared via a hard-template nanocasting approach using KIT-6 silica as the mother template (see Figure 5.6).[53] The unique, highly branched and intertwined 3-D channel network is likely to provide accessible entrances and channels as well as to serve as a highly opened pores host with easy and direct access for particles, which may result in a higher activity when this type of carbon is used as a support.[53b] Maiyalagan *et al.*, who studied the catalytic effectiveness of Pt-Ru/CMK-8 for methanol oxidation, found excellent performance that they attributed to better mass transfer resulting from the relatively large pore volume (1.48 cm^3/g), greatly enhanced surface area (1149 m^2/g) and large pore diameter (3.2 nm) .[47]

Figure 0.6: A framework of mesopores carbon CMK-8. Reproduced from Kawase *et al*.[52]

The mesopores structure of another synthetic carbon material, NCCR-41, exhibits two dimensional (2-D) hexagonal pore structure,[48b] which may help to achieve fine dispersion of metal nanoparticles and to eliminate diffusion problems.[48b] Selvam and Kuppan studied P/NCCR-41 as a catalyst for methanol oxidation and found that it performed in an excellent manner due to greatly enhanced surface area (1080 m^2/g), suitable pore diameter (2.2 nm) and appropriate pore volume (0.83 cm^3/g).[48b] The high activity of gold particles immobilized on the mesopores carbons, such as CMK-3, CMK-8 and NCCR-41, is attributed to excellent

dispersion and utilization of noble metal nanoparticles, which essentially originate from a high surface area, large pore volume and narrow pore size distribution.[37a, 47, 48b]

Gold nanoparticles dispersed on proper supports have recently been found to exhibit high heterogeneous catalytic activity and selectivity in certain oxidation reactions.[54] However, when different carbon materials with different textural and chemical properties are used, they can exhibit large differences of catalytic activity, which suggests that the role of the support is very complex.[55] The aim of the present chapter is to gain a deeper insight into the role of the nature of support by looking at the behaviour of gold nanoparticles immobilized on different types of activated carbons in the oxidation of benzyl alcohol under optimized conditions.

5.2 Results and discussion

The gold catalysts were 1.0 wt% Au_{101}/C where the immobilisation support was various types of carbon. The supported catalysts were washed with toluene or NaOH in MilliQ water (0.1 M) followed by calcination under static air or vacuum at 100 ^{o}C for 3 hours, as described in Chapter 4 (see in Chapter 4, Sections 4.2.3.1– 4.2.3.2). Test reactions were performed using 50 mg of catalysts. Under mild conditions for 3 hours – *i.e.*, benzyl alcohol: 2.5 mmol, base: 2.5 mmol, anisole: 1.25 mmol, methanol: 25 mL, temperature: 80 ^{o}C, oxygen gas pressure: 73 psi, stirring: 750 rpm, time: 24 h and Au_{101}/C: 50 mg.

5.2.1 Support effect on the catalytic activity and selectivity of Au_{101} particles

We hypothesised that different types of activated carbon could be efficient supports for improving the catalytic activity of gold nanocatalysts for benzyl alcohol oxidation.[28d] The key aim was to pinpoint supports which yield the best catalysts under these conditions of catalyst

preparation (see more detail in Chapter 4) and testing (see more detail in Chapter 3). These carbon supports include Norit activated carbon samples with different physical presentations (*i.e.*, powder, granular and granular which we powdered) and surface area, granular Norit modified with –SH and $–SO_3H$ groups, mesopores carbons CMK-3, CMK-8 and NCCR-41, and Vulcan carbon. We also performed detailed characterizations to clarify the particle-size effects on catalytic activity. Some of the properties of these supports that could affect the catalytic activity of gold catalysts (surface area, pore diameter and pore volume)[23a] are listed in Table 5.2.

Table 0.2: Structural properties of various carbons support were used in this thesis.

Carbon code	Surface area, BET (m^2g^{-1})	Pore diameter, D (nm)	Pore volume, Vp (cm^3g^{-1})
Powder (Norit)	813	3.2	0.44
Granular (Norit)	1227	2.1	0.58
CMK-3	997	4	1.3
CMK-8	1905	2.9	1.6
NCCR-41	1080	2.2	0.83
Vulcan	254	Broad	0.67

5.2.1.1 Comparisons of conversion and selectivity among gold nanoparticles immobilized on powder, granular and powdered Norit activated carbon

Commercially available Norit activated carbon was donated to the University of Canterbury in the powder form (SX1G 8001-9, BET: 813 m^2/g) and granular form (RX 3 EXTRA 570104, BET: 1227 m^2/g) (see more details in Chapter 2, Section 2.5.1.1). In the catalyst code designations, these are designated C and C_g, respectively. Samples were also produced that were made form granular Norit carbon that was ground at the University of Canterbury, and were designated C_{g+p}.

Table 0.3: Comparisons of conversion and selectivity achieved using activated gold particles immobilized on powder, granular and powdered granular Norit activated carbon for 3 hours reaction time.

#Catalyst code	***Activation**	**Conversion%**	**Selectivity%**		
			Benzaldehyde	**Benzoic acid**	**Methyl benzoate**
1.0% Au_{101}/C	W+ static air	75	0	24	76
1.0% Au_{101}/C	W+ vacuum	91	0	24	74
1.0% Au_{101}/C_g	W+ static air	1	59	27	14
1.0% Au_{101}/C_g	W+ vacuum	3	60	26	14
1.0% Au_{101}/C_{g+p}	W+ static air	1	65	24	13
1.0% Au_{101}/C_{g+p}	W+ vacuum	6	66	24	12

#Catalyst code: Au_{101}/C_g and $Au101/C_{g+p}$ = Au_{101} particles immobilized on Granular Norit activated carbon and Granular Norit activated carbon which we powdered, respectively. ***Activations:** Gold catalysts washed with toluene followed by calcination under static air or vacuum at 100 ^oC for 3 hours.

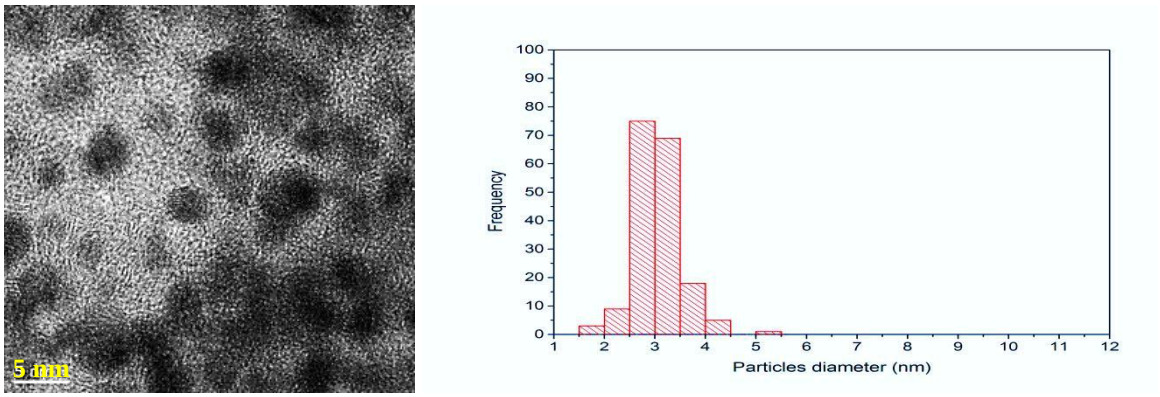

Figure 0.7: Left: a representative TEM image of treated 1.0 wt%Au_{101}/C (washed with toluene followed by calcination under static air at 100 ^oC for 3 hours) deposited onto carbon film coated copper TEM grid; Right: Particles size distribution histogram. The average particle size of gold particles was determined to be 3.0 ± 0.1 nm (two standard deviations of the mean).

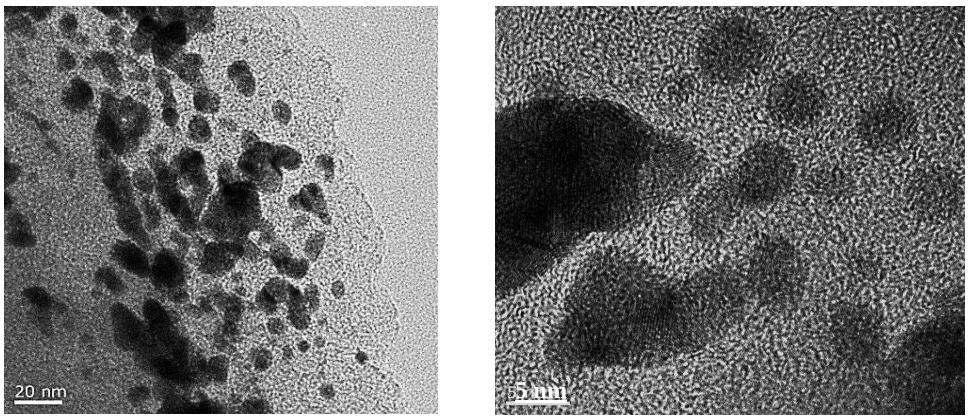

Figure 0.8: Representative TEM images (left: low magnification and right: high magnification) of treated 1.0 wt%Au_{101}/C_g (washed with toluene followed by calcination under static air at 100 ^oC for 3 hours) deposited onto carbon film coated copper TEM grid.

TEM images of Au_{101}/C_g showed that many gold particles aggregate to give very big particles when immobilized on granular Norit activated carbon (see Figure 5.8). Although, a few small gold particles were also, negligible conversions (no more than 7%) were observed (see Table 5.3) for both types of granular carbons (*i.e.*, C_g and C_{g+p}) whether they be calcined under static air or vacuum. However, the results showed reasonable selectivity for benzaldehyde as the main product (approximately 60%) with the remaining products split ~2:1 benzoic acid to methyl benzoate. In contract, the gold Au_{101} immobilized on powder Norit activated carbon demonstrated much higher activity (75%) and selectivity towards methyl benzoate as the main product in a product ratio of ~3:1 ester to acid and no significant production of the aldehyde (see Table 5.3). The TEM image of 1.0 wt% Au_{101}/C showed the average particle diameter was 3 ± 0.1 nm with a narrow size distribution indicating far lesser gold particle aggregation (see Figure 5.7). Both Norit activated carbons have high surface areas, along with relatively large pore diameters and volumes. The difference between them might be different functional groups. For better understanding of this tests using temperature programmed desorption (TPD) are suggested for future work.[39]

5.2.1.2 Comparisons of conversion and selectivity of gold nanoparticles immobilized on Norit carbon (powder) and modified Norit granular carbons (– SH and $–SO_3H$)

Au_{101} was immobilized on RX 3 EXTRA 570104 granular Norit activated carbon (BET: 1227 m2/g) that was functionalised (see in Chapter 2, Section 2.5.1.1) with –SH or $–SO_3H$ groups to give catalysts designated, $Au_{101}/C_{g.-SH}$ and $Au_{101}/C_{g.-SO3H}$). [26] These catalysts did not show any improvement in benzyl alcohol conversion (see Table 5.4).

Table 0.4: Comparison of conversion and selectivity between gold particles immobilized on granular Norit activated carbon which was modified (–SH and $–SO_3H$) and Norit activated carbon (powder) for 3 hours reaction time.

#**Catalyst code**	***Activation**	**Conversion%**	**Selectivity%**		
			Benzaldehyde	**Benzoic acid**	**Methyl benzoate**
1.0% Au_{101}/C	W+ static air	75	0	24	76
1.0% Au_{101}/C	W+ vacuum	91	0	24	74
1.0% $Au_{101}/C_{g.-SH}$	W+ static air	0	0	0	0
1.0% Au_{101}/ $C_{g.-SH}$	W+ vacuum	0	0	0	0
1.0% Au_{101}/ $C_{g.-SO3H}$	W+ static air	0	0	0	0
1.0% $Au_{101/}$ $C_{g.-SO3H}$	W+ vacuum	0	0	0	0

#**Catalyst code:** Au_{101}/ $C_{g.-SH}$ and Au_{101}/ $C_{g.-SO3H}$ = Au_{101} particles immobilized on Granular Norit activated carbon which was modified by –SH and $–SO_3H$, respectively. *__Activations:__ Gold catalysts washed with toluene followed by calcination under static air or vacuum at 100 ^oC for 3 hours.

5.2.1.3 Comparisons of conversion and selectivity of gold particles immobilized on Norit activated carbon (powder) and mesopores carbons (CMK-3, CMK-8 and NCCR-41)

The mesopores carbons CMK-3, CMK-8 and NCCR-41 (provided by Doctor Balaiah Kuppan and Professor Parasuraman Selvam Institute of Technology, Madras (see in Chapter 2, Section 2.5.1.1) with a variety of pore structures, pore volumes and surface areas were used as a supports for Au_{101} to give catalysts, abbreviated, respectively, as Au_{101}/C_3, Au_{101}/C_8 and Au_{101}/C_{41}. All of these gave high catalytic activities (summarise in Table 5.5) that were comparable to 1.0 wt% Au_{101}/C and which are discussed below.

Table 0.5: Comparisons of conversion and selectivity between gold particles immobilized on Norit activated carbon (powder) and different types of meso-pores carbons including CMK-3, CMK-8 and NCCR-41 for 3 hours reaction time.

[#]Catalyst code	[*]Activation	Conversion%	Selectivity%		
			Benzaldehyde	Benzoic acid	Methyl benzoate
1.0% Au_{101}/C	W+ static air	75	0	24	76
1.0% Au_{101}/C	W+ vacuum	91	0	24	74
1.0% Au_{101}/C_3	W+ static air	72	0	16	84
1.0% Au_{101}/C_3	W+ vacuum	78	0	19	81
1.0% Au_{101}/C_8	W+ static air	96	0	16	84
1.0% Au_{101}/C_8	W+ vacuum	95	0	16	85
1.0% Au_{101}/C_{41}	W+ static air	35	1	10	89
1.0% Au_{101}/C_{41}	W+ vacuum	88	0	12	88

[#]**Catalyst code:** Au_{101}/C_3, Au_{101}/C_8 and Au_{101}/C_{41}= Au_{101} particles immobilized on CMK-3, CMK-8 and NCCR-41carbon mesopores, respectively. [*]**Activations:** Gold catalysts washed with toluene followed by calcination under static air or vacuum at 100 ^{o}C for 3 hours.

5.2.1.3.1 Mesopores structure of CMK-3

Gold particles immobilized on CMK-3 activated by washing with toluene followed by calcination at 100 ^{o}C for 3 hours under static air and vacuum showed high activities with conversions of 72% and 78%, respectively. These conversions, comparable to Norit activated carbon powder, which is possibly a reflection of similarities of the surface area, pore size, average particle diameter (3.1 ± 0.1 nm), and size distributions.[56] The main product was methyl ester (selectivity ~83%) with benzoic acid as the minor product (selectivity ~17%) and no benzaldehyde (see Table 5.5). This is the first time that such a significant improvement occurred in terms of achieving high selectivity of gold catalysts towards methyl benzoate as the main product (81% and 84%).

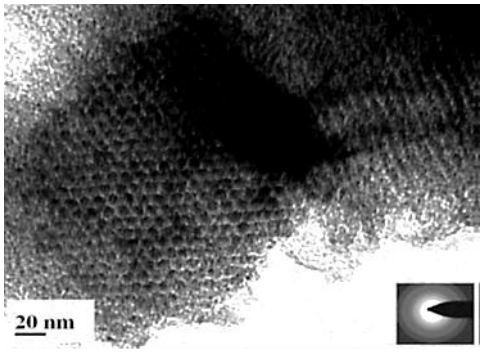

Figure 0.9: A TEM image of carbon mesopores CMK-3 carbon deposited onto carbon film coated copper TEM grid. Reproduced from Kuppan *et al*.[37a]

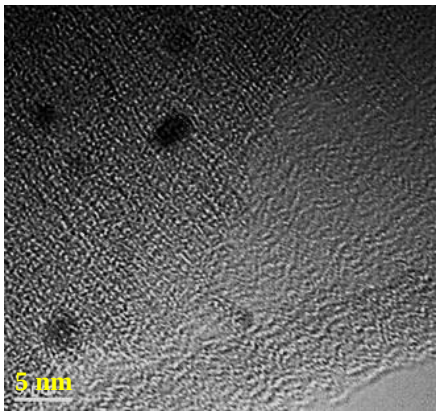

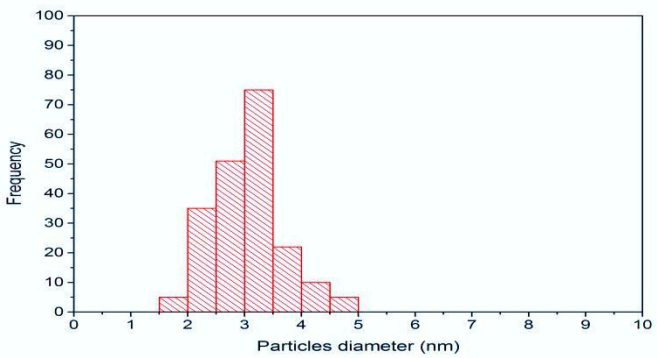

Figure 0.10: Left: a representative TEM image of treated gold nanoparticles immobilized on carbon meso-pores CMK-3 (washed with toluene followed by calcination under static air at 100 ^{o}C for 3 hours) deposited onto carbon film coated copper TEM grid; Right: Particle size distribution histogram. The average particle size of gold particles was determined to be 3.1 ± 0.1 nm (two standard deviations).

5.2.1.3.2 Mesopores structure of CMK-8

Mesopores CMK-8 has a highly ordered pore structure (as illustrated in Figure 5.11). The catalyst made from Au_{101} particles supported on CMK-8 (Au_{101}/C_8) is highly effective, giving the highest benzyl alcohol conversion (~96 %) of any type considered in this Section, irrespective of calcination under static air or vacuum. This probably because the 3-D mesopores structure[52] permits easy diffusion of reactants and products.[47] Additionally, it could be related to the high surface area (1905 m^2/g), ideal particles diameters and distribution (~3 nm), and appropriate pore diameters (~ 2.9 nm) (see Table 5.2 and Figure 5.12). The selectivity was strongly towards the methyl ester with a product ratio of approximately 5:1 (ester to acid). This is the second time (in addition to CMK-3) that such a significant improvement occurred in terms of achieved selectivity of gold catalysts towards methyl benzoate as the main product (~85%).

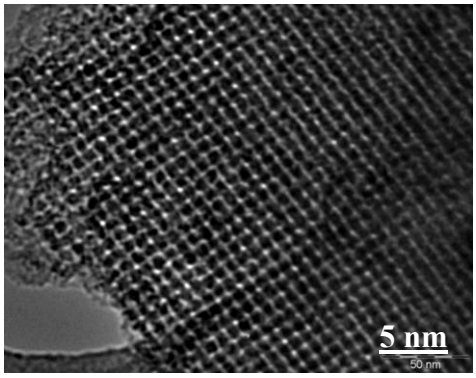

Figure 0.11: A TEM image of mesopores carbon CMK-8 carbon deposited onto carbon film coated copper TEM grid. Reproduced from Lang *et al*.[53a]

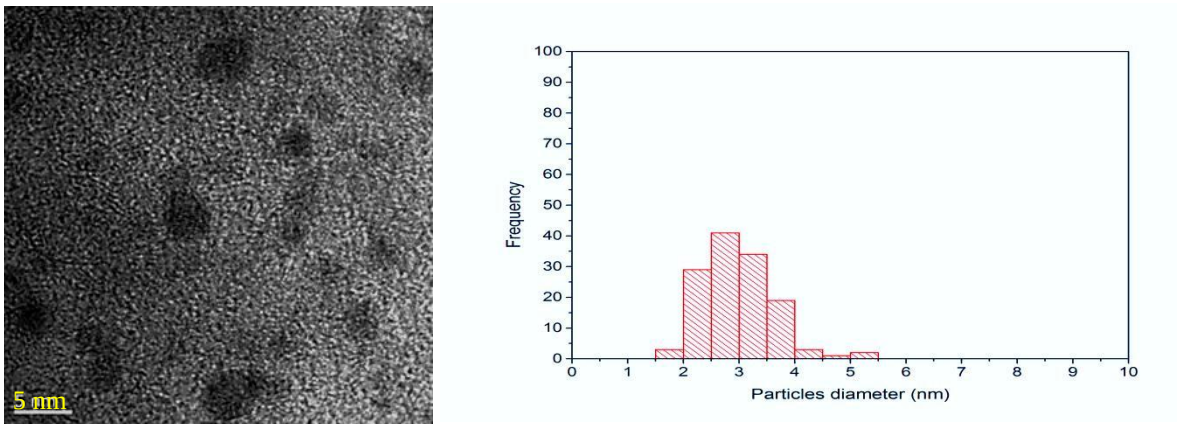

Figure 0.12: Left: a representative TEM image of treated gold nanoparticles immobilized on carbon mesopores CMK-8 (washed with toluene followed by calcination under static air at 100 ^{o}C for 3 hours) deposited onto carbon film coated copper TEM grid; Right: Particle size distribution histogram. The average particle size of gold particles was determined to be 3.0 ± 0.1 nm (two standard deviations of the mean).

5.2.1.3.3 Mesopores structure of NCCR-41

Table 5.5 and a comparison between Figures 5.14 and 5.15 indicate reasonable differences between gold particles sizes and catalytic activity of relevant 1.0 wt% Au_{101}/C_{41} when calcined under static air or vacuum. The average gold particles diameters were 3.3 ± 0.1 and 2.6 ± 0.1 nm, respectively. Calcination under static air gave only 35% conversion whereas calcination under vacuum gave a much higher 88% conversion. In both cases, the product ratio was approximately 9:1 for methyl benzoate to benzoic acid, the highest selectivity towards methyl ester obtained from any system considered in this thesis.

This is the first time such a large difference was observed between the catalytic activities of materials that differed only in being calcined under static air (35%) or a vacuum (88%).

Surprisingly, however, the average particle diameters were only slightly different (3.3 ± 0.1 nm for static-air calcined and 2.6 ± 0.1 nm for vacuum calcined). The TEM images provided no evidence as to why there should be such a big difference, but it may be related to the ways in which functional groups, surface area, pore diameter and pore volume can be influenced by calcination atmospheres and temperatures.[38a, 57] Further characterization is required and will be considered as a part of future work.

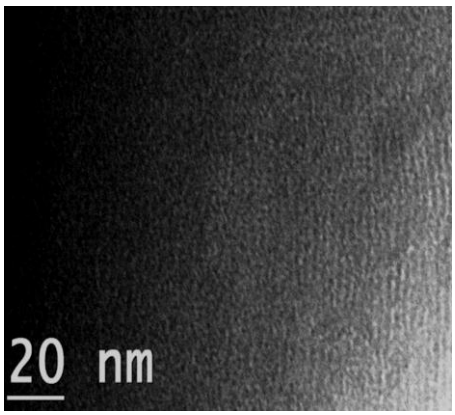

Figure 0.13: A TEM image of carbon mesopores NCCR-41deposited onto carbon film coated copper TEM grid. Reproduced from Selvam *et al.*[48b]

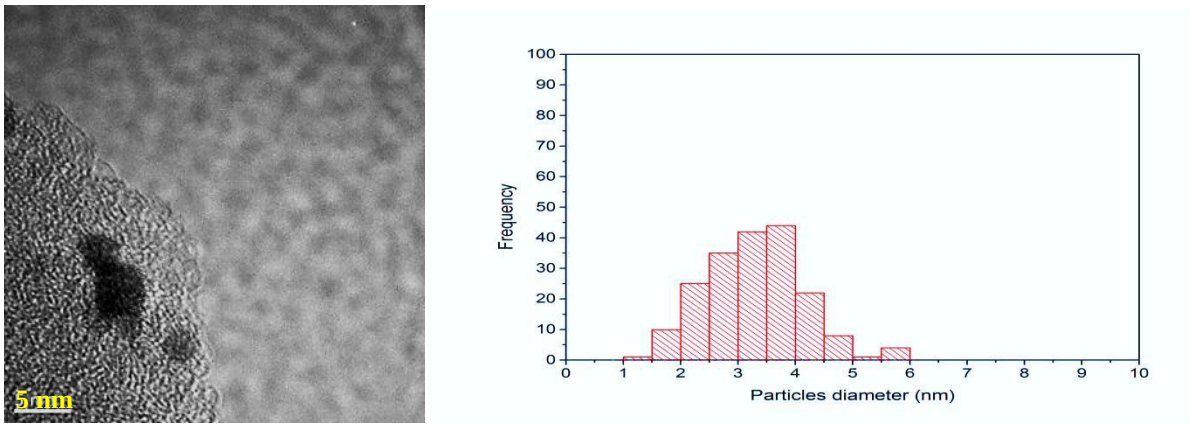

Figure 0.14: Left: a representative TEM image of treated gold nanoparticles immobilized on carbon meso-pores NCCR-41 (washed with toluene followed by calcination under static air at 100 ^{o}C for 3 hours) deposited onto carbon film coated copper TEM grid; Right: Particle size distribution histogram. The average particle size of gold particles was determined to be 3.3 ± 0.1 nm (two standard deviations of the mean).

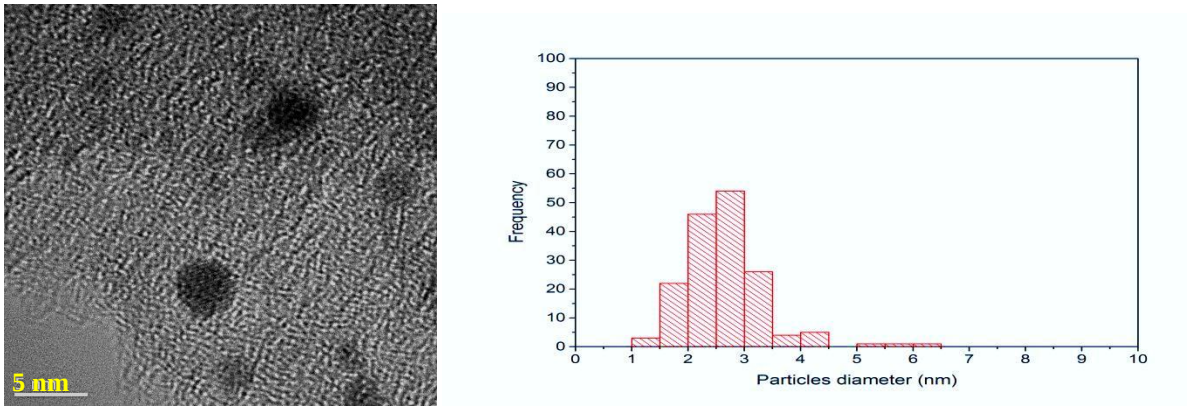

Figure 0.15: Left: a representative TEM image of treated gold nanoparticles immobilized on carbon mesopores NCCR-41 (washed with toluene followed by calcination under vacuum at 100 ^{o}C for 3 hours) deposited onto carbon film coated copper TEM grid; Right: Particle size distribution histogram. The average particle size of gold particles was determined to be 2.6 ± 0.1 nm (two standard deviations of the mean).

In summary, among gold nanocatalysts fabricated using synthetic mesopores carbon supports, that using CMK- 8 carbon showed the highest conversion of benzyl alcohol (≤ 95% with 3.0 ± 0.1 nm) which is even better than high-surface-area micropores Norit activated carbon (powder).[42] This high activity could be due to the pores 3-D structure of this CMK-8,[52] which improves the accessibility of gold particles to the reactants.[37a] Gold particles immobilized on CMK-3 and NCCR-41 were less active, which may be related to lesser porosity.[37a, 48b] Gold particles immobilized on mesopores carbons (CMK-3, CMK-8 and NCCR-41) showed higher selectivity (bigger than 81%) towards methyl benzoate as the main product compared to the particles immobilized on Norit activated carbon (~76%). These results confirm that the activity and selectivity of gold catalysts depend both on types of support and calcination conditions.

5.2.1.3.4 Comparisons of conversion and selectivity between gold particles immobilized on Norit activated carbon (powder) and Vulcan carbon

In this Section, the performance of catalysts made using Norit activated carbon was compared with the performance of analogues fabricated using Vulcan carbon as a support (see Figure 5.16). Au_{101} (1.6 ± 0.1 nm),[58] *"naked"* gold particles (3.2 ± 0.2 nm),[59] and gold citrate (12.6 ±

0.2 nm)[60] were selected to investigate the effects of different initial particle sizes (see more details in Chapter 2, Section 2.4.1) with different types of carbon.

For catalysts immobilized on Vulcan carbon we estimated full deposition of the gold particles by visually observing colour changes from brown (Au_{101}), light red (Au_{naked}) or strong red ($Au_{citrate}$) to colourless (see in Chapter 2, Sections 2.5.1.1.1 – 2.5.1.1.3). In future work, Au content of the samples could be quantitatively determined by using double-focusing inductively coupled plasma mass spectrometry (ICP-MS) or atomic absorption spectroscopy (AAS).

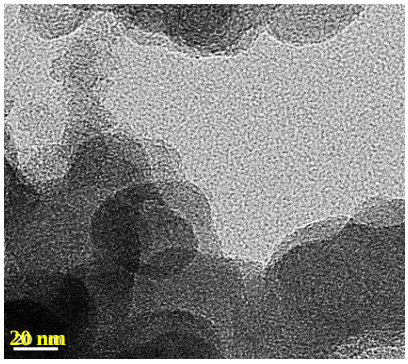

Figure 0.16: A TEM image of Vulcan carbon deposited onto carbon film coated copper TEM grid.

5.2.1.3.4.1 1.6 nm Au_{101} particles

As presented in Table 5.6, Au_{101} immobilized on Norit activated carbon powder showed high activity and selectivity for benzyl alcohol oxidation when activated by washing followed by calcination under static air (75%) or vacuum (87%) at 100 ^{o}C for 3 hours. However, when the support was changed to Vulcan carbon, no conversion was observed.

Table 0.6: Comparisons of conversion and selectivity between Au_{101} particles immobilized on Norit activated carbon (powder) and Vulcan carbon for 3 hours reaction time.

[#]Catalyst code	[*]Activation	Conversion%	Selectivity%		
			Benzaldehyde	Benzoic acid	Methyl benzoate
1.0% Au_{101}/C	W+ static air	75	0	24	76
1.0% Au_{101}/C	W+ vacuum	91	0	24	76
1.0% Au_{101}/C_V	W+ static air	0	0	0	0
1.0% Au_{101}/C_V	W+ vacuum	0	0	0	0

[#]**Catalysts code:** Au_{101}/C_v= Au_{101} particles immobilized on Vulcan carbon. [*]**Activations:** Gold catalysts washed with toluene followed by calcination under static air or vacuum at 100 ^oC for 3 hours.

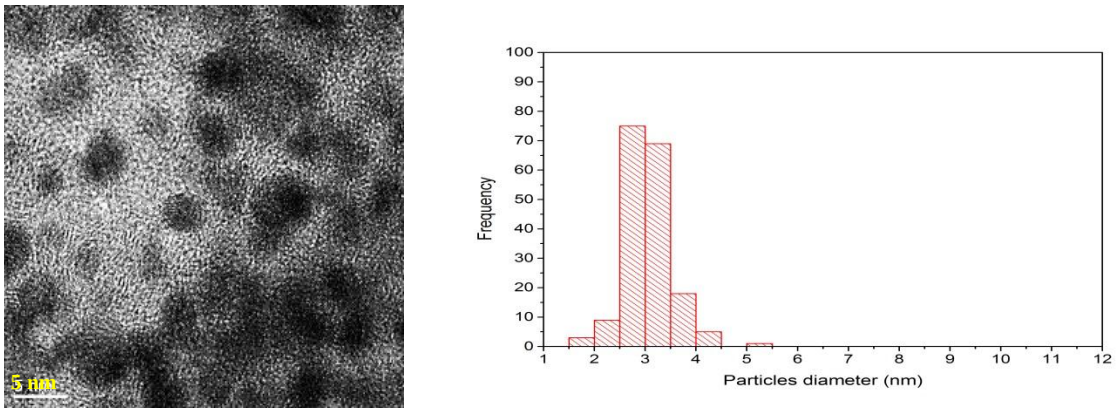

Figure 0.17: Left: a representative TEM image of treated gold nanoparticles (Au_{101}) immobilized on Norit activated carbon (washed with Toluene followed by calcination under static air at 100 ^oC for 3 hours) deposited onto carbon film coated copper TEM grid; Right: Particle size distribution histogram. The average particle size of gold particles was determined to be 3.0 ± 0.1 nm (two standard deviations of the mean).

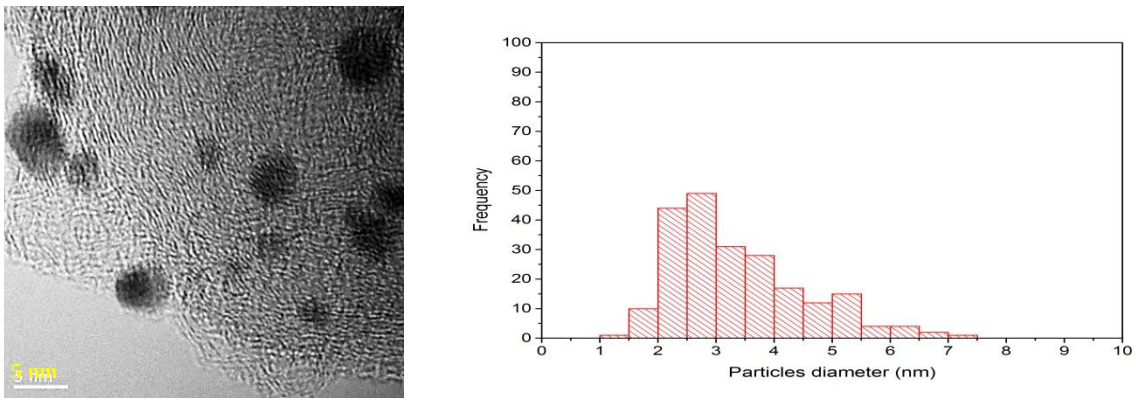

Figure 0.18: Left: a representative TEM image of treated gold nanoparticles (Au_{101}) immobilized on Vulcan carbon deposited onto carbon film coated copper TEM grid; Right: Particle size distribution histogram. The average particle size of gold particles was determined to be 3.4 ± 0.2 nm (two standard deviations of the mean).

a) 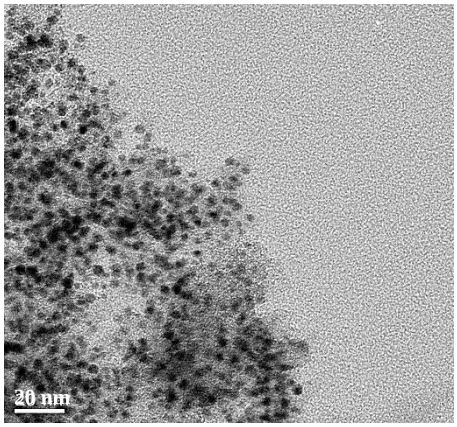

b) 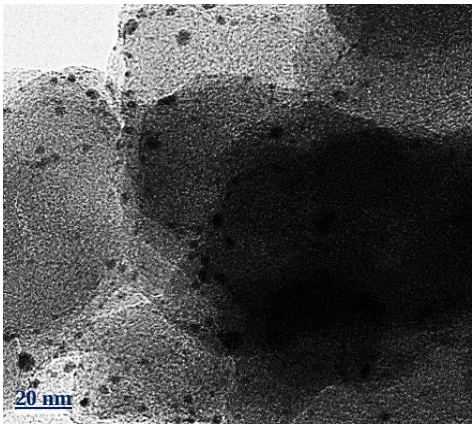

Figure 0.19: Low magnifications TEM images of Au_{101} particles immobilized on a) powder Norit activated carbon & b) Vulcan carbon deposited onto carbon film coated copper TEM grid.

The differences between the average sizes, size distribution and dispersion of gold particles on Norit activated carbon powder and Vulcan carbon are clearly visualized in the TEM images depicted in Figures 5.17 – 5.19. The images for Vulcan carbon show a broad size distribution, a low surface density and high dispersion of particles, possibly due to significantly high number of micropores (~2 nm) compared with of mesopores (2 to 9 nm).[45b, 46] Small gold nanoparticles of around 2 nm may block the micropores when their diameters nearly equal to those of the micropores.[45b] The gold nanoparticles immobilized on Norit activated carbon showed a narrow particle size distribution, a high surface density and low dispersion. Norit carbon has a larger surface area than Vulcan carbon and, more importantly, a higher fraction of this area is mesopores.[47] Additionally, gold nanoparticles could be mobile, and hence more prone to aggregation, on Vulcan carbon than on Norit carbon because gold-support interactions are weaker.[61] Bigger pore volumes, greater prevalence of mesopores region and higher surface areas of activated carbon are generally possessed by activated carbons[42] and led to the high activity of the gold nanocatalysts for benzyl alcohol oxidation (see Table 5.2 and Figure 5.19.a).

5.2.1.3.4.2 3.2 nm *"Naked"* gold particles

The support effect was studied of Norit activated carbon powder and Vulcan carbon on *"naked"* gold particles (3.2 nm) activated using selected treatments (for more details see Chapter 4, in section 4.2.3.1 and 4.2.3.2). Martin *et al.* proposed that these colloidal particles do not contain strongly bound stabilizing agents and hence named them "*naked*" to highlight this characteristic.[59]

Table 0.7: Comparisons of conversion and selectivity for 3 hours reaction time of naked gold immobilized on Norit activated carbon (powder) and Vulcan carbon.

#Catalyst code	***Activation**	**Conversion%**	**Selectivity%**		
			Benzaldehyde	**Benzoic acid**	**Methyl benzoate**
1.0% Au_{naked}/C	W+ static air	73	0	13	87
1.0% Au_{naked}/C	W+ vacuum	88	0	16	84
1.0% Au_{naked}/C_v	W+ static air	20	2	13	85
1.0% Au_{naked}/C_v	W+ vacuum	32	2	9	89

#Catalyst code: Au_{naked}/C_v= "*Naked*" gold particles immobilized on Vulcan carbon. ***Activations:** Gold catalysts washed with toluene followed by calcination under static air or vacuum at 100 ^oC for 3 hours.

Table 5.7 displays benzyl alcohol conversion and selectivity of activated (washed with toluene followed by calcinations under static air or vacuum at 100 ^oC for 3 hours) of *"naked"* gold particles immobilized on Norit activated carbon powder and Vulcan carbon. The results show higher conversion (73% for air calcination and 88% for vacuum calcination) when the naked gold is immobilized on Norit activated carbon. The product ratio was approximately 9:1 methyl benzoate to benzoic acid close to those found for "*naked*" gold nanoparticles immobilized on carbons support. The nanocatalysts calcined under vacuum exhibited higher conversions (Norit: 88% and Vulcan: 32%) than when the catalysts were calcined under static air (Norit: 73% and Vulcan: 20%). The selectivity of "*naked*" gold particles immobilized on Vulcan carbon was towards methyl benzoate as the main product (static air: 85% and vacuum: 89%). Benzaldehyde appeared as a very minor product (2%) when gold naked was immobilized on Vulcan carbon.

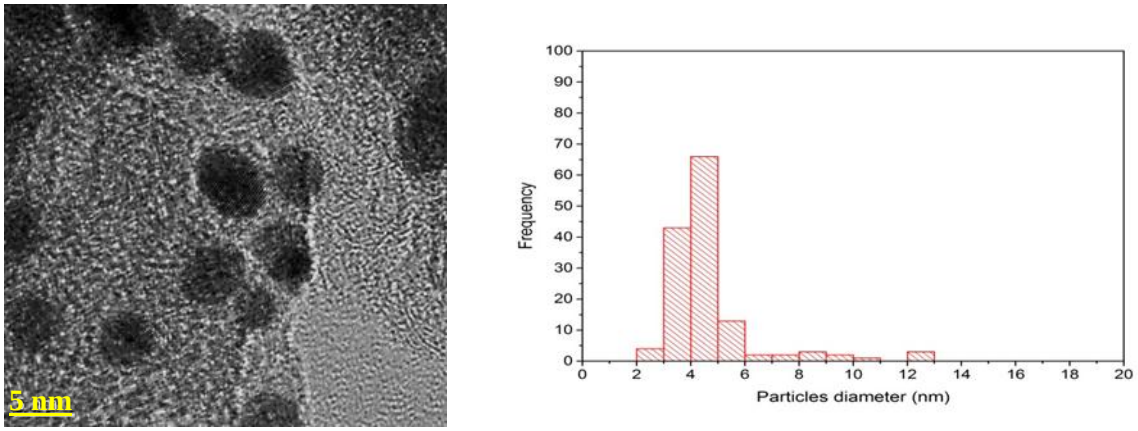

Figure 0.20: Left: a representative TEM image of treated gold naked nanoparticles immobilized on Norit activated carbon (washed with toluene followed by calcination under static air at 100 ^{o}C for 3 hours) deposited onto carbon film coated copper TEM grid; Right: Particle size distribution histogram. The average particle size of gold particles was determined to be 4.2 ± 0.1 nm (two standard deviations of the mean).

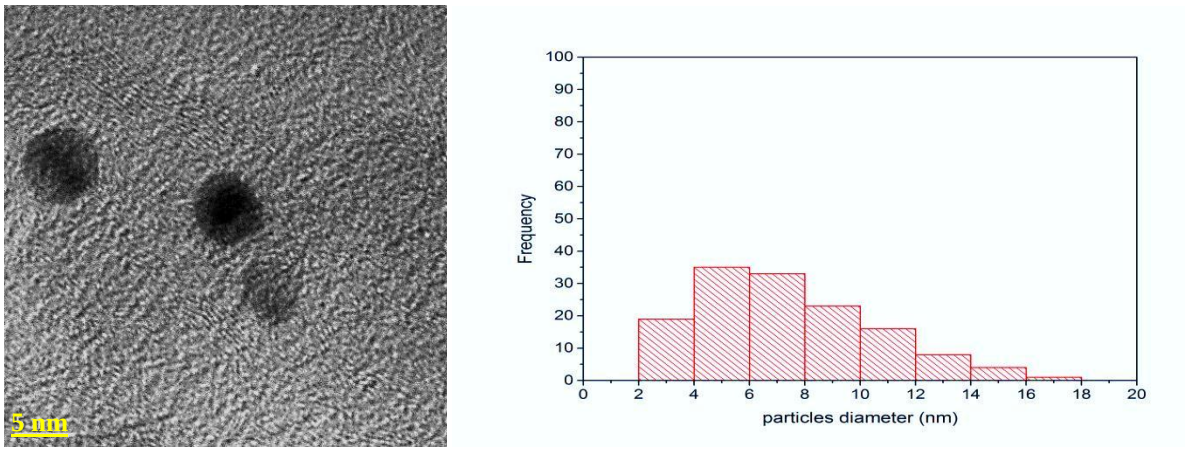

Figure 0.21: Left: a representative TEM image of treated "naked" gold nanoparticles immobilized Vulcan carbon (washed with toluene followed by calcination under static air at 100 ^{o}C for 3 hours) deposited onto carbon film coated copper TEM grid; Right: Particle size distribution histogram. The average particle size of gold particles was determined to be 7.4 ± 0.5 nm (two standard deviations of the mean).

a) 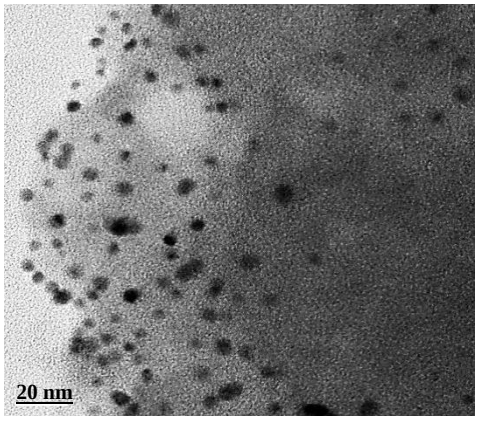

b) 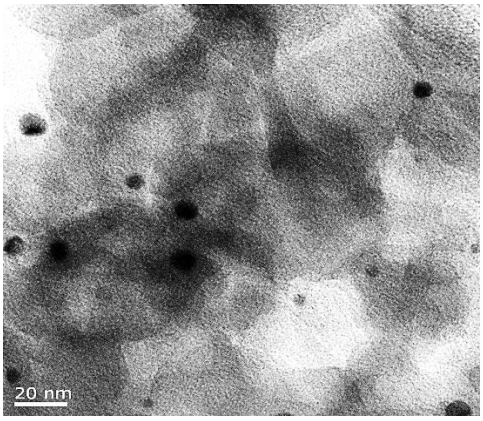

Figure 0.22: Low magnifications TEM images of "*naked"* gold particles immobilized on a) powder Norit activated carbon & b) Vulcan carbon deposited onto carbon film coated copper TEM grid.

The size, size distribution and dispersion of gold particles on immobilized Norit activated carbon powder and Vulcan carbon are visualized by the TEM images presented in Figures 5.20 – 5.22. The average diameter of as-made *"naked"* gold particles was 3.8 ± 0.1 nm (see in Chapter 2, Section 2.5.1.1.3). A high surface density and low dispersion of the gold nanoparticles with a narrow distribution of particle sizes around a slightly enlarged average particle diameter of 4.2 ± 0.1 nm result when immobilized on Norit activated carbon.[62] The big pore size and high surface area of Norit activated carbon may lead to the high activity of the gold nanocatalysts (see Table 5.1).[42] Additionally, gold nanoparticles could be more mobile and hence more likely to aggregate on Vulcan carbon than on Norit carbon because there are no strong gold-support interactions in the case of the former.[61] Vulcan carbon has a significant amount of ~2 nm micropores (compared with mesopores).[45b] This, combined with a lower surface area means that sintering is more likely, giving rise to a large average particle diameter (7.5± 0.5 nm) and a broad size distribution (see Figures 5.21 and 5.22.b).

5.2.1.3.4.3 12.6 nm Gold citrate colloidal particles

The support effect of Norit activated carbon powder and Vulcan carbon on activated gold citrate colloidal particles was studied in this section. Previous benzyl alcohol oxidation studies of gold citrate particles (15 nm) immobilized on the surface of fused-silica capillaries

surfaces showed 59.4% conversion, with 95.2% selectivity towards benzoic acid and with benzaldehyde as a minor product.[63]

Table 0.8: Comparisons of conversion and selectivity between gold citrate immobilized on Norit activated carbon (powder) and Vulcan carbon for 3 hours reaction time.

[#]**Catalyst code**	[*]**Activation**	**Conversion%**	**Selectivity%**		
			Benzaldehyde	**Benzoic acid**	**Methyl benzoate**
1.0% $Au_{citrate}$/ C	W+ static air	70	0	25	75
1.0% $Au_{citrate}$/ C	W+ vacuum	79	0	27	73
1.0% $Au_{citrate}$/ C_v	W+ static air	52	0	13	87
1.0% $Au_{citrate}$/ C_v	W+ vacuum	56	0	16	84

[#]**Catalyst code:** $Au_{citrate}$ /C_v= Gold citrate colloids immobilized on Vulcan carbon. [*]**Activations:** Gold catalysts washed with NaOH in MilliQ water (0.1 M) followed by calcinations under static air or vacuum at 100 ^{o}C for 3 hours.

Table 5.8 shows high conversion and selectivity for benzyl alcohol oxidation when the gold nanoparticles were immobilized on Norit carbon and then activated by being washed with toluene followed by static air calcination (70%) or vacuum calcination (79%). The product ratio was approximately 3:1 the ester to acid. Lower conversions were observed for the activated gold citrate immobilized on Vulcan carbon (static air calcination: 52% and Vacuum calcination: 56%), and the product ratio of approximately 5:1 was shifted further in favour of methyl benzoate.

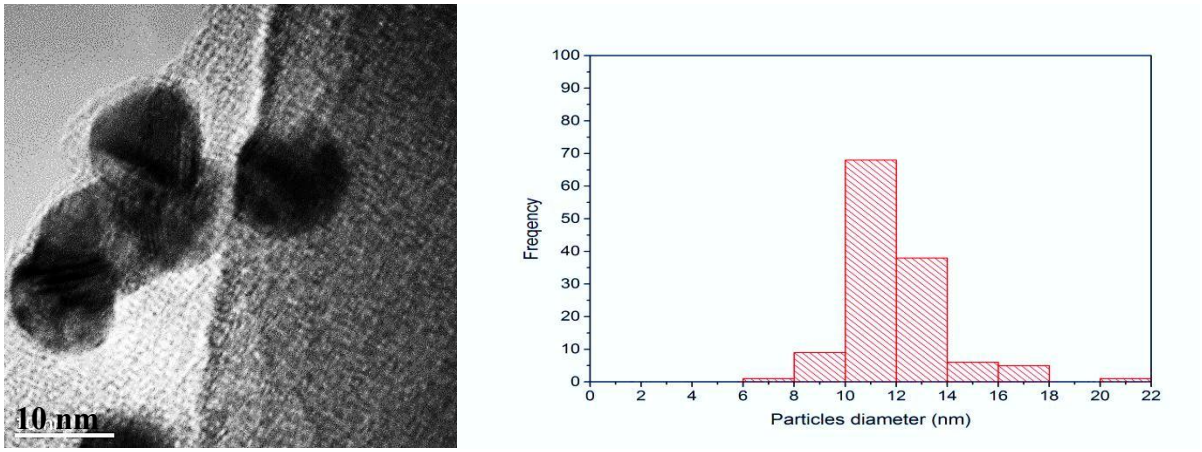

Figure 0.23: Left: a representative TEM image of treated gold citrate immobilized on Norit activated carbon (washed with NaOH in MilliQ water (0.1 M) followed by calcination under static air at 100 ^{o}C for 3 hours) deposited onto carbon film coated copper TEM grid; Right: Particle size distribution histogram. The average particle size of gold particles was determined to be 11.5 ± 0.6 nm (two standard deviations of the mean).

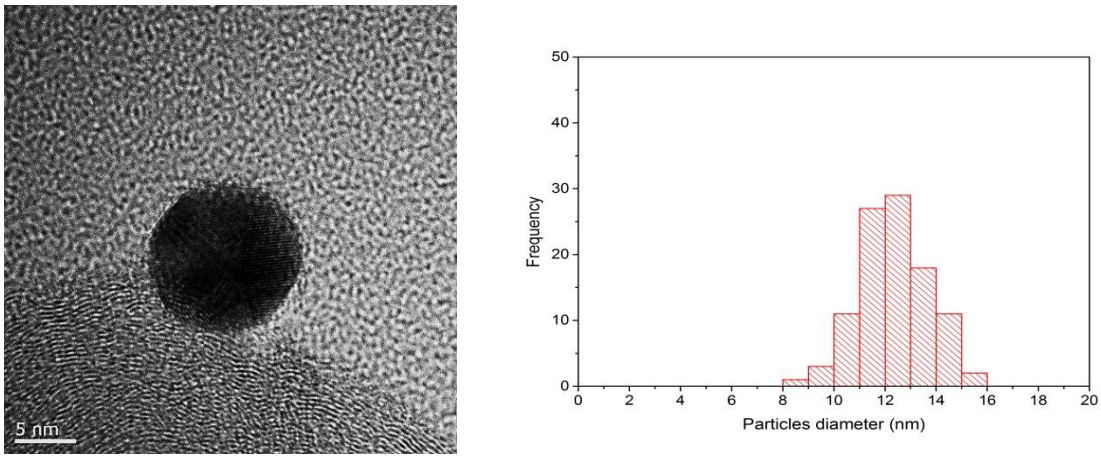

Figure 0.24: Left: a representative TEM image of treated gold citrate immobilized on Vulcan carbon (washed with NaOH in MilliQ water (0.1 M) followed by calcination under static air at 100 ^{o}C for 3 hours) deposited onto carbon film coated copper TEM grid; Right: Particle size distribution histogram. The average particle size of gold particles was determined to be 12.3 ± 0.3 nm (two standard deviations of the mean).

a) 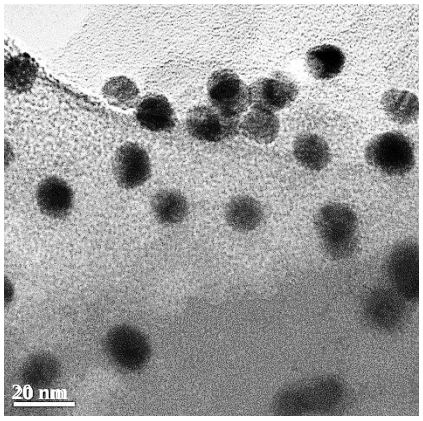

b) 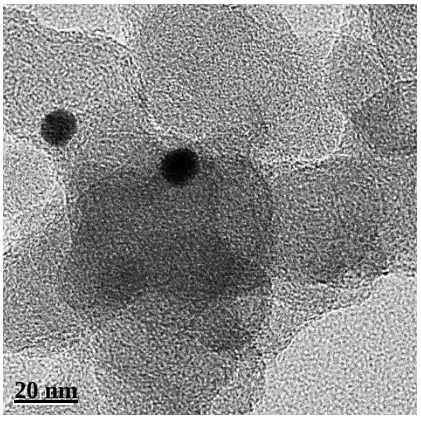

Figure 0.25: Low magnifications TEM images of activated (washed with toluene or NaOH in MilliQ water (0.1 M) followed by calcination under static air at 100 ^{o}C for 3 hours) with gold citrate colloidal particles immobilized on a) Norit activated carbon & b) Vulcan carbon deposited onto carbon film coated copper TEM grid.

The differences in average sizes, size distributions and dispersions of the gold particles for calcination under static air are visualized in the TEM images presented in Figures 5.23 – 5.25. The histograms of Figures 5.23 and 5.25 show that the average diameter of particles immobilized on Norit activated carbon is 11.5 ± 0.6 nm and that there is a high surface density and low dispersion. Gold particles immobilized on Vulcan carbon exhibited slightly greater aggregation (average particle diameter of 12.3 ± 0.3 nm) (see Figure 5.24) which reflects the greater mobility on the surface of Vulcan carbon,[61] and probably led to the higher surface density of colloidal particles (evident in Figure 5.25.).

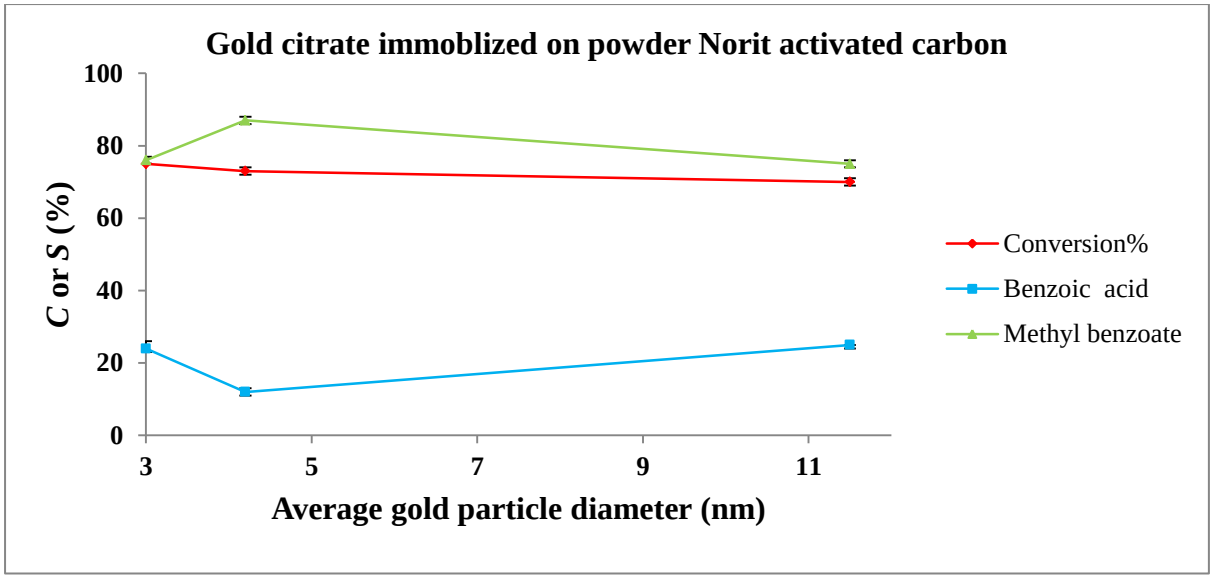

Figure 0.26: The size effect on conversion (*C*%) and selectivity (*S*%) of gold particles (Au_{101}, Au_{naked} and $Au_{citrate}$) immobilized on Norit activated carbon (powder).

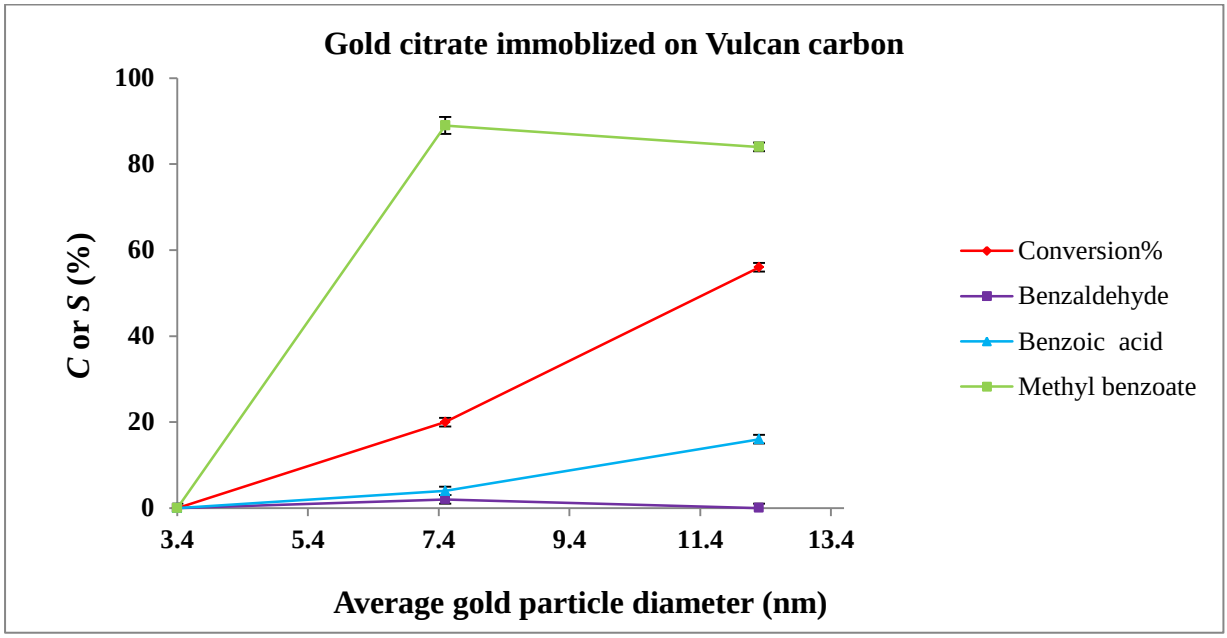

Figure 0.27: The effect size on conversion (*C*%) and selectivity (*S*%) of gold particles (Au_{101}, Au_{naked} and $Au_{citrate}$) immobilized on Vulcan carbon.

Figures 5.26 and 5.27 demonstrate plots of conversions and selectivities as a function of particle diameters, increasing in the order $Au_{101} < Au_{naked} < Au_{citrate}$ for Vulcan carbon supports. However, in Norit activated carbon this order appears in reverse – *i.e.*, $Au_{101} > Au_{naked} > Au_{citrate}$. Generally, the conversions for benzyl alcohol oxidation (70-75%) are greater and much less size dependent for the Norit-based systems than the Vulcan-based ones

(0-50%). For the Norit systems the highest conversion (≤ 75%) occurred for the smallest, 3.0 ± 0.1 nm, Au_{101} particles (see red curve Figure 5.26). However, among the Vulcan systems, the largest, 12.3± 0.3 nm, $Au_{citrate}$ particles gave the highest conversion (52% -- see red curve in Figure 5.27). In all cases where the conversion was non-zero, selectivity was substantially in favour of methyl benzoate and fairly independent of particles size. These results indicate that the structure of the support can have a profound influenced on the particle-size dependence of conversion efficiency, whereas selectivity shows only weak dependence on these variables.

5.2.2 Size effect on the catalytic activity of supported gold particles

Although, the catalytic activity of Au_{101} nanoparticles (with[64] or without[65] support) is well researched, the relationship between activity, selectivity and gold particle size requires further investigation. Benzyl alcohol oxidation was studied using nearly mono-disperse gold nanoparticles with diameters ranging from ~ 0.8 to ~ 12.6 nm immobilized on Norit activated carbon powder and Vulcan carbon.

5.2.2.1 Comparisons of conversion and selectivity among Au_{101} particles, Au_9 and Au_8 clusters immobilized on Norit activated carbon (powder)

Phosphine-stabilized Au_8, Au_9 and Au_{101} clusters were deposited on Norit activated carbon powder, washed with toluene the calcined under static air or vacuum at 100 ^oC for 3 hours. The only active systems involved Au_{101}, with 75% conversion after static air calcination and 91% conversion under vacuum calcination. For both of these systems, selectively is ~3:1 in favour of methyl benzoate over benzoic acid (see Table 5.9).

Table 0.9: Comparisons of conversion and selectivity among Au_{101} particles, Au_8 and Au_9 clusters immobilized on Norit activated carbon (powder) for 3 hours reaction time.

Catalyst code	*Activation	Conversion%	Selectivity%		
			Benzaldehyde	Benzoic acid	Methyl benzoate
1.0% Au_{101}/C	W+ static air	75	0	24	76
1.0% Au_{101}/C	W+ vacuum	91	0	24	74
1.0% Au_8/C	W+ static air	0	0	0	0
1.0% Au_8/C	W+ vacuum	0	0	0	0
1.0% Au_9/C	W+ static air	0	0	0	0
1.0% Au_9/C	W+ vacuum	0	0	0	0

***Activation:** Gold catalysts washed with toluene followed by calcinations under static air or vacuum at 100 ^oC for 3 hours.

5.2.2.1.1 Au_{101} particles

According to the TEM images of Figures 5.28 – 5.29, the average particle diameters for the Au_{101} systems were 3.0 ± 0.1 and 3.5 ± 0 nm, respectively, after calcination under air or vacuum. Both had narrow size distributions and high dispersions of the gold particles. The results presented in Table 5.8 showed higher activity for the larger vacuum-calcinated catalyst. Hence, as small gold particles (Au_{101}) were active catalysts for benzyl alcohol oxidation, we hypothesise that small gold clusters (*i.e.*, Au_8 and Au_9 clusters) can be active catalysts; in particular both gold clusters and particles have similar structures – *i.e.*, their core diameters are surrounded with the same capping agent (PPh_3).

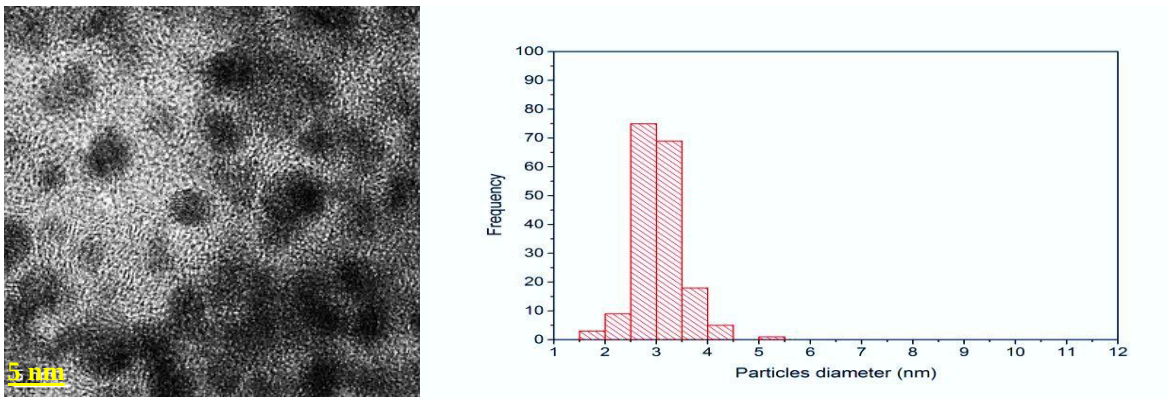

F***igure 0.28:*** Left: a representative TEM image of treated 1.0 wt% Au_{101}/C (washed with toluene followed by calcination under static air at 100 ^oC for 3 hours) deposited onto carbon film coated copper TEM grid; Right: Particle size distribution histogram. The average particle size of gold particles was determined to be 3.0 ± 0.1 nm (two standard deviations of the mean).

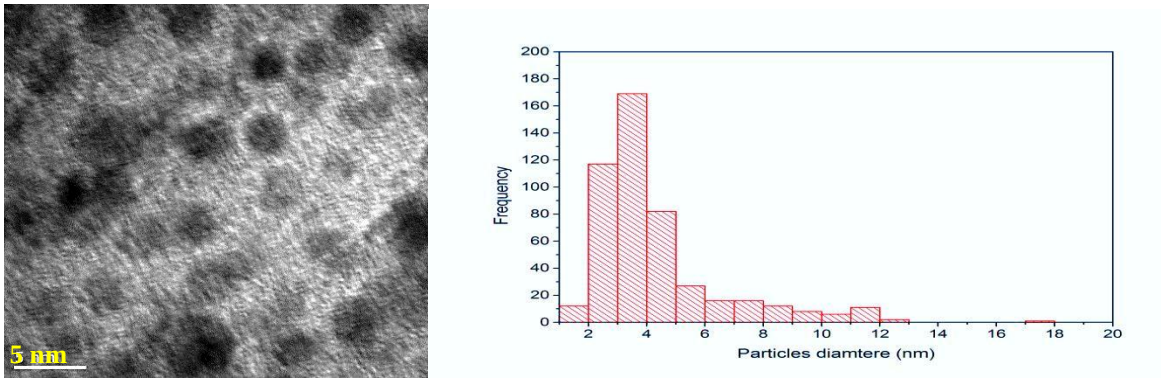

Figure 0.29: Left: a representative TEM image of activated 1.0 wt% Au_{101}/C (washed with toluene and followed by calcination under vacuum at 100 ^{o}C for 3 hours) deposited onto carbon film coated copper TEM grid; Right: Particle size distribution histogram. The average particle size of gold particles was determined to be 3.5 ± 0.1 nm (two standard deviations of the mean).

5.2.2.1.2 Au_9 nanoclusters

Figure 5.30 displays TEM images of Au_9 nanoclusters deposited on Norit activated carbon (powder) without washing or calcination. Only very few (about five) large gold particles with diameters up to 3.5 nm were evident. The University of Canterbury TEM cannot detect immobilized particles smaller than 1 nm, so any other particles must have diameters smaller than this. Since the diameter of as-synthesized Au_9 nanoclusters (prior to immobilization) is about 0.9 nm,[14b, 66] the lack of particle images indicates that the any other Au_9 particles must essentially have undergone no aggregation during initial deposition. After washing with toluene and calcination under static air at 100 ^{o}C for 3 hours, large particles with diameters around 10.5 nm were observed (see Figure 5.31).[66] These results confirmed that the Au_9 nanoclusters had been deposited on the support and that they were sensitive to aggregation during activation.[64, 66-67] The activated small gold clusters (*i.e.*, Au_9 with ~ 0.9 nm size) were not active for benzyl alcohol because the clusters fully aggregated after activation and made very big particles (see Figure 5.29).[68]

Features in the optical spectra of small phosphine-stabilized gold clusters are known to be associated with the ligand shell bound to the gold core of the cluster.[69] However, gold

clusters can aggregate when ligands are still weakly bound to the gold cores of the clusters. Hence, the big particles formed during activation when the gold clusters were predominantly phosphine-free.[66] Intriguingly, gold citrate immobilized on Norit activated carbon with average gold particles diameter (11.5±0.6 nm) bigger than the gold clusters (Au_9: 10.5± 0.7 nm) showed high activity (72%). This will be explained in more detail in Section 5.2.2.2.3.1.

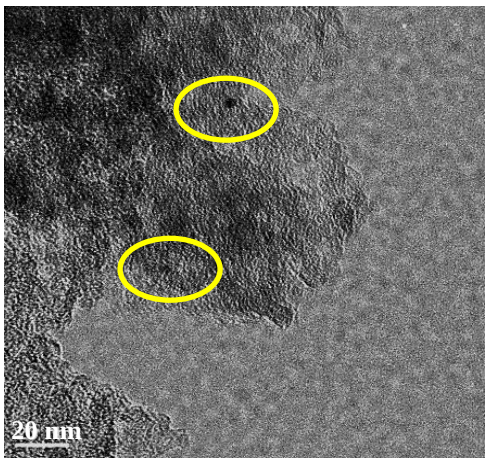

Figure 0.30: A TEM image of Au_9/C (un-treated) deposited onto carbon film coated copper TEM grid. The average gold particle diameter was approximately 3.5 nm ***(just for 5 particles which were found on the grid).***

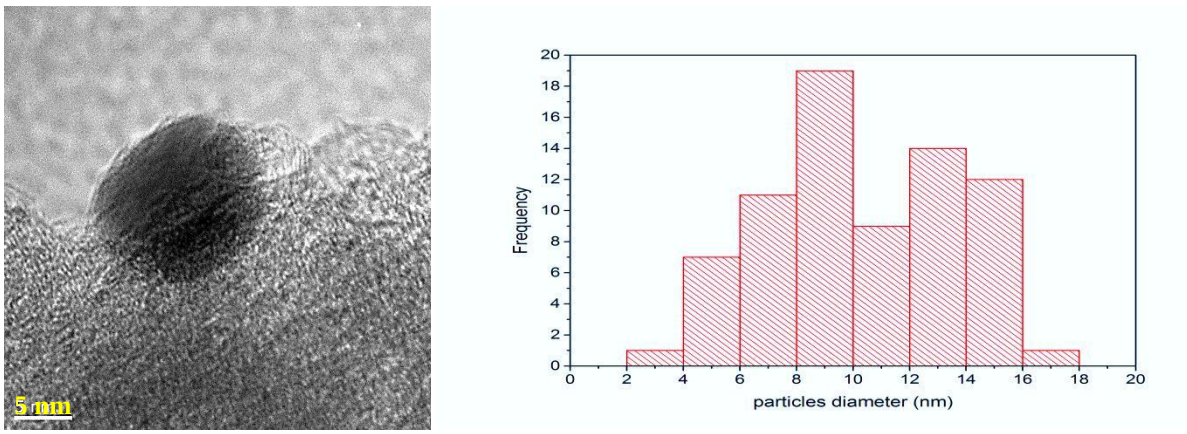

Figure 0.31: Left: a representative TEM image of treated 1.0 wt% Au_9/C (washed with toluene followed by calcination under static air at 100 ^oC for 3 hours) deposited onto carbon film coated copper TEM grid; Right: Particle size distribution histogram. The average particle size of gold particles was determined to be 10.5 ± 0.7 nm (two standard deviations of the mean).

5.2.2.1.3 Au_8 nanoclusters

The TEM image in Figure 5.32 demonstrates that the Au_8 nanoclusters (like Au_9) aggregate during treatment by washing and calcination, with their average diameter rising from ~0.8[14a]

to ~22.5 nm. As for supported, activated and aggregated Au_9, no conversion was observed for the large Au_8 nanocatalysts (see Table 5.9).[68]

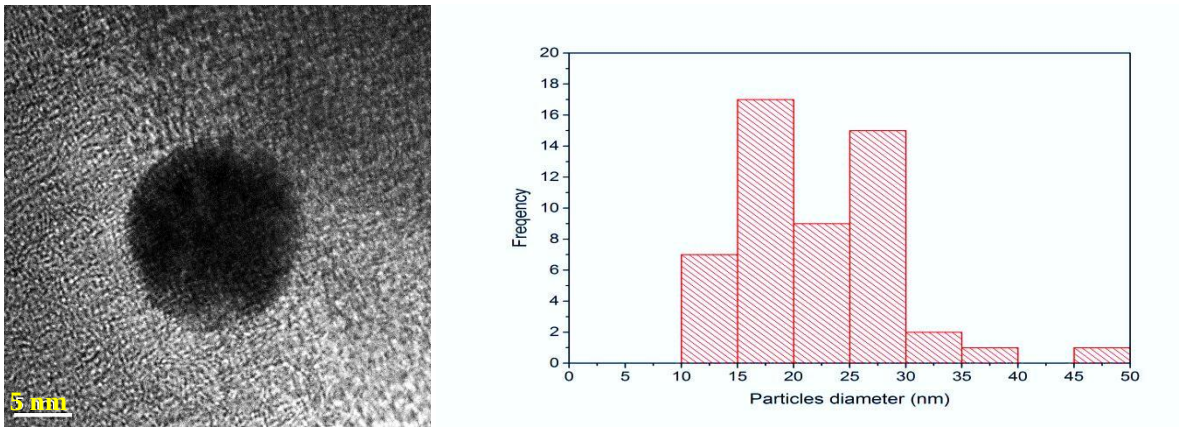

Figure 0.32: Left: a representative TEM image of treated 1.0 wt% Au_8/C (washed with toluene followed by calcination under static air at 100 ^oC for 3 hours) deposited onto carbon film coated copper TEM grid; Right: Particle size distribution histogram. The average particle size of gold particles was determined to be 22.0 ± 2.0 nm (two standard deviations of the mean).

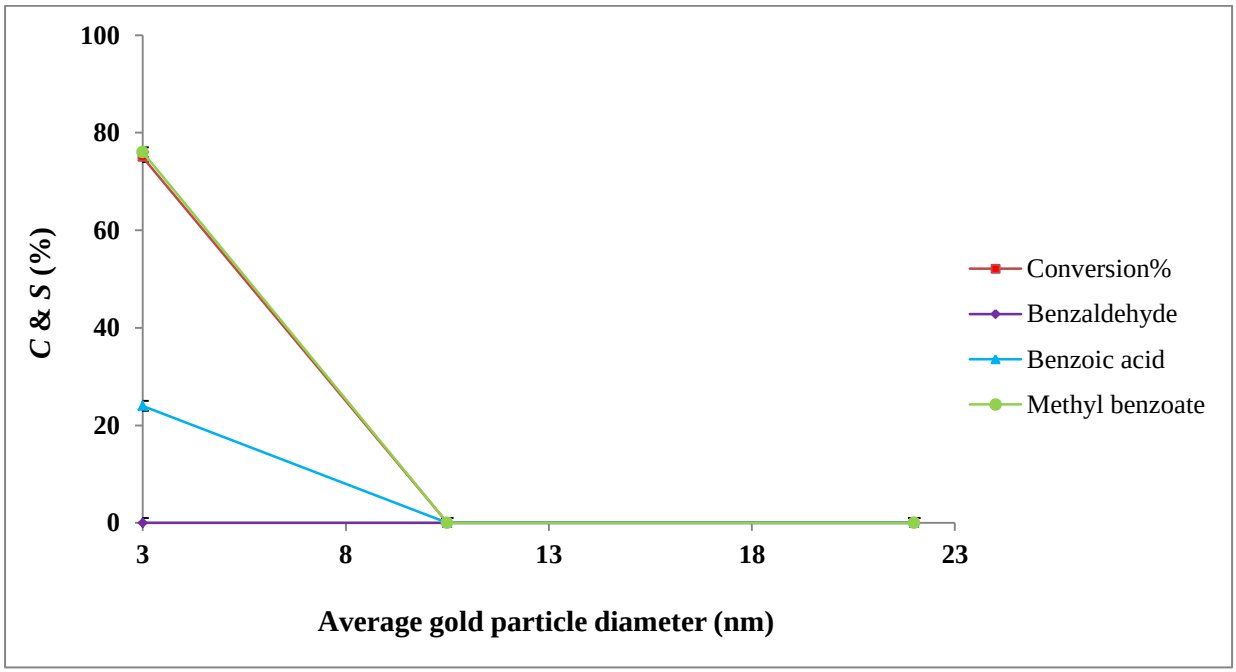

Figure 0.33: The size effect on conversion (*C%*) and selectivity (*S%*) of Au_8/C, Au_9/C and Au_{101}/C gold nanocatalysts. The selectivity for methyl benzoate lies almost exactly on the curve for conversion.

After treatment, the particle sizes increase in the order Au_{101}< Au_9< Au_8. Figure 5.33 shows the effect of the size of activated nanocatalysts on conversion and selectivity for benzyl alcohol oxidation. Au_{101}/C, with a gold particle diameter of approximately 3±0.1 nm, was the

most active catalyst with 75% conversion.[28a, 56] Au_8 and Au_9 clusters proved to be inactive due to substantial gold aggregation.[64, 66-67] Activated $Au_{citrate}$/C with ~11.5 nm particle size showed reasonable activity but the very large gold particles obtained as a result of cluster (*i.e.*, Au_8 and Au_9) aggregation upon immobilization and activation did not show any conversion. Evidently gold particles prepared with PPh_3 capping agents are more sensitive to activation conditions.[64, 66-67]

5.2.2.2 Comparisons of the catalytic activity among $Au_{101,}$ *"naked"* gold and gold citrate particles immobilized on different types of carbon

The Au_{101}, *"naked"* gold and gold citrate (1.0 wt %) immobilized on Norit activated carbon powder and Vulcan carbon, with average particle diameters ranging from 1.6 to 12 nm, was used to investigate the effect of gold particle size on benzyl alcohol oxidation.

5.2.2.2.1 Au_{101}, *"naked"* gold and gold citrate immobilized on Norit activated carbon (powder)

The 1.0 wt% Au_{101}/C washed with toluene followed by calcination under vacuum at 100 ^{o}C for 3 hours showed the highest activity of 91%. However, the highest selectivity of 7:1 towards methyl benzoate belonged to 1.0 wt % Au_{naked}/C calcined under static air. Overall, gold particles calcined under vacuum showed higher activity than the calcination under static air.

Table 0.10: Comparisons of conversion and selectivity among 1.0 wt % Au_{101}, Au_{naked} and $Au_{citrate}$ immobilized on Norit activated carbon (powder) for 3 hours reaction time.

Catalyst code	*Activation	Conversion%	Selectivity%		
			Benzaldehyde	Benzoic acid	Methyl benzoate
1.0% Au_{101}/C	W+ static air	75	0	24	76
1.0% Au_{101}/C	W+ vacuum	91	0	24	74
1.0% Au_{naked}/C	W+ static air	73	0	12	87
1.0% Au_{naked}/C	W+ vacuum	88	0	16	84
1.0% $Au_{citrate}$/C	W+ static air	70	0	25	75
1.0% $Au_{citrate}$/C	W+ vacuum	79	0	27	73

*__Activation:__ Gold catalysts washed with toluene or NaOH in MilliQ water (0.1 M) followed by calcination under static air or vacuum at 100 ^{o}C for 3 hours.

5.2.2.2.1.1 Au_{101} nanoparticles

Figures 5.34 – 5.36 present HRTEM images and associated particle size distributions for Au_{101} immobilized on Norit activated carbon, either un-treated or activated. The low activity un-treated nanocatalysts had an average gold particle diameter of 2.6 ± 0.1 nm. Activity rose substantially for systems with larger particle diameter (≤ 3.5 nm). The highest conversion of 91% was recorded for 1.0 wt% Au_{101}/C washed with toluene and calcined under vacuum at 100 ^{o}C for 3 hours, for which the average particle size was 3.5±0.1 nm, with particles as large as ~ 6.6 nm also being present.[28a, 56]

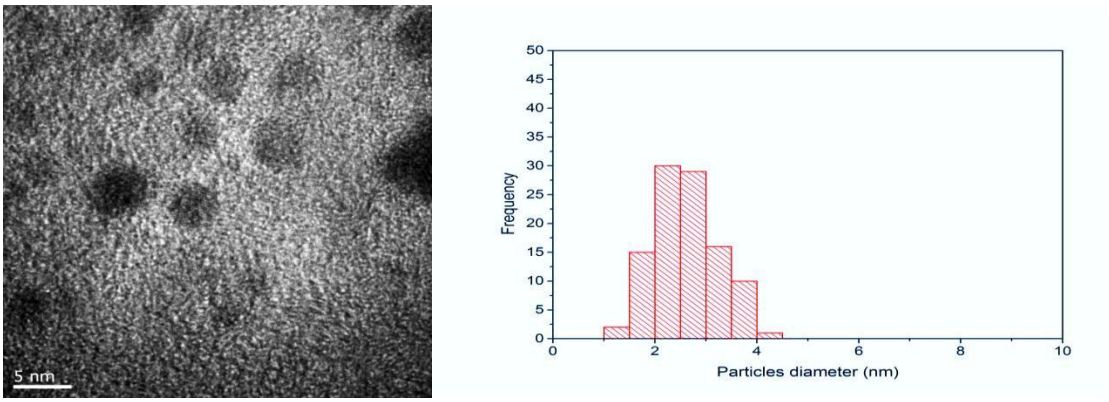

Figure 0.34: Left: a representative TEM image of gold nanoparticles immobilized on Norit activated carbon (un-treated) deposited onto carbon film coated copper TEM grid; Right: Particle size distribution histogram. The average particle size of gold particles was determined to be 2.6 ± 0.1 nm (two standard deviations of the mean).

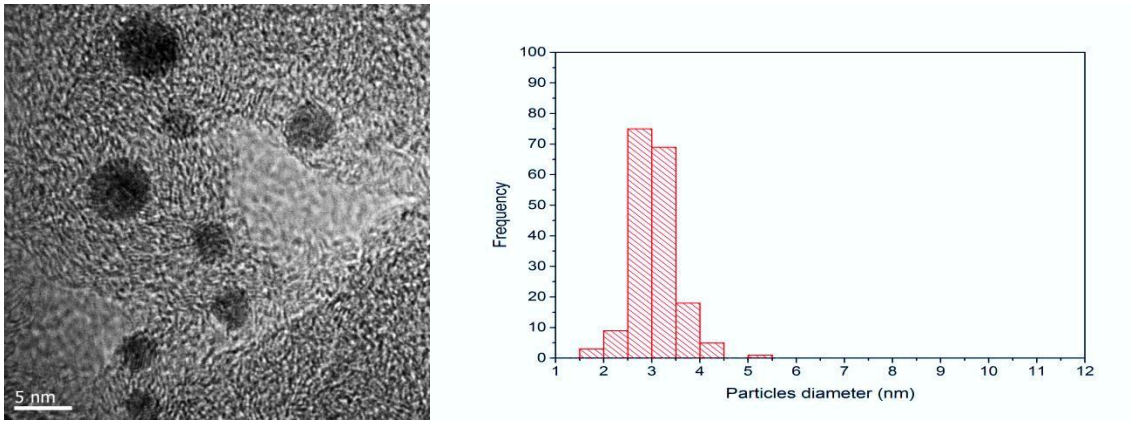

Figure 0.35: Left: a representative TEM image of treated of Au_{101}/C (washed with toluene followed by calcination under static air at 100 ^{o}C for 3 hours) deposited onto carbon film coated copper TEM grid; Right: Particle size distribution histogram. The average particle size of gold particles was determined to be 3.0 ± 0.1 nm (two standard deviations of the mean).

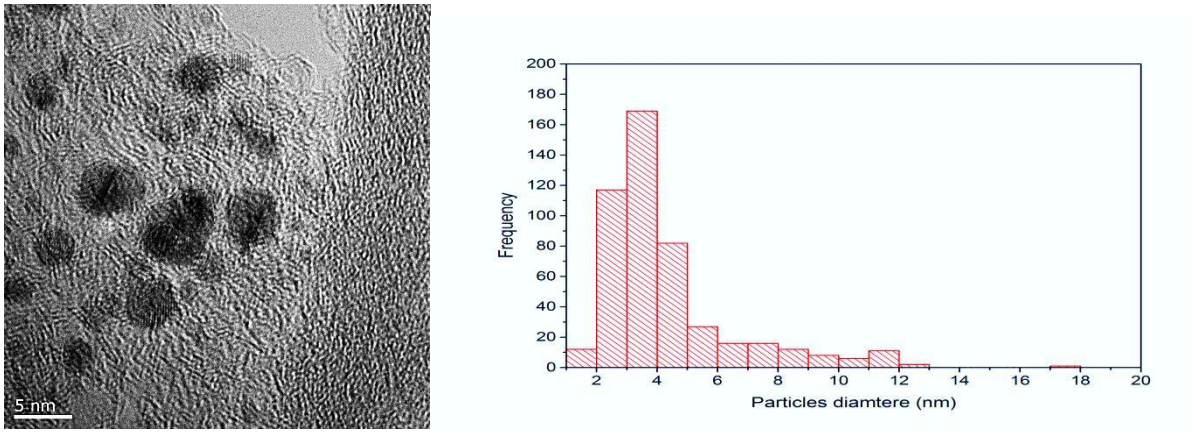

Figure 0.36: Left: a representative TEM image of treated Au_{101}/C (washed with toluene followed by calcination under static air at 100 ^{o}C for 3 hours) deposited onto carbon film coated copper TEM grid; Right: Particle size distribution histogram. The average particle size of gold particles was determined to be 3.5 ± 0.1 nm (two standard deviations of the mean).

5.2.2.2.1.2 *"Naked"* gold nanoparticles

Figures 5.37 – 5.39 show that the average particles size of *"naked"* gold particles increased from 3.8 ± 0.1 nm (un-treated) to 4.2 ± 0.1 nm when washed with toluene and calcined under static air or 4.4 ± 0.1 nm when washed with toluene and calcined under vacuum. Although, the treated gold naked nanocatalysts with the lower average particle diameters (~4.2) nm showed reasonable conversion of 73%, higher conversion (88%) was achieved by the catalyst with 4.4 nm average diameter. The main product was methyl benzoate (static air calcination: 87% and vacuum calcination: 84%).

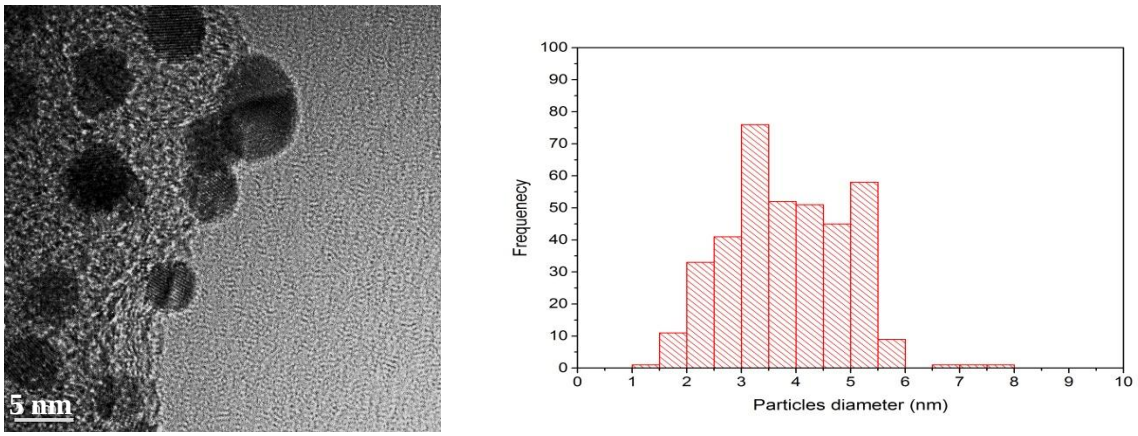

Figure 0.37: Left: a representative TEM image of gold naked immobilized on Norit activated carbon (un-treated) deposited onto carbon film coated copper TEM grid; Right: Particle size distribution histogram. The average particle size of gold particles was determined to be 3.8 ± 0.1 nm (two standard deviations of the mean).

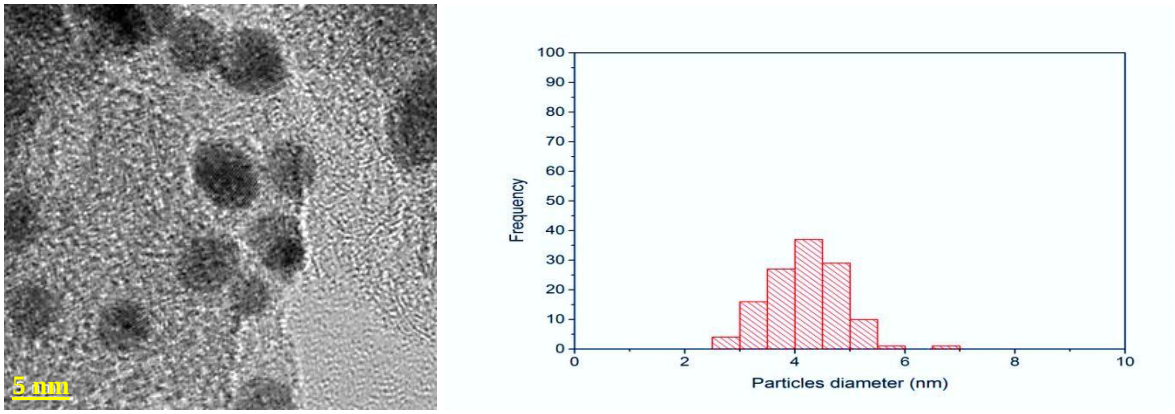

Figure 0.38: Left a representative TEM image of treated gold naked immobilized on Norit activated carbon (washed with toluene followed by calcination under static air at 100 ^{o}C for 3 hours) deposited onto carbon film coated copper TEM grid; Right: Particle size distribution histogram. The average particle size of gold particles was determined to be 4.2 ± 0.1 nm (two standard deviations of the mean).

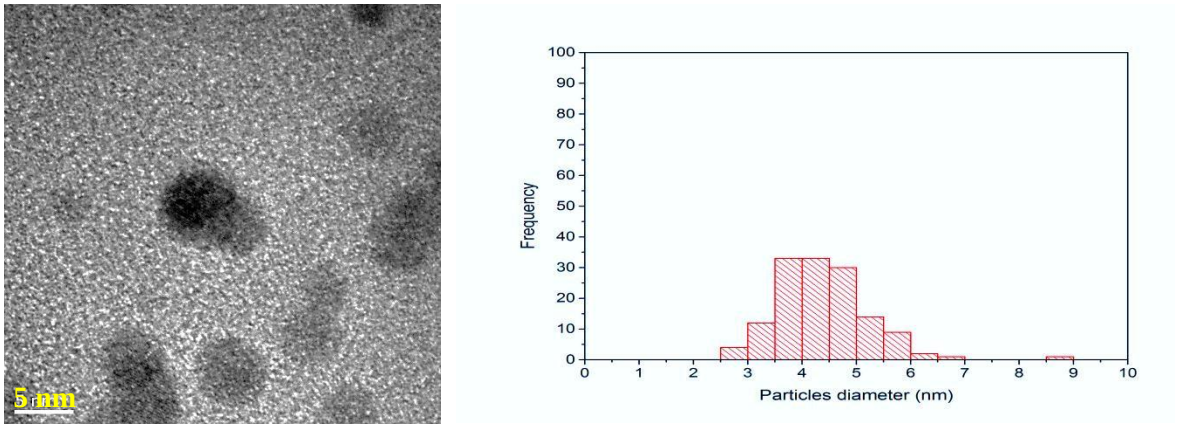

Figure 0.39: Left: a representative TEM image of treated gold naked immobilized on Norit activated carbon (washed with toluene followed by calcination under vacuum at 100 ^{o}C for 3 hours) deposited onto carbon film coated copper TEM grid; Right: Particle size distribution histogram. The average particle size of gold particles was determined to be 4.4 ± 0.1 nm (two standard deviations of the mean).

5.2.2.2.1.3 Gold citrate colloids

After immobilization on the activated carbon support gold citrate colloidal particles form a type of "chain" arrangement with the average diameters of the individual gold particles insignificantly changed from 12.6 ± 0.2 nm as synthesized (see in Chapter 2, Section 2.4.1.6) to 12.5 ± 0.2 nm. Treatment by washing with toluene followed by calcination under static air at 100 ^{o}C for 3 hours caused the gold particle size to increase to 13.1± 0.2 nm (see Figures 5.40 and 5.41). The resulting material showed no conversion (see Table 5.10). For gold citrate catalysts washed with 0.1 M NaOH in MilliQ water, then calcined under static air or vacuum at 100 ^{o}C for 3 hours, the gold particles size decreased from ~12.5 to ~ 11.1 and ~11.5 nm, respectively (see Figures 5.42-5.43). At the same time, chain arrangements of the gold particles were broken down. Comparisons of the TEM images between un-treated and activated gold citrate nanocatalysts confirmed that the washing procedure removed the citrate from the gold cores and consequently separated the gold particles. The catalytic activity of the gold particles increased to 72% after calcination under static air and 79% after calcination under vacuum. The product ratio was approximately 3:1 in favour of methyl benzoate.

It can be inferred that the catalytic performance for this type of gold particles is directly related to the distance between particles for more connection between the gold particles and reactants.[42] In addition, washed Au clusters deposited on silica with NaOH solution (0.1 M) showed that the gold clusters preserved their size and so the clusters survived as individual entities under such condition.[70]

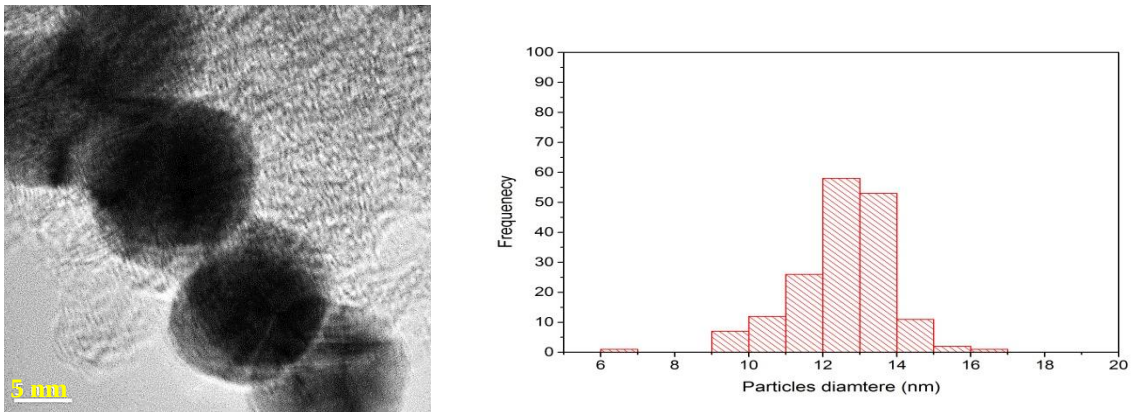

Figure 0.40: Left: a representative TEM image of gold citrate nanoparticles immobilized on Norit activated carbon (un-treated) deposited onto carbon film coated copper TEM grid; Right: Particle size distribution histogram. The average particle size of gold particles was determined to be 12.5 ± 0.2 nm (two standard deviations of the mean).

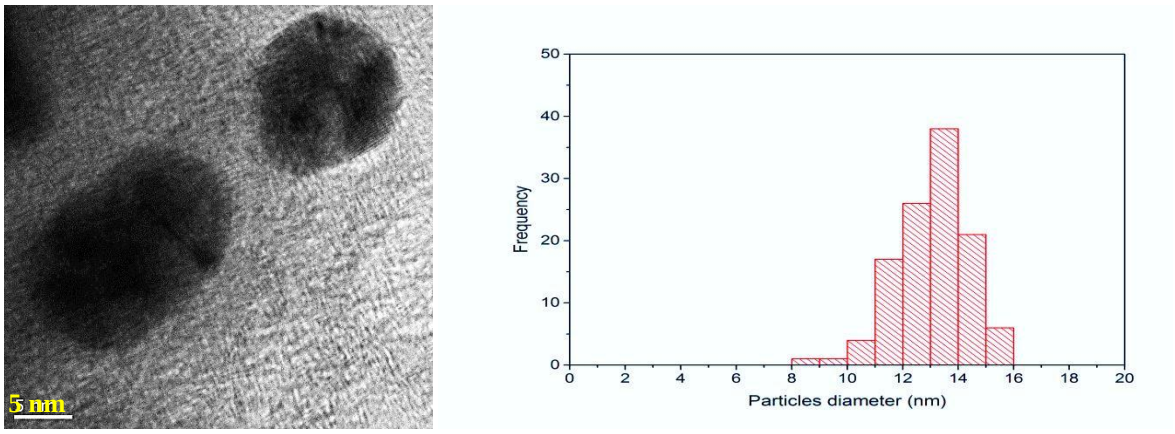

Figure 0.41: Left: a representative TEM image of treated gold citrate nanoparticles immobilized on Norit activated carbon (washed with toluene followed by calcination under static air at 100 ^{o}C for3 hours) deposited onto carbon film coated copper TEM grid; Right: Particle size distribution histogram. The average particle size of gold particles was determined to be 13.1 ± 0.2 nm (two standard deviations of the mean).

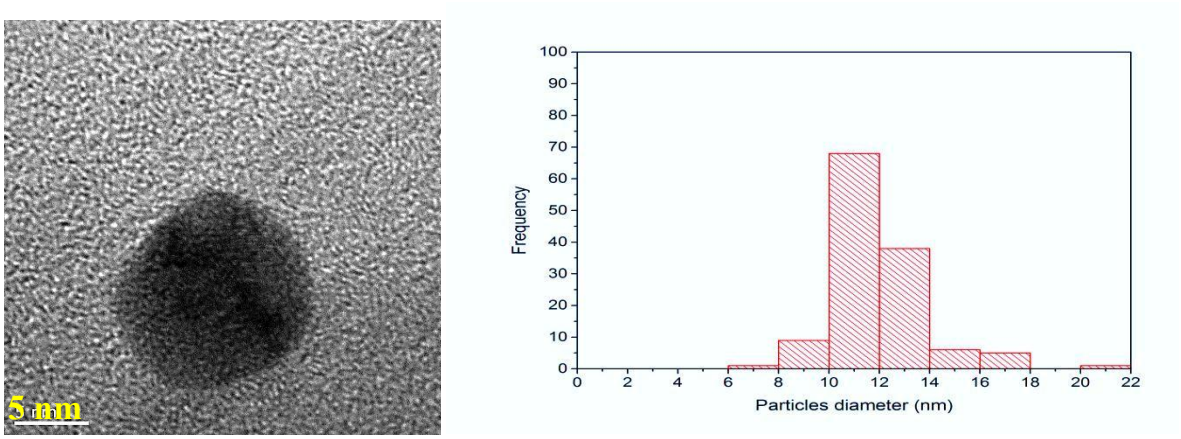

Figure 0.42: Left: a representative TEM image of treated gold citrate nanoparticles immobilized on Norit activated (washed with NaOH in MilliQ water (0.1 M) at water followed by calcination under static air at 100 ^{o}C for 3 hours) deposited onto carbon film coated copper TEM grid; Right: Particle size distribution histogram. The average particle size of gold particles was determined to be 11.5 ± 0.6 nm (two standard deviations of the mean).

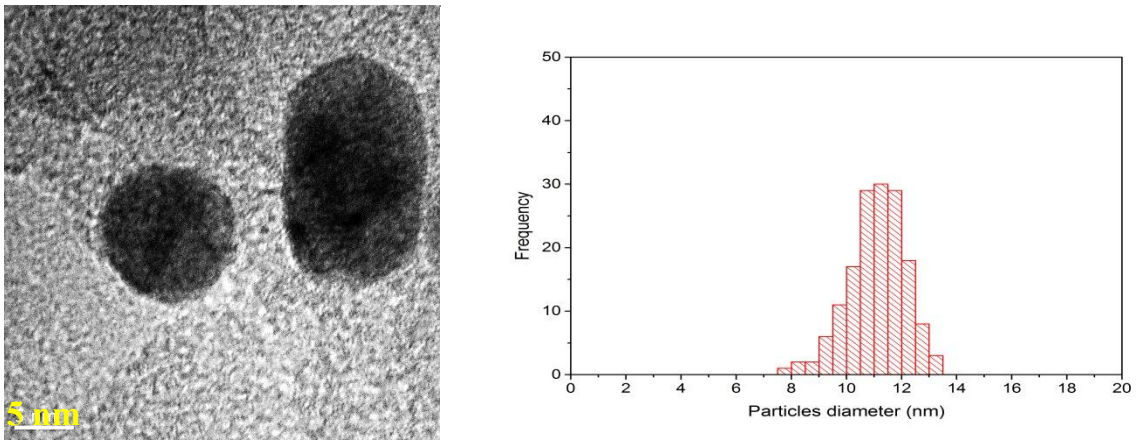

Figure 0.43: Left: a representative TEM image of treated gold citrate nanoparticles immobilized on Norit activated (washed with NaOH in MilliQ water (0.1 M) at water followed by calcination under vacuum at 100 ^{o}C for 3 hours) deposited onto carbon film coated copper TEM grid; Right: Particle size distribution histogram. The average particle size of gold particles was determined to be 11.1 ± 0.2 nm (two standard deviations of the mean).

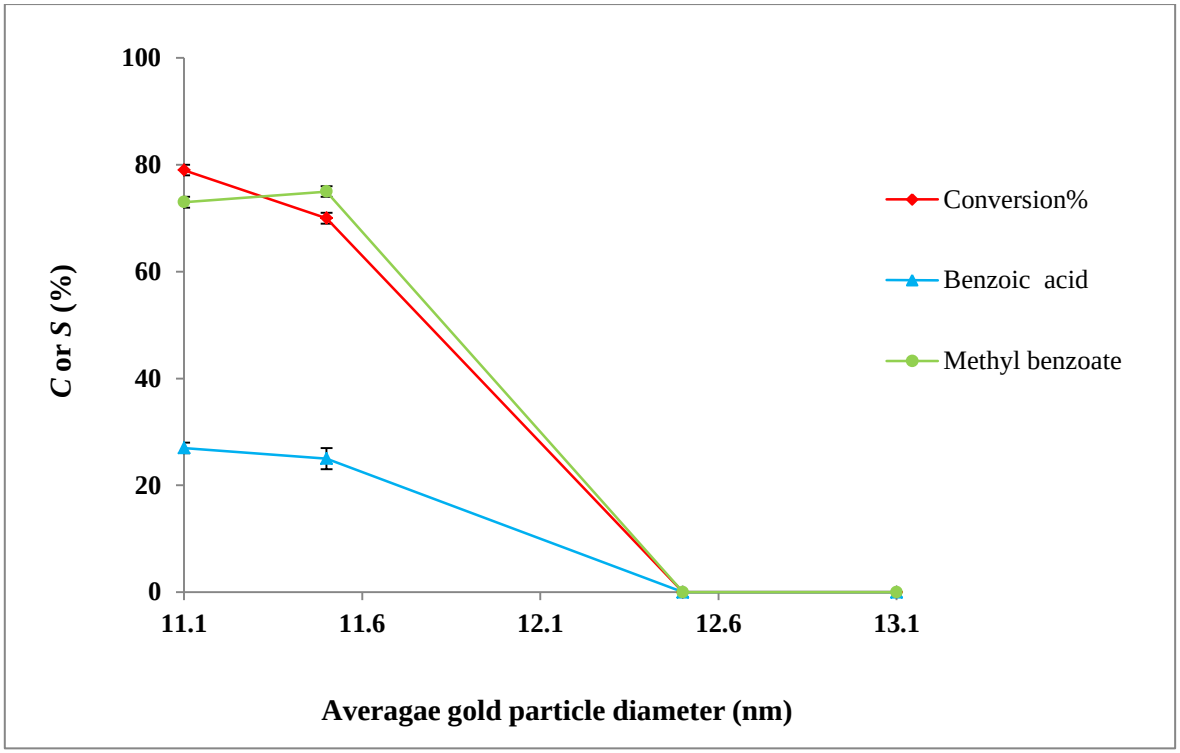

Figure 0.44: The particle size effect on the conversion (*C%*) and selectivity (*S%*) of gold citrate immobilized on Norit activated carbon.

Figure 5.44 shows the dependence of catalytic activity of gold citrate on size. When the average particle diameter decreased from 12.5 ± 0.2 to 11.5 ± 0.6 or 11.1 ± 0.2 the activity of the gold catalysts increased to ~70% or 79%, respectively. Washing with 0.1 M NaOH reduced the distance between the gold particles and reactants by removing citrate from the gold cores.[42, 70] The selectivity of the gold catalyst was towards methyl benzoate with a 3:1 product ratio in favour of methyl benzoate.

5.2.2.2.2 Au_{101}, gold citrate and *"naked"* gold immobilized on Vulcan carbon

In this part, "*naked*" gold and gold citrate nanoparticles are compared with Au_{101} nanoparticles deposited on Vulcan carbon.

Table 0.11: Comparisons of conversion and selectivity among Au_{101}, Au_{naked} and $Au_{citrate}$ immobilized on Vulcan carbon (1.0 wt%) for 3 hours reaction time.

[#]Catalyst code	[*]Activation	Conversion%	Selectivity%		
			Benzaldehyde	Benzoic acid	Methyl benzoate
1.0% Au_{101}/C_v	W+ static air	0	0	0	0
1.0% Au_{101}/C_v	W+ vacuum	0	0	0	0
1.0% Au_{naked}/C_v	W+ static air	20	2	13	85
1.0% Au_{naked}/C_v	W+ vacuum	32	2	11	87
1.0% $Au_{citrate}/C_v$	W+ static air	52	0	13	87
1.0% $Au_{citrate}/C_v$	W+ vacuum	56	0	16	84

[#]**Catalyst code:** Au_{101}/C_v, Au_{naked}/C_v and $Au_{citrate}/C_v$=Au_{101}, Au_{naked} and $Au_{citarte}$ particles immobilized on Vulcan carbon, respectively. [*]**Activations:** Gold catalysts washed with toluene or NaOH in MilliQ water (0.1 M) followed by calcinations under static air or vacuum at 100 C for 3 hours.

The highest activity of the gold nanocatalysts belonged to the activated gold citrate immobilized on Vulcan carbon 52% (washed and static air calcination) and 56% (washed and vacuum calcination) as shown in Table 5.11. There was no conversion for Au_{101} immobilized on Vulcan carbon. The main product was methyl benzoate with 87% and 84% for calcination under static air or vacuum, respectively. Benzaldehyde appeared as a very minor product (2%) for naked gold immobilized on Vulcan carbon.

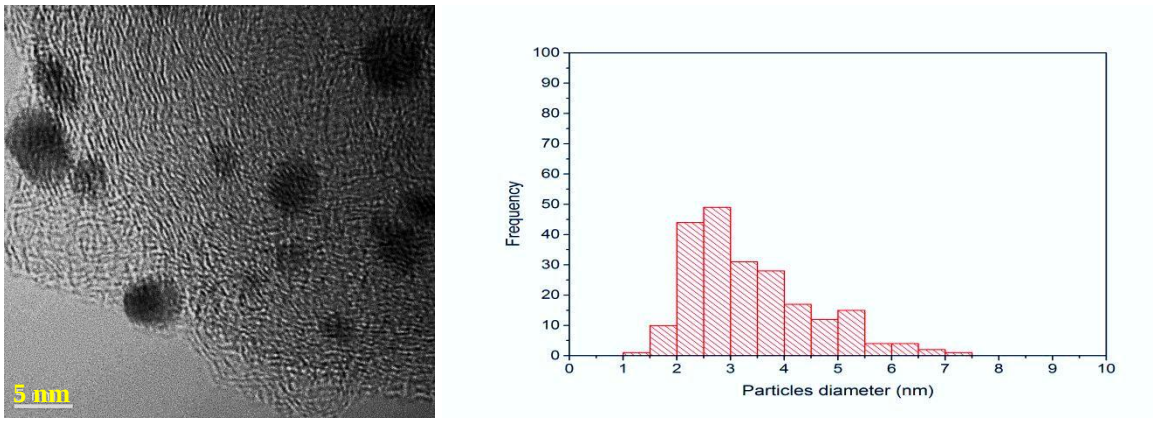

Figure 0.45: Left: a representative TEM image of treated of Au_{101}/C_v (washed with toluene followed by calcination under static air at 100 ^oC for 3 hours) deposited onto carbon film coated copper TEM grid; Right: Particle size distribution histogram. The average particle size of gold particles was determined to be 3.4 ± 0.2 nm (two standard deviations of the mean).

Figure 5.45 shows that the average particle size of activated Au_{101} nanoparticles immobilized on Vulcan carbon (washed with toluene followed by static air calcination at 100 ^oC for 3

hours) was 3.4 ± 0.2 nm. Despite there being many small gold particles of around 3 nm diameter for this type of catalysts, no conversion benzyl alcohol was observed. The small gold nanoparticles might block the Vulcan carbon pores when the particles size is nearly equal or smaller than pore size.[42] Additionally, small gold particles are inaccessible for reactants in Vulcan carbon (see Section 5.2.1.3.4.1).[45b]

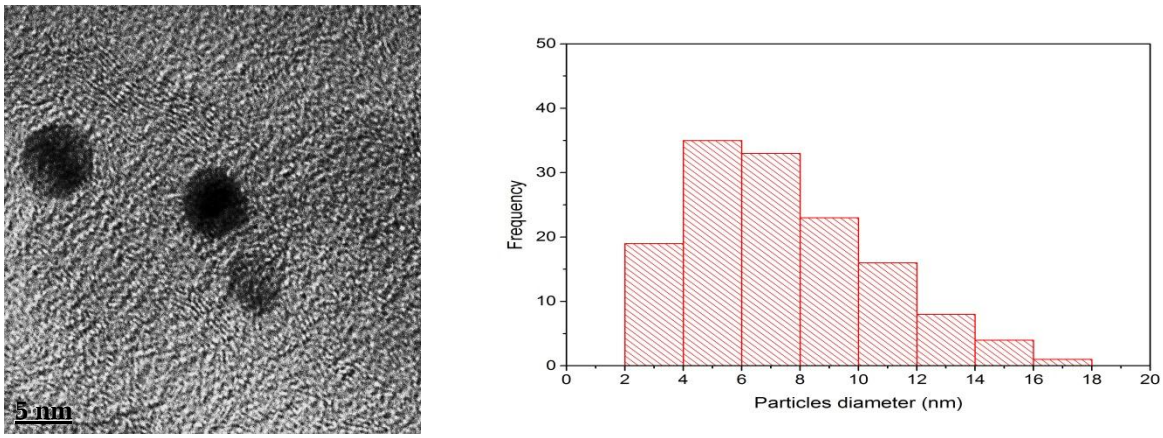

Figure 0.46: Left: a representative TEM image of treated of Au_{naked}/C_v (washed with toluene followed by calcination under static air at 100 ^oC for 3 hours) deposited onto carbon film coated copper TEM grid; Right: Particle size distribution histogram. The average particle size of gold particles was determined to be 7.4 ± 0.5 nm (two standard deviations of the mean).

According to Figure 5.46 and Table 5.11, the catalytic activity (32%) of the treated "*naked*" gold nanocatalysts (washed with toluene and followed by calcination under static air at 100 ^oC for 3 hours) increased reasonably as the average particle diameter increased from ~3.8 ± 0.1 (un-treated) to 7.5± 0.5 nm after catalyst activation.

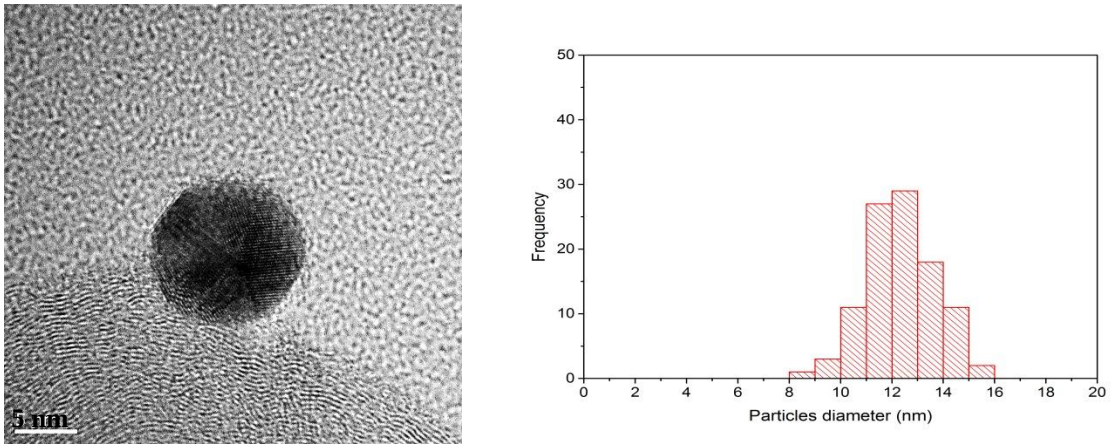

Figure 0.47: Left: a representative TEM image of treated of $Au_{citrate}/C_v$ (washed with NaOH in MilliQ water (0.1 M) followed by calcination under static air at 100 ^oC for 3 hours) deposited onto carbon film coated copper TEM grid; Right: Particle size distribution histogram. The average particle size of gold particles was determined to be 12.3 ± 0.3 nm (two standard deviations of the mean).

Based on Figure 5.47, the gold citrate immobilized on Vulcan carbon and then treated (washed with 0.1 M NaOH in MilliQ water followed by calcination under static air at 100 ^oC for 3 hours) showed a slight decrease in average particle diameter from ~12.5 to ~12.3 nm due to the removal of citrate from the gold core. Washing caused size-preservation and reduced the distance between gold particles and reactants by removing citrate from the gold core particles which led to a better connection between the gold particles and reactants.[42, 70] This can be related with reasonable conversion (52%) of benzyl alcohol with the gold catalysts (see Table 5.11).

5.3 Conclusions

The catalytic activity for benzyl alcohol oxidation of gold nanoparticles can be greatly affected by the size of the gold particles. Small activated gold nanoparticles immobilized on powder Norit activated carbon (1.0 wt% Au_{101}/C) demonstrated the highest activity when the size of gold particles was ~3.5 nm. When the size of gold citrate particles increased, their catalytic activity decreased. The catalytic activity of activated gold particles immobilized on Norit activated carbon powder decreased in the order: $Au_{101}/C > Au_{naked}/C > Au_{citrate}/C$. No conversion was observed when supported gold citrate particles were washed using toluene as

a solvent. However, washing with 0.1 M NaOH in MilliQ caused a big improvement in catalytic activity of this gold catalyst.

While no conversion was observed for small gold particles (Au_{101}: 3.4 ± 0.2), reasonable conversions were observed for bigger particles (*i.e.,* Au_{naked}: 7.4 ± 0.5 nm and $Au_{citrate}$: 12.3 ± 0.3 nm) immobilized on Vulcan carbon. The activity of gold particle immobilized on Vulcan carbon increased in the order: $Au_{101}/C_v < Au_{naked}/C_v < Au_{citrate}/C_v$. Catalysts made using Vulcan carbon as a support demonstrated lower activity in comparison with ones made using Norit carbon. Hence, the average gold particles diameter and the activity of gold catalysts seem to be affected by the nature of carbon support.

Support immobilization of noble metal nanoparticles plays a key role in defining the catalytic activity and selectivity due to both the support structure and specific interactions occurring between the gold particles and the support. Small gold nanoparticles (Au_{101}: ~1.6 nm) immobilized on Norit activated carbon powder and mesopores carbons (*i.e.,* CMK-3, CMK-8 and NCCR-41) showed higher activity in comparison with, Vulcan carbon or granular Norit activated carbon, even when the latter was modified with –SH or $–SO_3H$ groups. The higher performance of gold nanoparticles immobilized on mesopores carbons is mainly due to the fact that the large pore diameter makes it easier for smaller gold particles to access the pore channels and also limits the agglomeration of the particles both in the pore entrance and on the pores surface of the support. Meanwhile, Au_{101} immobilized on CMK-8 mesopores carbons, with the largest pore diameter and 3-D network structure as key factors, showed higher performance in comparison with powder Norit activated carbon. Gold nanoparticles immobilized on Vulcan carbon demonstrated lower activity in comparison with powder Norit activated carbon and meso-pores carbons, too. Gold particles smaller than ~ 4 nm probably block Vulcan carbon pores and reduce accessibility for the reactants.

Overall, the catalytic testing showed that carbon supports for activated (washed and followed by calcinations under static air at 100 ^{o}C for 3 hours) small gold particles (Au_{101}) behave in the following order: mesopores CMK-8 > powder Norit activated carbon > mesopores CMK-3 > mesopores CMK-41 > Vulcan carbon. However, when calcination was swapped to under-vacuum, the gold catalysts behaved in the following order: mesopores CMK-8 > Norit activated carbon (powder) > mesopores CMK-41> mesopores CMK-3 > Vulcan carbon.

Overall, activated 1% Au_{101}/C_{41} (washed with toluene followed by calcination under vacuum at 100 ^{o}C for 3 hours) with 2.6 ± 0.1 nm gold particle size showed high conversion (*C*%: 88%). In fact, it also showed the highest selectivity towards methyl benzoate as the main product (*S*%: 88%) after 3 hours reaction time. However, according to the findings discussed in Chapter 4 of this thesis, activated 1% Au_{101}/C (calcination in O_2 -H_2 at 100 ^{o}C for 3 hours) with 6.6 ± 0.3 nm gold particle size showed the highest selectivity towards benzoic acid as the main product (*S*%: 86%); the catalyst exhibited high conversion (*C*%: 94%) after 24 hours reaction time. In addition, activated 1% Au_{101}/C_{8} (washed with toluene followed by calcination under vacuum or in static air at 100 ^{o}C for 3 hours) with 3.0 ± 0.1 nm gold particle size showed the highest conversion (*C*%: 96%) after 3 hours reaction time.

References

1. (a) Rao, C. N. R.; Kulkarni, G. U.; John Thomas, P.; Edwards, P. P., Size-dependent chemistry: Properties of nanocrystals. *Chem.Eur. J.* **2002,** *8* (1), 28-35; (b) Bond, G.; Thompson, D., Gold-catalysed oxidation of carbon monoxide. *Gold Bull.* **2000,** *33* (2), 41-50.
2. Herzing, A. A.; Kiely, C. J.; Carley, A. F.; Landon, P.; Hutchings, G. J., Identification of active gold nanoclusters on iron oxide supports for CO oxidation. *Science* **2008,** *321* (5894), 1331-1335.
3. Bamwenda, G. R.; Tsubota, S.; Nakamura, T.; Haruta, M., The influence of the preparation methods on the catalytic activity of platinum and gold supported on TiO_2 for CO oxidation. *Catal. Lett.* **1997,** *44* (1-2), 83-87.
4. Valden, M.; Lai, X.; Goodman, D. W., Onset of catalytic activity of gold clusters on titania with the appearance of nonmetallic properties. *Science* **1998,** *281* (5383), 1647-1650.
5. Boronat, M.; Corma, A.; Illas, F.; Radilla, J.; Ródenas, T.; Sabater, M. J., Mechanism of selective alcohol oxidation to aldehydes on gold catalysts: Influence of surface roughness on reactivity. *J. Catal.* **2011,** *278* (1), 50-58.
6. Haruta, M., Spiers Memorial Lecture Role of perimeter interfaces in catalysis by gold nanoparticles. *Faraday Discuss.* **2011,** *152* (0), 11-32.
7. Mavrikakis, M.; Stoltze, P.; Nørskov, J. K., Making gold less noble. *Catal. Lett.* **2000,** *64* (2-4), 101-106.
8. Bond, G., Gold: A relatively new catalyst. *Gold Bulletin* **2001,** *34* (4), 117-119.
9. Xing, X.; Yoon, B.; Landman, U.; Parks, J. H., Structural evolution of Au nanoclusters: From planar to cage to tubular motifs. *Phys. Rev. B: Condens. Matter Mater. Phys.* **2006,** *74* (16).
10. Cox, D. M.; Brickman, R.; Creegan, K.; Kaldor, A., Gold clusters: Reactions and deuterium uptake. *Z. Phys. D: At., Mol. Clusters* **1991,** *19* (4), 353-355.
11. (a) Chi, L. F.; Rakers, S.; Hartig, M.; Gleiche, M.; Fuchs, H.; Schmid, G., Monolayers of nanosized Au_{55}-clusters: Preparation and characterization. *Colloids Surf., A* **2000,** *171* (1-3), 241-248; (b) Zhang, H.; Mautes, D.; Hartmann, U., Negative differential resistance and nonclassical capacitive behaviour in networks of metal clusters. *Nanotechnology* **2007,** *18* (6), 065202.
12. Schmid, G.; Corain, B., Nanoparticulated gold: Syntheses, structures, electronics, and reactivities. *Eur. J. Inorg. Chem.* **2003,** (17), 3081-3098.
13. Yuan, Y.; Kozlova, A. P.; Asakura, K.; Wan, H.; Tsai, K.; Iwasawa, Y., Supported Au catalysts prepared from Au phosphine complexes and As-precipitated metal hydroxides: Characterization and low-temperature CO oxidation. *J. Catal.* **1997,** *170* (1), 191-199.
14. (a) Van der Velden, J. W. A.; Bour, J. J.; Bosman, W. P.; Noordik, J. H., Reactions of cationic gold clusters with Lewis bases. Preparation and x-ray structure investigation of $[Au_8(PPh_3)_7](NO_3)_{2.2}CH_2Cl_2$ and $Au_6(PPh_3)_4[Co(CO)_4]_2$. *Inorg. Chem.* **1983,** *22* (13), 1913-1918; (b) Wen, F.; Englert, U.; Gutrath, B.; Simon, U., Crystal structure, electrochemical and optical properties of $[Au_9(PPh_3)_8](NO_3)_3$. *Eur. J. Inorg. Chem.* **2008,** *2008* (1), 106-111; (c) Schmid, G.; Pfeil, R.; Boese, R.; Bandermann, F.; Meyer, S.; Calis, G. H. M.; Vandervelden, W. A., $AU_{55}[P(C_6H_5)_3]_{12}CL_6$ - A gold cluster of an exceptional size. *Chem. Ber. Recl.* **1981,** *114* (11), 3634-3642.
15. Fenske; Longoni, G.; Schmid, G., Clusters in ligand shells. In *Cluster and colloids; From theoedry to applications*, Schmid, G., Ed. VCH: Weinheim (Federal Republic of Germany), 1994; Vol. 99, pp 89-289.
16. Turner, M.; Golovko, V. B.; Vaughan, O. P. H.; Abdulkin, P.; Berenguer-Murcia, A.; Tikhov, M. S.; Johnson, B. F. G.; Lambert, R. M., Selective oxidation with dioxygen by gold nanoparticle catalysts derived from 55-atom clusters. *Nature* **2008,** *454* (7207), 981-983.
17. Roldán, A.; González, S.; Ricart, J. M.; Illas, F., Critical size for O_2 dissociation by Au nanoparticles. *ChemPhysChem* **2009,** *10* (2), 348-351.
18. Pei, Y.; Shao, N.; Gao, Y.; Zeng, X. C., Investigating active site of gold nanoparticle $Au_{55}(PPh_3)_{12}Cl_6$ in selective oxidation. *ACS Nano* **2010,** *4* (4), 2009-2020.
19. Haruta, M., Spiers memorial lecture role of perimeter interfaces in catalysis by gold nanoparticles. *Faraday Discuss.* **2011,** *152*, 11-32.

20. Porta, F.; Prati, L.; Rossi, M.; Coluccia, S.; Martra, G., Metal sols as a useful tool for heterogeneous gold catalyst preparation: Reinvestigation of a liquid phase oxidation. *Catal. Today* **2000,** *61* (1-4), 165-172.
21. (a) Boronat, M.; Corma, A., Molecular approaches to catalysis: Naked gold nanoparticles as quasi-molecular catalysts for green processes. *J. Catal.* **2011,** *284* (2), 138-147; (b) Comotti, M.; Della Pina, C.; Matarrese, R.; Rossi, M., The catalytic activity of "naked" gold particles. *Angew. Chem., Int. Ed.* **2004,** *43* (43), 5812-5815.
22. Gao, W.; Chen, X. F.; Li, J. C.; Jiang, Q., Is Au_{55} or Au_{38} cluster a threshold catalyst for styrene epoxidation? *J. Phys. Chem. C* **2009,** *114* (2), 1148-1153.
23. (a) Kitahara, H.; Sakurai, H., Anti-addition mechanism in the intramolecular hydroalkoxylation of alkenes catalyzed by PVP-stabilized nanogold. *Molecules* **2012,** *17* (3), 2579-2586; (b) Prati, L.; Martra, G., New gold catalysts for liquid phase oxidation. *Gold Bull.* **1999,** *32* (3), 96-101.
24. (a) Zhu, Y.; Wu, Z.; Gayathri, C.; Qian, H.; Gil, R. R.; Jin, R., Exploring stereoselectivity of Au_{25} nanoparticle catalyst for hydrogenation of cyclic ketone. *J. Catal.* **2010,** *271* (2), 155-160; (b) Qi, C.; Huang, J.; Bao, S.; Su, H.; Akita, T.; Haruta, M., Switching of reactions between hydrogenation and epoxidation of propene over Au/Ti-based oxides in the presence of H_2 and O_2. *J. Catal.* **2011,** *281* (1), 12-20.
25. Nigra, M. M.; Arslan, I.; Katz, A., Gold nanoparticle-catalyzed reduction in a model system: Quantitative determination of reactive heterogeneity of a supported nanoparticle surface. *J. Catal.* **2012,** *295*, 115-121.
26. Haider, P.; Urakawa, A.; Schmidt, E.; Baiker, A., Selective blocking of active sites on supported gold catalysts by adsorbed thiols and its effect on the catalytic behavior: A combined experimental and theoretical study. *J. Mol. Catal. A: Chem.* **2009,** *305* (1-2), 161-169.
27. Liu, Y.; Tsunoyama, H.; Akita, T.; Tsukuda, T., Size effect of silica-supported gold clusters in the microwave-assisted oxidation of benzyl alcohol with H_2O_2. *Chem. Lett.* **2010,** *39* (3), 159-161.
28. (a) Nielsen, I. S.; Taarning, E.; Egeblad, K.; Madsen, R.; Christensen, C. H., Direct aerobic oxidation of primary alcohols to methyl esters catalyzed by a heterogeneous gold catalyst. *Catal. Lett.* **2007,** *116* (1-2), 35-40; (b) Oliveira, R. L.; Kiyohara, P. K.; Rossi, L. M., Clean preparation of methyl esters in one-step oxidative esterification of primary alcohols catalyzed by supported gold nanoparticles. *Green Chem.* **2009,** *11* (9), 1366-1370; (c) Su, F.-Z.; Ni, J.; Sun, H.; Cao, Y.; He, H.-Y.; Fan, K.-N., Gold supported on nanocrystalline β-Ga_2O_3 as a versatile bifunctional catalyst for facile oxidative transformation of alcohols, aldehydes, and acetals into esters. *Chem. Eur. J.* **2008,** *14* (24), 7131-7135; (d) Ishida, T.; Nagaoka, M.; Akita, T.; Haruta, M., Deposition of gold clusters on porous coordination polymers by solid grinding and their catalytic activity in aerobic oxidation of alcohols. *Chem.- Eur. J.* **2008,** *14* (28), 8456-8460.
29. (a) Li, Y.; El-Sayed, M. A., The effect of stabilizers on the catalytic activity and stability of Pd colloidal nanoparticles in the suzuki ractions in aueous slution†. *J. Phys. Chem. B.* **2001,** *105* (37), 8938-8943; (b) Zhang, Y.; Quek, X.-Y.; Wu, L.; Guan, Y.; Hensen, E. J., Palladium nanoparticles entrapped in polymeric ionic liquid microgels as recyclable hydrogenation catalysts. *J. Mol. Catal. A: Chem.* **2013,** *379* (0), 53-58.
30. Kulkarni, A.; Lobo-Lapidus, R. J.; Gates, B. C., Metal clusters on supports: Synthesis, structure, reactivity, and catalytic properties. *Chem. Commun.* **2010,** *46* (33), 5997-6015.
31. Tsubota, S.; Cunningham, D. A. H.; Bando, Y.; Haruta, M., Preparation of nanometer gold strongly interacted with TiO_2 and the structure sensitivity in low-temperature oxidation of CO. *Stud. Surf. Sci. Catal.* **1995,** *91* (c), 227-235.
32. Azad, A.-M.; Duran, M. J.; McCoy, A. K.; Abraham, M. A., Development of ceria-supported sulfur tolerant nanocatalysts: Pd-based formulations. *Appl. Catal., A.* **2007,** *332* (2), 225-236.
33. Roggenbuck, J.; Tiemann, M., Ordered mesoporous magnesium oxide with high thermal stability synthesized by exotemplating using CMK-3 carbon. *J. Am. Chem. Soc.* **2005,** *127* (4), 1096-1097.
34. (a) Liu, C. Y.; Tan, Y. Z.; Lin, S. S.; Li, H.; Wu, X. J.; Li, L.; Pei, Y.; Zeng, X. C., CO self-promoting oxidation on nanosized gold clusters: triangular Au^{-3} active site and CO induced O-O scission. *J. Am. Chem. Soc.* **2013,** *135* (7), 2583-2595; (b) Bulushev, D. A.; Yuranov, I.; Suvorova, E.

I.; Buffat, P. A.; Kiwi-Minsker, L., Highly dispersed gold on activated carbon fibers for low-temperature CO oxidation. *J. Catal.* **2004,** *224* (1), 8-17.
35. Guillois, K.; Mangematin, S.; Tuel, A.; Caps, V., Gold-catalyzed aerobic epoxidation of trans-stilbene in methylcyclohexane. Part II: Identification and quantification of a key reaction intermediate. *Catal. Today* **2013,** *203*, 111-115.
36. Bianchi, C. L.; Biella, S.; Gervasini, A.; Prati, L.; Rossi, M., Gold on carbon: Influence of support properties on catalyst activity in liquid-phase oxidation. *Catal. Lett.* **2003,** *85* (1-2), 91-96.
37. (a) Kuppan, B.; Selvam, P., Platinum-supported mesoporous carbon (Pt/CMK-3) as anodic catalyst for direct methanol fuel cell applications: The effect of preparation and deposition methods. *Prog. Natural Sci.* **2012,** *22* (06), 616-623; (b) Celorrio, V.; Montes de Oca, M. G.; Plana, D.; Moliner, R.; Fermín, D. J.; Lázaro, M. J., Electrochemical performance of Pd and Au–Pd core–shell nanoparticles on surface tailored carbon black as catalyst support. *Int. J. Hydrogen Energy* **2012,** *37* (8), 7152-7160.
38. (a) Pigamo, A.; Besson, M.; Blanc, B.; Gallezot, P.; Blackburn, A.; Kozynchenko, O.; Tennison, S.; Crezee, E.; Kapteijn, F., Effect of oxygen functional groups on synthetic carbons on liquid phase oxidation of cyclohexanone. *Carbon* **2002,** *40* (8), 1267-1278; (b) Pereira, M. F. R.; Órfão, J. J. M.; Figueiredo, J. L., Oxidative dehydrogenation of ethylbenzene on activated carbon catalysts. Influence of surface chemical groups. *Appl. Catal., A.* **1999,** *184* (1), 153-160.
39. Figueiredo, J. L.; Pereira, M. F. R.; Freitas, M. M. A.; Órfão, J. J. M., Modification of the surface chemistry of activated carbons. *Carbon* **1999,** *37* (9), 1379-1389.
40. Monk, J.; Singh, R.; Hung, F. R., Effects of pore size and pore loading on the properties of ionic liquids confined inside nanoporous CMK-3 carbon materials. *J. Phys. Chem. C* **2011,** *115* (7), 3034-3042.
41. (a) Erturk, E.; Haberal, M.; Piskin, E., Towards the commercialization of a haemoperfusio column. Part I: Selection of activated carbon. *Clin. Mater.* **1987,** *2* (1), 55-65; (b) Brunauer, S.; Emmett, P. H.; Teller, E., Adsorption of gases in multimolecular layers. *J.Am. Chem. Soc.* **1938,** *60* (2), 309-319.
42. Park, G. G.; Yang, T. H.; Yoon, Y. G.; Lee, W. Y.; Kim, C. S., Pore size effect of the DMFC catalyst supported on porous materials. *Int. J. Hydrogen Energy* **2003,** *28* (6), 645-650.
43. Bianchi, C.; Porta, F.; Prati, L.; Rossi, M., Selective liquid phase oxidation using gold catalysts. *Top. Catal.* **2000,** *13* (3), 231-236.
44. Rolison, D. R., Catalytic nanoarchitectures - The importance of nothing and the unimportance of periodicity. *Science* **2003,** *299* (5613), 1698-1701.
45. (a) Foley, H. C., Carbogenic molecular sieves: synthesis, properties and applications. *Microporous Mater.* **1995,** *4* (6), 407-433; (b) Raghuveer, V.; Manthiram, A., Mesoporous carbons with controlled porosity as an electrocatalytic support for methanol oxidation. *J. Electrochem. Soc.* **2005,** *152* (8), A1504-A1510.
46. Raghuveer, V.; Manthiram, A., Mesoporous carbon with larger pore diameter as an electrocatalyst support for methanol oxidation. *Electrochem. Solid-State Lett.* **2004,** *7* (10), A336-A339.
47. Maiyalagan, T.; Nassr, A. B. A.; Alaje, T. O.; Bron, M.; Scott, K., Three-dimensional cubic ordered mesoporous carbon (CMK-8) as highly efficient stable Pd electro-catalyst support for formic acid oxidation. *J. Power Sources* **2012,** *211* (0), 147-153.
48. (a) Corma, A., From microporous to mesoporous molecular sieve materials and their use in catalysis. *Chem. Rev.* **1997,** *97* (6), 2373-2419; (b) Selvam, P.; Kuppan, B., Synthesis, characterization and electrocatalytic properties of nano-platinum-supported mesoporous carbon molecular sieves, Pt/NCCR-41. *Catal. Today* **2012,** *198* (1), 85-91; (c) Lesaint, C.; Lebeau, B.; Marichal, C.; Patarin, J., Synthesis of mesoporous silica materials functionalized with n-propyl groups. *Microporous Mesoporous Mater.* **2005,** *83* (1-3), 76-84.
49. Lysenko, N. D.; Opanasenko, M. V.; Yaremov, P. S.; Shvets, A. V.; Il'in, V. G., Structural and sorption properties of carbon replicas obtained by matrix carbonization of organic precursors in SBA-15 and KIT-6. *Theor. Exp. Chem.* **2010,** *46* (1), 51-57.
50. Baikousi, M.; Bourlinos, A. B.; Douvalis, A.; Bakas, T.; Anagnostopoulos, D. F.; Tuček, J.; Šafářová, K.; Zboril, R.; Karakassides, M. A., Synthesis and characterization of γ-Fe_2O_3/carbon

hybrids and their application in removal of hexavalent chromium ions from aqueous solutions. *Langmuir* **2012,** *28* (8), 3918-3930.
51. Garcia, T.; Murillo, R.; Agouram, S.; Dejoz, A.; Lazaro, M. J.; Torrente-Murciano, L.; Solsona, B., Highly dispersed encapsulated AuPd nanoparticles on ordered mesoporous carbons for the direct synthesis of H_2O_2 from molecular oxygen and hydrogen. *Chem. Commun.* **2012,** *48* (43), 5316-5318.
52. Kawase, T.; Yoshitake, H., Cathodes comprising Li_2MnSiO_4 nanoparticles dispersed in the mesoporous carbon frameworks, CMK-3 and CMK-8. *Microporous Mesoporous Mater.* **2012,** *155* (0), 99-105.
53. (a) Lang, J.-W.; Yan, X.-B.; Yuan, X.-Y.; Yang, J.; Xue, Q.-J., Study on the electrochemical properties of cubic ordered mesoporous carbon for supercapacitors. *J. Power Sources* **2011,** *196* (23), 10472-10478; (b) Maiyalagan, T.; Alaje, T. O.; Scott, K., Highly stable Pt–Ru nanoparticles supported on three-dimensional cubic ordered mesoporous carbon (Pt–Ru/CMK-8) as promising electrocatalysts for methanol oxidation. *J. Phys. Chem. C* **2011,** *116* (3), 2630-2638.
54. (a) Abad, A.; Corma, A.; García, H., Catalyst parameters determining activity and selectivity of supported gold nanoparticles for the aerobic oxidation of alcohols: The molecular reaction mechanism. *Chem.- Eur. J.* **2008,** *14* (1), 212-222; (b) Prati, L.; Rossi, M., Gold on carbon as a new catalyst for selective liquid phase oxidation of diols. *J. Catal.* **1998,** *176* (2), 552-560; (c) Okumura, M.; Nakamura, S.; Tsubota, S.; Nakamura, T.; Azuma, M.; Haruta, M., Chemical vapor deposition of gold on Al_2O_3, SiO_2, and TiO_2 for the oxidation of CO and of H_2. *Catal. Lett.* **1998,** *51* (3-4), 53-58; (d) Miedziak, P.; Sankar, M.; Dimitratos, N.; Lopez-Sanchez, J. A.; Carley, A. F.; Knight, D. W.; Taylor, S. H.; Kiely, C. J.; Hutchings, G. J., Oxidation of benzyl alcohol using supported gold–palladium nanoparticles. *Catal. Today* **2011,** *164* (1), 315-319.
55. Zielasek, V.; Xu, B. J.; Liu, X. Y.; Baumer, M.; Friend, C. M., Absence of subsurface oxygen effects in the oxidation of olefins on Au: Styrene oxidation over sputtered Au(111). *J. Phys. Chem. C* **2009,** *113* (20), 8924-8929.
56. Dimitratos, N.; Lopez-Sanchez, J. A.; Morgan, D.; Carley, A. F.; Tiruvalam, R.; Kiely, C. J.; Bethell, D.; Hutchings, G. J., Solvent-free oxidation of benzyl alcohol using Au-Pd catalysts prepared by sol immobilisation. *PCCP* **2009,** *11* (25), 5142-5153.
57. (a) Choudhary, V. R.; Dumbre, D. K., Solvent-free selective oxidation of benzyl alcohol to benzaldehyde by tert-butyl hydroperoxide over U_3O_8-supported nano-gold catalysts. *Appl. Catal., A* **2010,** *375* (2), 252-257; (b) Valente, A.; Palma, C.; Fonseca, I. M.; Ramos, A. M.; Vital, J., Oxidation of pinane over phthalocyanine complexes supported on activated carbon: Effect of the support surface treatment. *Carbon* **2003,** *41* (14), 2793-2803.
58. Hutchinson, J. E.; Foster, E. W.; Warner, M. G.; Reed, S. M.; Weare, W. W., Triphenylphosphine-stabilised gold nanoparticles. In *Inorganic synthsis*, Shapley, J. R., Ed. John Wiley & Sons: 2004; Vol. 34 pp 228-232.
59. Martin, M. N.; Basham, J. I.; Chando, P.; Eah, S.-K., Charged gold nanoparticles in non-polar solvents: 10-min synthesis and 2D self-assembly. *Langmuir* **2010,** *26* (10), 7410-7417.
60. Turkevich, J.; Stevenson, P. C.; Hillier, J., A study of the nucleation and growth processes in the synthesis of colloidal gold. *Disc. Faraday Soc.* **1951,** *11*, 55-75.
61. Kilmartin, J. Molecular gold clusters as precursors to heterogeneous catalysts University College London, London, England, 2010.
62. Zhang, X.; Qu, Z.; Li, X.; Wen, M.; Quan, X.; Ma, D.; Wu, J., Studies of silver species for low-temperature CO oxidation on Ag/SiO_2 catalysts. *Sep. Purif. Technol.* **2010,** *72* (3), 395-400.
63. Ftouni, J.; Penhoat, M.; Girardon, J. S.; Addad, A.; Payen, E.; Rolando, C., Immobilization of gold nanoparticles on fused silica capillary surface for the development of catalytic microreactors. *Chem. Eng. J.* **2013,** *227*, 103-110.
64. Anderson, D. P.; Alvino, J. F.; Gentleman, A.; Qahtani, H. A.; Thomsen, L.; Polson, M. I. J.; Metha, G. F.; Golovko, V. B.; Andersson, G. G., Chemically-synthesised, atomically-precise gold clusters deposited and activated on titania. *PCCP* **2013,** *15* (11), 3917-3929.
65. Chang, C. M.; Cheng, C.; Wei, C. M., CO oxidation on unsupported Au_{55}, Ag_{55}, and $Au_{25}Ag_{30}$ nanoclusters. *J. Chem. Phys.* **2008,** *128* (12), 124710/1-124710/4.

66. Donoeva, B. G.; Ovoshchnikov, D. S.; Golovko, V. B., Establishing a Au nanoparticle size effect in the oxidation of cyclohexene using gradually changing Au catalysts. *ACS Catalysis* **2013,** *3* (12), 2986-2991.
67. Anderson, D. P.; Adnan, R. H.; Alvino, J. F.; Shipper, O.; Donoeva, B.; Ruzicka, J. Y.; Al Qahtani, H.; Harris, H. H.; Cowie, B.; Aitken, J. B.; Golovko, V. B.; Metha, G. F.; Andersson, G. G., Chemically synthesised atomically precise gold clusters deposited and activated on titania. Part II. *PCCP* **2013,** *15* (35), 14806-14813.
68. Zheng, N.; Stucky, G. D., A general synthetic strategy for oxide-supported metal nanoparticle catalysts. *J. Am. Chem. Soc* **2006,** *128* (44), 14278-14280.
69. Woehrle, G. H.; Hutchison, J. E., Thiol-functionalized undecagold clusters by ligand exchange: Synthesis, mechanism, and properties. *Inorg. Chem.* **2005,** *44* (18), 6149-6158.
70. Lim, D. C.; Dietsche, R.; Ganteför, G.; Kim, Y. D., Chemical properties of size-selected Au clusters treated under ambient conditions. *Chem. Phys. Lett.* **2008,** *457* (4-6), 391-395.

Chapter 6: Catalysis by Palladium Nanoparticles Immobilized on Wool

6.1 Introduction

Platinum group metals, such as platinum itself, ruthenium and palladium, have long been known as active and selective catalysts in many applications, even in their bulk phases;[1] but, as bulk materials, their industrial utility is diminished by their high cost and low surface area.[2] Recently, nanoscale palladium has been extensively studied because nanoparticulate materials can provide a greater surface area at much lower costs, and have been found to exhibit remarkable properties as highly active and selective catalysts, particularly for a broad range of hydrogenation reactions involving unsaturated substrates,[3] such as cyclohexene,[4] hex-1-ene,[4-5] styrene,[4, 6] acrylic acid[4, 7] and allyl alcohol.[8] Table 6.1 provides selected examples illustrating the use of supported palladium nanoparticles as a high-performance catalyst in various types of reactions.

In the majority of current industrial applications, metal nanoparticles are immobilized on robust supports, such as oxides or activated carbon.[9] In recent years, however, polymeric supports have attracted attention because they provide additional qualities, such as tunable surface chemistry and mechanical process-ability. In principle, the choice of a specific polymer with certain functional groups could be used to fine-tune the performance of such systems.

Polymers can stabilize metal nanoparticles by incorporation them into the polymer framework or by binding weakly to the nanoparticle through stabilizer ligands.[10] Following the polymerization initiation process, the polymer chains grow, by consuming monomers, until they reach a termination length that depends on the polymer composition, reaction conditions, the solvent, *etc*. Stabilizer ligands or surfactants may also play a major role in prevention of particles aggregation and precipitation.[10, 11]

Table 0.1: **Example of reactions catalysed by supported palladium nanoparticles.**

Catalyst code	Reaction	*C%	TOF	*Y%	Reference
Pd/Fe_3O_4/s-G	Suzuki–Miyaura cross-coupling reaction	90	—	—	Hu *et al.*[12]
Pd^{II}/50WX2	3-hexyn-1-ol hydrogenation	90	—	—	Marrodan *et al.*[3]
Pd/Glass-polymer	Ethyl cinnamate hydrogenation	100	—	—	Mennecke *et al.*[13]
Pd/Polyelectrolyte	Un-saturated alcohols hydrogenation	—	~1500	—	Kidambi *et al.*[7]
Pd/Al_2O_3	Un-saturated alcohols hydrogenation	—	60 –700	—	Kidambi *et al.*[7]
Pd/Polyacrylic acid	propyne hydrogenation	20<C< 80	—	—	Gröschel *et al.*[14]
Pd/SiO_2 – CS	Ketone hydrogenation	—	—	30<Y< 100	Yin *et al.*[15]
Pd/Cellulose	Heck reaction of acrylic acid or styrene with aryl iodides	—	—	~ 90	Xu *et al.*[16]
Pd/Wool	Ortho- or para-substituted styrene hydration	—	—	~ 90	Wang *et al.*[6]
Pd/Wool	Diacetone alcohol hydrogenation	—	—	30<Y< 70	Yin *et al.*[17]
Pd/Wool	3-methyl-2-butanone hydrogenation	—	—	90<Y< 100	Yin *et al.*[17]

*C%: How much of a reactant was reacted & Y**%**: The amount of a specific product.

The catalytic properties of nanosized metal particles dispersed within a polymeric matrix can be tailored by adjusting the natures of both the nanoparticles and the support materials.[18] Miyazaki *et al.* found that the polymer can also help to control the morphology and size of metal particles.[19] They used poly (N-vinyl-2-pyrrolidone) (PVP), poly (*N*-isopropylacrylamide) (NIPA) and sodium poly (acrylate) (SPA) and found that the Pt nanocrystals shapes were hexagonal, square and triangular with the average sizes of 6.9, 13.6 and 14.6 nm, respectively.[19]

Metal nanoparticles stabilized by polymers have shown promising results in terms of catalytic efficiency and selectivity because of their small size and relatively narrow dispersity.[20] Polymers, such as PVP,[13, 21] poly (ethylene glycol) (PEG) [4], poly–acrylonitrile and poly (acrylic acid) (see Figure 6.1)[14] have been utilized as efficient supports for catalysis.

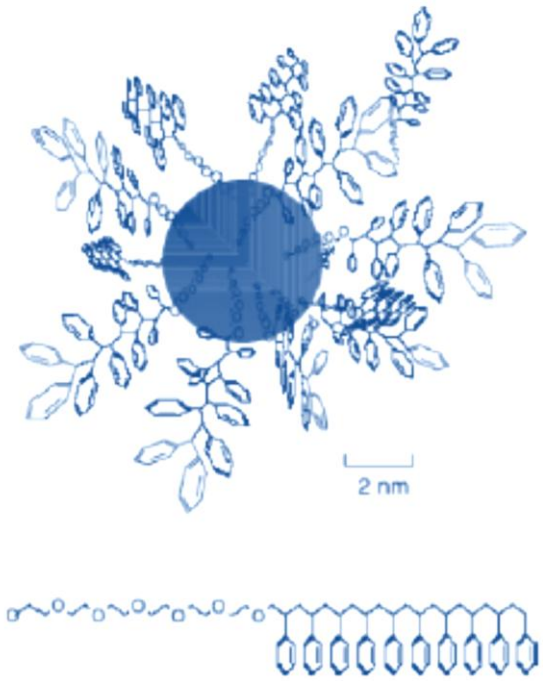

Figure 0.1: Palladium particles stabilized by poly-acrylic acid. The stabilizing effect is due to interactions of the nanoparticle with the polar part of the block copolymer. Reproduced from Groschel *et al.*[14]

Suspensions of nanoparticles stabilized by polymeric composite materials are sometimes used as homogeneous catalysts.[22] As an example, palladium nanoparticles are stabilized in organic solvent by poly-acrylic acid, with the help of the latter's hydrophilic and lipophilic components. The hydrophilic polyethylene oxide chain adsorbs to the electropositive surface of the nanoparticles, while the lipophilic polystyrene section orients towards the solvent (see Figure 6.1).[14] As another example, catalytic hydrogenation of a range of olefins was carried out by palladium nanoparticles dispersed in polyethylene glycols (PEGs), with the double bond of cyclohexene being hydrogenated with 100% selectivity.[4] However, as mentioned earlier, homogeneous catalysts lead to separation difficulties,[14] and the catalyst system can become contaminated by ligand residues in the products.[23]

In recent years polymers have also been developed as "*heterogeneous"* supports for noble metal particles.[24] This type of catalyst systems contains multiple types of active sites, located on the outer and inner surfaces of polymer films (see Figures 6.2).[23a, 25] The outer surface is directly in contact with the reactants, which diffuse through the polymer to the metal particles where the reaction occurs.[25] The ratio of polymer to metal particles is important to the catalytic activity; a ratio greater than one can lead to an increase of the surface area and hence provides better accessibility of the reactants to the active sites of catalyst.[11]

Multilayer polyelectrolyte films attached to solid substrates, such as alumina or silica particles, are utilized as efficient composite supports for catalyst materials occupying the niche between truly homogeneous and heterogeneous classes. Such catalytic systems have shown excellent properties in facilitating mass transfer of reactants to the active sites at the metal nanoparticles, especially in hydrogenation reactions.[13]

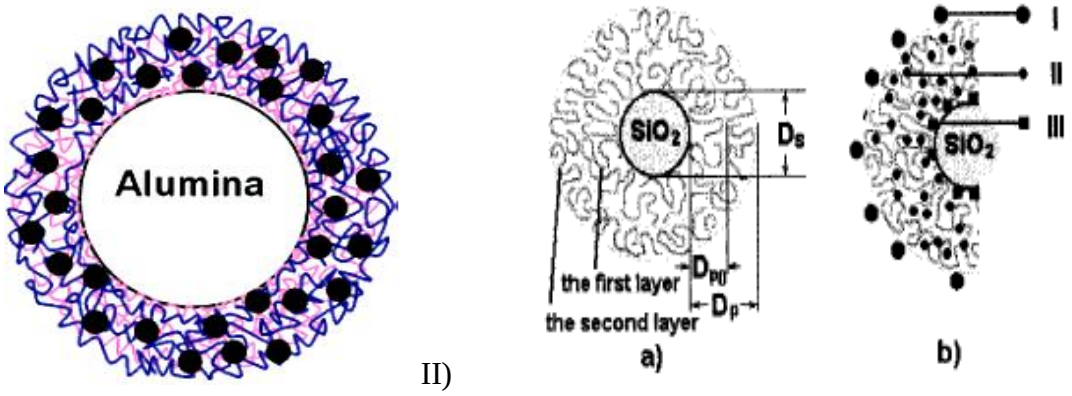

Figure 0.2: Model of Pd particles (black dots) attached on polymer layers on alumina I) & silica II) surfaces. Reproduced from Kidambi *et al*[7] and Huang *et al.,*[11] respectively.

Polymer brushes are another type of appealing polymeric support. The polymer chains are attached at one end, in relatively high coverage, to an interface (*i.e.,* a solid support, like gold) from which they stretch into solution to form a brush-like structure.[26] The metal ion particles reside on top of, or within, the brush. The whole system is maintained in suspension by

interactions between the polymer brush and the solvent.[26-27] In addition, a polar end group (attached to a hydrocarbon chain) is insoluble in polar solvents.[26]

The catalytic activities of the embedded metal nanoparticles in polymer-brush systems are strongly affected by the nature of the polymers.[27] One type of system is shown in Figure 6.3. Here, the metal nanoparticles reside within the brush layer, near the surface of the core heterogeneous support particles. The external layer is directly in contact with the reactants, which diffuse rapidly through the polymer brush to the metal particles.[25, 27] The nanoparticles have partial freedom of movement within the brush.

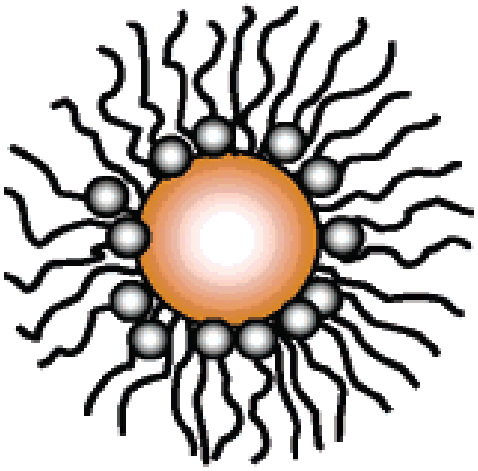

Figure 0.3: A schematic illustration of Pd particles in spherical polyelectrolyte brushes. Reproduced Mei *et al*.[27]

Micro- and meso-porous materials with large specific surface areas are potentially of great practical value in the fields of catalysis,[28] due to their ability to capture metal nanoparticles within a matrix (see Figure 6.4).[29] For example, Ogasawara *et al*. recently reported that porous polymeric supports could be used to minimize, or prevent, aggregation of palladium nanoparticles with narrow size distributions.[29] Such supports can also control the growth of Pd particles involving dendrimeric ligands (see Figure 6.4), for example by limiting the size of Pd-containing particles to a diameter ~2 nm.[29] Such flexible materials can be used as supports for fabrication of truly heterogeneous catalytic systems for processes like carbon cross-coupling reactions, with both high activity and selectivity.[29]

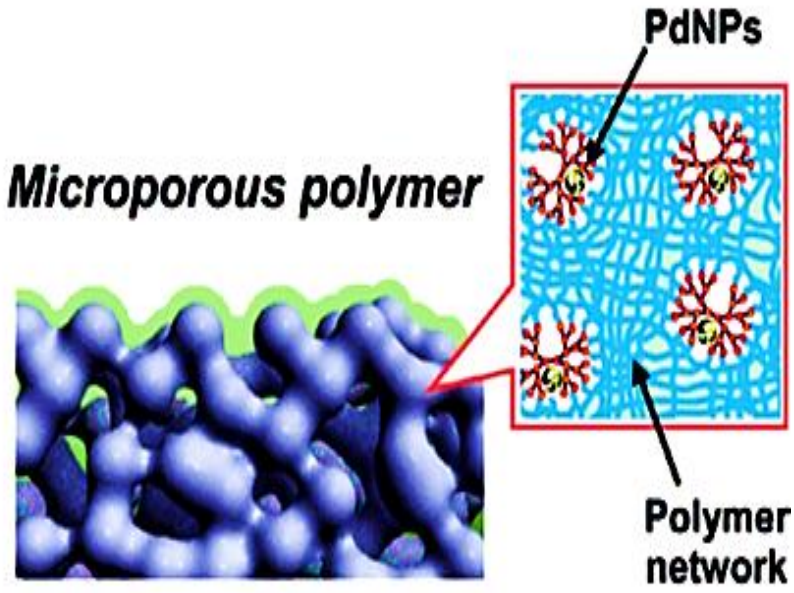

Figure 0.4: Schematic outline of micro-porous polymers (dendrimer structures) containing Pd particles. Reproduced from Ogasawara Kato.[29]

Recently, environmental pollution has been one of the biggest concerns for scientists.[30] Despite concerns about plastics contamination, plastics are widely used in many industries, as packaging, in construction, medical devices, electronics, automotive and aerospace materials.[31] In 2009, about 230 million tonnes of non-bio-degradable plastics was produced globally.[32] Micro-plastic materials don't fully degrade; they simply break down, due to effects of heat, light and physicochemical processes,[33] into very small (ultimately microscopic) fragments that can contaminate both soil and water (see Figure 6.5).[34] They are dangerous to living organisms because they have rather significant environmental lifetimes. For example, the degradation dust of a plastic six-pack collar is estimated to last approximately 450 years.[35] Another disadvantage of the use of synthetic polymeric supports in catalytic systems is their current feed-stocks, which are derived from non-renewable organic substances such as oil and natural gas.

In recent years, with increasing concerns of environmental protection, development of environmentally benign chemical processes and methodologies has received much attention, along with a strengthening interest in renewable materials.[4] Although some catalysts made

using synthetic polymeric supports exhibit remarkable activity and selectivity, they are resilient to bio-degradation and consequently can accumulate in the environment.

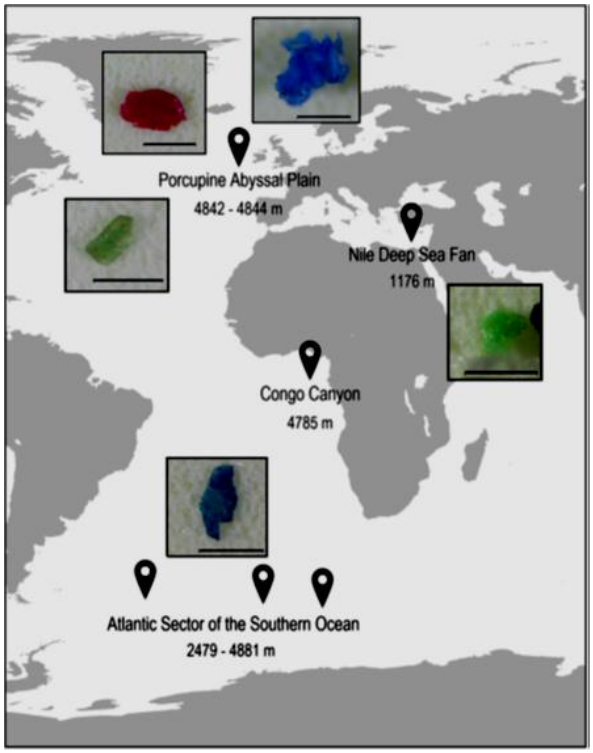

Figure 0.5: Locations of the sites collected sampled of micro-plastic. Reproduced from Cauwenberghe *et al*.[30b]

Potential alternatives to synthetic polymer include natural bio-polymeric fibers, and recently there have been developments of catalysts based on these supports. Bio-polymers have several advantageous properties; in particular they are environmentally friendly (*e.g.*, they are renewable and bio-degradable, although one must remember that waste generated by natural fiber industries is still substantial).[18, 36] Wool can degrade within one to five years, while cotton can degrade within one to five months.[35] They also have variability in characteristics which affects their porosity and hence their diffusion properties and accessibility to internal sites, *etc*.[25] Thus far, researchers have predominantly focused on a few selected natural bio-polymers, such as chitosan,[15] cellulose,[16, 37] silk[38] and wool,[6, 20b, 24] in pioneering developments of novel metal systems. Each of these could be used reasonably cheaply for certain applications without any additional treatment.[24]

Important studies have been performed using synthetic polymers that take a leading position in the world fibre market in terms of production and consumption. However, the emerging fields of interactive textiles and smart fabrics have recently attracted much attention.[23b] The potential applications of thermal conductivity fibres span a wide range of fields from traditional clothing sectors, including sportswear and work clothing, to home ware (carpet, upholstery) and industrial textiles (building, automotive and filtration), as well as highly innovative electronics and biomedical end-uses.[16, 39] For instance, recent advances in wool grading and processing in New Zealand have led to the emergence of high-tech clothing brands, such as *"Icebreaker",* yet most of New Zealand wool is sold at relatively low premium to carpet manufacturers.[40]

Wool is a natural, multi-cellular staple fibre (see Figure 6.6) predominantly composed of amino acids and other organic substances, such as sugars, lipids and DNA/RNA *etc*.[24] It is estimated that wool contains more than 170 different proteins, which are not uniformly distributed throughout the fibre with proteins of different structures being located in specific regions. The proteins, in turn, are composed of more than 20 amino acids. The amino acids are cross-linked by S–S bonds (see Scheme 6.1).[17] This heterogeneous composition is responsible for the different physical and chemical properties of the various regions of wool.

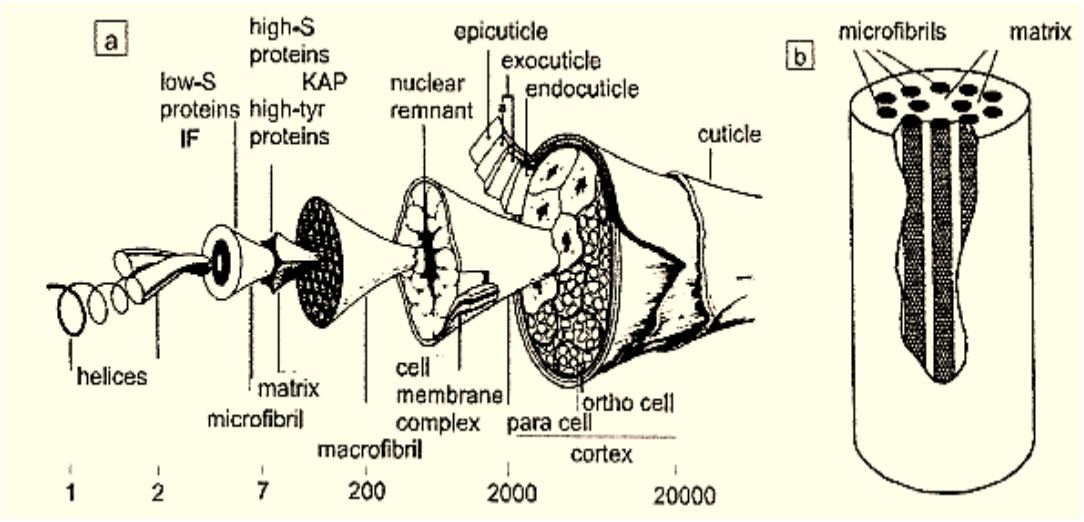

Figure 0.6: Schematic structures of a) wool fibre & b) micro-fibril/ matrix assembly.[41]

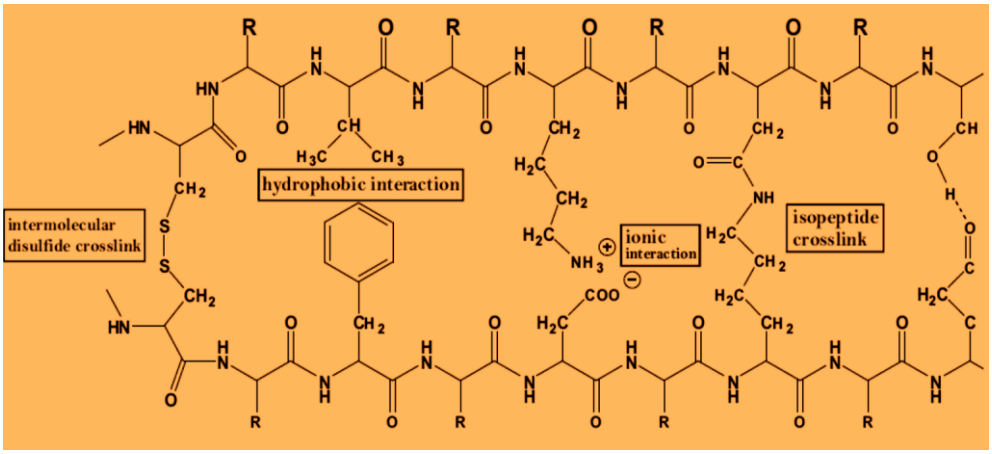

Scheme 0.1: Chemical structure of a wool fibre.[42]

Different grades of wool fibres have somewhat different structures leading to variations in texture, staple, elasticity and crimp formation.

Wool has attracted interest in the field of heterogeneous catalysis because its fibres can be used as a solid-phase ligating (*i.e.*, containing functional groups capable of acting as ligands) support with no need for further functionalization. It is also renewable, bio-compatible, bio-degradable, hydrophobic and capable of supporting well-dispersed nanoparticles. Researchers have claimed that nanoparticles are distributed at surface defects and /or at edges of the wool fibre cells (Figure 6.7), with aggregation being prevented due to interactions with structurally

ordered amino acid chains.[43] However, wool's potential in such applications largely remains unexplored.[18]

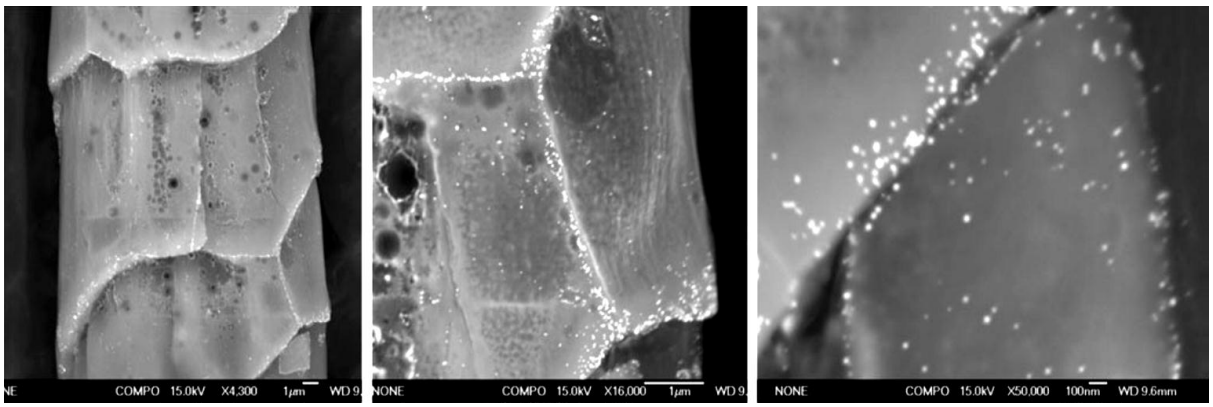

Figure 0.7: SEM images at increasing magnification (left to right) of a nanogold wool fibre showing gold nanoparticles (white dots) on the surface of the fibre, particularly along the cuticle edges. Rreproduced from Johnston *et al.*[40]

$R–NH_2 + HCl \rightarrow RNH_3^+ + Cl^-$

$2RNH_3^+ + PdCl_4^{2-} \rightarrow (RNH_3^+)_2PdCl_4^{2-}$

Scheme 0.2: Interaction between palladium atoms and wool fibres. Reproduced from Yu *et al*.[20b]

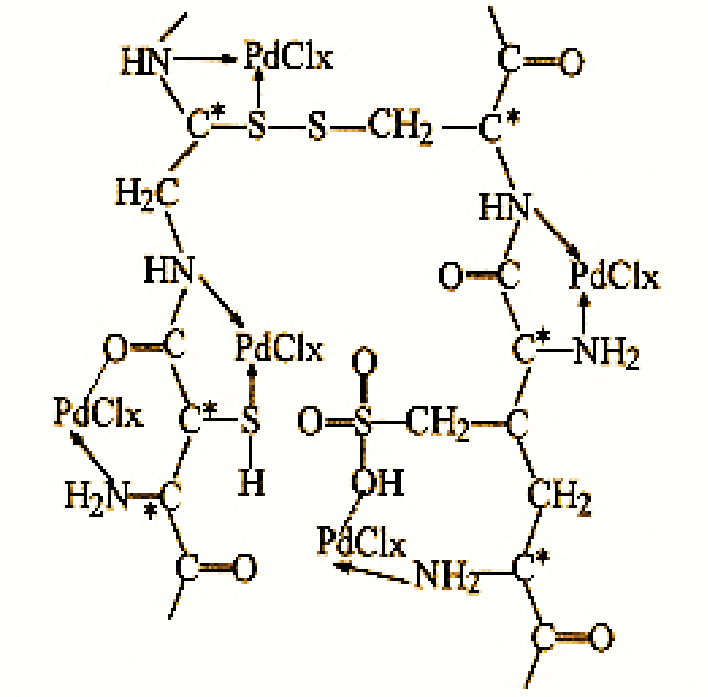

Scheme 0.3: The possible structure of palladium atoms embedded on wool fibres. Reproduced from Yin *et al*.[17]

Metal particles fabricated and/or supported on wool have been proposed for use in a wide range of potential applications, such as colourfast pigments for high-end boutique textiles[40, 44] and antibacterial textiles.[43b, 45] Compared to the overall number of relevant studies on synthesis, characterization and various other applications of such materials, there are only a very few examples of their use in catalysis. Professor James Johnston and co-workers at Victoria University of Wellington have fabricated a range of safe and environmentally friendly materials containing metal nanoparticles of Au (Figure 6.7),[40, 46] Ag (Figure 6.8)[44] and Pd[43a] supported on natural bio-polymeric supports such as Merino and/ or crossbred wool fibres. However, among all of the materials developed by his research group the only catalytic trial has been for 3-hexyne hydrogenation by gold particles immobilized on wool.[46]

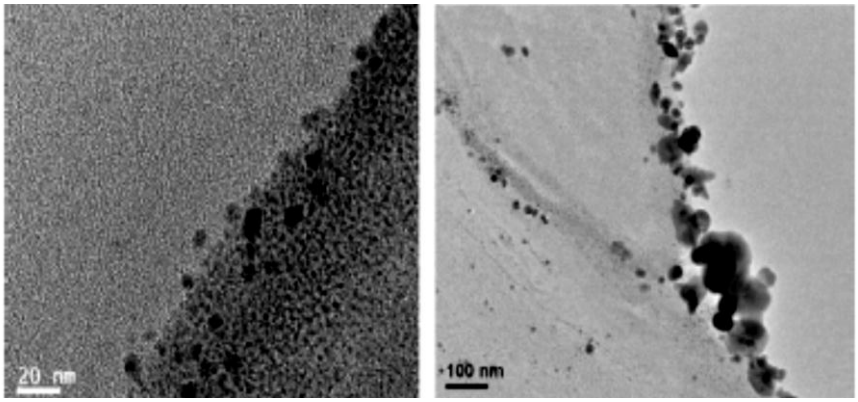

Figure 0.8: TEM images of a cross section showing silver nanoparticles immobilized on Merino wool fibres. Reproduced from Johnston *et al.*[44]

A pioneering study by Yin *et al.* in 1999 reported the use of Pd nanoparticles immobilized on wool fibres (Pd/wool) as a catalyst for asymmetric hydrogenation of diacetone alcohol at 30 ^{o}C for 10 hours under 1 atm of H_2.[17] They investigated the effect of Pd content (mmol/g) and reproducibility on the catalytic activity of the Pd catalysts.[17] In a more recent study, Ma *et al*. reported heterogeneous catalysts using Pd/wool for water-mediated coupling reactions of aryl iodides and bromides with arylboronic acid in the presence of potassium carbonate (as a base) for 5 hours between 25 and 85 ^{o}C.[24] Importantly, this specific catalyst system has the advantage of substantial catalyst recyclability.[24]

The novelty of wool as an "*environmentally friendly*" support and the potential of adding value to wool by fabricating Pd/wool catalysts was the stimulation for the project work undertaken in this thesis. The aims for this chapter are to test Pd /wool composites as catalysts in liquid-phase hydrogenation of cyclohexene to cyclohexane, as a simple model reaction of hydrogenation of a double bond (C = C), to assess their performance and stability and compare them to commercially available Pd particles on charcoal. I also will briefly outline a simple and general synthesis procedure originally developed by Professor Johnston's group (as I described in Chapter 2, Section 2.5.3) to obtain Pd nanoparticles stabilized by wool fibres. Effects of various parameters of this process will be discussed in detail below.

6.2 Results and discussion

Hydrogenation of cyclohexene to cyclohexane[47] was chosen as a model reaction because Pd is known to be an active catalyst for hydrogenation of unsaturated hydrocarbons. It was hypothesized that the catalytic activity of Pd/wool would depend on reaction conditions such as stirring rate, gas pressure and target temperature. The reaction was investigated using Pd/wool samples provide in two batches from the Johnston laboratory. These were labelled $S_{n,1}$/ $S_{n,2}$ where the *1* and *2* indicate the first and second batch, respectively, and *n* corresponds to a specific sample number within each batch. $S_{n,1}$ catalysts were received 27 January, 2010, whereas $S_{n,2}$ catalysts were received 18 December, 2010. S_5 and S_6 catalysts were received in the second batch only (as described at 7.3, Catalytic testing of supported palladium nanocatalysts). Generally, reactions were performed in triplicate with analysis by using the GC-FID method described at section 7.3.1, Apparatus and hydrogenation reaction. The conversion results are reported as means with uncertainties corresponding to two standard errors (± 2SE) of the mean.

For industrially relevant catalysis, the use of a neat starting material, with no solvent, would help to minimize costs and the need of separation, and also to improve safety and minimize environmental risks. However, in the case of these test reactions, there are practical limitations that require the use of a solvent. To achieve affective stirring, the volume of liquid in the reactor must be no less than about 25 mL, which corresponds to 20.3 g (0.247 mol) of cyclohexene. An H_2 gas pressure of 400 psi was chosen, which is within the safe operating range of the reactor and corresponds to mild pressure conditions.[48] By running reactions with 100% conversion using commercial Pd-on-charcoal catalysts, this pressure was found to correspond to ~0.13 mol H_2 within the reactor. Consequently, any reaction using more than ~0.13 mol (10.7 g or 13.2 mL) of cyclohexene, will be limited by the amount of H_2 and calculations based on the initial amount of cyclohexene will realise an erroneously low conversion factor. To circumvent this problem while maintaining an appropriate liquid volume, reactions were performed with ~10 g of cyclohexene (~12.3 mL or 0.122 mol) diluted with ~10 g (12.8 mL) of cyclohexane, which was chosen because it is miscible with the reactant and (as the reaction product) will not interfere with the test reaction.

6.2.1 Effect of the stirring rate

Stirring rate is an important factor in batch-style heterogeneous catalytic tests since it can affect mass transfer. The results using $S_{1,1}$ and under solvent-free conditions (*i.e.*, initially with pure cyclohexene reagent) at 40 ^{o}C and 400 psi hydrogen gas pressure for 24 h are given in Table 6.2.

Table 0.2: The effect of stirring rate on the conversion of cyclohexene over 24 hours.

Sample # (Pd/wool)	Stirring rate (rpm)	Initial mass of cyclohexene (g)	Initial mass of cyclohexane (g)	Conversion%
$S_{1,1}$	1100	20.01	0.00	29 ± 6
$S_{1,1}$	750	20.35	0.00	97 ± 5
$S_{1,1}$	0.0	20.35	0.00	16 ± 5

The Parr reactor can operate at stirrer rates up to 1200 rpm, but control below 750 rpm is not very reproducible. Tests using $S_{1,1}$ at a high stirring rate of 1100 rpm, usually regarded as near optimal for minimizing mass transfer limitations, resulted in only 29 ± 6% conversion. Such low value can be explained by visually observed mechanical damage to the fragile catalyst system at the end of the test (see Figure 6.9.B). A test using $S_{1,1}$ catalyst without any stirring (bottom entry in Table 6.2) gave an even poorer result of only ~16 ± 5% conversion. However the intermediate stirring rate of 750 rpm (the lowest stable rate) led to substantially improved conversions, with $C \approx 97 \pm 5\%$. Importantly, under such conditions visual examination confirmed that damage of Pd/wool material (Figure 6.9.A) was not anywhere near as pronounced as for the higher stirring rate.

a)  b) 

Figure 0.9: The effect of stirring rate a) 750 rpm & b) 1100 rpm on the mechanical damage of wool fibres after 24 hours reaction time. At the higher stirring rate the damage is visually much more substantial.

Results from these experiments suggest that mechanical instability of Pd/wool impairs its catalytic activity at high stirring rates. Without stirring, activity is also limited, presumably due to poor mass transfer.[49] Comparison among different ranges of stirring rates of Pd/wool showed that Pd/wool can be active catalysts only under moderate rates of stirring (*i.e.*, 750 rpm) due to reasonable mass transfer without substantial physical degradation.[50] All further tests were performed using stirring rate of 750 rpm.

6.2.2 Optimization of H_2 introduction

Hydrogen pressure can be an important parameter in obtaining the highest conversion[51] because of its consequence on determining surface coverage by H_2.[52] The effect of this was studied using two protocols while keeping other parameters fixed (~10 g: ~10 g; reactant and solvent composition, stirring rate: 750 rpm and target temperature: 40 ± 2 ^{o}C).

- **Protocol 1:** The reactor was initially purged with dry H_2 gas three times and then pressurized with hydrogen gas to 400 psi prior to heating to 40 ^{o}C.
- **Protocol 2:** The reactor was initially purged three times with dry N_2 gas and then pressurized to 3 psi with dry nitrogen gas to avoid exposure of hydrogen to atmospheric oxygen during the heating step. The temperature was raised to 40 ^{o}C, at which point the reactor was flushed and pressurized to 400 psi with hydrogen.

From Table 6.3 it can be seen that the method of introducing H_2 gas had no significant effect on the conversion of cyclohexene. For further experiments it was decided to use the simpler procedure of pressurising the reactor with 400 psi of H_2 gas from the start.

Table 0.3: Effect of the way H_2 gas was introduced during the test on the conversion over 24 hours.

Sample # (Pd/wool)	**Initial mass cyclohexene (g)**	**Initial mass cyclohexane (g)**	**Initial pressure H_2 (psi)**	**Initial pressure N_2 (psi)**	**Pressure H_2 (psi) at 40 ^{o}C**	***C*%**
$S_{1,1}$	10.16	10.12	400	0	0	83 ± 5
$S_{1,1}$	10.14	10.06	0	3	400	76 ± 6

6.2.3 Reaction temperature

The target temperature at which the reaction was carried out was considered as another option for optimization. Reactions were carried out at 30, 40 and 50 ± 2 ^{o}C while keeping all other parameters fixed (~10 g: ~10 g reactant and solvent composition; 750 rpm stirring rate; initial H_2 gas pressure of 400 psi). The conversion increased from 46% to 83% when the temperature was increased from 30 to 40 ^{o}C, but then decreased to 66% when the temperature was increased further to 50 ^{o}C (see Table 6.4). The palladium catalysts seem to be less active at higher temperatures (above 40 ^{o}C); perhaps at the elevated temperature, the wool fibers are less stable, leading to mechanical degradation.[53]

Table 0.4: The effect of temperature on conversion over 24 hours.

Sample # (Pd/wool)	**Initial mass of cyclohexene (g)**	**Initial mass of cyclohexane (g)**	**Temperature (^{o}C)**	***C*%**
$\mathbf{S_{1,1}}$	10.01	10.03	30	46 ± 5
$\mathbf{S_{1,1}}$	10.16	10.12	40	83 ± 5
$\mathbf{S_{1,1}}$	10.23	10.31	50	66 ± 4

6.2.4 Comparison with palladium on charcoal

Palladium nanoparticles immobilized on charcoal (Pd/C) are recognized as effective catalysts for hydrogenation of organic compounds, so commercially available Pd/C was used as a benchmark against which to measure the catalytic activity of Pd/wool for hydrogenation of cyclohexene to cyclohexane. Tables 6.5 and 6.6 show that 95 ± 5% conversion can be obtained by using the second batch of S_1 of Pd/wool catalyst over 5 hours. However, under the same conditions the commercial Pd particles immobilized on carbon (Pd/C) catalysts achieved effectively 100% conversion in just an hour.

This comparison suggests that the catalytic activity of palladium nanoparticles strongly depends on the type of support.[54] The main constituent of a wool fibre is keratin, a complex protein containing amine, sulfur, carboxylate and hydroxyl functional groups[41] that can bind

to Pd nanoparticles.[43a] Keratin at the cuticle edges has higher levels of sulfur to which the Pd can preferentially bind, as confirmed by the SEM and EDS presented in Figure 6.10.[43a] TEM images show the palladium nanoparticles have a poly-disperse size distribution over a core-diameter range from 2 to 30 nm because SEM and EDS images showed larger Pd particles (>5 nm) located on the surface of the fibre and smaller particles (<5 nm) within the fibres.[43a]

Table 0.5: Size and size distributions of the Pd/wool complexes. Reproduced from Fonseca-Paris and Johnston.[43a]

Sample # Pd/wool	**Mean size (nm)**	**Size distributions**	**Concentration of $PdCl_2$ (mg/L)**	**Types of wool**
S_1	4.9 ± 0.1	2 - 30	260	Merino
S_2	4.5 ± 0.2	2 - 20	260	Crossbred

From Table 6.5 and Figures 6.10 – 6.12 the Pd particles in S_1 and S_2were typically approximately 5 nm in core diameter size with some larger particles of 20 – 30 nm corresponding to agglomerates. The size of the Pd particles was also found to depend on the concentration of $PdCl_2$ and the type (*i.e.,* Merino or crossbred) of the wool fibres.[43a]

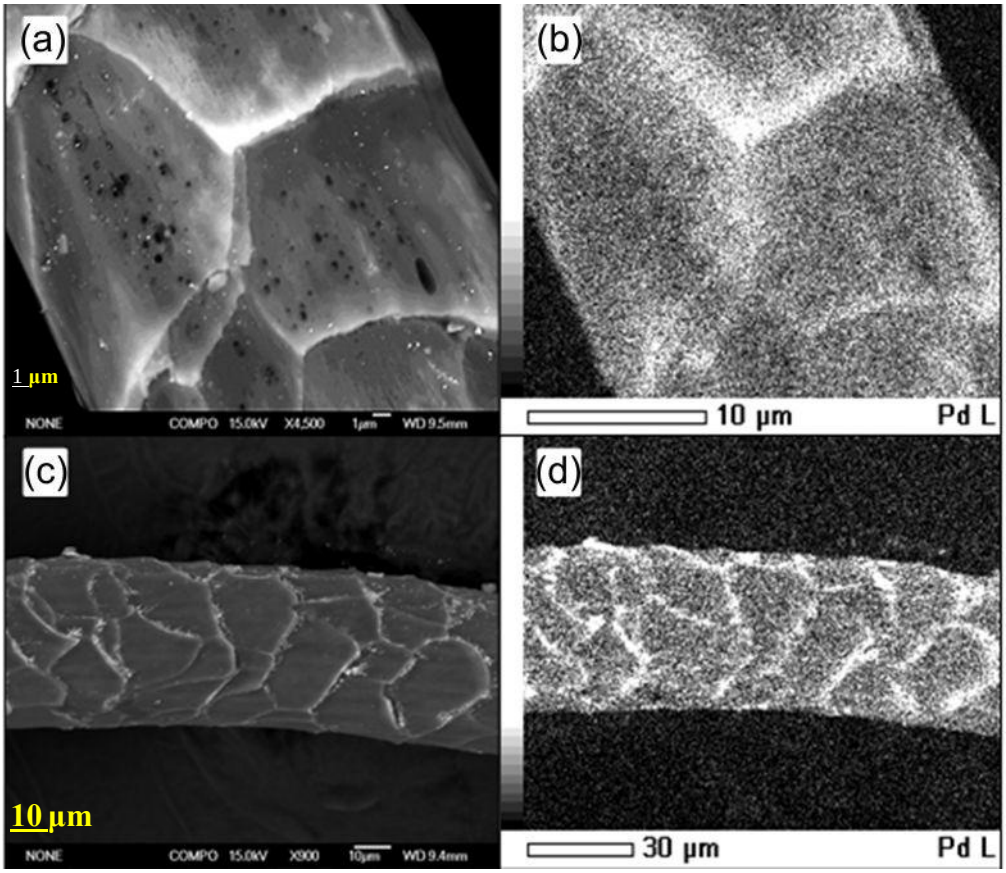

Figure 0.10: a) Backscatter SEM images of nanopalladium–Merino wool composite prepared from a 260 mg. L^{-1} of Pd^{2+} solution at 100 ˚C and pH 3.0; b) corresponding EDS elemental maps for Pd. c) Backscatter SEM images of a palladium nanoparticle – Merino wool composite from a 260 mg. L^{-1} Pd^{2+} solution at 100 ˚C and pH 3.0; d) corresponding EDS elemental maps for Pd. The images were taken by Fonseca-Paris at Victoria University of Wellington.

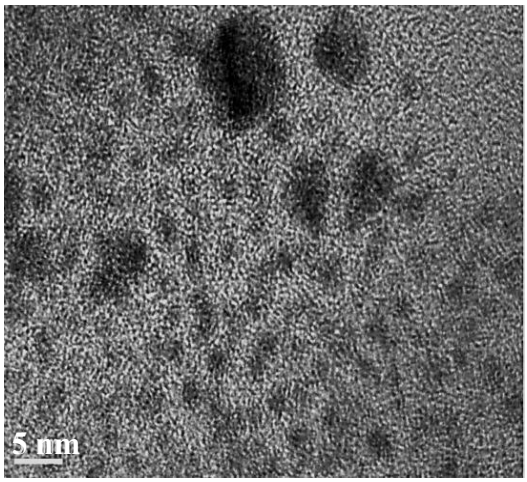

Figure 0.11: A representative TEM image of S_1 (Pd/wool) was taken by Fonseca-Paris at Victoria University of Wellington.

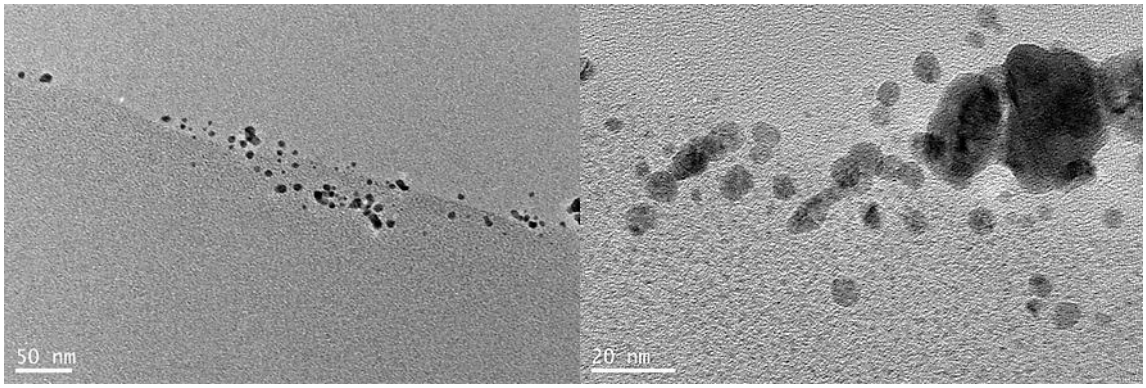

Figure 0.12: TEM images of a cross section of a nanopalladium – Merino wool catalyst at different magnifications showing the palladium nanoparticles on the surface of the merino wool fibre were taken by Fonseca-Paris at Victoria University of Wellington.

It seems that not only size and size distributions,[55] but also the locations of the Pd particles,[22, 56] affect the catalytic activity of the Pd/wool. It is likely that Pd particles with diameters smaller than 3 nm are more intrinsically effective than larger ones for hydrogenation of organic compounds.[55b, 57] However, since the very small particles are encapsulated within the wool fibres, it will be difficult for the reactants to access them. It therefore seems likely that the observed catalytic activity for these samples actually arises from particles with diameters of ~5 nm or larger located at the fibre surfaces.[55a, 56, 58] Negligible conversions by samples $S_{5,2}$ and $S_{6,2}$, both with very small particles sizes and narrow size distributions from 1 to 4 nm, support this hypothesis.

According to previous research, metal loading is also one of the important factors that can affect the catalytic activity of nanocatalysts.[59] In our preliminary studies, catalysts S_1 and S_2 with 2.6 wt% Pd loadings, showed appreciable activity (initially estimated indirectly by monitoring the H_2 pressure drop) and thus their testing was performed using shorter, 5-hour test runs. S_3 to S_6 (*i.e.*, for both batches), with loadings between 1.6 and 6.4 wt% Pd, gave low conversions (see Tables 6.6 and 6.7), even in 24-hour tests. $S_{1,2}$ from *"the second batch"* of catalysts, consistently showed the best performance with a H_2 pressure drop of 280 psi within the first hour and $C = 95 \pm 5\%$ over 5 hours, a conversion comparable with

commercial Pd/C albeit over a substantially longer reaction time. In comparison, $S_{1,1}$ managed just $C = 83 \pm 6\%$ after a much longer period of 24 hours (see Tables 6.4 and 6.7). The difference was that $S_{1,2}$ was tested very much sooner after its synthesis, which suggests that the freshly made catalysts have higher activity.

Table 0.6: The catalytic activity of *"the second batch"* of Pd/wool nanocatalysts.

Sample # (Pd/wool)	Initial mass of cyclohexene (g)	Initial mass of cyclohexane (g)	Time (h)	Conversion% (First run)
$S_{1,2}$	10.16	10.12	5	95 ± 5
$S_{2,2}$	10.26	10.01	5	78 ± 6
$S_{3,2}$	10.08	10.21	24	2 ± 1
$S_{4,2}$	10.13	10.19	24	9 ± 5
$S_{5,2}$	10.10	10.10	24	1 ± 1
$S_{6,2}$	10.01	10.01	24	2 ± 1

Table 0.7: Comparison the reproducibility of Pd/wool nanocatalysts tests between *"the first batch"* and *"the second batch"*.

Sample # (Pd/wool)	Initial mass of cyclohexene (g)	Initial mass of cyclohexane (g)	Time (h)	Conversion% (First run)
$S_{1,2}$	10	10	5	95 ± 5
$S_{1,2}$	10	10	5	95 ± 6
$S_{1,1}$	10	10	24	83 ± 6
$S_{2,2}$	10	10	5	78 ± 4
$S_{2,2}$	10	10	5	55 ± 5
$S_{3,2}$	10	10	24	2 ± 1
$S_{3,1}$	10	10	24	3 ± 1
$S_{3,1}$	10	10	24	2 ± 1
$S_{4,2}$	10	10	24	6 ± 2
$S_{4,1}$	10	10	24	5 ± 2
$S_{4,1}$	10	10	24	4 ± 1
$S_{5,2}$	10	10	24	1 ± 1
$S_{6,2}$	10	10	24	2 ± 1
$S_{6,2}$	10	10	24	1 ± 1

It is apparent from Tables 6.6 and 6.7 that factors in addition to metal loading are important in defining catalytic activity. A study is pending of how catalyst morphology (*i.e.*, accessibility of the metal nanoparticles to the reagents and the presence of functional groups capable of influencing catalytic activity of metal nanoparticles in the matrix of the support) affects catalytic performance.

In Table 6.7, results are shown for repeated triplicate tests for some samples. The results are generally quite reproducible for the same sample from the same batch. However, the reproducibility between batches is not as strong, even for the same particle size. For example, the activity of $S_{1,2}$ is very reproducible (C = ~95% over 5 hours), but significantly greater than for $S_{1,1}$ (C = ~83% over 24 hours) even though the samples are ostensibly the same. Since every sheep's wool is unique it is possible this difference can affect the catalytic activity of the catalyst.

The TEM images show that the nanoparticles of palladium range from 2 to 50 nm in diameter localized on the surface and within the fibre. The nanoparticles have a poly-disperse particle size distribution with larger nanoparticles located on the surface of the fibre and smaller particles within the fibres. It seems that the location of particles provides accessibility of Pd catalysts for the reactants. The small particles in S_3 to S_6 are incorporated into the fibres and cannot interact with the reactants efficiently. However, for S_1 and S_2 the big particles are at the surface of fibres where they are easily accessible to the reactants.

6.3 Conclusions

This study investigated the catalytic activity of Pd/wool with loadings from 1.56 to 6.4 wt% controlling the stirring rate, pressure and target temperature. It is inferred that the catalytic activity of nanocatalysts can be influenced by the few controllable reaction parameters in play here, along with the nature of the wool (its surface chemistry *etc.*), which can affect the accessible metal loading, as well as the size and size distributions of Pd nanoparticles that are accessible (*i.e.*, on the surface of the fiber). Samples S_1 and S_2, with average particles sizes around 5 nm and broad size distributions (2 – 30 nm) proved to be the most active catalysts. S_1 and S_2 with Pd particles on Merino wool fibres showed higher activity than those with particles on crossbred fibres. However, sensitivity of Pd/wool catalysts to mechanical damage

upon stirring and high temperature, as well as low reproducibility between different batches of the supposedly the same material, make wool as a support for catalysts inferior compared with currently industrially used activated carbon. Indeed, current study showed that the activity of Pd/C is far superior to that of Pd/wool implying that Pd/wool catalyst cannot be considered as a highly active catalyst under catalytic testing conditions used in this study.

References

1. (a) Matsura, V. A.; Potekhin, V. V.; Platonov, V. V.; Tatsenko, O. M.; Ukraintsev, V. B.; Khokhryakov, K. A., Hydrogention and oxidation of allyl alcohol in the presence of colloid palladium in situ. *Russ. J. Gen. Chem.* **2003,** *73* (12), 1900-1903; (b) Ford, J. W.; Chaudhari, R. V.; Subramaniam, B., Supercritical deoxygenation of a model bio-oil oxygenate. *Ind. Eng. Chem. Res.* **2010,** *49* (21), 10852-10858.
2. Beal, J. H. L.; Etchegoin, P. G.; Tilley, R. D., Transition metal polysulfide complexes as single-source precursors for metal sulfide nanocrystals. *J. Phys. Chem. C* **2010,** *114* (9), 3817-3821.
3. Marrodan, C. M.; Berti, D.; Liguori, F.; Barbaro, P., In situ generation of resin-supported Pd nanoparticles under mild catalytic conditions: a green route to highly efficient, reusable hydrogenation catalysts. *Catal. Sci. Technol* **2012,** *2* (11), 2279-2290.
4. Ma, X.; Jiang, T.; Han, B.; Zhang, J.; Miao, S.; Ding, K.; An, G.; Xie, Y.; Zhou, Y.; Zhu, A., Palladium nanoparticles in polyethylene glycols: Efficient and recyclable catalyst system for hydrogenation of olefins. *Catal. Commun.* **2008,** *9* (1), 70-74.
5. Alshammari, H.; Miedziak, P. J.; Bawaked, S.; Knight, D. W.; Hutchings, G. J., Solvent-free Liquid-phase oxidation of 1-hexene using supported gold catalysts. *ChemCatChem* **2012,** *4* (10), 1565-1571.
6. Wang, S.; Zhang, Z.; Chi, C.; Wu, G.; Ren, J.; Wang, Z.; Huang, M.; Jiang, Y., Asymmetric hydration of ortho- or para-substituted styrenes catalyzed by biopolymer-metal complex wool-Pd. *React. Funct. Polym.* **2008,** *68* (1), 424-430.
7. Kidambi, S.; Dai, J.; Li, J.; Bruening, M. L., Selective hydrogenation by Pd nanoparticles embedded in polyelectrolyte multilayers. *J. Am. Chem. Soc.* **2004,** *126* (9), 2658-2659.
8. Wilson, O. M.; Knecht, M. R.; Garcia-Martinez, J. C.; Crooks, R. M., Effect of Pd nanoparticle size on the catalytic hydrogenation of allyl alcohol. *J. Am. Chem. Soc.* **2006,** *128* (14), 4510-4511.
9. (a) Palomares, A. E.; Franch, C.; Yuranova, T.; Kiwi-Minsker, L.; García-Bordeje, E.; Derrouiche, S., The use of Pd catalysts on carbon-based structured materials for the catalytic hydrogenation of bromates in different types of water. *Appl. Catal., B* **2014,** *146*, 186-191; (b) Colmenares, J. C.; Magdziarz, A.; Łomot, D.; Chernyayeva, O.; Lisovytskiy, D., A new photocatalytic tool in VOCs abatement: Effective synergetic combination of sonication and light for the synthesis of monometallic palladium-containing TiO_2. *Appl. Catal., B* **2014,** *147*, 624-632.
10. Charbonnier, A.; Brochon, C.; Cloutet, E.; Navarro, C.; Hadziioannou, G., Synthesis of functional polymer particles by dispersion polymerization in organic media: A tool toward stable electrophoretic inks. *J. Polym. Sci., Part A: Polym. Chem.* **2013,** *51* (21), 4608-4617.
11. Huang, A.; Liu, Y.; Chen, L.; Hua, J., Synthesis and property of nanosized palladium catalysts protected by chitosan/silica. *J. Appl. Polym. Sci.* **2002,** (5), 989-994.
12. Hu, J.; Wang, Y.; Han, M.; Zhou, Y.; Jiang, X.; Sun, P., A facile preparation of palladium nanoparticles supported on magnetite/s-graphene and their catalytic application in Suzuki-Miyaura reaction. *Catal. Sci. Technol.* **2012,** *2* (11), 2332-2340.
13. Mennecke, K.; Cecilia, R.; Glasnov, T. N.; Gruhl, S.; Vogt, C.; Feldhoff, A.; Vargas, M. A. L.; Kappe, C. O.; Kunz, U.; Kirschning, A., Palladium(0) nanoparticles on glass-polymer composite materials as recyclable catalysts: A comparison study on their use in batch and continuous flow processes. *Adv. Synth. Catal.* **2008,** *350* (5), 717-730.
14. Gröschel, L.; Haidar, R.; Beyer, A.; Reichert, K. H.; Schomäcker, R., Characterization of palladium nanoparticles adsorpt on polyacrylic acid particles as hydrogenation catalyst. *Catal. Lett.* **2004,** *95* (1-2), 67-75.
15. Yin, M. Y.; Yuan, G. L.; Wu, Y. Q.; Huang, M. Y.; Jiang, Y. Y., Asymmetric hydrogenation of ketones catalyzed by a silica-supported chitosan-palladium complex. *J. Mol. Catal. A: Chem.* **1999,** *147* (1-2), 93-98.
16. Xu, Y.; Zhang, L.; Cui, Y., Catalytic performance of cellulose supported palladium complex for Heck reaction in water. *J. Appl. Polym. Sci.* **2008,** *110* (5), 2996-3000.
17. Yin, M.-Y.; Yuan, G.-L.; Huang, M.-Y.; Jiang, Y.-Y., Catalytic behavior of a Wool–Pd complex in asymmetric hydrogenation of diacetone alcohol and 3-methyl-2-butanone. *J. Mol. Catal. A: Chem.* **1999,** *147* (1–2), 89-92.

18. Cui, H.; Zayat, M.; Levy, D., A chemical strategy to control the shape of oxide nanoparticles. *J. Nanopart. Res.* **2009,** *11* (6), 1331-1338.
19. Miyazaki, A.; Balint, I.; Nakano, Y., Morphology control of platinum nanoparticles and their catalytic properties. *J. Nanopart. Res.* **2003,** *5* (1-2), 69-80.
20. (a) Chandler, B. D.; Gilbertson, J. D., Dendrimer-encapsulated bimetallic nanoparticles: Synthesis, characterization, and applications to homogeneous and heterogeneous catalysis. *Top. Organomet. Chem.* **2006,** *20*, 97-120; (b) Yu, D.; Wang, W.; Wu, J., Preparation of conductive wool fabrics and adsorption behaviour of Pd (II) ions on chitosan in the pre-treatment. *Synth. Met.* **2011,** *161* (1-2), 124-131.
21. Gallezot, P.; Richard, D.; Bergeret, G. A., In novel materials in heterogeneous catalysis. In *Symposium series No. 437* Baker, R. T. K.; Murrell, L. L., Eds. American chemical society: Washington DC, 1990; pp 150-159.
22. Copéret, C.; Chabanas, M.; Petroff Saint-Arroman, R.; Basset, J.-M., Homogeneous and heterogeneous catalysis: Bridging the gap through surface organometallic chemistry. *Angew. Chem. Int. Ed.* **2003,** *42* (2), 156-181.
23. (a) Widegren, J. A.; Finke, R. G., A review of the problem of distinguishing true homogeneous catalysis from soluble or other metal-particle heterogeneous catalysis under reducing conditions. *J. Mol. Catal. A: Chem.* **2003,** *198* (1–2), 317-341; (b) Buisson, P.; Quignard, F., Polysaccharides: Natural polymeric supports for aqueous phase catalysts in allylic substitution reactions. *Aust. J. Chem.* **2002,** *55* (1-2), 73-78.
24. Ma, H.-c.; Cao, W.; Bao, Z.-k.; Lei, Z.-Q., Biopolymer-metal complex wool-Pd as a highly active catalyst for Suzuki reaction in water. *Catal. Sci. Technol.* **2012,** *2* (11), 2291-2296.
25. Guibal, E., Heterogeneous catalysis on chitosan-based materials: A review. *Prog. Polym. Sci.* **2005,** *30* (1), 71-109.
26. Milner, S. T., Polymer brushes. *Science* **1991,** *251* (4996), 905-914.
27. Mei, Y.; Lu, Y.; Polzer, F.; Ballauff, M.; Drechsler, M., Catalytic activity of palladium nanoparticles encapsulated in spherical polyelectrolyte brushes and core−shell microgels. *Chem. Mater.* **2007,** *19* (5), 1062-1069.
28. Hoffmann, F.; Cornelius, M.; Morell, J.; Fröba, M., Silica-based mesoporous organic-inorganic hybrid materials. *Angew. Chem. Int. Ed.* **2006,** *45* (20), 3216-3251.
29. Ogasawara, S.; Kato, S., Palladium nanoparticles captured in microporous polymers: A tailor-made catalyst for heterogeneous carbon cross-coupling reactions. *J. Am. Chem. Soc.* **2010,** *132* (13), 4608-4613.
30. (a) Gianfreda, L.; Iamarino, G.; Scelza, R.; Rao, M. A., Oxidative catalysts for the transformation of phenolic pollutants: A brief review. *Biocatal. Biotransform.* **2006,** *24* (3), 177-187; (b) Van Cauwenberghe, L.; Vanreusel, A.; Mees, J.; Janssen, C. R., Microplastic pollution in deep-sea sediments. *Environ. Pollut.* **2013,** *182* (0), 495-499.
31. Goodship, V., *Introduction to plastics recycling*. Smithers Rapra Technology Limited UK 2007; p 184.
32. (a) Plastics - the Facts 2013 (an analysis of European latest plastics production, demand and waste data). http://www.plasticseurope.org/cust/documentrequest.aspx?DocID=59108 (accessed Nov 26, 2013); (b) Green paper. www.aztex.com/green (accessed Nov 27, 2013).
33. Moezzi, M.; Ghane, M.; Nicoletto, G.; Nedoushan, R. J., Analysis of the mechanical response of a woven polymeric fabric with locally induced damage. *Mater. Des.* **2014,** *54*, 279-290.
34. Nuelle, M.-T.; Dekiff, J. H.; Remy, D.; Fries, E., A new analytical approach for monitoring microplastics in marine sediments. *Environ. Pollut.* **2014,** *184* (0), 161-169.
35. The Life Span of Commonly Discarded Litter. http://www.dot.state.pa.us/Internet/pdkids.nsf/StartlingStatistics?OpenForm (accessed Nov 26, 2013).
36. Borrmann, T.; Dominis, A.; McFarlane, A. J.; Johnston, J. H.; Richardson, M. J.; Kane-Maguire, L. A. P.; Wallace, G. G., Immobilisation of fully sulfonated polyaniline on nanostructured calcium silicate. *J. Nanosci. Nanotechnol.* **2007,** *7* (12), 4303-4310.
37. Small, A. C.; Johnston, J. H., Novel hybrid materials of magnetic nanoparticles and cellulose fibers. *J. Colloid Interface Sci.* **2009,** *331* (1), 122-126.
38. Monguchi, Y.; Sajiki, H., Polymer-supported palladium catalysts for chemoselective hydrogenation. *Kobunshi Ronbunshu* **2011,** *68* (5), 232-241.

39. (a) Astruc, D., Palladium nanoparticles as efficient green homogeneous and heterogeneous carbon-carbon coupling precatalysts: A unifying view. *Inorg. Chem.* **2007,** *46* (6), 1884-1894; (b) Hu, J. Y.; Li, Y.; Chang, Y. F.; Yeung, K. W.; Yuen, C. W., Transport properties of fabrics treated with nano-wool fibrous materials. *Colloids Surf., A* **2007,** *300* (1-2 SPEC. ISS.), 136-139.
40. Johnston, J.; Lucas, K., Nanogold synthesis in wool fibres: novel colourants. *Gold Bull.* **2011,** *44* (2), 85-89.
41. Hearle, J. W. S., A critical review of the structural mechanics of wool and hair fibres. *Int. J. Biol. Macromol.* **2000,** *27* (2), 123-138.
42. The chemical & physical structure of merino wool. http://www.csiro.au/Organisation-Structure/Divisions/CMSE/Fibre-Science/The-chemical-and-physical-structure-of-merino-wool.aspx (accessed Nov 20, 2013).
43. (a) Fonseca-Paris, C.; Johnston, J. H. In *Characterization of palladium nanoparticles embedded in a wool substrate*, Proceedings of the NSTI TechConnect 2011 Boston, Boston, 2011; pp 511-514; (b) Johnston, J. H.; Nilsson, T. In *Paper fibres functionalised with nanogold and nanosilver, properties and potential applications*, 2011; pp 97-103.
44. Kelly, F. M.; Johnston, J. H., Colored and functional silver nanoparticle−wool fiber composites. *ACS Appl. Mater. Inter.* **2011,** *3* (4), 1083-1092.
45. Johnston, J. H.; Lucas, K. A. In *Novel nanogold coloured and antimicrobial nanosilver woollen textiles: The journey of discovery, the nanoscience and pathway to commercialisation*, 2013; pp 510-513.
46. Borrmann, T.; Lim, T. H.; Cope, H.; Lucas, K.; Lorden, M., Gold nanoparticles on wool in a comparative study with molecular gold catalysts. *Gold Bull.* **2013,** *46* (1), 13-18.
47. Yu, J.; Liu, T., Preparation of palladium nano-particles by electrospinning and its application in hydrogenations. *Adv. Mater. Res.* **2011,** *217-218*, 75-78.
48. Li, Q.; Zhang, Y.; Chen, G.; Fan, J.; Lan, H.; Yang, Y., Ultra-low-gold loading Au/CeO_2 catalysts for ambient temperature CO oxidation: Effect of preparation conditions on surface composition and activity. *J. Catal.* **2010,** *273* (2), 167-176.
49. La Scala, J.; Wool, R. P., Effect of FA composition on epoxidation kinetics of TAG. *J. Am. Oil Chem. Soc.* **2002,** *79* (4), 373-378.
50. Mennecke, K.; Cecilia, R.; Glasnov, T. N.; Gruhl, S.; Vogt, C.; Feldhoff, A.; Vargas, M. A. L.; Kappe, C. O.; Kunz, U.; Kirschning, A., Palladium(0) nanoparticles on glass-polymer composite materials as recyclable catalysts: A comparison study on their use in batch and continuous flow processes. *Adv. Synth. Catal.* **2008,** *350* (5), 717-730.
51. (a) Edwards, J. K.; Pritchard, J.; Piccinini, M.; Shaw, G.; He, Q.; Carley, A. F.; Kiely, C. J.; Hutchings, G. J., The effect of heat treatment on the performance and structure of carbon-supported Au–Pd catalysts for the direct synthesis of hydrogen peroxide. *J. Catal.* **2012,** *292* (0), 227-238; (b) Li, X.; Liu, J.; Huang, Q.; Vogel, W.; Akins, D. L.; Yang, H., Effect of heat treatment on stability of gold particle modified carbon supported Pt–Ru anode catalysts for a direct methanol fuel cell. *Electrochim. Acta* **2010,** *56* (1), 278-284; (c) Vollmer, C.; Redel, E.; Abu-Shandi, K.; Thomann, R.; Manyar, H.; Hardacre, C.; Janiak, C., Microwave irradiation for the facile synthesis of transition-metal nanoparticles (NPs) in ionic liquids (ILs) from metal–carbonyl precursors and Ru-, Rh-, and Ir-NP/IL dispersions as biphasic liquid–liquid hydrogenation nanocatalysts for cyclohexene. *Chem. – Eur. J.* **2010,** *16* (12), 3849-3858.
52. Pritchard, J.; Piccinini, M.; Tiruvalam, R.; He, Q.; Dimitratos, N.; Lopez-Sanchez, J. A.; Morgan, D. J.; Carley, A. F.; Edwards, J. K.; Kiely, C. J.; Hutchings, G. J., Effect of heat treatment on Au-Pd catalysts synthesized by sol immobilisation for the direct synthesis of hydrogen peroxide and benzyl alcohol oxidation. *Catal. Sci.Technol.* **2013,** *3* (2), 308-317.
53. Aksakal, B.; Alekberov, V., The effect of temperature and water on the mechanical properties of wool fibres investigated with different experimental methods. *Fiber. Polym.* **2009,** *10* (5), 673-680.
54. (a) Edwards, J. K.; Thomas, A.; Carley, A. F.; Herzing, A. A.; Kiely, C. J.; Hutchings, G. J., Au-Pd supported nanocrystals as catalysts for the direct synthesis of hydrogen peroxide from H_2 and O_2. *Green Chem.* **2008,** *10* (4), 388-394; (b) Abad, A.; Corma, A.; García, H., Catalyst parameters determining activity and selectivity of supported gold nanoparticles for the aerobic oxidation of alcohols: The molecular reaction mechanism. *Chem.- Eur. J.* **2008,** *14* (1), 212-222.

55. (a) Hu, J.; Zhou, Z.; Zhang, R.; Li, L.; Cheng, Z., Selective hydrogenation of phenylacetylene over a nano-Pd/α-Al_2O_3 catalyst. *J. Mol. Catal. A: Chem.* **2014,** *381*, 61-69; (b) Tsunoyama, H.; Ichikuni, N.; Sakurai, H.; Tsukuda, T., Effect of electronic structures of au clusters stabilized by poly(N-vinyl-2-pyrrolidone) on aerobic oxidation catalysis. *J. Am. Chem. Soc.* **2009,** *131* (20), 7086-7093; (c) Arul Dhas, N.; Gedanken, A., Sonochemical preparation and properties of nanostructured palladium metallic clusters. *J. Mater. Chem.* **1998,** *8* (2), 445-450.
56. Astruc, D.; Lu, F.; Aranzaes, J. R., Nanoparticles as Recyclable Catalysts: The Frontier between Homogeneous and Heterogeneous Catalysis. *Angew. Chem. Int. Ed.* **2005,** *44* (48), 7852-7872.
57. Zhang, Y.; Quek, X. Y.; Wu, L.; Guan, Y.; Hensen, E. J., Palladium nanoparticles entrapped in polymeric ionic liquid microgels as recyclable hydrogenation catalysts. *J. Mol. Catal. A: Chem.* **2013,** *379*, 53-58.
58. Abbenhuis, H. C. L., Advances in Homogeneous and Heterogeneous Catalysis with Metal-Containing Silsesquioxanes. *Chem–Eur J.* **2000,** *6* (1), 25-32.
59. (a) Pojanavaraphan, C.; Luengnaruemitchai, A.; Gulari, E., Effect of support composition and metal loading on Au catalyst activity in steam reforming of methanol. *Int. J. Hydrogen Energy* **2012,** *37* (19), 14072-14084; (b) Cárdenas-Lizana, F.; Gómez-Quero, S.; Keane, M. A., Ultra-selective gas phase catalytic hydrogenation of aromatic nitro compounds over Au/Al_2O_3. *Catal. Commun.* **2008,** *9* (3), 475-481.

Chapter 7: Activation of Catalysts Based on the Shape-Specific Ru Nanocrystals Immobilized on Silica for Cyclohexene Hydrogenation

7.1 Introduction

Catalysis by an ideally flat surface of a transition-metal single crystal depends on the type of the exposed face.[1] When heterogeneous nanocatalysts are used, the reaction usually occurs on the surface of nanoparticles,[2] where the active site is a collection of surface atoms that adsorb reactants and facilitate transformations of chemical bonds. The nature this active site can have a strong influence on the outcome of heterogeneous catalytic reactions (see Figure 7.1).[3] Structure-sensitive reactions show a dependence of activity and selectivity on the specific exposed crystallographic face of a metal or the particle size and shape (*via* the relative proportions of atoms occupying vertices, edges and faces) of a catalyst.[4] Surface reconstruction or dissolution of active atoms on corners or edges by one or more of the reactants or even the solvent is expected to take place during catalysis.[5] Such crystal restructuring can influence the catalytic efficiency.[6]

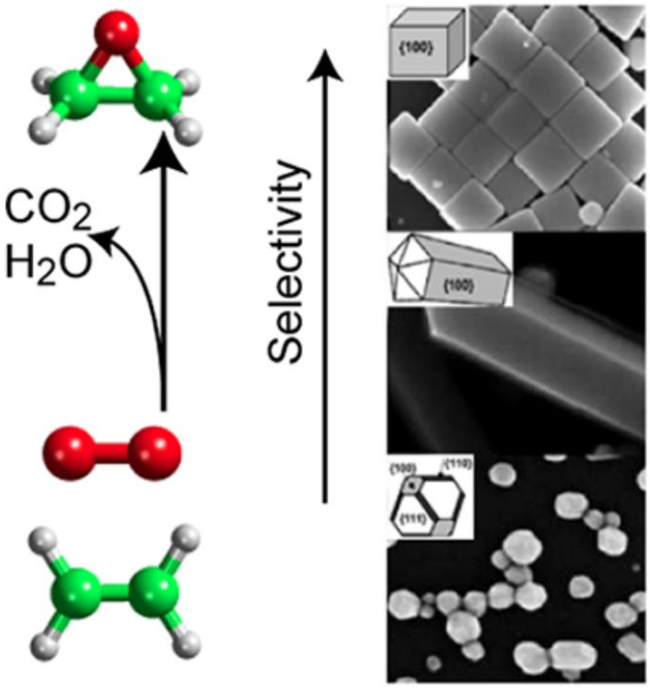

Figure 0.1: Shape-dependent selectivity of metal catalysts towards CO oxidation shows the highest selectivity of CO_2 for cubic particles (100). Reproduced from Linic *et al*.[3]

The surface chemistry of heterogeneous catalysts is complex, with numerous surface phenomena playing important roles–surface defects (steps and kinks) affect chemisorption and catalytic activity, while adsorbate-induced restructuring of surfaces can control adsorbate mobility under reaction conditions.[7] For example, the catalytic activity of platinum nanocatalysts covered with a strongly adsorbed carbonaceous monolayer has been investigated for hydrocarbon hydrogenation and dehydrogenation. The results showed that bond breaking and chemical rearrangement of the reactants takes place at uncovered sites of the metal catalysts.[8] Among three commonly exposed crystal faces of Pt, (111) is relatively defect free, while high concentrations of steps and kinks in the steps exist in the higher Miller index (557) and (679) surfaces.[9]

Metal particles with different shapes have various facets (resulting from the loss of atoms at their locations); consequently, the ratios of the numbers of atoms on corners and edges to those on facets are different.[2-3] This has opened possibilities for the design of heterogeneous catalytic materials that have different shapes and surface facets.[3, 10] For example, the catalytic reaction between hexacyanoferrate (III) and thiosulfate ions using tetrahedral, cubic, or "near spherical" platinum nanocrystals has demonstrated that the catalytic activity of these nanocatalysts is correlated with the fraction of surface atoms located on corners and edges.[11] An ability to control the specific type of surface facet exposed to reactants could therefore lead to fine-tuning of the outcome of catalytic processes.[3]

Nanostructured metals have been of significant interest for technological applications in several areas of science and industry, particularly in catalysis.[1, 3, 5-6] Their catalytic activity and selectivity are believed to be related to particles size,[12] the nature of the support,[13] and particle shape (number of corners, edges and face atoms available for adsorption and activation of the substrate).[2, 4] As an example, Lee *et al.* investigated the conversion of cis-

and trans-2-butenes on shaped-specific platinum particles and found that cubic Pt particles promote isomerization to 1-butene and retard hydrogenation to butane in comparison with tetrahedral Pt particles.[6] Specific-shaped metals can be catalytically active for hydrogenation of organic compounds, such as light olefins.[14] Somorjai *et al.* showed the importance of the shape and surface structure by using ethylene hydrogenation and carbon monoxide adsorption and oxidation as surface reaction probes.[15] The influence of the shape and surface structure of Pt nanoparticles supported on carbon on the selective hydrogenation of crotonaldehyde (C_4H_6O) and cinnamaldehyde (C_9H_8O) was studied.[16] The results showed that catalytic activity and selectivity depend on the surface structure of the Pt catalysts. Despite Pt(100)/C showing higher conversion of reactants, Pt(111)/C exhibited higher selectivity towards cinnamyl alcohol.[16] Although, specific-shape nanocatalysts possess a number of advantages, they do have significant problems in application. One of the critical problems is that shaped metal nanocatalysts particles can be easily reshaped during catalytic process.[2, 5]

The complexity of the metal-support interaction and the difficulty of obtaining metal particles with well-defined morphologies have motivated researchers to fabricate model supported-metal catalysts using lithography.[17] Lithography is a physical method of transferring a pattern to a photosensitive material by selective exposure to a radiation source, such as light[18] or an electron beam,[17, 19] which makes the properties of the exposed part of surface distinctly different from those of the unexposed part (see Figure 7.2).[18] Somorjai used electron-beam lithography as a method of preparing model Pt-based catalysts with uniform and relatively large (~50 nm) particles sizes.[7] Somorjai also fabricated model catalysts using optical lithography, which allowed spatial control over the metal particles in the micrometre size range.[7]

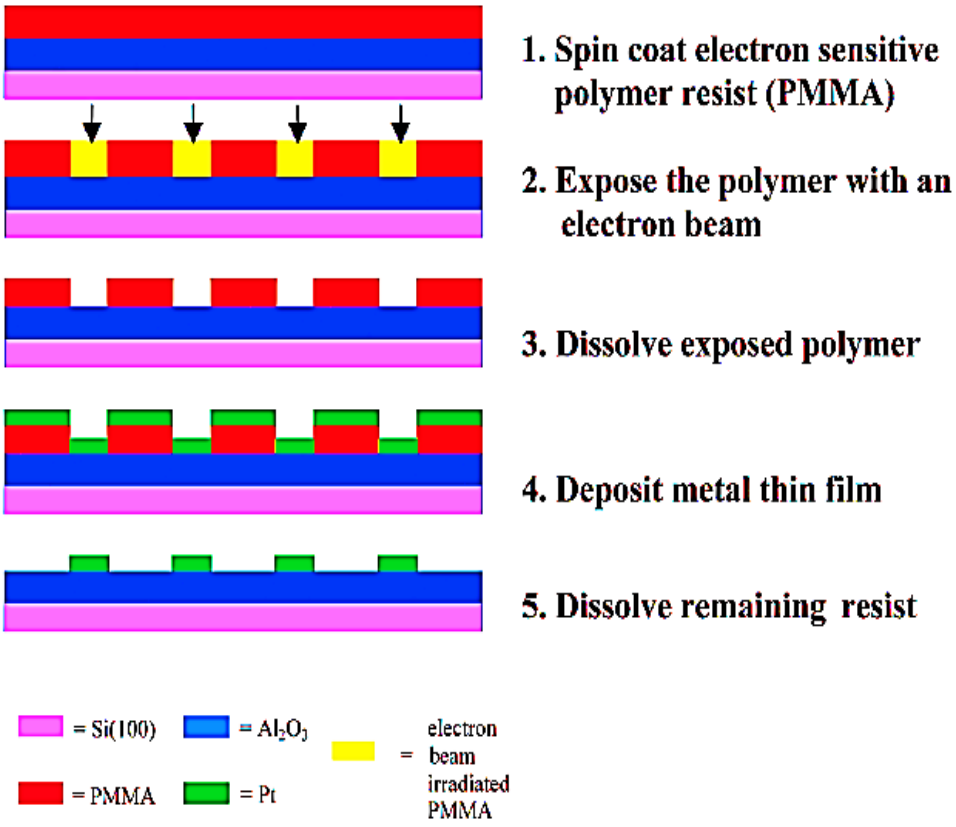

Figure 0.2: A schematic diagram of sample preparation of a Pt-patterned surface with the electron beam lithography (EBL) process. Reproduced from Grunes *et al.*[17b]

Metal nanostructures have been fabricated over a large area with high uniformity using various lithographic techniques, including electron-beam lithography,[20] soft lithography,[21] nanosphere lithography[22] and colloidal lithography,[23] which uses hexagonally ordered colloidal nanoparticles. These methods are strong candidates for generating nanoscopic metal nanostructures with at least some control over their morphology. However, flat surfaces and/or big particles size are considered as the biggest limitations of lithographic methods in fabrication of shaped metal particles as catalysts due to low catalytic performance.[7, 24]

Another common, physical, surface-science approach towards control of the particle size is to evaporate metal onto a flat oxide support under ultrahigh-vacuum (UHV) conditions and to attempt to control the particle size distribution by carefully controlling the nucleation conditions.[25] TiO_2-supported Au nanoclusters have been fabricated in this way and were used

for low-temperature catalysts CO oxidation.[25b] However, it is very hard to achieve good particle shape control using this approach.

Chemical synthesis opens other opportunities in controlling particle shape. A multitude of shape-specific nanosized materials, such as fibres[26], spheres, tetrahedral, stars (see Figure 7.3),[27] rods, tubes, sheets, wheels, cages, wires (see Figure 7.4.a),[28] cubes (see Figure 7.4.b)[28] and dendrites have been fabricated by a variety of synthetic approaches involving self-assembly. However, such synthetic materials have been very rarely used to prepare supported heterogeneous catalysts.[29]

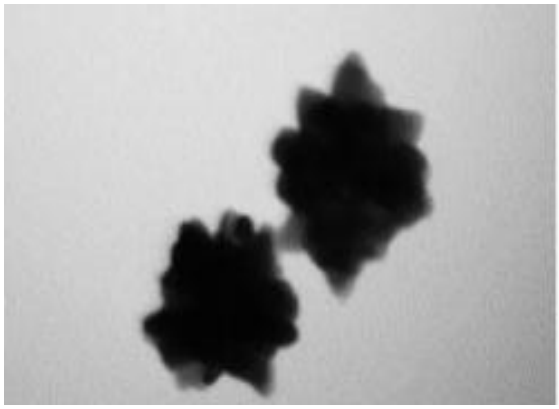

Figure 0.3: A TEM image of gold nanostars. Reproduced from Minati *et al.*[30]

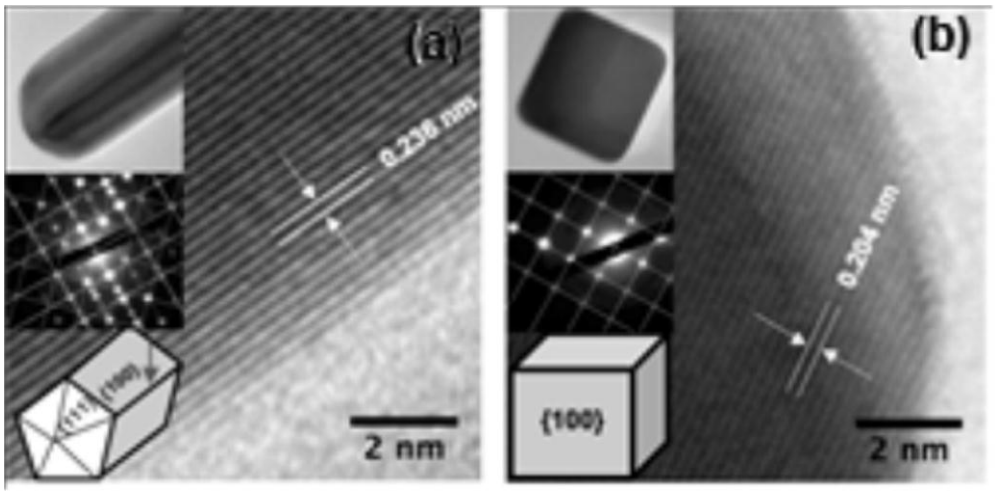

Figure 0.4: HRTEM images of silver nanostructures a) nanowire and b) nanocube. Reproduced from Christopher *et al.*[28]

The morphology of metal nanostructures fabricated by chemical methods is strongly influenced by the reduction methods and conditions.[15, 31] For example, Pt nanoparticles can be formed as cuboctahedra, cubes or porous particles depending on manipulation within the reduction method (see Scheme 7.1).[15] Additionally, the choice of a protective polymer or capping agent can be important for controlling the particle morphology as well as for the stabilization and suspension/solvation of the resulting colloids.[32] The effect of the surfactants oleyl-amine and hexadecylamine on the growth of ruthenium hourglass nanocrystals was investigated by Tilley *et al.*[33] with oleyl-amine as the stabilizer, the nanocrystals were 14± 7 nm long and resembled ill-defined hourglasses and other irregular shapes. With hexadecylamine as the stabilizer, the nanocrystals had dimensions of 9 ± 6 nm and near-spherical, worm-like or irregular shapes.[33] Overall, fabrication by chemical methods can be more appropriate than fabrication by physical methods if one aims to obtain small, well-defined and uniform shaped metal particles.[34]

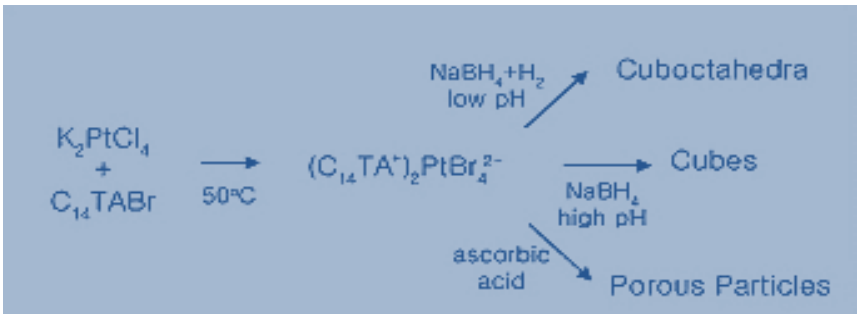

Scheme 0.1: Reduction of a metal-surfactant complex can be kinetically controlled to produce cuboctahedra, cubes and porous particles. Reproduced from Lee *et al.*[15]

Recently, some researchers have proposed that in some cases the presence of capping agents or surfactants can be essential for the catalytic activity of some systems because the metal particle remains isolated on the support surface and can easily agglomerate.[35] As an example, Jin *et al*. hypothesised that a core-shell (thiolate) structure is primarily responsible for the catalytic activities of thiolated gold clusters.[36] However, other researchers believe otherwise; while surfactants and organic ligands can be indispensable in the synthesis of metal particles,

they can be detrimental to catalysis because they block the access of the reactant molecules to surface particles.[6] Chemical reactions can also occur effectively on catalytically un-covered particles when the reactants are adsorbed more strongly to the particle surface (see Figure 7.5).[35e] Surface impurities, ligands and/or surfactants can block a significant proportion of metal catalysts active sites.[35e] Hence, for catalytic applications of chemically made nanoparticles, it is critical to establish procedures for surface cleaning and removal of surfactants without inducing particle size and morphology changes.[6, 35e]

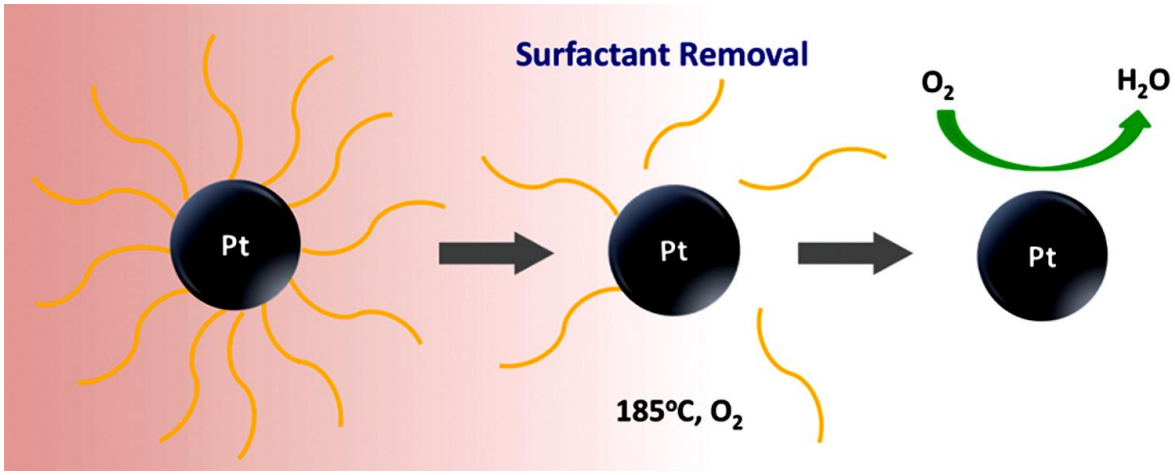

Figure 0.5: The effect of surfactant removal on the catalytic activity of Pt nanocatalysts. Reproduced from Li *et al.*[35e]

Calcination under various oxidative or reductive conditions can be used for activation of catalysts by removing surface impurities that would otherwise impair catalytic performance (see Chapter 1, Section 1.7, for a review of catalysts activation).[3] Methods that have been applied to remove oleyl-amine surfactant include thermal annealing, acid treatments (using, *e.g.*, acetic acid[37] or hydrogen chloride acid[38]) and UV–ozone irradiation.[37-39] Tests using the resulting materials as electro-catalysts for the oxygen reduction[35e] have suggested that low-temperature (~185 °C) thermal annealing in air is the most effective way for surface cleaning without inducing particle-size and morphology changes.[35e] Removal of oleyl-amine adsorbed onto Y_2O_3-doped CeO_2 nanocrystals surfaces has also been attempted by heating to 200 °C under an oxygen atmosphere and by treatment in aqueous H_2O_2 solution in an autoclave at

200 °C.[40] Ru nanocatalysts display oxophilicity (*i.e.*, a tendency to oxidise by hydrolysis or abstraction of oxygen), and hence oxidative treatments would cause poisoning by formation of an oxide layer.[41] However, recent studies have shown that reductive treatments can improve the catalytic activity of Ru nanocatalysts by removing the oxide (RuO_2) layer.[41-42]

Another important challenge is that shaped metal nanocatalysts can be spontaneously deactivated due to effects including sintering, leaching of active components, poisoning (by heteroatom-containing molecules, deposition of inactive metal or metal oxide, and impurities in solvents and reagents), structural or morphological changes of the active sites and surface oxidation.[41, 43] In addition, surface deposition of products can reduce activity, stability and recyclability.[6] Thermal treatment has been considered as a method for reactivating the catalytic properties of supported Ru nanoparticles.[14a, 42, 44] Lenzi *et al.* showed that drying in vacuum at 200 ^{o}C for 24 hours and calcination under air at 600 ^{o}C for 5 hours increased the surface area of Ru/SiO_2 (as determined by BET) from 301 to 515 m^2/g.[42b] Ma *et al.* activated Ru/SiO_2 through temperature-programmed reduction (TPR). The catalyst samples were heated in Ar at 350 ^{o}C for 0.5 hour before being subjected to a flow (20 ml/min) of 4.97% H_2 in Ar at a heating rate of 15 ^{o}C. min^{-1}. A cold trap (liquid nitrogen and iso-propanol) was used to remove water that was produced during TPR activation. The resulting catalysts were utilized for hydrogenolysis of glycerol with 17% conversion.[42a]

Shape-specific metal particles fabricated and immobilized on a support have been proposed for use in a wide range of catalytic applications. Associate Professor Richard Tilley and co-workers (our collaborators at Victoria University of Willington) synthesized some specific-shape particles and crystals with a variety of morphologies, such as branched nickel nanoparticles (monopod, linear bipod, bent bipod, tripod, regular tetrapod and planar tetrapod – see Figure 7.6.a)[45] and ruthenium hourglass nanocrystals (*i.e.*, a crystalline nanoparticle –

see Figure 7.6.b).[33] Despite this success, examples of the use of such shape-specific materials in catalysis are still very limited.

a) 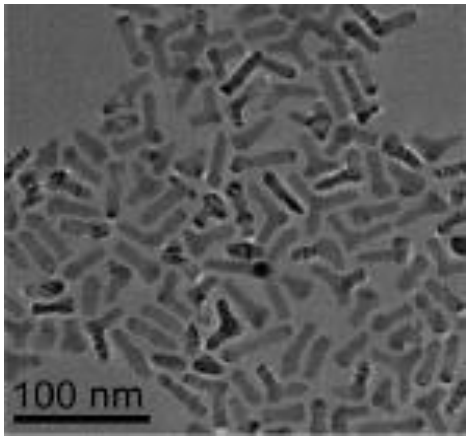

b) 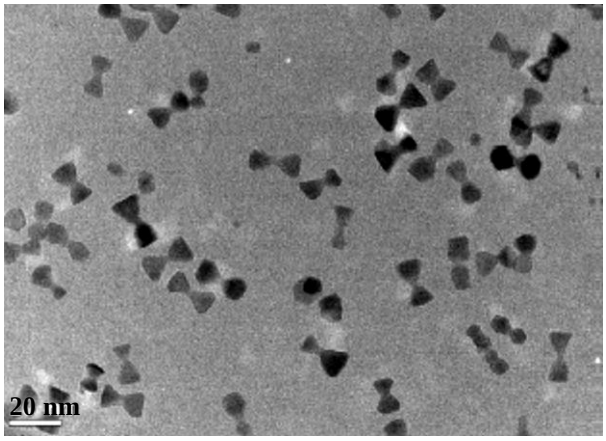

Figure 0.6: Transmission electron microscopy of a) branched nickel nanoparticles (monopod) & b) ruthenium hourglass nanoparticles. Reproduced from Tilley *et al*.[33, 45]

The novelty of shape-specific Ru nanocrystals and the potential for fabricating Ru/SiO_2 catalysts containing shape-specific particles has stimulated the work presented in this chapter. There is a major concern about deactivation of Ru catalysts. The effectiveness of the treatments for removing protective layers of surfactant and reduction of the Ru surface (for removing RuO_2) while retaining the particle shape is of particular interest.[42b, 44a] The aims here are to assess the catalysts' performance of shape-specific Ru catalysts in liquid-phase hydrogenation of cyclohexene to cyclohexane as a simple model reaction of hydrogenation of a double bond (C = C).[14a] A series of catalysts was made by depositing pre-synthesised, shape-specific Ru nanoparticles onto SiO_2 and then activating them in different ways. The effects of various activation protocols, such as thermal treatments under specific conditions on the catalytic performance were determined by conducting tests under mild conditions to prevent Ru crystals from aggregating.[14a, 44a] It was hypothesised that activated catalysts would show better activity due to the removal of surfactants from the metal surface[46] and/or reduction of the surface oxide layer of metal particles[41, 43] which could lead to a stronger Ru-support interaction.

7.2 Results and discussion

A brief outline of the simple and general Ru particle-synthesis procedure developed by Tilley's group was presented in Chapter 2 (see section 2.4.2). The Ru crystals were immobilized on silica under as mild as possible conditions by David Anderson from Doctor Golovko's group (as described in Chapter 2, Section 2.5.1.2) to give 0.1 wt% Ru/SiO_2. Catalysts described as "as-made" were not subject to any additional activation treatments.

The result of various activation procedures was investigated by carrying out test reactions involving the catalytic hydrogenation of cyclohexene in ~10g:10g mixtures of cyclohexene/cyclohexane in a Parr reactor while controlling the stirring rate (1200 rpm), H_2 pressure (400 psi) and target temperature (75 ^{o}C). After each catalytic test, the product mixtures were separated from the catalyst, which was recovered by washing with fresh cyclohexane (50 mL), centrifugation (5000 rpm, 15 minutes) and drying under vacuum for one day to remove reactant and product residues. To check the recyclability of ruthenium catalysts, each test was run three times using the same catalyst with a fresh reaction mixture.

7.2.1 "As-made" catalyst Ru nanocrystals as deposited on SiO_2

As shown in Table 7.1, the results for "as-made" 0.1% Ru/SiO_2 indicate poor recyclability of the un-activated catalyst, with a ten-fold drop in conversion (from 43% to only 4%) over three cycles. Experiments (such as AAS and TEM) to establish the cause of this decrease were not performed due to limited time and equipment access (due to earthquake-related shut down of facilities), along with a judgement that the reason was of much lower priority that the empirical observations of an underperforming system. This decrease could be due to catalyst reshaping, products depositing on the catalyst surface, Ru leaching or particle aggregation (particularly in organic solvents).[2, 11a, 44a, 47]

Table 0.1: The effect of recyclability of 0.1 wt% Ru/SiO_2 catalysts ("as-made") on cyclohexene conversion.

0.1 wt% Ru/SiO_2	Mass of cyclohexene (g)	Mass of cyclohexane (g)	C_x%	Time (h)
1st run (fresh)	10.06	10.02	43	24
1st recycle	10.08	10.03	13	24
2nd recycle	10.12	10.05	4	24

The observed decrease in activity with recycling is in line with earlier observations.[48] Narayanan and El-Sayed showed that size and shape of colloidal shape-specific Pt particles changed during catalysis of the electron-transfer reaction between hexacyanoferrate (III) and thiosulfate to form hexacyanoferrate (II) and tetrathionate ions. TEM images proved that tetrahedral Pt particles of approximately 5 nm size changed to spherical particles (~5.2 nm) after the first cycle and that the spherical particles increased to ~5.7 nm after the second cycle.[48] Manyar *et al.* found that 1 wt% Ru/SiO_2 significantly loses activity in the hydrogenation of butan-2-one on recycling, from 100% to 85% for the second cycle, and then to 25% for the third cycle. They attributed deactivation to the fast oxidation of the catalyst surface to RuO_2 by air.[44a]

7.2.2 Effect of different catalyst activation protocols

Thermal activation (calcination) treatments were performed in a vacuum (in a Schlenk tube) or in a hydrogen-containing atmosphere in a tube furnace (MTI). The activated 0.1 wt% Ru/SiO_2 samples were tested in the hydrogenation of cyclohexene using exactly the same experimental conditions as above.

After calcination in a vacuum using a Schlenk tube (as described in Chapter 2, Section 2.6.2), 0.1 wt% Ru/SiO_2 nanocatalysts exhibited 77% conversion after 24 hours. Hence, improving the catalytic activity by partially removing the surfactants or/and RuO_2 can be considered as an effective catalyst activation method.[39, 49] A significant increase in conversion from 43% (un-treated) to 77% was observed when Ru catalysts were activated using a Schlenk tube

under vacuum at 200 ^{o}C for 2 hours. It is hypothesised that this increase is due to removal of the surfactant from the catalysts surface by vacuum calcination.[42b] However, further experiments are necessary to confirm retention of particle shape or removal of surfactant using this activation treatment.

In the next stage, for improvement of the catalytic activity of 0.1 wt% Ru/SiO_2, the Ru catalyst was activated by calcination using time-programmed temperature protocols.[14a, 42, 44b] Ru catalyst deactivation is attributed to fast oxidation of surface Ru to RuO_2, whose presence has been confirmed by X-ray line broadening. Reduction by hydrogen was chosen as a means to reduce any ruthenium oxide species.[42, 44a] The minimum temperature for such reduction is approximately 200 ^{o}C.[42] The temperature, gas composition and duration of each reaction stage could be critical in determining the activity of the catalyst due to associated chemical changes of the key components of the catalyst system.[42, 44a]

The furnace was programmed according to the five protocols based on calcination temperature (200, 400 ^{o}C), lengths of time of calcination (1 & 2 hours) and high or low reduction gas flow rates; these protocols are presented in Figures 7.7, 7.9, 7.11, 7.12 and 7.13. All measurements were carried out in a flow of H_2/N_2, except for protocol No. 5 which was carried out in pure H_2. The temperature was ramped from: a) 20 to 100 ^{o}C for protocols No.2 and 3, or 200 ^{o}C for protocols No.4 and 5 at a rate of 5 ^{o}C/min; b) 100 to 200 ^{o}C for protocols No.1, 2 and 3, or 400 ^{o}C for protocols No. 4 and 5 at a rate of 9 ^{o}C/min. The Ru/SiO_2 catalysts were calcined at 200 ^{o}C over 60 (protocol No.1) or 120 minutes (protocols No. 2 and 3) in the first three protocols. In protocol No.3, the activated sample was kept under vacuum at 22 ^{o}C over 24 hours before performing the catalytic testing experiments. In protocols No.4 and 5, a calcination temperature of 400 ^{o}C was used over a period of 60 minutes under hydrogen and nitrogen gas or hydrogen gas, respectively.

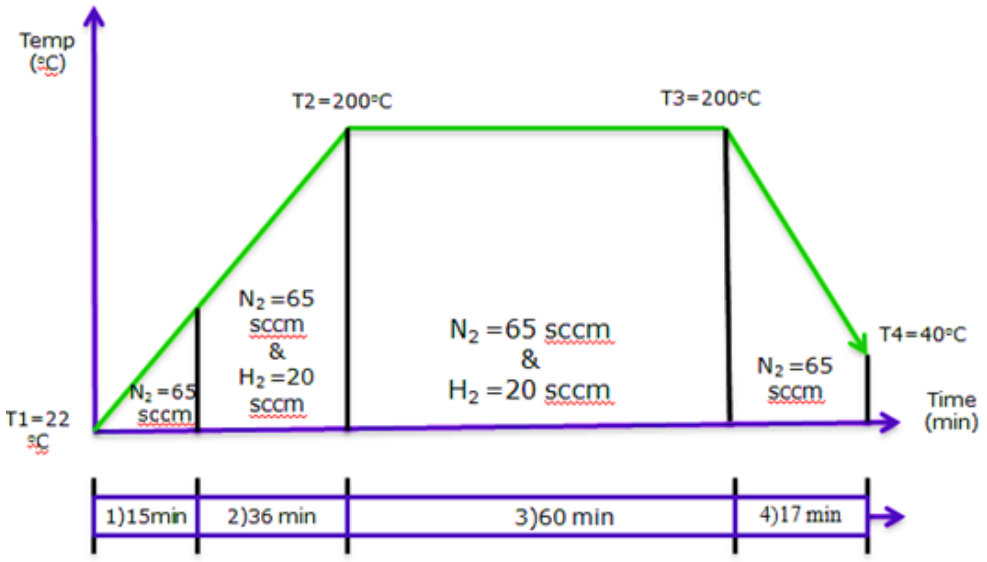

Figure 0.7: Furnace temperature, gas flow and time programme for protocol No.1.

Figure 7.8 displays TEM images taken after treatment according to protocol No.1. In comparison with Figure 7.10 the shape of Ru particles is relatively preserved with a little thickening at the necks of the hourglass Ru nanocrystals. An explanation for the relatively small degree of change could be that the calcination was performed at a relatively low temperature (200 ^{o}C) over only one hour (see Figure 7.7). The TEM images in Figure 7.8 also confirm that low-temperature reduction prevented significant aggregation of the Ru particles, which is in line with an earlier report by Ma *et al*.[42a]

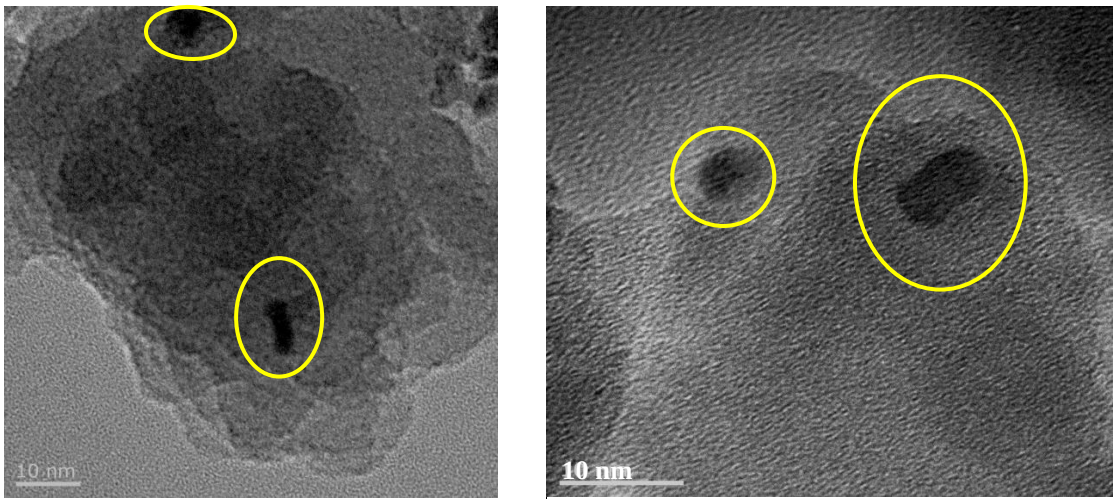

Figure 0.8: TEM images of the activated Ru nanocrystals using protocol No.1.

The Ru catalysts activated using protocol No.1 showed the highest activity (100% and 49% conversion over 24 hours and 4.5 hours of reaction time, respectively) among the activated Ru nanocatalysts (see Table 7.3). My hypothesis is that such high activity is attained due to the cleaned surfaces and preserved shapes of the Ru nanoparticles, although it was difficult to make a detailed estimate of the change in shape due to the limited number of Ru samples studied and limited number of TEM images received from our collaborators.

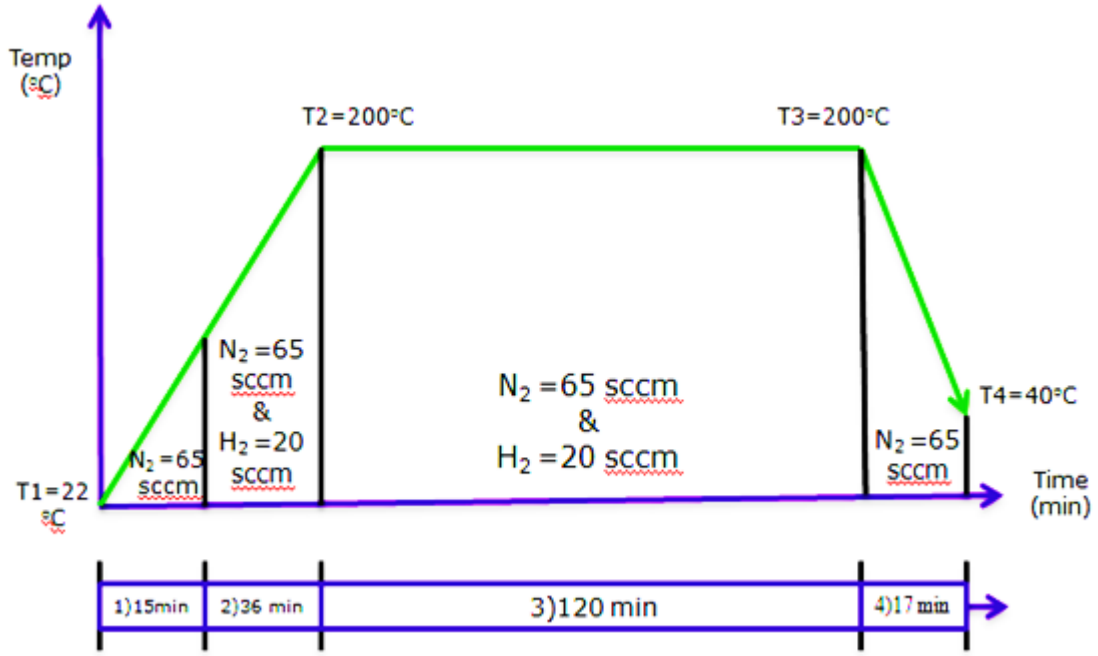

Figure 0.9: Furnace temperature, gas flow and time programme for protocol No.2.

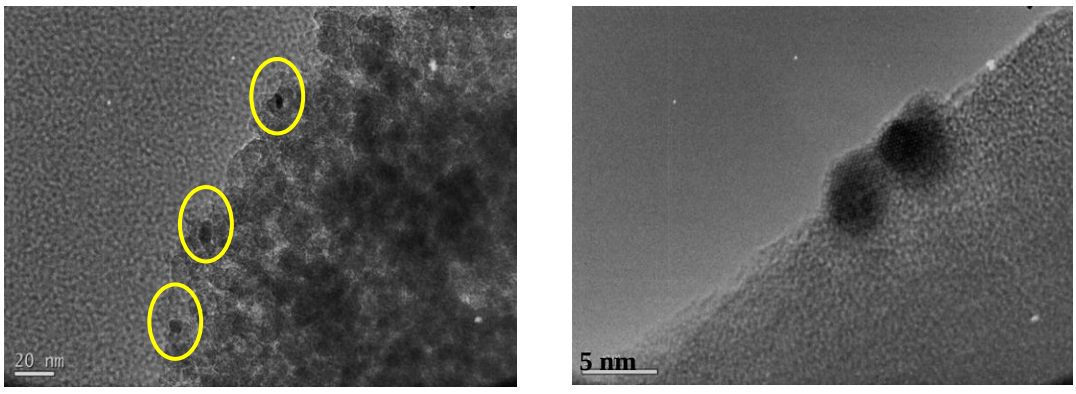

Figure 0.10: TEM images of the activated Ru nanocrystals using protocol No.2 (TEM images were taken by the group of Tilley at VUW).

Figure 7.10 displays TEM images of Ru nanoparticles after activation at 200 ^{o}C for 2 hours according to protocol No.2. These particles were slightly deformed with necks that were nearly broken to give two particles. Catalytic testing results showed 74% conversion over 24 hours using this activation protocol. If treatment under an atmosphere of 65 sccm N_2 and 20 sccm H_2 at 200 ^{o}C results in removal of surfactant and/or RuO_2 layer (as expected based on earlier reports) the longer treatment time of 120 minutes in protocol No.2 (compared with 60 minutes in protocol No.1) should give a greater degree of removal. Hence, the lower conversion suggests that, as Ru nanocrystals substantially lose their shape, their catalytic activity decreases (see Table 7.2), despite a cleaner surface being available for the reaction.

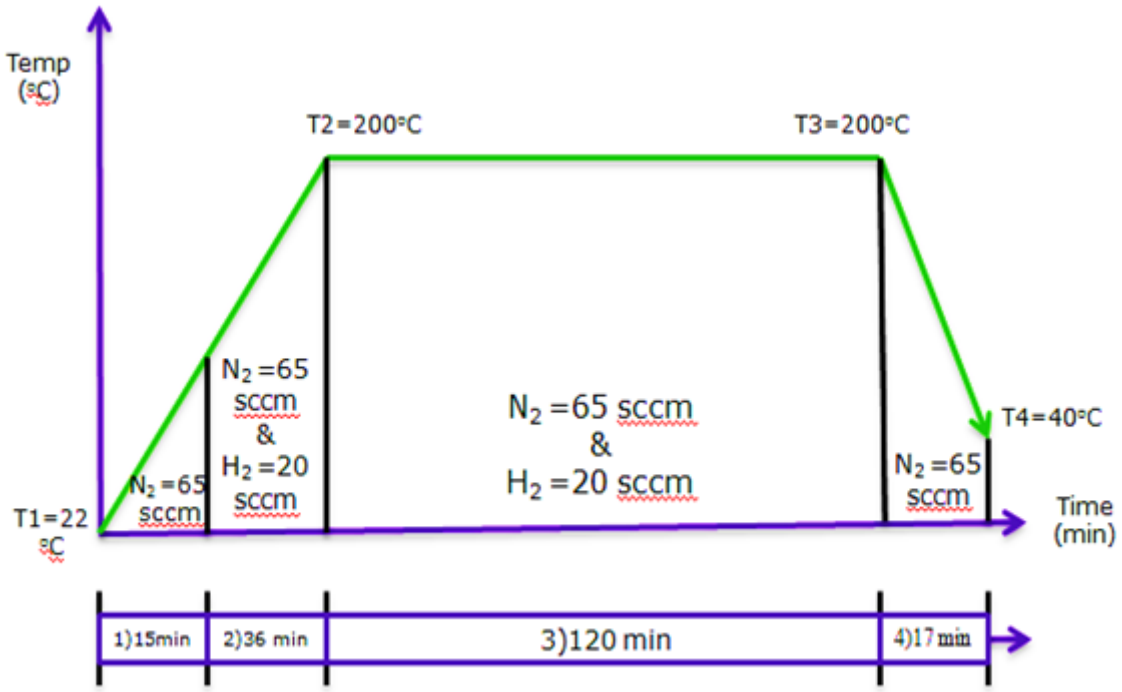

Figure 0.11: Furnace temperature, gas flow and time programme for protocol No.3.

The only difference between protocols No.2 (Figure 7.9) and No. 3 (Figure 7.11) is that, in the case of the latter, the activated sample was kept in vacuum overnight prior to the catalytic test in order to check the storage stability of the catalyst. Despite being kept under vacuum, the cyclohexene conversion decreased to 63%. Perhaps even traces of oxygen present under

the relatively low vacuum achieved using rotary vacuum pump can result in mild passivation of catalysts during storage. This result suggests that catalytic testing should be performed immediately after activation. Indeed, all other catalytic experiments reported in this chapter were performed immediately after activation.

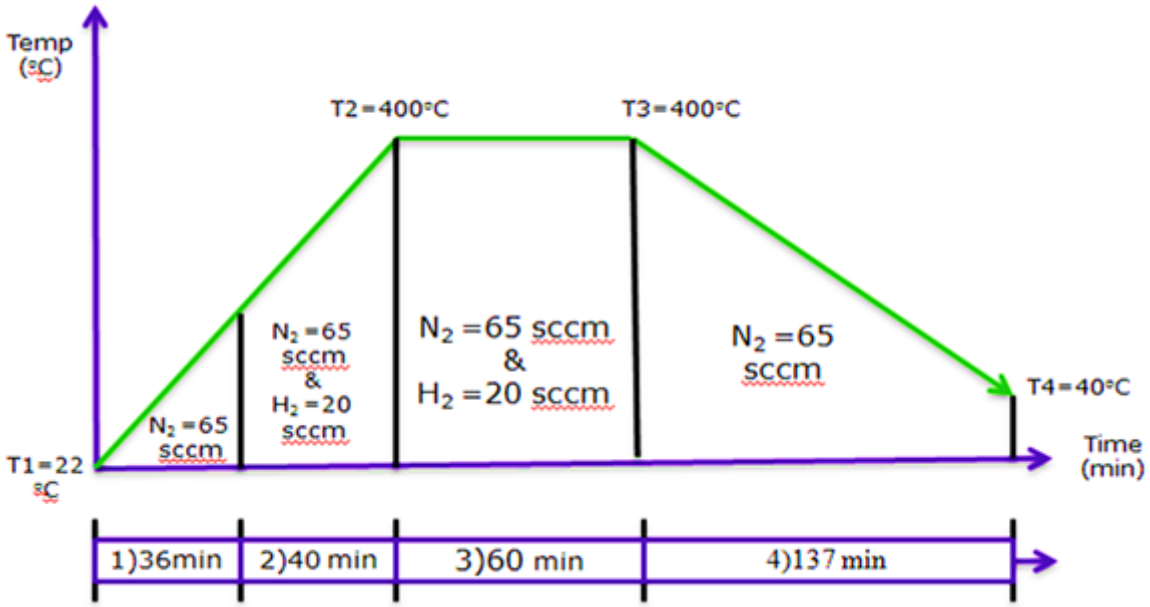

Figure 0.12: Furnace temperature, gas flow and time programme for protocol No.4.

In protocol No.4 (see Figure 7.12) the sample was activated at a higher temperature (400 ^{o}C) for 60 min under a mixture of 65 sccm N_2 and 20 sccm H_2. The resultant catalyst showed the lowest cyclohexene hydrogenation conversion (7%). TEM images of these samples were not obtained.

Figure 7.14 demonstrates that the shapes of the Ru particles changed very significantly during activation using protocol No.5 (activation at 400 ^{o}C for 60 minutes under pure H_2). As expected (based on earlier studies of the effect of temperature on particle aggregation discussed in Chapter 4, Section 4.1), this result showed that calcination at high temperature (400 ^{o}C) under a reductive (H_2) atmosphere may accelerate aggregation of Ru particles and lead to shape deformation.[42]

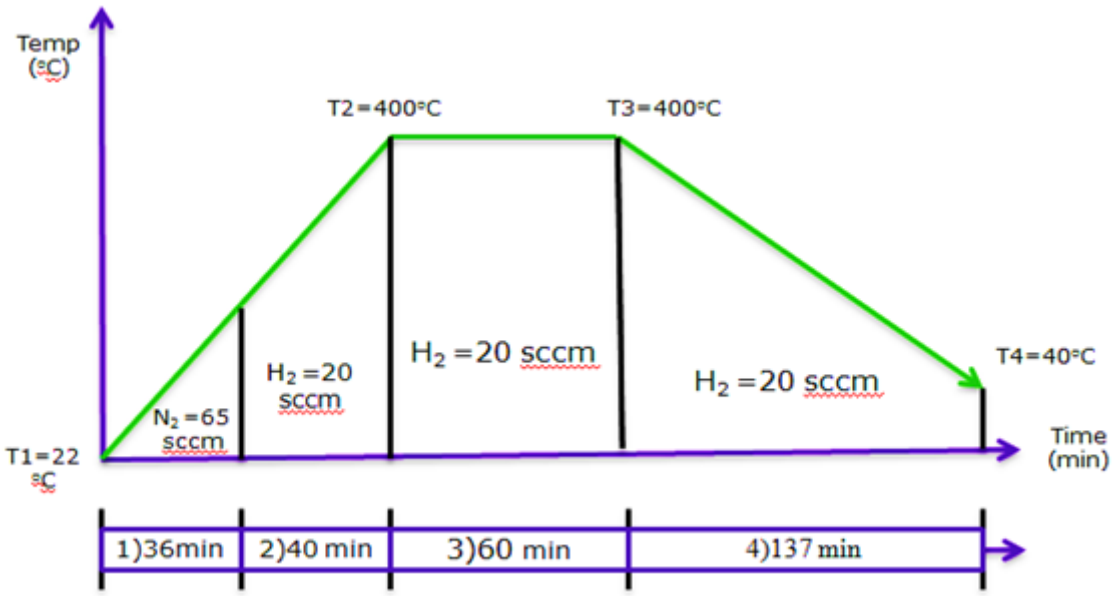

Figure 0.13: Furnace temperature, gas flow and time programme for protocol No.5

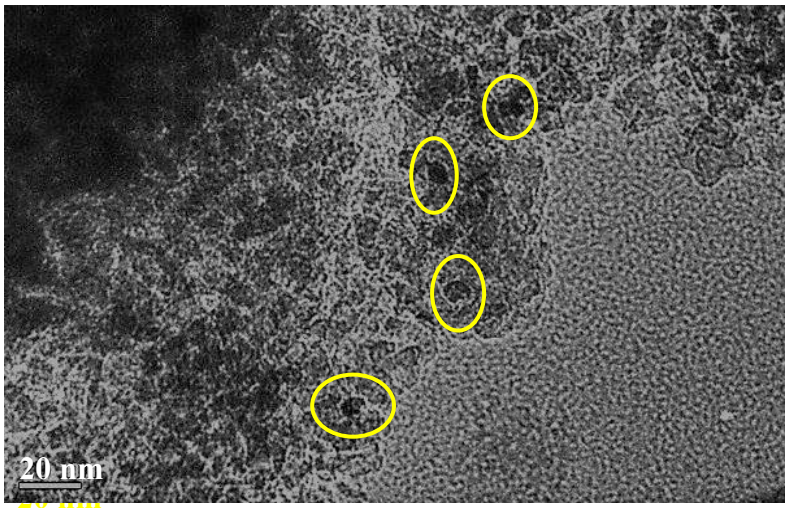

Figure 0.14: A TEM image of the Ru nanocatalysts activated using protocol No.5.

Ma *et al.* found the crystal size of Ru catalysts increased from 15 to 16 and then 18 nm when calcined in H_2 at 350 and 450 ^oC, respectively.[42a] Therefore, a high reduction temperature leads to a decrease in catalytic performance of Ru/SiO_2.[42a] Changes in metal core morphology (both size and shape) are responsible for decreased conversion (47%) achieved using 0.1 wt% Ru/SiO_2 nanocatalysts activated using this protocol (see Table 7.2). Based on earlier reports, one could expect that surfactant removal[35e] and Ru oxide reduction[42] would be more efficient at the higher temperature used here (*cf.* 200 ^oC used earlier in this chapter).

Hence, this analysis allows us to hypothesise that the low activity observed here is due to the changes of the metal core rather than poisoning due to surfactant or oxide.

Table 0.2: The effect of thermal treatments of 0.1 wt% Ru/SiO_2 catalysts on cyclohexene conversion (in the first test run).

Protocol No.	Calcination temperature (^oC)	Calcination period (min)	N_2:H_2	Mass of cyclohexene (g)	Mass of cyclohexane (g)	C_x (%)	Reaction time (h)
1	200	60	65:20	10.25	10.00	100	24
2	200	120	65:20	10.05	10.00	72	24
3	200	120	65:20	10.34	10.10	63	24
4	400	60	65:20	10.41	10.66	7	24
5	400	60	0:20	10.45	10.20	47	24

Comparison between the catalytic activity of protocols No.4 and 5 shows that hydrogen is more effective at activating these nanocatalysts in the absence of nitrogen, which suggests that pure hydrogen, is better at reducing RuO_2. However, a detailed TEM study (which was not performed due to poor performance of materials activated by protocol No. 4) is required to rule out the possibility that this significant drop in activity was not due to severe aggregation under the mixed atmosphere.

Recyclability of the catalyst is another important criterion for the development of industrially relevant catalysts. We investigated the long-term recyclability of the material produced after treatment protocol No.1 since this was the most active. The material was freshly activated before the first catalytic run and then recovered and re-used for each of the four consecutive experiments (1^{st} to 4^{th} recycles of Table 7.3). As shown in Table 7.3, a significant drop in conversion, from 100% in the first catalytic run to only 16% in the 4^{th} recycle experiment.

Table 0.3: Recyclability of 0.1wt% Ru/SiO_2 catalysts samples for protocol No.1.

Protocol No.	**0.1 wt% Ru/SiO_2**	**Mass of cyclohexene (g)**	**Mass of cyclohexane (g)**	**C_x (%)**	**Reaction time (h)**
1	1^{st} run (fresh)	10.25	10.00	100	24
1	1^{st} recycle	10.07	10.01	36	24
1	2^{nd} recycle	10.09	10.13	22	24
1	3^{rd} recycle	10.02	10.07	17	24
1	4^{th} recycle	10.08	10.19	10	24

7.3 Conclusions

The effects of catalyst activation treatments on the performance of catalysts based on shape-specific Ru nanoparticles immobilized on SiO_2 have been investigated using a model reaction – the hydrogenation of cyclohexene to cyclohexane. "As-made" catalyst, a catalyst calcined under vacuum at 200 ^oC or activated under reductive atmospheres (mixture of N_2 and H_2 or pure H_2) at 200 or 400 ^oC and over 1 or 2 hours has been tested under systematically identical catalytic conditions. The highest activity (100 %) was achieved during the first test run of a catalyst activated by calcination by protocol No.1 in a furnace under the mildest reductive conditions studied here (temperature of 200 ^oC over the shortest calcination time of 1 hour). HRTEM showed only minor deformation of the Ru nanoparticles and minimal aggregation, implying that both size and shape are important to achieving the highest activity. It seems that reduction of Ru/SiO_2 nanocatalysts in pure H_2 is more efficient at removing RuO_2 species than reduction under H_2 plus N_2 mixtures, although a further TEM study is required to rule out an alternative scenario of severe particles aggregation. A higher temperature and/or longer activation time (for protocols No.2 to 5) caused decreases in the activity of 0.1 wt% Ru/SiO_2 catalysts. The catalysts studied here suffer from poor recyclability as evidenced by two tests of long-term recyclability. The observed decreases in activity could be due to metal leaching, particle aggregation during reaction or formation of oxide species upon exposure to air.

References

1. Ahmadi, T. S.; Logunov, S. L.; El-Sayed, M. A., Picosecond dynamics of colloidal gold nanoparticles. *J. Phys. Chem.* **1996,** *100* (20), 8053-8056.
2. Mahmoud, M. A.; Narayanan, R.; El-Sayed, M. A., Enhancing colloidal metallic nanocatalysis: Sharp edges and corners for solid nanoparticles and cage effect for hollow ones. *Acc. Chem. Res.* **2013,** *46* (8), 1795-1805.
3. Linic, S.; Christopher, P.; Xin, H.; Marimuthu, A., Catalytic and photocatalytic transformations on metal nanoparticles with targeted geometric and plasmonic properties. *Acc. Chem. Res.* **2013,** *46* (8), 1890-1899.
4. Boudart, M., Catalysis by supported metals. 1969; Vol. 20, pp 153-166.
5. Narayanan, R.; El-Sayed, M. A., Changing catalytic activity during colloidal platinum nanocatalysis due to shape changes: Electron-transfer reaction. *J. Am. Chem. Soc.* **2004,** *126* (23), 7194-7195.
6. Lee, I.; Zaera, F., Catalytic conversion of olefins on supported cubic platinum nanoparticles: Selectivity of (100) versus (111) surfaces. *J. Catal.* **2010,** *269* (2), 359-366.
7. Somorjai, G. A., New model catalysts (platinum nanoparticles) and new techniques (SFG and STM) for studies of reaction intermediates and surface restructuring at high pressures during catalytic reactions. *Appl. Surf. Sci.* **1997,** *121–122* (0), 1-19.
8. Davis, S. M.; Zaera, F.; Somorjai, G. A., The reactivity and composition of strongly adsorbed carbonaceous deposits on platinum. Model of the working hydrocarbon conversion catalyst. *J. Catal.* **1982,** *77* (2), 439-459.
9. Somorjai, G. A., Reactions on single-crystal surfaces. *Acc. Chem. Res.* **1976,** *9* (7), 248-256.
10. (a) Zhang, J.; Hou, C.; Huang, H.; Zhang, L.; Jiang, Z.; Chen, G.; Jia, Y.; Kuang, Q.; Xie, Z.; Zheng, L., Surfactant-concentration-dependent shape evolution of Au–Pd alloy nanocrystals from rhombic dodecahedron to trisoctahedron and hexoctahedron. *Small* **2013,** *9* (4), 538-544; (b) Zhang, L.; Niu, W.; Li, Z.; Xu, G., Facile synthesis and electrochemiluminescence application of concave trisoctahedral Pd@Au core-shell nanocrystals bound by {331} high-index facets. *Chem. Commun.* **2011,** *47* (37), 10353-10355; (c) Zhang, L.; Chen, D.; Jiang, Z.; Zhang, J.; Xie, S.; Kuang, Q.; Xie, Z.; Zheng, L., Facile syntheses and enhanced electrocatalytic activities of Pt nanocrystals with {hkk} high-index surfaces. *Nano Research* **2012,** *5* (3), 181-189.
11. (a) Narayanan, R.; El-Sayed, M. A., Shape-dependent catalytic activity of platinum nanoparticles in colloidal solution. *Nano Lett.* **2004,** *4* (7), 1343-1348; (b) Wang, Z. L.; Ahmad, T. S.; El-Sayed, M. A., Steps, ledges and kinks on the surfaces of platinum nanoparticles of different shapes. *Surf. Sci.* **1997,** *380* (2-3), 302-310.
12. Campbell, P. S.; Santini, C. C.; Bayard, F.; Chauvin, Y.; Collière, V.; Podgoršek, A.; Costa Gomes, M. F.; Sá, J., Olefin hydrogenation by ruthenium nanoparticles in ionic liquid media: Does size matter? *J. Catal.* **2010,** *275* (1), 99-107.
13. Cárdenas-Lizana, F.; Gómez-Quero, S.; Keane, M. A., Ultra-selective gas phase catalytic hydrogenation of aromatic nitro compounds over Au/Al_2O_3. *Catal. Commun.* **2008,** *9* (3), 475-481.
14. (a) Vollmer, C.; Redel, E.; Abu-Shandi, K.; Thomann, R.; Manyar, H.; Hardacre, C.; Janiak, C., Microwave irradiation for the facile synthesis of transition-metal nanoparticles (NPs) in ionic liquids (ILs) from metal–carbonyl precursors and Ru-, Rh-, and Ir-NP/IL dispersions as biphasic liquid–liquid hydrogenation nanocatalysts for cyclohexene. *Chem. – Eur. J.* **2010,** *16* (12), 3849-3858; (b) Campbell, P. S.; Santini, C. C.; Bouchu, D.; Fenet, B.; Philippot, K.; Chaudret, B.; Padua, A. A. H.; Chauvin, Y., A novel stabilisation model for ruthenium nanoparticles in imidazolium ionic liquids: in situ spectroscopic and labelling evidence. *PCCP* **2010,** *12* (16), 4217-4223.
15. Lee, H.; Habas, S. E.; Kweskin, S.; Butcher, D.; Somorjai, G. A.; Yang, P., Morphological control of catalytically active platinum nanocrystals. *Angew. Chem. Int. Ed.* **2006,** *45* (46), 7824-7828.
16. Serrano-Ruiz, J. C.; López-Cudero, A.; Solla-Gullón, J.; Sepúlveda-Escribano, A.; Aldaz, A.; Rodríguez-Reinoso, F., Hydrogenation of α, β unsaturated aldehydes over polycrystalline, (111) and (100) preferentially oriented Pt nanoparticles supported on carbon. *J. Catal.* **2008,** *253* (1), 159-166.
17. (a) Eppler, A. S.; Rupprechter, G.; Anderson, E. A.; Somorjai, G. A., Thermal and chemical stability and adhesion strength of Pt nanoparticle arrays supported on silica studied by transmission electron microscopy and atomic force microscopy. *J. Phys. Chem. B* **2000,** *104* (31), 7286-7292; (b)

Grunes, J.; Zhu, J.; Anderson, E. A.; Somorjai, G. A., Ethylene hydrogenation over platinum nanoparticle array model catalysts fabricated by electron beam lithography: Determination of active metal surface area. *J. Phys. Chem. B* **2002,** *106* (44), 11463-11468.
18. An information portal for the MEMS and nanotechnology community http://www.memsnet.org/mems/processes/lithography.html (accessed Nov 23, 2013).
19. Gervinskas, G.; Seniutinas, G.; Rosa, L.; Juodkazis, S., Arrays of arbitrarily shaped nanoparticles: Overlay-errorless direct Ion write. *Adv. Optical Mater.* **2013,** *1* (6), 456-459.
20. Grigorenko, A. N.; Roberts, N. W.; Dickinson, M. R.; Zhang, Y., Nanometric optical tweezers based on nanostructured substrates. *Nat. Photonics* **2008,** *2* (6), 365-370.
21. Malyarchuk, V.; Hua, F.; Mack, N. H.; Velasquez, V. T.; White, J. O.; Nuzzo, R. G.; Rogers, J. A., High performance plasmonic crystal sensor formed by soft nanoimprint lithography. *Opt. Express* **2005,** *13* (15), 5669-5675.
22. (a) Colson, P.; Henrist, C.; Cloots, R., Nanosphere lithography: A powerful method for the controlled manufacturing of nanomaterials. *J.Nano Mat.* **2013,** *2013*; (b) Zhenga, H.; Wua, K., Enhanced light emission of ingan light-emitting-diodes by nanosphere lithography generated photonic crystals with different geometries. *ECS J. Solid State Sci. Technol* **2013,** *2* (11), R241-R244.
23. (a) Park, J. H.; Hwang, S.; Kim, B. K.; Kwak, J., Soft colloidal lithography by strong physical contact using swollen magnetic microspheres and magnetic force. *Electrochem. Commun.* **2013,** *30*, 99-102; (b) Pendergraph, S. A.; Park, J. Y.; Hendricks, N. R.; Crosby, A. J.; Carter, K. R., Facile colloidal lithography on rough and non-planar surfaces for asymmetric patterning. *Small* **2013,** *9* (18), 3037-3042.
24. Dieringer, J. A.; McFarland, A. D.; Shah, N. C.; Stuart, D. A.; Whitney, A. V.; Yonzon, C. R.; Young, M. A.; Zhang, X.; Van Duyne, R. P., Surface enhanced Raman spectroscopy: New materials, concepts, characterization tools, and applications. *Faraday Discuss.* **2006,** *132*, 9-26.
25. (a) Valden, M.; Pak, S.; Lai, X.; Goodman, D. W., Structure sensitivity of CO oxidation over model Au/TiO_2 catalysts. *Catal. Lett.* **1998,** *56* (1), 7-10; (b) Rodríguez-Reyes, J. C. F.; Friend, C. M.; Madix, R. J., Origin of the selectivity in the gold-mediated oxidation of benzyl alcohol. *Surf. Sci.* **2012,** *606* (15–16), 1129-1134.
26. Guo, H.; Al-Hunaiti, A.; Kemell, M.; Rautiainen, S.; Leskelä, M.; Repo, T., Gold catalysis outside nanoscale: Bulk gold catalyzes the aerobic oxidation of π-activated alcohols. *ChemCatChem* **2011,** *3* (12), 1872-1875.
27. Somorjai, G. A.; Park, J. Y., Colloid science of metal nanoparticle catalysts in 2D and 3D Structures. Challenges of nucleation, growth, composition, particle shape, size control and their influence on activity and selectivity. *Top. Catal.* **2008,** *49* (3-4), 126-135.
28. Christopher, P.; Linic, S., Shape- and size-specific chemistry of Ag nanostructures in catalytic ethylene epoxidation. *ChemCatChem* **2010,** *2* (1), 78-83.
29. (a) Yoo, J. W.; Hathcock, D.; El-Sayed, M. A., Characterization of Pt nanoparticles encapsulated in Al_2O_3 and their catalytic efficiency in propene hydrogenation. *J. Phys. Chem. A* **2002,** *106* (10), 2049-2054; (b) Kónya, Z.; Puntes, V. F.; Kiricsi, I.; Zhu, J.; Alivisatos, P.; Somorjai, G. A., Novel two-step synthesis of controlled size and shape platinum nanoparticles encapsulated in mesoporous silica. *Catal. Lett.* **2002,** *81* (3-4), 137-140; (c) Miyazaki, A.; Balint, I.; Nakano, Y., Morphology control of platinum nanoparticles and their catalytic properties. *J. Nanopart. Res.* **2003,** *5* (1-2), 69-80.
30. Minati, L.; Benetti, F.; Chiappini, A.; Speranza, G., One-step synthesis of star-shaped gold nanoparticles. *Colloids Surf., A* **2014,** *441* (0), 623-628.
31. Khurshid, H.; Li, W.; Chandra, S.; Phan, M.-H.; Hadjipanayis, G. C.; Mukherjee, P.; Srikanth, H., Mechanism and controlled growth of shape and size variant core/shell FeO/Fe_3O_4 nanoparticles. *Nanoscale* **2013,** *5* (17), 7942-7952.
32. Bradley, J. S., The chemistry of transition metal colloids. In *Cluster and colloids; From theory to applications*, Schmid, G., Ed. VCH Weinheim (Federal Republic of Germany), 1994; Vol. 99, pp 459-537.
33. Watt, J.; Yu, C.; Chang, S. L. Y.; Cheong, S.; Tilley, R. D., Shape control from thermodynamic growth conditions: The case of HCP ruthenium hourglass nanocrystals. *J. Am. Chem. Soc.* **2013,** *135* (2), 606-609.

34. Gao, M.; Lyalin, A.; Taketsugu, T., Role of the support effects on the catalytic activity of gold clusters: A density functional theory study. *Catalysts* **2011,** *1*, 18-39.
35. (a) Yin, H.; Ma, Z.; Overbury, S. H.; Dai, S., Promotion of $Au(en)_2Cl_3$-Derived Au/Fumed SiO_2 by Treatment with $KMnO_4$. *J. Phys. Chem. C* **2008,** *112* (22), 8349-8358; (b) Martra, G.; Prati, L.; Manfredotti, C.; Biella, S.; Rossi, M.; Coluccia, S., Nanometer-sized gold particles supported on SiO_2 by deposition of gold sols from $Au(PPh_3)_3Cl$. *J. Phys. Chem. B* **2003,** *107* (23), 5453-5459; (c) Budroni, G.; Corma, A., Gold-organic-inorganic high-surface-area materials as precursors of highly active catalysts. *Angew. Chem., Int. Ed.* **2006,** *45* (20), 3328-3331; (d) Alvino, J. F.; Bennett, T.; Anderson, D.; Donoeva, B.; Ovoshchnikov, D.; Adnan, R. H.; Appadoo, D.; Golovko, V.; Andersson, G.; Metha, G. F., Far-infrared absorption spectra of synthetically-prepared, ligated metal clusters with Au_6, Au_8, Au_9 and Au_6Pd metal cores. *RSC Adv.* **2013,** *3* (44), 22140-22149; (e) Li, D.; Wang, C.; Tripkovic, D.; Sun, S.; Markovic, N. M.; Stamenkovic, V. R., Surfactant removal for colloidal nanoparticles from solution synthesis: The effect on catalytic performance. *ACS Catalysis* **2012,** *2* (7), 1358-1362.
36. Zhu, Y.; Qian, H.; Jin, R., An atomic-level strategy for unraveling gold nanocatalysis from the perspective of Aun(SR)m nanoclusters. *Chem. Eur. J.* **2010,** *16* (37), 11455-11462.
37. Choi, S.-I.; Xie, S.; Shao, M.; Odell, J. H.; Lu, N.; Peng, H.-C.; Protsailo, L.; Guerrero, S.; Park, J.; Xia, X.; Wang, J.; Kim, M. J.; Xia, Y., Synthesis and characterization of 9 nm Pt–Ni octahedra with a record high activity of 3.3 A/mgPt for the oxygen reduction reaction. *Nano Lett.* **2013,** *13* (7), 3420-3425.
38. Li, C. C.; Chang, S. J.; Tai, M. Y., Surface chemistry and dispersion property of TiO_2 nanoparticles. *J. Am. Ceram. Soc.* **2010,** *93* (12), 4008-4010.
39. Kang, Y.; Murray, C. B., Synthesis and Electrocatalytic Properties of Cubic Mn−Pt Nanocrystals (Nanocubes). *J. Am. Chem. Soc.* **2010,** *132* (22), 7568-7569.
40. Goto, Y.; Takahashi, K.; Omata, T.; Otsuka-Yao-Matsuo, S., Synthesis of Y_2O_3-doped CeO_2 nanocrystals and their surface modification. *J. Phys.: Conf. Ser.* **2009,** *165*.
41. Wakita, H.; Ukai, K.; Takeguchi, T.; Ueda, W., Deactivation of Ru/Al_2O_3 catalyst for preferential CO oxidation in the presence of low-concentration NH_3 by nitrosyl species. *Chem. Lett.* **2006,** *35* (7), 734-735.
42. (a) Ma, L.; He, D., Influence of catalyst pretreatment on catalytic properties and performances of $Ru-Re/SiO_2$ in glycerol hydrogenolysis to propanediols. *Catal. Today* **2010,** *149* (1-2), 148-156; (b) Lenzi, G. G.; Lenzi, M. K.; Baesso, M. L.; Bento, A. C.; Jorge, L. M. M.; Santos, O. A. A., Cobalt, nickel and ruthenium-silica based materials synthesized by the sol-gel method. *J. Non-Cryst. Solids* **2008,** *354* (42-44), 4811-4815.
43. (a) Besson, M.; Gallezot, P., Deactivation of metal catalysts in liquid phase organic reactions. *Catal. Today* **2003,** *81* (4), 547-559; (b) Bartholomew, C. H., Sintering kinetics of supported metals: new perspectives from a unifying GPLE treatment. *Appl. Catal., A* **1993,** *107* (1), 1-57.
44. (a) Manyar, H. G.; Weber, D.; Daly, H.; Thompson, J. M.; Rooney, D. W.; Gladden, L. F.; Hugh Stitt, E.; Jose Delgado, J.; Bernal, S.; Hardacre, C., Deactivation and regeneration of ruthenium on silica in the liquid-phase hydrogenation of butan-2-one. *J. Catal.* **2009,** *265* (1), 80-88; (b) Yan, Q. G.; Wu, T. H.; Weng, W. Z.; Toghiani, H.; Toghiani, R. K.; Wan, H. L.; Pittman, C. U., Partial oxidation of methane to H_2 and CO over Rh/SiO_2 and Ru/SiO_2 catalysts. *J. Catal.* **2004,** *226* (2), 247-259.
45. LaGrow, A. P.; Cheong, S.; Watt, J.; Ingham, B.; Toney, M. F.; Jefferson, D. A.; Tilley, R. D., Can polymorphism be ued to form banched mtal nnostructures? *Adv. Mater.* **2013,** *25* (11), 1552-1556.
46. Choudhary, T. V.; Goodman, D. W., Oxidation catalysis by supported gold nano-clusters. *Top. Catal.* **2002,** *21* (1), 25-34.
47. Zhu, J.; Carabineiro, S. A. C.; Shan, D.; Faria, J. L.; Zhu, Y.; Figueiredo, J. L., Oxygen activation sites in gold and iron catalysts supported on carbon nitride and activated carbon. *J. Catal.* **2010,** *274* (2), 207-214.
48. Narayanan, R.; El-Sayed, M. A., Catalysis with transition metal nanoparticles in colloidal solution: Nanoparticle shape dependence and stability. *J. Phys. Chem. B* **2005,** *109* (26), 12663-12676.

49. Wang, C.; Daimon, H.; Lee, Y.; Kim, J.; Sun, S., Synthesis of monodisperse Pt nanocubes and their enhanced catalysis for oxygen reduction. *J. Am. Chem. Soc.* **2007,** *129* (22), 6974-6975.

Chapter 8: Summary and Future Work

8.1 Summary

Noble metal nanoparticles have been reported to show remarkable catalytic activity for oxidation and hydrogenation of organic compounds. Palladium nanoparticles often show particularly remarkable catalytic activity and selectivity for the hydrogenation of unsaturated hydrocarbons. Catalytic hydrogenation of liquid-phase cyclohexene to cyclohexane, using a Parr high-pressure reactor, was used as a model reaction to investigate the catalytic activity of palladium nanoparticles immobilized on wool (Pd/wool). Optimized conditions, including a H_2 gas pressure of 400 psi and stirring rate of 750 rpm at a temperature of 40 ^oC, proved that the catalysts were not very effective for the conversion of cyclohexene to cyclohexane.

The catalytic activity and selectivity of noble metal nanoparticles are often said to be related to the particle size and shape, as well as the nature of the support. Comparison of the catalytic activity of small (≤ 10 nm) nanoparticles may highlight the effects of particles shape and their interaction with support material. Shape-controlled (specific-shape) ruthenium nanoparticles immobilized on silica (0.1 wt% Ru/SiO_2) were studied for the hydrogenation of cyclohexene by using a H_2 gas pressure of 400 psi and stirring rate of 1200 rpm at a temperature of 75 ^oC for approximately 24 hours. The Ru/SiO_2 was calcined using a Schlenk tube or one of five time-programmed temperature protocols (from 200 ^oC to 400 ^oC) involving a furnace. The highest activity was achieved when the catalyst was calcined at 200 ^oC over 60 minutes (protocol No.1). It seems that higher calcination temperatures (~ 400 ^oC) caused the ruthenium nanocatalysts to be reshaped, which consequently decreased their catalytic activity.

Gold nanoparticles and nanoclusters immobilized on different types of carbon were studied for oxidation of benzyl alcohol in methanol. The effects of activation methods, including

washing with toluene or NaOH in MiiliQ water (by reflux) and calcinations, along with size and support materials, were investigated using a mini reactor. The conclusions drawn are:

- Under optimized conditions, carbon-supported Au_{101} gold nanoparticles (Au_{101}/C) are effective nanocatalysts for benzyl alcohol oxidation with benzoic acid and methyl benzoate being the main products. The activity and selectivity depend on the amounts of benzyl alcohol and base, the temperature, gold loading and the nature of the solvent. Gold appears to be a very promising catalyst for sustainable processes using simple and relatively environmentally benign reagents, particularly O_2, often in aqueous solution or in the presence of a solvent (methanol), under mild conditions.
- Un-treated gold nanocatalysts were found to be reasonably active over 24 hours reaction periods.
- Some of the gold nanocatalysts showed high activity after only 3 hours. Washing with toluene followed by calcinations under static air (75%) or vacuum (91%) at 100 ^{o}C for 3 hours, proved to be an effective for removal of the stabilising phosphine ligands from the gold nanocatalysts. In line with previous research, catalysts calcined at mild temperatures (100 – 200 ^{o}C) are more active than those calcined at higher temperatures (more than 200 ^{o}C), probably because of sintering of particles at the higher temperatures. Thermal treatments at a lower temperature (100 ^{o}C) allow more control over ligand removal while avoiding the formation of larger particles.
- Better control on the size and stability of gold nanoparticles could be achieved by further optimization of the activation processes. The catalytic activity of gold nanoparticles is partly related to their size and size distribution, particularly in the nanometre range. No conversion was observed for benzyl alcohol oxidation using gold nanoclusters with sizes smaller than 1 nm (*e.g.*, Au_9 and Au_8 nanoclusters) immobilized on Norit activated carbon. However, bigger nanoparticles (*e.g.*, Au_{101},

Au_{naked} and $Au_{citrate}$ particles) immobilized on Norit activated carbon showed high activity for benzyl alcohol oxidation. The higher conversion may be related to factors including the particle size, size distribution and gold dispersion. The highest conversion was obtained when the average particle diameters were 3.5 ± 0.1 nm for Au_{101}/C; whereas the lowest conversions were observed for average gold particles diameters of 10.5 ± 0.7 and 22 ± 2.0 nm for Au_9/C and Au_8/C, respectively. The results of this study support the view that particle size plays a key (but far from exclusive) role on the catalytic performance of gold catalysts.

- Support materials also play important role in the catalytic activity of gold catalysts due to the interaction of the gold particles with the support substrates. Activated carbon has the advantage of being an oxide support with a high specific surface area of up to 1000 m^2/g. The choice of the support has been also directly connected with the reaction to be catalysed by gold catalysts. Gold nanoparticles immobilized on mesoporous carbons, such as CMK-8, exhibited the highest activity (~96% conversion) for benzyl alcohol oxidation for 3 hours. Granular activated carbon, even when modified with $–SO_3H$ and –SH, showed essentially no activity. Interestingly, good correlations were observed between gold size, size distribution, dispersion carbon support and catalytic activity of gold catalysts.

8.2 Future work

The results presented in this work, particularly those for benzyl alcohol oxidation, open new perspectives for future experiments to gain deeper insights on:

- The activation of supported noble metal nanoparticles: other methods (post- and pre-treatments) at lower temperatures and for shorter times might be more effective at promoting catalytic activity for oxidation or hydrogenation reactions.

- Bi-metallic catalysts (*e.g.*, iron or ruthenium components in gold nanoparticles) could have properties that enhance the activities, selectivities and stabilities of nanocatalysts.
- Benzyl alcohol has been used as a model reactant for oxidation. Catalytic applications could be expanded to other reactions, for example alkenes, cyclic alkenes and alkynes. Further research should address nanocatalytic oxidation and/or hydrogenation of other alcohols and other types of organic compounds.
- Further work should investigate different types of reducible (*e.g.*, TiO_2) and irreducible (*e.g.*, carbon bases like MOFs) supports.
- It may be possible to reduce sintering during thermal treatments by substituting support calcination pre-treatments by catalyst calcination post-treatments. It would be interesting to repeat the low-temperature ligand-removal experiments, which might allow further control over the rate at which particles degrade to larger metal particles.
- Supported gold particles with average gold particle sizes around 20 nm were found to be more active than smaller particles for selective hydrogenation. It seems that the large gold particles, like gold citrate, immobilized on an appropriate support, can be considered to be active catalysts for hydrogenation of organic compounds.
- The modification of supports can improve the catalytic activity of supported metal nanoparticles. Investigations into improving the catalytic activity of gold catalysts on other types of carbon could be interesting.
- Appropriate characterizations for metal nanocatalysts are suggested as below:
    - X – ray photoelectron spectroscopy (XPS) to provide an estimate of the chemical composition of the few uppermost layers of the materials in order to

get further insights into the nature of the functional groups on the catalyst surfaces.

- Infrared **(**IR) spectroscopy for characterization of ligands on supported metal clusters and to probe the local surface structure of surface-bound species.
- Temperature programmed desorption (TPD) profiles for the determination of the amount of oxygen – containing functional groups on the carbon surface.
- Atomic adsorption spectroscopy (AAS) and CO **–** TPD experiments can be considered as further studies needed to understand the effect of gold loading on the gold particle size. Specifically, such studies could explain why higher gold loadings reported in the current thesis resulted in smaller gold particle sizes.

The present study is one of fundamental research. Future work should aim to discover and develop nanocatalysts for industrial applications. Rational approaches need to be developed in the direction of novel, attractive and eco-friendly catalysts for oxidation and hydrogenation processes.

Appendix

Notation and calculations

The following calculations are used to calculate the conversion and selectivity for the catalysed hydrogenation of cyclohexene to cyclohexane.

Notation:

-Cyclohexene = e

-Cyclohexane = a

-Decane = d

-Other product = o

-Initial amount = i

-Final amount = f

-Mass (g) = *m*

-Amount (mole) = *n*

-mole ratio = *x*

-Number of moles from chromatography (GC-FID) result = *g*

-Conversion = *C*

-Selectivity = *S*

We have two competing processes:

a) $e \xrightarrow[H_2,\Delta]{} a$

and

b) $e \xrightarrow[H_2,\Delta]{} o$

The initial amounts (mole) of reaction components are $(n_e)_i$ *and* $(n_a)_i$.

After the reaction, we have amounts $(n_e)_f$, $(n_a)_f$ and n_o.

Conversion and selectivity are, respectively, defined:

$$C = \frac{(n_e)_i - (n_e)_f}{(n_e)_i} = 1 - \frac{(n_e)_f}{(n_e)_i}$$

$$S = \frac{(n_a)_f - (n_a)_i}{(n_e)_i - (n_e)_f}$$

The total mass of the product mixture is

$$m_{prod} = (m_e)_f + (m_a)_f + m_o$$

A sample of mass m_{samp} is taken from the product mixture and spiked with an amount n_d of decane, which acts as an internal GC standard. Hence, the amounts in the sample are

$$g_e = \frac{m_{samp} \times (n_e)_f}{m_{prod}}$$

$$g_a = \frac{m_{samp} \times (n_a)_f}{m_{prod}}$$

These can be determined by chromatography (GC-FID), and then rearranging gives

$$(n_e)_f = \frac{m_{prod} \times g_e}{m_{samp}}$$

$$(n_a)_f = \frac{m_{prod} \times g_a}{m_{samp}}$$

Now substituting these expressions in to those for *C* and *S* from above;

$$C = 1 - \frac{m_{\text{prod}}}{m_{\text{samp}}} \times \frac{ge}{(n_e)_i}$$

$$S = \frac{\frac{m_{\text{prod}}}{m_{\text{samp}}} \times g_a - (n_a)_i}{(n_e)_i - \frac{m_{\text{prod}}}{m_{\text{samp}}} \times g_e}$$

So, we need to know:

a) The initial amounts of cyclohexane and cyclohexene (which are readily obtained from the initial masses)

b) The chromatography results on the final product mixture.

c) The ratio of the total mass of the product mixture to the mass of the sample (to be spiked).

The main problem lies with determining the mass of the product. Since there is the possibility of side products, this mass may not be determined purely by the degree of conversion. There are several methods (1- 4 below) to deal with part c):

1. Measure the mass of the whole product mixture before the sample is removed, and then measure the mass of the sample before it is spiked.

2. Spike the whole product mixture. In that case, we have

$$\frac{m_{\text{prod}}}{m_{\text{samp}}} = 1$$

hence:

$$C = 1 - \frac{g_e}{(n_e)_i}$$

$$S = \frac{g_a - (n_a)_i}{(n_e)_{i-} g_e}$$

3. Assume that there are no side products in which case

$$S = \frac{(n_a)_f - (n_a)_i}{(n_e)_i - (n_e)_f} = 1$$

So we have

$$(n_a)_f + (n_e)_f = (n_a)_i + (n_e)_i = n_a + n_e$$

That is the total amount of cyclohexane and cyclohexene is unchanged (due to the 1:1 stoichiometry).

Defining:

$$x_i = \frac{(n_e)_i}{n_e + n_a}$$

$$x_f = \frac{(n_e)_f}{n_e + n_a}$$

then, we have

$$C_x = 1 - \frac{x_f}{x_i}$$

where x_i is obtained from the original amounts;

$$x_i = \frac{(n_e)_i}{(n_e)_i + (n_a)_i}$$

and

x_f is obtained from the chromatography data;

$$x_f = \frac{g_e}{g_e + g_a} = \frac{1}{1 + \frac{g_a}{g_e}}$$

4. Calculate the final mass of the product mixture from the initial masses of cyclohexane and cyclohexene also the change in the mass of H_2 gas.

$m_{prod} = (m_a)_i + (m_e)_i - \Delta m\mathrm{H_2(g)}$

$\Delta m\mathrm{H_2(g)} = \left(m\mathrm{H_2(g)}\right)_f - \left(m\mathrm{H_2(g)}\right)_i$

$= \left[\left(n\mathrm{H_2(g)}\right)_f - \left(n\mathrm{H_2(g)}\right)_i\right] \times \left(M_R\mathrm{H_2(g)}\right)$

$= \left[\frac{p_{f\times V_f}}{RT_f} - \frac{p_{i\times V_i}}{RT_i}\right] \times \left(M_R\mathrm{H_2(g)}\right)$

Assuming that, the gas volume does not change significantly throughout the reaction.

$\Delta m\mathrm{H_2(g)} = \frac{M_{R(\mathrm{H_2})g\times V}}{RT}\left[\frac{p_f}{T_f} - \frac{p_i}{T_i}\right]$

Abbreviations/Glossary

AAS	Atomic adsorption spectroscopy
Au_1	$AuClPPh_3$
Au_8	$Au_8 (PPh_3)_8(NO_3)_2$
Au_9	$Au_9 (PPh_3)_8(NO_3)_3$
Au_{55} and Au_{101}	$Au_{101} (PPh_3)_{21}Cl_5$
$Au_{citrate}$	Gold citrate colloids
Au_{naked}	*"Naked"* gold particles
Aqua regia	2:1, v/v mixture of concentrated HCl and HNO_3
C_{CMK-3}	Mesopores carbon CMK - 3
C_{CMK-8}	Mesopores carbon CMK - 8
$C_{NCCR-41}$	Mesopores carbon NCCR - 41
C_g	Granular activated carbon
$C_{g.p}$	Granular activated carbon was powdered
C_{-SH}	Granular Norit activated carbon was modified with –SH
C_{-SO3H}	Granular Norit activated carbon was modified with $–SO_3H$
C_V	Vulcan carbon
$CHCl_3$	Chloroform
CH_2Cl_2	Dichloromethane
C	Conversion
DOWEX®50WX2	Cation-exchange resin
EtOH	Ethanol
FE-SEM	Field Emission Scanning Electron Microscope
FTIR	Fourier transform infrared spectroscopy
GC-FID	Gas chromatography - flame ionization detector
HPLC	High-performance liquid chromatography
$HAuCl_4.3H_2O$	Hydrogen tetrachloroaurate (III) hydrate
IR	Infrared **(**IR) spectroscopy
MHz	Mega hertz
MeOH	MeOH
mM	Millimolar
mL	Millilitre
min	Minutes
MQ	MilliQ
$NaBH_4$	Sodium borohydride
nm	Nanometers
NMR	Nuclear magnetic resonance
NMNPs	Noble metal nanoparticles
No	Number
PPh_3	Triphenylphosphine
Psi	Pounds per square inch, as to measure the amount of pressure per area (1 bar = 14.5 psi).
sccm	A standard cubic per minute (sccm) is an effective measurement of gas flow that indicates how many cubic centimetre of air pass a stationary point in one minute under standard conditions of temperature (32 ^oF = 0 ^oC = 273 K) and pressure (14.72 psi = 1 atm = 1.014 bar).
S	Selectivity

s	Second
SEM	Scanning electron microscope
s-G	Sulfonated graphene
SiO_2 – CS	Silica-supported chitosan
TEM	Transmission Electron Microscopy
THF	Tetrahydrofuran
TOABr	Tetraoctylammonium
TOFs	Turnover of frequencies
TPD	Temperature programmed desorption
UC	The University of Canterbury
UV-Vis	Ultraviolet-visible spectroscopy
VUW	The University of Victoria of Wellington
XPS	X-ray photoelectron spectroscopy
Y	Yield

9.3 Appendix three: Powder Norit activated carbon characterization

Sample: 5x16 8001-9 (powder carbon)
Operator: csm
File Name: C:\...\BAXTER\001-378.SMP

Started: 12/6/2012 2:31:30PM Analysis Adsorptive: N2
Completed: 12/7/2012 7:59:31AM Analysis Bath: 77.24 K
Report Time: 12/10/2012 10:26:26AM Thermal Correction: No
Sample Weight: 0.0523 g Smoothed Pressures: No
Warm Freespace: 27.9696 cm³ MEASURED Cold Freespace: 89.4856 cm³
Equil. Interval: 25 secs Low Pressure Dose: 10.00 cm³/g STP

Analysis Log

Relative Pressure	Pressure (mmHg)	Vol Adsorbed (cm³/g STP)	Elapsed Time (HR:MN)	Saturation Press.(mmHg)
			02:00	751.78809
0.000000000	0.00000	10.1916	02:16	
0.000000921	0.00069	20.3817	02:29	
0.000001957	0.00147	30.5723	02:49	
0.000003081	0.00232	40.7643	03:08	
0.000004442	0.00334	50.9562	03:28	
0.000006385	0.00480	61.1451	03:47	
0.000009706	0.00730	71.3331	04:07	
0.000015336	0.01153	81.5126	04:27	
0.000024968	0.01877	91.6679	04:46	
0.000042018	0.03158	101.7879	05:06	
0.000073803	0.05548	111.8468	05:25	
0.000135760	0.10205	121.9465	05:45	
0.000256930	0.19313	131.9413	06:06	
0.000490550	0.36873	141.7259	06:27	
0.000924595	0.69497	151.1238	06:48	
0.001628265	1.22387	159.9636	07:08	
0.002825378	2.12364	168.1207	07:29	
0.004616810	3.47010	175.1817	07:46	
			07:56	751.61902
0.007173338	5.39072	181.5415	08:04	
0.010176288	7.64597	186.5597	08:13	
0.013709269	10.29855	190.8460	08:22	
0.017628738	13.24068	194.4953	08:30	
0.021806251	16.37560	197.5980	08:38	
0.026180584	19.65767	200.2868	08:45	
0.030778221	23.10642	202.6729	08:52	
0.035542688	26.67938	204.8255	08:59	
0.040327733	30.26674	206.7365	09:06	
0.045232835	33.94314	208.4688	09:13	
0.050194240	37.66150	210.0455	09:19	
0.055193147	41.40618	211.4858	09:26	
0.060279595	45.21543	212.8454	09:33	
0.079555728	59.66687	217.1521	09:39	
0.100919580	75.68185	221.0205	09:44	
0.121653365	91.21911	224.2805	09:50	
0.160812762	120.56676	229.3173	09:56	
			09:58	749.70239
0.182462536	136.78557	231.8146	10:03	
0.202237206	151.60057	233.8902	10:09	
0.249853770	187.28516	238.7777	10:14	
0.277153882	207.73807	241.5208	10:19	

Sample: 5x16 8001-9 (powder carbon)
Operator: csm
File Name: C:\...\BAXTER\001-378.SMP

Started: 12/6/2012 2:31:30PM Analysis Adsorptive: N2
Completed: 12/7/2012 7:59:31AM Analysis Bath: 77.24 K
Report Time: 12/10/2012 10:26:26AM Thermal Correction: No
Sample Weight: 0.0523 g Smoothed Pressures: No
Warm Freespace: 27.9696 cm³ MEASURED Cold Freespace: 89.4856 cm³
Equil. Interval: 25 secs Low Pressure Dose: 10.00 cm³/g STP

Analysis Log

Relative Pressure	Pressure (mmHg)	Vol Adsorbed (cm³/g STP)	Elapsed Time (HR:MN)	Saturation Press.(mmHg)
0.301812538	226.20677	243.9366	10:25	
0.326044444	244.35588	246.2850	10:30	
0.350228041	262.46692	248.6169	10:35	
0.399875587	299.65515	253.7061	10:41	
0.425770665	319.04376	255.9991	10:46	
0.450137058	337.28494	258.4024	10:51	
0.499930504	374.57175	263.5288	10:57	
0.525562773	393.75641	266.4454	11:02	
0.550682379	412.55502	269.4855	11:07	
0.599926664	449.41965	276.0224	11:13	
0.625758552	468.74683	279.9899	11:18	
0.650896535	487.55225	284.1908	11:23	
0.699505108	523.92462	293.8449	11:30	
0.725920640	543.68170	299.8160	11:35	
0.750965230	562.40424	306.2662	11:41	
0.799068966	598.39258	321.0015	11:47	
0.850654218	636.97693	340.9510	11:54	
			12:01	748.75433
0.890161089	666.72943	359.8229	12:52	
0.900910262	674.80212	365.3210	12:57	
0.944847013	707.76605	390.0456	13:09	
0.979078560	733.44574	413.3848	13:17	
0.989333168	741.16083	425.3603	13:24	
0.982504928	736.06897	420.9193	13:29	
0.975498666	730.84808	416.9054	13:35	
0.952639949	713.81805	406.5135	13:56	
0.924984890	693.12256	395.6961	14:02	
			14:04	749.34351
0.899983865	674.45654	386.1084	14:10	
0.875138093	655.90436	376.4272	14:17	
0.849825833	636.98932	366.6892	14:23	
0.824893319	618.36469	357.1681	14:30	
0.799278490	599.22467	347.7470	14:37	
0.750665970	562.83740	331.2105	14:44	
0.699362507	524.42480	316.1855	14:51	
0.649460292	487.05515	304.0075	14:58	
0.599829379	449.87466	294.0351	15:04	
0.549737628	412.33591	285.6640	15:09	
0.499920060	375.00281	278.3911	15:15	
0.453816971	340.46469	262.1311	15:24	
0.399679004	299.87106	253.6376	15:29	
			16:09	750.72034

Sample: 5x16 8001-9 (powder carbon)
Operator: csm
File Name: C:\...\BAXTER\001-378.SMP

Started: 12/6/2012 2:31:30PM Analysis Adsorptive: N2
Completed: 12/7/2012 7:59:31AM Analysis Bath: 77.24 K
Report Time: 12/10/2012 10:26:26AM Thermal Correction: No
Sample Weight: 0.0523 g Smoothed Pressures: No
Warm Freespace: 27.9696 cm^3 MEASURED Cold Freespace: 89.4856 cm^3
Equil. Interval: 25 secs Low Pressure Dose: 10.00 cm^3/g STP

Analysis Log

Relative Pressure	Pressure (mmHg)	Vol Adsorbed (cm^3/g STP)	Elapsed Time (HR:MN)	Saturation Press.(mmHg)
0.305814191	229.58093	244.3616	16:48	
0.251656958	188.92400	239.0122	17:25	
0.195456378	146.73308	233.0233	17:30	

Sample: 5x16 8001-9 (powder carbon)
Operator: csm
File Name: C:\...\BAXTER\001-378.SMP

Started: 12/6/2012 2:31:30PM Analysis Adsorptive: N2
Completed: 12/7/2012 7:59:31AM Analysis Bath: 77.24 K
Report Time: 12/10/2012 10:26:26AM Thermal Correction: No
Sample Weight: 0.0523 g Smoothed Pressures: No
Warm Freespace: 27.9696 cm³ MEASURED Cold Freespace: 89.4856 cm³
Equil. Interval: 25 secs Low Pressure Dose: 10.00 cm³/g STP

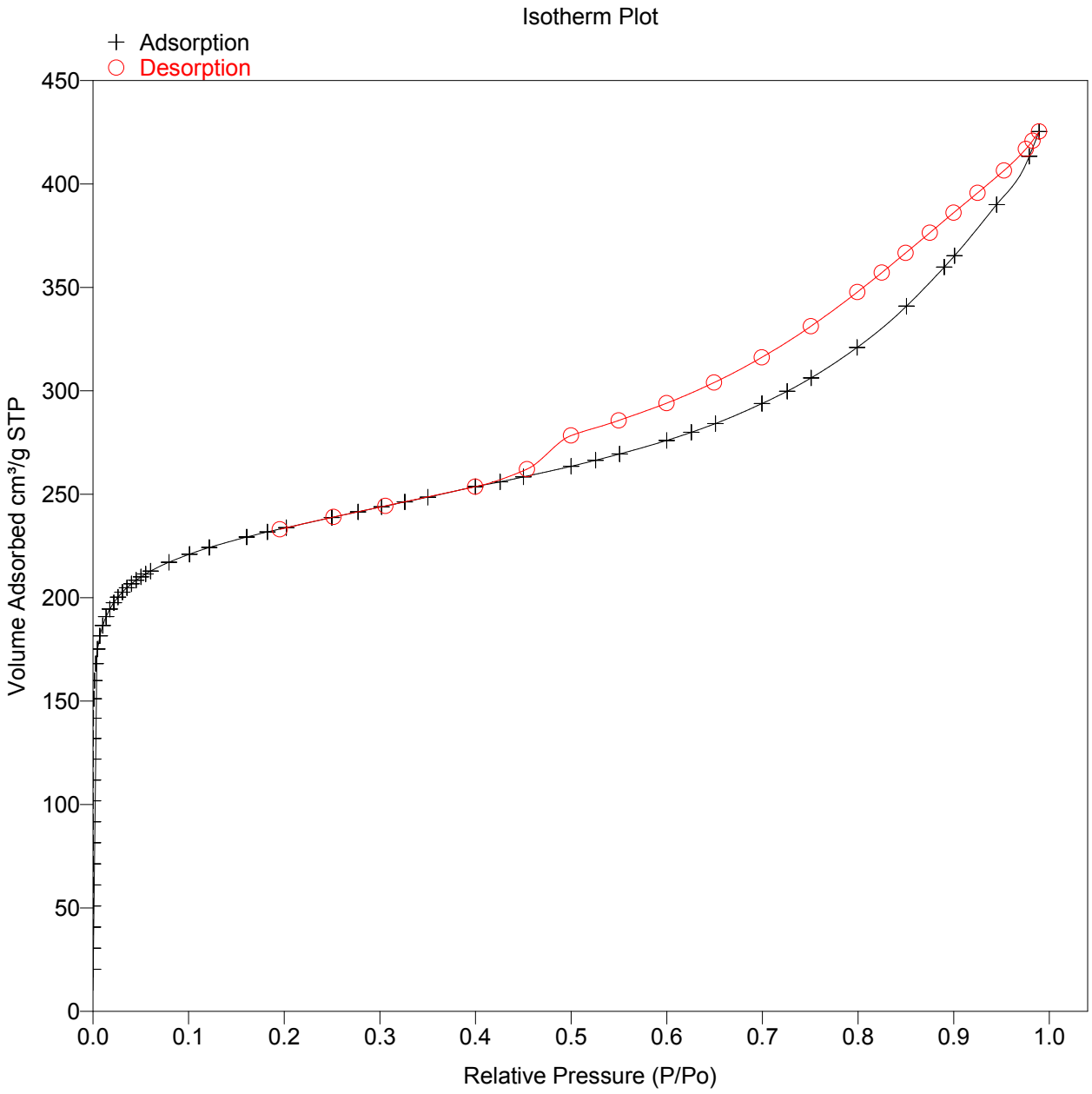

Sample: 5x16 8001-9 (powder carbon)
Operator: csm
File Name: C:\...\BAXTER\001-378.SMP

Started: 12/6/2012 2:31:30PM Analysis Adsorptive: N2
Completed: 12/7/2012 7:59:31AM Analysis Bath: 77.24 K
Report Time: 12/10/2012 10:26:26AM Thermal Correction: No
Sample Weight: 0.0523 g Smoothed Pressures: No
Warm Freespace: 27.9696 cm³ MEASURED Cold Freespace: 89.4856 cm³
Equil. Interval: 25 secs Low Pressure Dose: 10.00 cm³/g STP

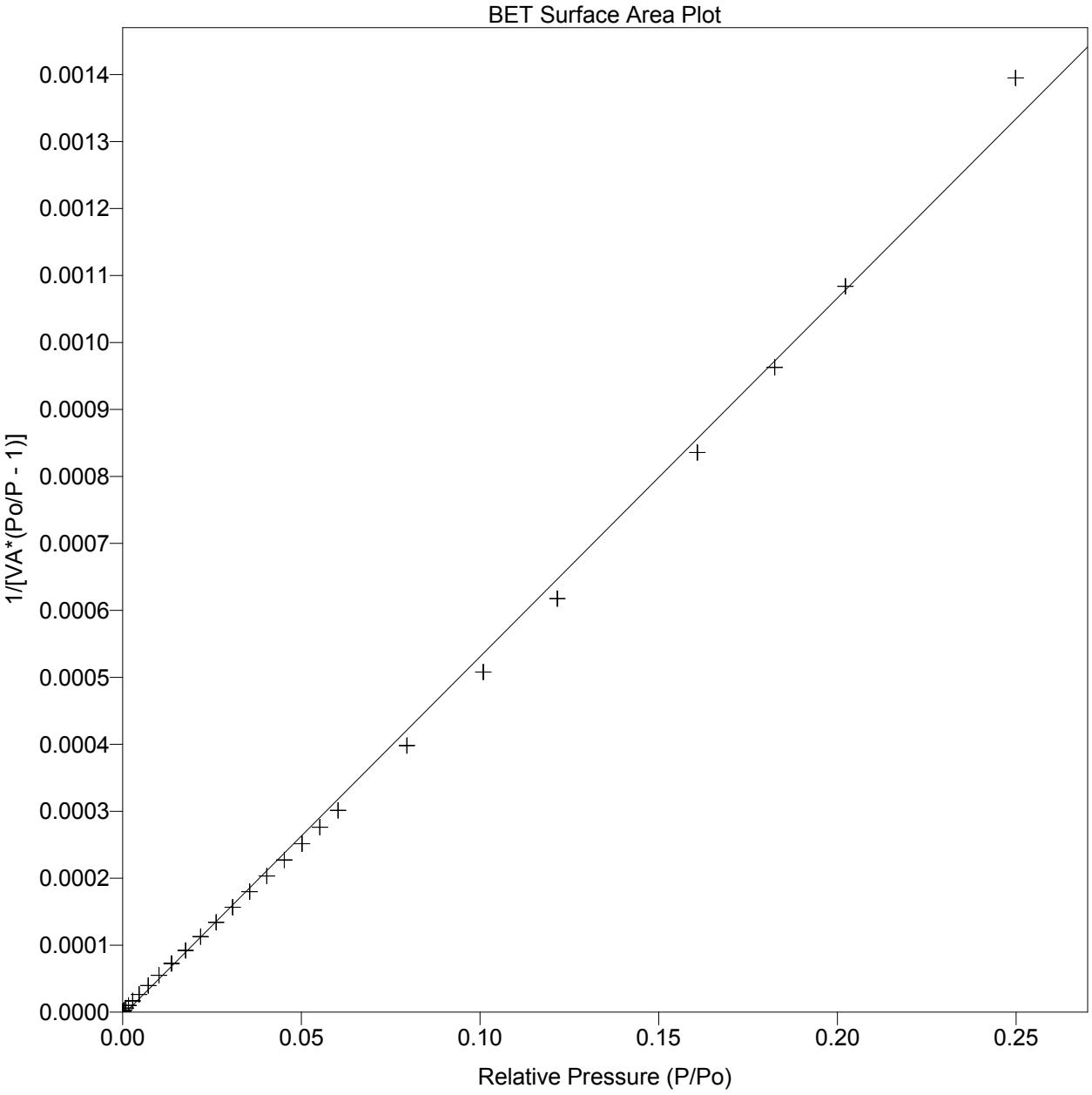

Sample: 5x16 8001-9 (powder carbon)
Operator: csm
File Name: C:\...\BAXTER\001-378.SMP

Started: 12/6/2012 2:31:30PM Analysis Adsorptive: N2
Completed: 12/7/2012 7:59:31AM Analysis Bath: 77.24 K
Report Time: 12/10/2012 10:26:26AM Thermal Correction: No
Sample Weight: 0.0523 g Smoothed Pressures: No
Warm Freespace: 27.9696 cm³ MEASURED Cold Freespace: 89.4856 cm³
Equil. Interval: 25 secs Low Pressure Dose: 10.00 cm³/g STP

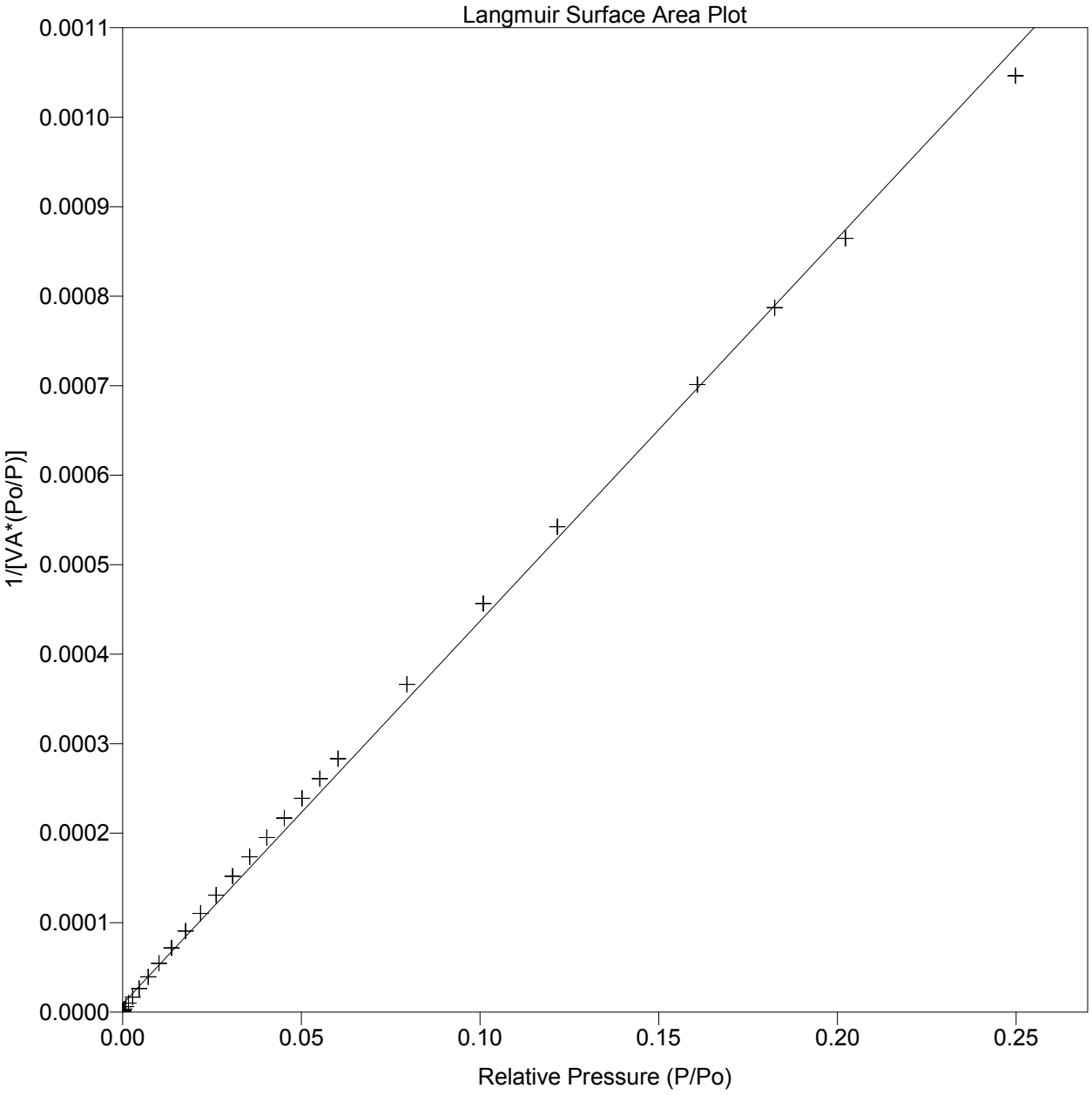

Sample: 5x16 8001-9 (powder carbon)
Operator: csm
File Name: C:\...\BAXTER\001-378.SMP

Started: 12/6/2012 2:31:30PM Analysis Adsorptive: N2
Completed: 12/7/2012 7:59:31AM Analysis Bath: 77.24 K
Report Time: 12/10/2012 10:26:26AM Thermal Correction: No
Sample Weight: 0.0523 g Smoothed Pressures: No
Warm Freespace: 27.9696 cm³ MEASURED Cold Freespace: 89.4856 cm³
Equil. Interval: 25 secs Low Pressure Dose: 10.00 cm³/g STP

---

t-Plot Report

Micropore Volume: -0.009613 cm³/g
Micropore Area: -139.9449 m²/g
External Surface Area: 953.3490 m²/g
Slope: 61.633630 ± 5.192782
Y-Intercept: -6.214969 ± 15.000108
Correlation Coefficient: 8.92450e-01
Thickness Range: 0.1500 to 0.5000 nm

t = [13.9900 / (0.0340 - log(P/Po))] 0.5000

Surface Area Correction Factor: 1.00
Density Conversion Factor: 0.001547
Total Surface Area (by BET): 813.4041

Relative Pressure	Statistical Thickness (nm)	Vol Adsorbed (cm³/g)
0.000000921	0.1518	20.3817
0.000001957	0.1561	30.5723
0.000003081	0.1588	40.7643
0.000004442	0.1612	50.9562
0.000006385	0.1636	61.1451
0.000009706	0.1665	71.3331
0.000015336	0.1699	81.5126
0.000024968	0.1737	91.6679
0.000042018	0.1781	101.7879
0.000073803	0.1833	111.8468
0.000135760	0.1894	121.9465
0.000256930	0.1965	131.9413
0.000490550	0.2046	141.7259
0.000924595	0.2135	151.1238
0.001628265	0.2226	159.9636
0.002825378	0.2327	168.1207
0.004616810	0.2430	175.1817
0.007173338	0.2534	181.5415
0.010176288	0.2628	186.5597
0.013709269	0.2716	190.8460
0.017628738	0.2797	194.4953
0.021806251	0.2873	197.5980
0.026180584	0.2942	200.2868
0.030778221	0.3008	202.6729
0.035542688	0.3071	204.8255
0.040327733	0.3130	206.7365
0.045232835	0.3186	208.4688
0.050194240	0.3239	210.0455

Sample: 5x16 8001-9 (powder carbon)
Operator: csm
File Name: C:\...\BAXTER\001-378.SMP

Started: 12/6/2012 2:31:30PM Analysis Adsorptive: N2
Completed: 12/7/2012 7:59:31AM Analysis Bath: 77.24 K
Report Time: 12/10/2012 10:26:26AM Thermal Correction: No
Sample Weight: 0.0523 g Smoothed Pressures: No
Warm Freespace: 27.9696 cm^3 MEASURED Cold Freespace: 89.4856 cm^3
Equil. Interval: 25 secs Low Pressure Dose: 10.00 cm^3/g STP

---

t-Plot Report

Relative Pressure	Statistical Thickness (nm)	Vol Adsorbed (cm^3/g)
0.055193147	0.3290	211.4858
0.060279595	0.3340	212.8454
0.079555728	0.3513	217.1521
0.100919580	0.3685	221.0205
0.121653365	0.3840	224.2805
0.160812762	0.4111	229.3173
0.182462536	0.4255	231.8146
0.202237206	0.4383	233.8902
0.249853770	0.4689	238.7777
0.277153882	0.4864	241.5208
0.301812538	0.5024	243.9366
0.326044444	0.5183	246.2850
0.350228041	0.5345	248.6169
0.399875587	0.5690	253.7061
0.425770665	0.5879	255.9991
0.450137058	0.6062	258.4024
0.499930504	0.6461	263.5288
0.525562773	0.6682	266.4454
0.550682379	0.6909	269.4855
0.599926664	0.7394	276.0224
0.625758552	0.7673	279.9899
0.650896535	0.7966	284.1908

Sample: 5x16 8001-9 (powder carbon)
Operator: csm
File Name: C:\...\BAXTER\001-378.SMP

Started: 12/6/2012 2:31:30PM Analysis Adsorptive: N2
Completed: 12/7/2012 7:59:31AM Analysis Bath: 77.24 K
Report Time: 12/10/2012 10:26:26AM Thermal Correction: No
Sample Weight: 0.0523 g Smoothed Pressures: No
Warm Freespace: 27.9696 cm³ MEASURED Cold Freespace: 89.4856 cm³
Equil. Interval: 25 secs Low Pressure Dose: 10.00 cm³/g STP

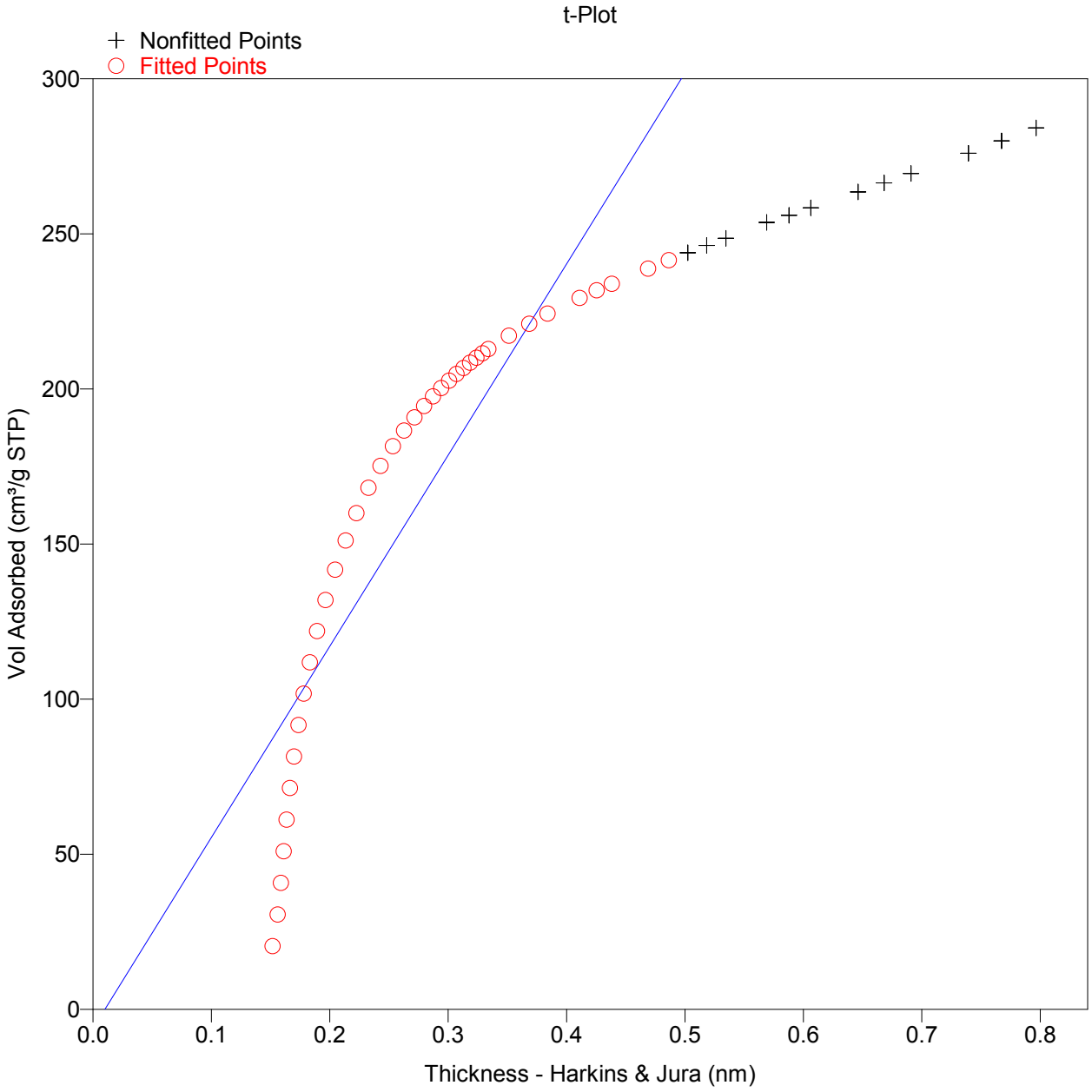

Sample: 5x16 8001-9 (powder carbon)
Operator: csm
File Name: C:\...\BAXTER\001-378.SMP

Started: 12/6/2012 2:31:30PM Analysis Adsorptive: N2
Completed: 12/7/2012 7:59:31AM Analysis Bath: 77.24 K
Report Time: 12/10/2012 10:26:26AM Thermal Correction: No
Sample Weight: 0.0523 g Smoothed Pressures: No
Warm Freespace: 27.9696 cm³ MEASURED Cold Freespace: 89.4856 cm³
Equil. Interval: 25 secs Low Pressure Dose: 10.00 cm³/g STP

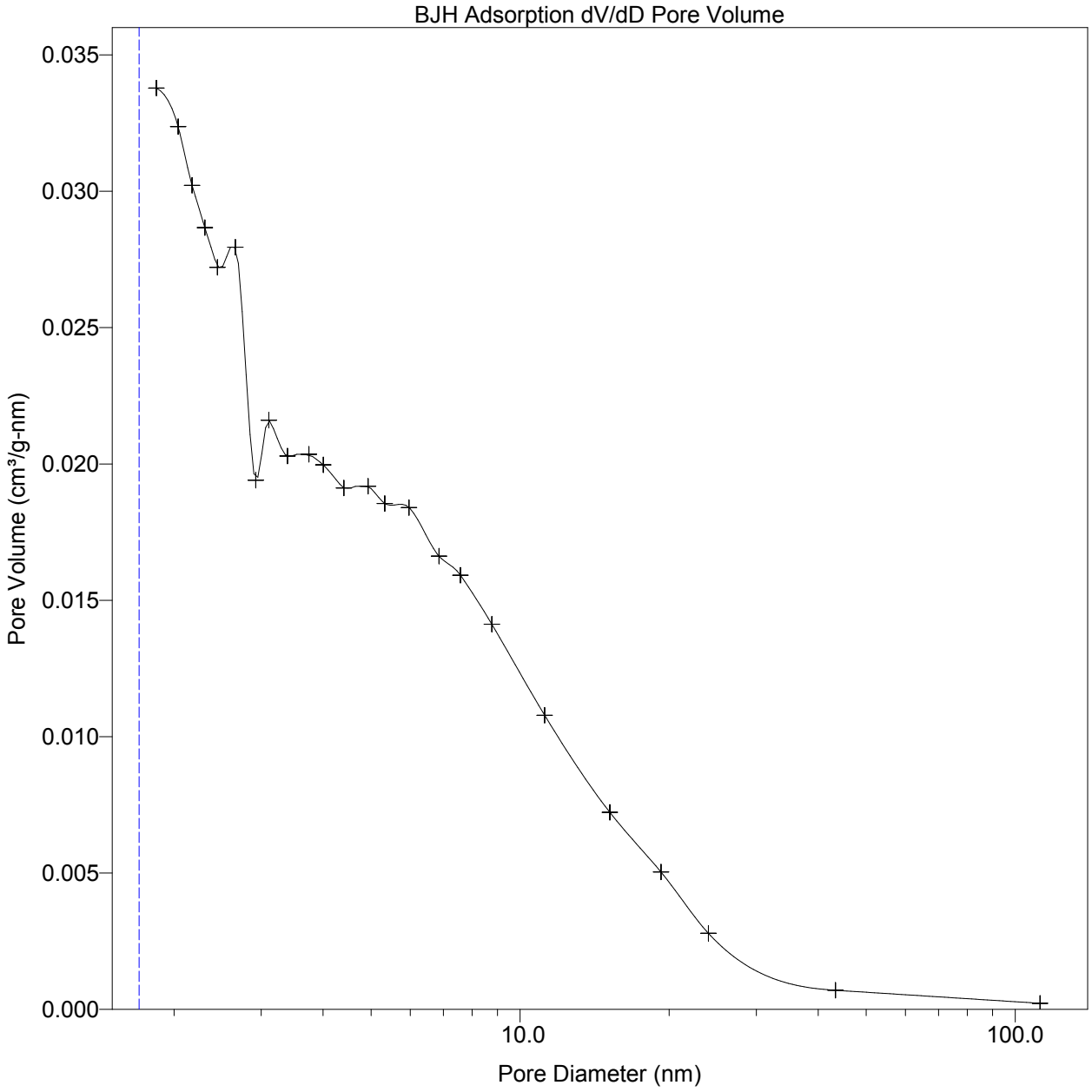

Sample: 5x16 8001-9 (powder carbon)
Operator: csm
File Name: C:\...\BAXTER\001-378.SMP

Started: 12/6/2012 2:31:30PM Analysis Adsorptive: N2
Completed: 12/7/2012 7:59:31AM Analysis Bath: 77.24 K
Report Time: 12/10/2012 10:26:26AM Thermal Correction: No
Sample Weight: 0.0523 g Smoothed Pressures: No
Warm Freespace: 27.9696 cm³ MEASURED Cold Freespace: 89.4856 cm³
Equil. Interval: 25 secs Low Pressure Dose: 10.00 cm³/g STP

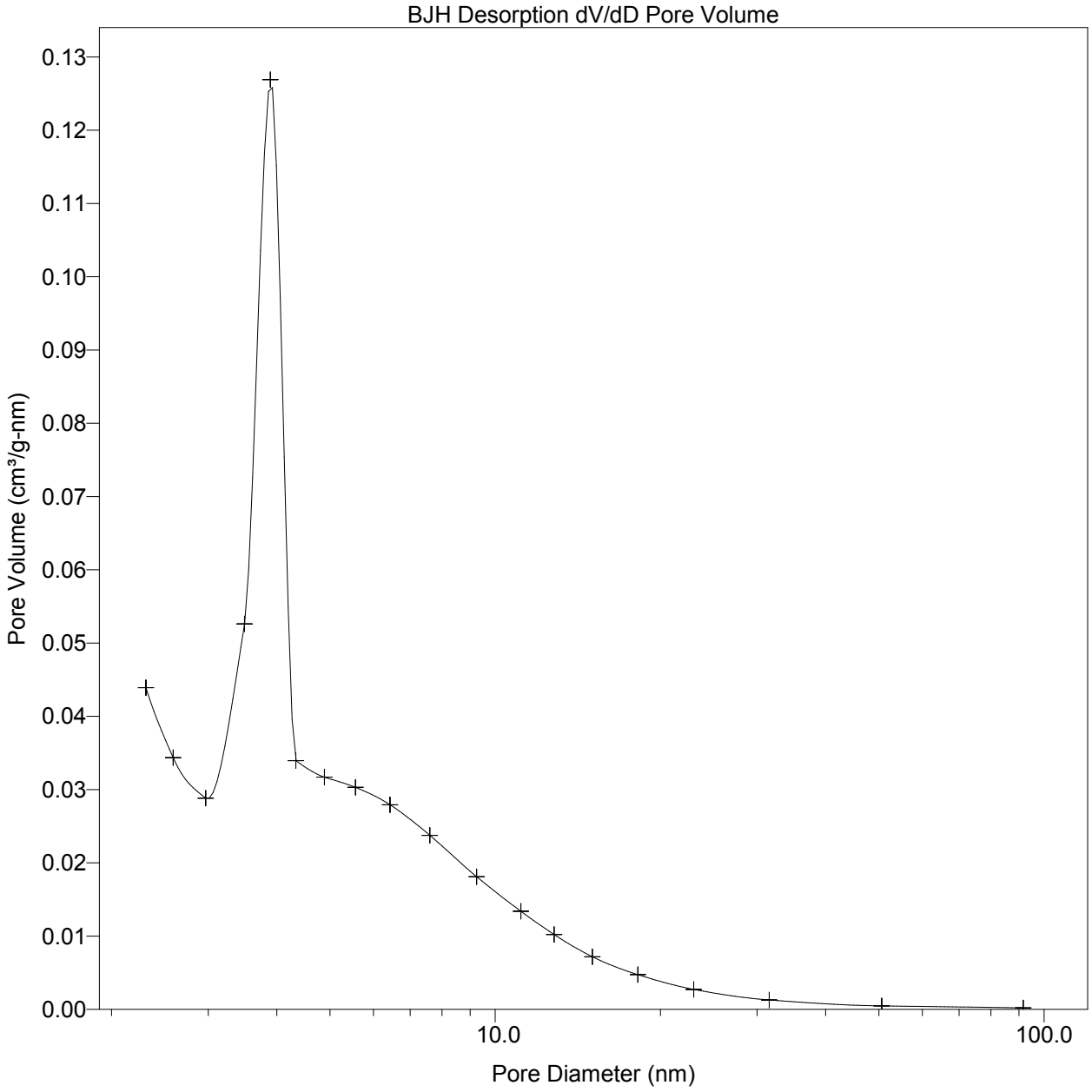

Sample: 5x16 8001-9 (powder carbon)
Operator: csm
File Name: C:\...\BAXTER\001-378.SMP

Started: 12/6/2012 2:31:30PM Analysis Adsorptive: N2
Completed: 12/7/2012 7:59:31AM Analysis Bath: 77.24 K
Report Time: 12/10/2012 10:26:26AM Thermal Correction: No
Sample Weight: 0.0523 g Smoothed Pressures: No
Warm Freespace: 27.9696 cm³ MEASURED Cold Freespace: 89.4856 cm³
Equil. Interval: 25 secs Low Pressure Dose: 10.00 cm³/g STP

Horvath-Kawazoe Report
Cylinder Pore Geometry (Saito/Foley)

Maximum Pore Volume:		0.439586 cm³/g
at Relative Pressure:		0.650896535
Median Pore Diameter:		1.2 nm
Relative Pressure Range:	9.210540E-07 to	0.999999881
Diameter of Adsorptive Molecule:		0.3000 nm
Diameter of Sample Atom:		0.3400 nm
Interaction Parameter:		3.73e-43 ergs-cm4
Density Conversion Factor:		0.001547

Absolute Pressure (mmHg)	Relative Pressure	Volume Adsorbed (cm³/g STP)	Pore Diameter (nm)	Cumulative Pore Volume (cm³/g)	Differential Pore Volume (cm³/g-nm)
0.00000	0.000000921	20.3817	0.7	0.0315	0.0425
0.00069	0.000001957	30.5723	0.8	0.0473	0.5202
0.00147	0.000003081	40.7643	0.8	0.0631	0.7961
0.00232	0.000004442	50.9562	0.8	0.0788	0.9344
0.00334	0.000006385	61.1451	0.8	0.0946	0.8905
0.00480	0.000009706	71.3331	0.8	0.1103	0.7261
0.00730	0.000015336	81.5126	0.9	0.1261	0.6219
0.01153	0.000024968	91.6679	0.9	0.1418	0.5392
0.01877	0.000042018	101.7879	0.9	0.1574	0.4596
0.03158	0.000073803	111.8468	1.0	0.1730	0.3831
0.05548	0.000135760	121.9465	1.0	0.1886	0.3170
0.10205	0.000256930	131.9413	1.1	0.2041	0.2630
0.19313	0.000490550	141.7259	1.2	0.2192	0.2193
0.36873	0.000924595	151.1238	1.2	0.2338	0.1835
0.69497	0.001628265	159.9636	1.3	0.2474	0.1639
1.22387	0.002825378	168.1207	1.4	0.2600	0.1319
2.12364	0.004616810	175.1817	1.5	0.2710	0.1080
3.47010	0.007173338	181.5415	1.6	0.2808	0.0918
5.39072	0.010176288	186.5597	1.7	0.2886	0.0782
7.64597	0.013709269	190.8460	1.8	0.2952	0.0685
10.29855	0.017628738	194.4953	1.9	0.3008	0.0610
13.24068	0.021806251	197.5980	2.0	0.3056	0.0548
16.37560	0.026180584	200.2868	2.1	0.3098	0.0500
19.65767	0.030778221	202.6729	2.2	0.3135	0.0456
23.10642	0.035542688	204.8255	2.2	0.3168	0.0429
26.67938	0.040327733	206.7365	2.3	0.3198	0.0395
30.26674	0.045232835	208.4688	2.4	0.3225	0.0366
33.94314	0.050194240	210.0455	2.5	0.3249	0.0345
37.66150	0.055193147	211.4858	2.5	0.3271	0.0324

Sample: 5x16 8001-9 (powder carbon)
Operator: csm
File Name: C:\...\BAXTER\001-378.SMP

Started: 12/6/2012 2:31:30PM Analysis Adsorptive: N2
Completed: 12/7/2012 7:59:31AM Analysis Bath: 77.24 K
Report Time: 12/10/2012 10:26:26AM Thermal Correction: No
Sample Weight: 0.0523 g Smoothed Pressures: No
Warm Freespace: 27.9696 cm^3 MEASURED Cold Freespace: 89.4856 cm^3
Equil. Interval: 25 secs Low Pressure Dose: 10.00 cm^3/g STP

Horvath-Kawazoe Report
Cylinder Pore Geometry (Saito/Foley)

Absolute Pressure (mmHg)	Relative Pressure	Volume Adsorbed (cm^3/g STP)	Pore Diameter (nm)	Cumulative Pore Volume (cm^3/g)	Differential Pore Volume (cm^3/g-nm)
41.40618	0.060279595	212.8454	2.6	0.3292	0.0310
45.21543	0.079555728	217.1521	2.8	0.3359	0.0273
59.66687	0.100919580	221.0205	3.1	0.3419	0.0232
75.68185	0.121653365	224.2805	3.3	0.3469	0.0210
91.21911	0.160812762	229.3173	3.8	0.3547	0.0171
120.56676	0.182462536	231.8146	4.0	0.3586	0.0151
136.78557	0.202237206	233.8902	4.3	0.3618	0.0133
151.60057	0.249853770	238.7777	4.9	0.3693	0.0120
187.28516	0.277153882	241.5208	5.3	0.3736	0.0108
207.73807	0.301812538	243.9366	5.7	0.3773	0.0094
226.20677	0.326044444	246.2850	6.1	0.3810	0.0088
244.35588	0.350228041	248.6169	6.6	0.3846	0.0080
262.46692	0.399875587	253.7061	7.6	0.3924	0.0077
299.65515	0.425770665	255.9991	8.2	0.3960	0.0061
319.04376	0.450137058	258.4024	8.7	0.3997	0.0066
337.28494	0.499930504	263.5288	9.9	0.4076	0.0065
374.57175	0.525562773	266.4454	10.6	0.4121	0.0069
393.75641	0.550682379	269.4855	11.3	0.4168	0.0072
412.55502	0.599926664	276.0224	12.7	0.4270	0.0073
449.41965	0.625758552	279.9899	13.4	0.4331	0.0083
468.74683	0.650896535	284.1908	14.2	0.4396	0.0083

Sample: 5x16 8001-9 (powder carbon)
Operator: csm
File Name: C:\...\BAXTER\001-378.SMP

Started: 12/6/2012 2:31:30PM Analysis Adsorptive: N2
Completed: 12/7/2012 7:59:31AM Analysis Bath: 77.24 K
Report Time: 12/10/2012 10:26:26AM Thermal Correction: No
Sample Weight: 0.0523 g Smoothed Pressures: No
Warm Freespace: 27.9696 cm³ MEASURED Cold Freespace: 89.4856 cm³
Equil. Interval: 25 secs Low Pressure Dose: 10.00 cm³/g STP

Horvath-Kawazoe Differential Pore Volume Plot
Cylinder Pore Geometry (Saito/Foley)

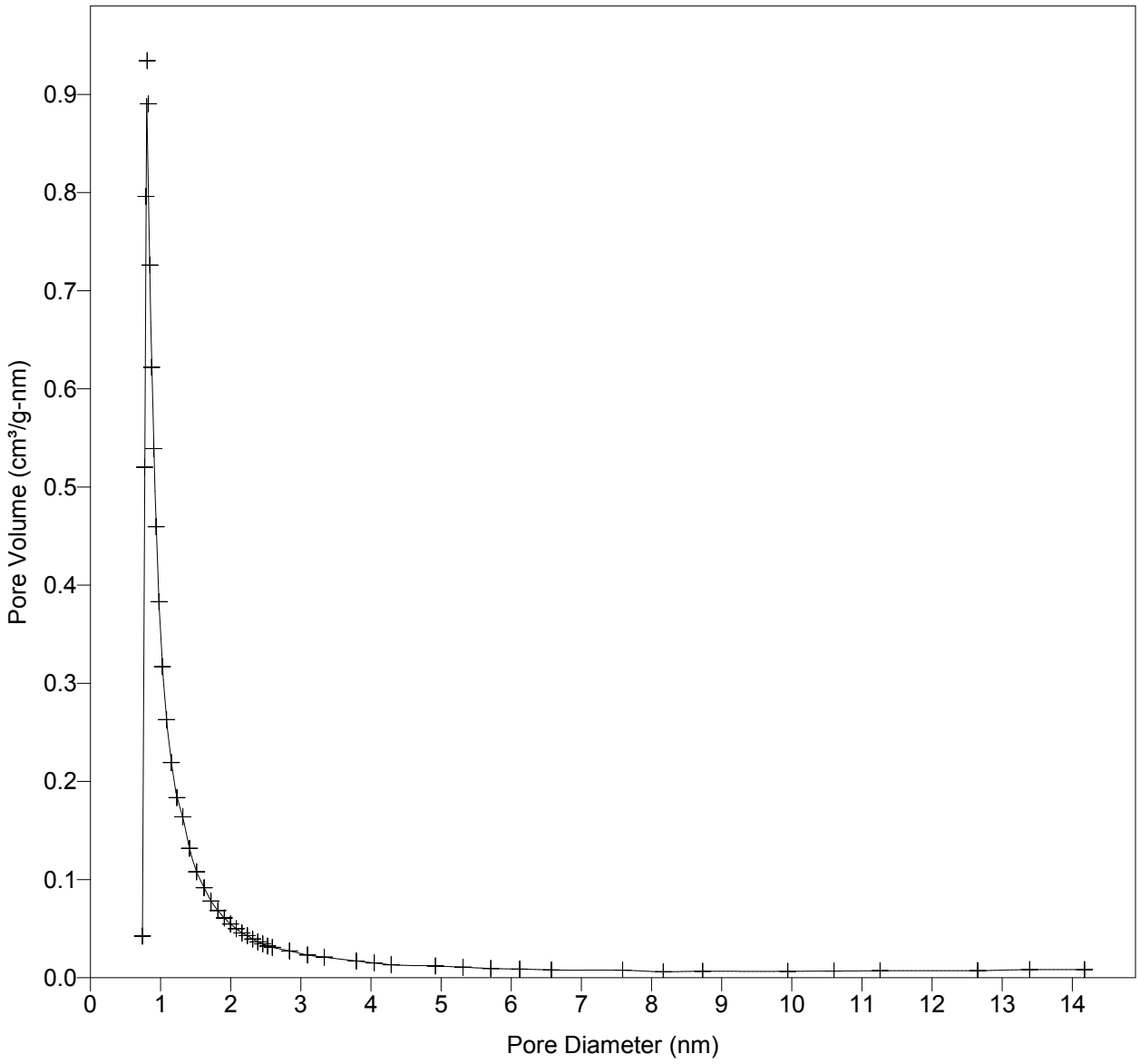

Sample: 5x16 8001-9 (powder carbon)
Operator: csm
File Name: C:\...\BAXTER\001-378.SMP

Started: 12/6/2012 2:31:30PM Analysis Adsorptive: N2
Completed: 12/7/2012 7:59:31AM Analysis Bath: 77.24 K
Report Time: 12/10/2012 10:26:26AM Thermal Correction: No
Sample Weight: 0.0523 g Smoothed Pressures: No
Warm Freespace: 27.9696 cm^3 MEASURED Cold Freespace: 89.4856 cm^3
Equil. Interval: 25 secs Low Pressure Dose: 10.00 cm^3/g STP

Summary Report

Area

Single Point Surface Area at P/Po 0.24985377 :	779.7372	m^2/g
BET Surface Area:	813.4041	m^2/g
Langmuir Surface Area:	1017.5395	m^2/g
Micropore Area:	-139.9449	m^2/g
External Surface Area:	953.3490	m^2/g
BJH Adsorption Cumulative Surface Area of pores between 1.700000 and 300.000000 nm Diameter:	187.6916	m^2/g
BJH Desorption Cumulative Surface Area of pores between 1.700000 and 300.000000 nm Diameter:	263.9949	m^2/g

Volume

Single Point Adsorption Total Pore Volume of pores less than 183.2088 nm Diameter at P/Po 0.98933317:	0.657947	cm^3/g
Micropore Volume:	-0.009613	cm^3/g
BJH Adsorption Cumulative Pore Volume of pores between 1.700000 and 300.000000 nm Diameter:	0.344059	cm^3/g
BJH Desorption Cumulative Pore Volume of pores between 1.700000 and 300.000000 nm Diameter:	0.410161	cm^3/g

Pore Size

Adsorption Average Pore Diameter (4V/A by BET):	3.2355	nm
BJH Adsorption Average Pore Diameter (4V/A):	7.3324	nm
BJH Desorption Average Pore Diameter (4V/A):	6.2147	nm

Horvath-Kawazoe

Sample: 5x16 8001-9 (powder carbon)
Operator: csm
File Name: C:\...\BAXTER\001-378.SMP

Started: 12/6/2012 2:31:30PM Analysis Adsorptive: N2
Completed: 12/7/2012 7:59:31AM Analysis Bath: 77.24 K
Report Time: 12/10/2012 10:26:26AM Thermal Correction: No
Sample Weight: 0.0523 g Smoothed Pressures: No
Warm Freespace: 27.9696 cm^3 MEASURED Cold Freespace: 89.4856 cm^3
Equil. Interval: 25 secs Low Pressure Dose: 10.00 cm^3/g STP

Summary Report

Maximum Pore Volume at Relative Pressure 0.650896535:	0.439586 cm^3/g
Median Pore Diameter:	1.1579 nm

9.4 Granular Norit activated carbon characterization

Sample: Rx3 EXTRA 570104
Operator: CSM
File Name: C:\...\BAXTER\001-379.SMP

Started: 12/7/2012 9:51:52AM Analysis Adsorptive: N2
Completed: 12/8/2012 11:44:07AM Analysis Bath: 77.35 K
Report Time: 12/10/2012 10:28:08AM Thermal Correction: No
Sample Weight: 0.2407 g Smoothed Pressures: No
Warm Freespace: 27.9527 cm³ MEASURED Cold Freespace: 92.4420 cm³
Equil. Interval: 25 secs Low Pressure Dose: 10.00 cm³/g STP

Analysis Log

Relative Pressure	Pressure (mmHg)	Vol Adsorbed (cm³/g STP)	Elapsed Time (HR:MN)	Saturation Press.(mmHg)
			02:19	752.10480
0.000001463	0.00110	10.1282	02:50	
0.000003065	0.00231	20.2559	03:17	
0.000004154	0.00313	30.3842	03:49	
0.000005067	0.00382	40.5126	04:21	
0.000006100	0.00460	50.6407	04:53	
0.000007563	0.00570	60.7691	05:25	
0.000009801	0.00739	70.8971	05:58	
0.000012840	0.00968	81.0250	06:30	
0.000016906	0.01276	91.1527	07:02	
0.000022442	0.01694	101.2797	07:34	
0.000029928	0.02260	111.4061	08:06	
0.000040179	0.03035	121.5304	08:34	
0.000054725	0.04135	131.6525	09:01	
0.000074905	0.05661	141.7725	09:28	
0.000104125	0.07872	151.8888	09:57	
0.000146131	0.11051	162.0009	10:23	
0.000208259	0.15755	172.1053	10:51	
0.000303955	0.23001	182.1968	11:18	
0.000454317	0.34389	192.2668	11:44	
0.000696213	0.52715	202.2999	12:10	
0.001090485	0.82594	212.2705	12:37	
0.001687986	1.27888	222.1648	13:04	
0.002661139	2.01683	231.9221	13:33	
0.004176815	3.16669	241.4623	14:05	
0.006374951	4.83541	250.7119	14:45	
			14:50	758.54401
0.009507148	7.21247	259.8734	15:05	
0.013634377	10.34473	268.8491	15:19	
0.018678863	14.17372	277.3633	15:33	
0.024727956	18.76599	285.5991	15:47	
0.031741508	24.09170	293.4643	16:03	
0.039567451	30.03550	300.8338	16:19	
0.048495453	36.81722	307.9396	16:34	
0.058457509	44.38574	314.6617	16:49	
			16:53	759.30695
0.069420786	52.71960	320.9274	17:07	
0.080228588	60.93707	326.1805	17:22	
0.101984368	77.47482	334.6262	17:38	
0.123558661	93.88134	340.9676	17:55	
0.167021423	126.92663	349.6824	18:11	
0.189218457	143.81358	352.7908	18:23	

Sample: Rx3 EXTRA 570104
Operator: CSM
File Name: C:\...\BAXTER\001-379.SMP

Started: 12/7/2012 9:51:52AM Analysis Adsorptive: N2
Completed: 12/8/2012 11:44:07AM Analysis Bath: 77.35 K
Report Time: 12/10/2012 10:28:08AM Thermal Correction: No
Sample Weight: 0.2407 g Smoothed Pressures: No
Warm Freespace: 27.9527 cm³ MEASURED Cold Freespace: 92.4420 cm³
Equil. Interval: 25 secs Low Pressure Dose: 10.00 cm³/g STP

Analysis Log

Relative Pressure	Pressure (mmHg)	Vol Adsorbed (cm³/g STP)	Elapsed Time (HR:MN)	Saturation Press.(mmHg)
0.210882416	160.29967	355.2878	18:35	
0.251570069	191.25247	358.8836	18:47	
0.280920126	213.58830	360.9528	18:57	
			18:59	760.33313
0.306831035	233.33171	362.5235	19:09	
0.328385394	249.75533	363.6918	19:17	
0.351733681	267.54776	364.8635	19:25	
0.398941648	303.50107	366.9566	19:34	
0.424643986	323.09125	368.0053	19:41	
0.449399573	341.96545	368.9684	19:48	
0.499015728	379.77579	370.8287	19:57	
0.524592691	399.28650	371.7801	20:04	
0.549604264	418.37125	372.6890	20:11	
0.598833938	455.90518	374.4685	20:19	
0.624238167	475.29996	375.4186	20:26	
0.649301150	494.43927	376.3338	20:33	
0.698323923	531.83887	378.1624	20:41	
0.723943859	551.41345	379.1620	20:48	
0.748857428	570.44513	380.1388	20:54	
0.797551087	607.62640	382.2090	21:03	
			21:05	761.88989
0.847581525	645.85687	384.7924	21:13	
0.898891960	685.07880	388.5215	21:23	
0.952769813	726.38959	395.6467	21:42	
0.978299837	746.06848	402.8572	21:58	
0.990059635	755.25415	409.0609	22:14	
0.965662286	736.78876	405.9712	22:25	
0.936113984	714.37225	402.5455	22:35	
0.908577116	693.45795	400.5076	22:43	
0.882303378	673.48969	399.1439	22:50	
0.856703348	654.03070	398.0704	22:57	
0.848709480	647.99786	397.7248	23:03	
0.822359519	627.94714	396.9028	23:09	
			23:11	763.61945
0.798570148	609.83081	396.2040	23:17	
0.750044567	572.80804	394.9442	23:25	
0.700210366	534.78143	393.7888	23:33	
0.649859814	496.35593	392.6928	23:41	
0.599898102	458.22287	391.6260	23:49	
0.549862012	420.02847	390.5233	23:57	
0.500730933	382.60309	385.2645	24:34	
0.447984687	342.37631	369.8990	25:04	

Sample: Rx3 EXTRA 570104
Operator: CSM
File Name: C:\...\BAXTER\001-379.SMP

Started: 12/7/2012 9:51:52AM Analysis Adsorptive: N2
Completed: 12/8/2012 11:44:07AM Analysis Bath: 77.35 K
Report Time: 12/10/2012 10:28:08AM Thermal Correction: No
Sample Weight: 0.2407 g Smoothed Pressures: No
Warm Freespace: 27.9527 cm^3 MEASURED Cold Freespace: 92.4420 cm^3
Equil. Interval: 25 secs Low Pressure Dose: 10.00 cm^3/g STP

Analysis Log

Relative Pressure	Pressure (mmHg)	Vol Adsorbed (cm^3/g STP)	Elapsed Time (HR:MN)	Saturation Press.(mmHg)
0.400286509	305.94974	366.7104	25:16	
			25:18	764.33820
0.299028074	228.55858	361.6182	25:29	
0.254402169	194.44930	358.5966	25:41	
0.196131041	149.91045	353.0441	25:55	

Sample: Rx3 EXTRA 570104
Operator: CSM
File Name: C:\...\BAXTER\001-379.SMP

Started: 12/7/2012 9:51:52AM Analysis Adsorptive: N2
Completed: 12/8/2012 11:44:07AM Analysis Bath: 77.35 K
Report Time: 12/10/2012 10:28:08AM Thermal Correction: No
Sample Weight: 0.2407 g Smoothed Pressures: No
Warm Freespace: 27.9527 cm³ MEASURED Cold Freespace: 92.4420 cm³
Equil. Interval: 25 secs Low Pressure Dose: 10.00 cm³/g STP

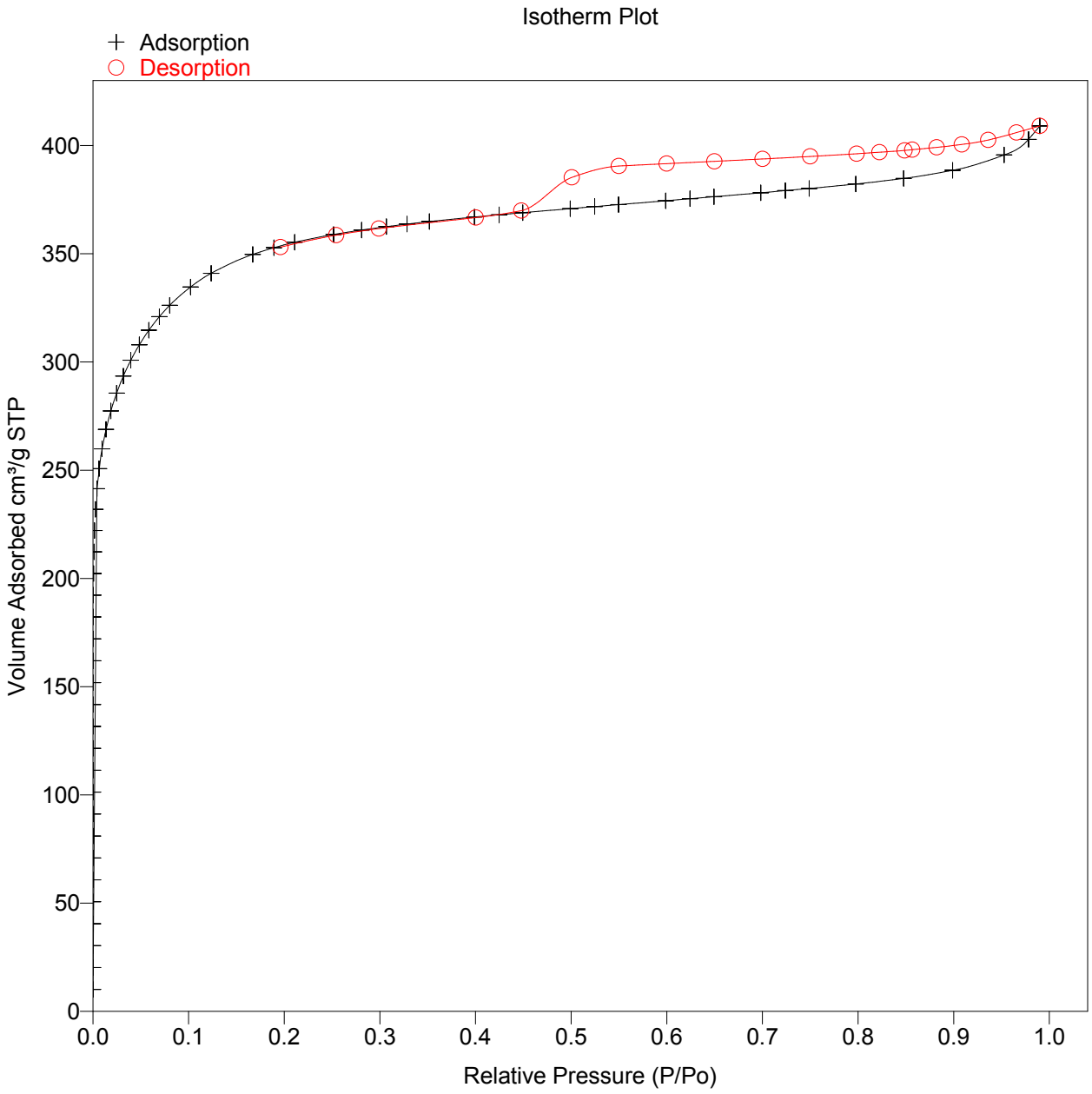

Sample: Rx3 EXTRA 570104
Operator: CSM
File Name: C:\...\BAXTER\001-379.SMP

Started: 12/7/2012 9:51:52AM Analysis Adsorptive: N2
Completed: 12/8/2012 11:44:07AM Analysis Bath: 77.35 K
Report Time: 12/10/2012 10:28:08AM Thermal Correction: No
Sample Weight: 0.2407 g Smoothed Pressures: No
Warm Freespace: 27.9527 cm³ MEASURED Cold Freespace: 92.4420 cm³
Equil. Interval: 25 secs Low Pressure Dose: 10.00 cm³/g STP

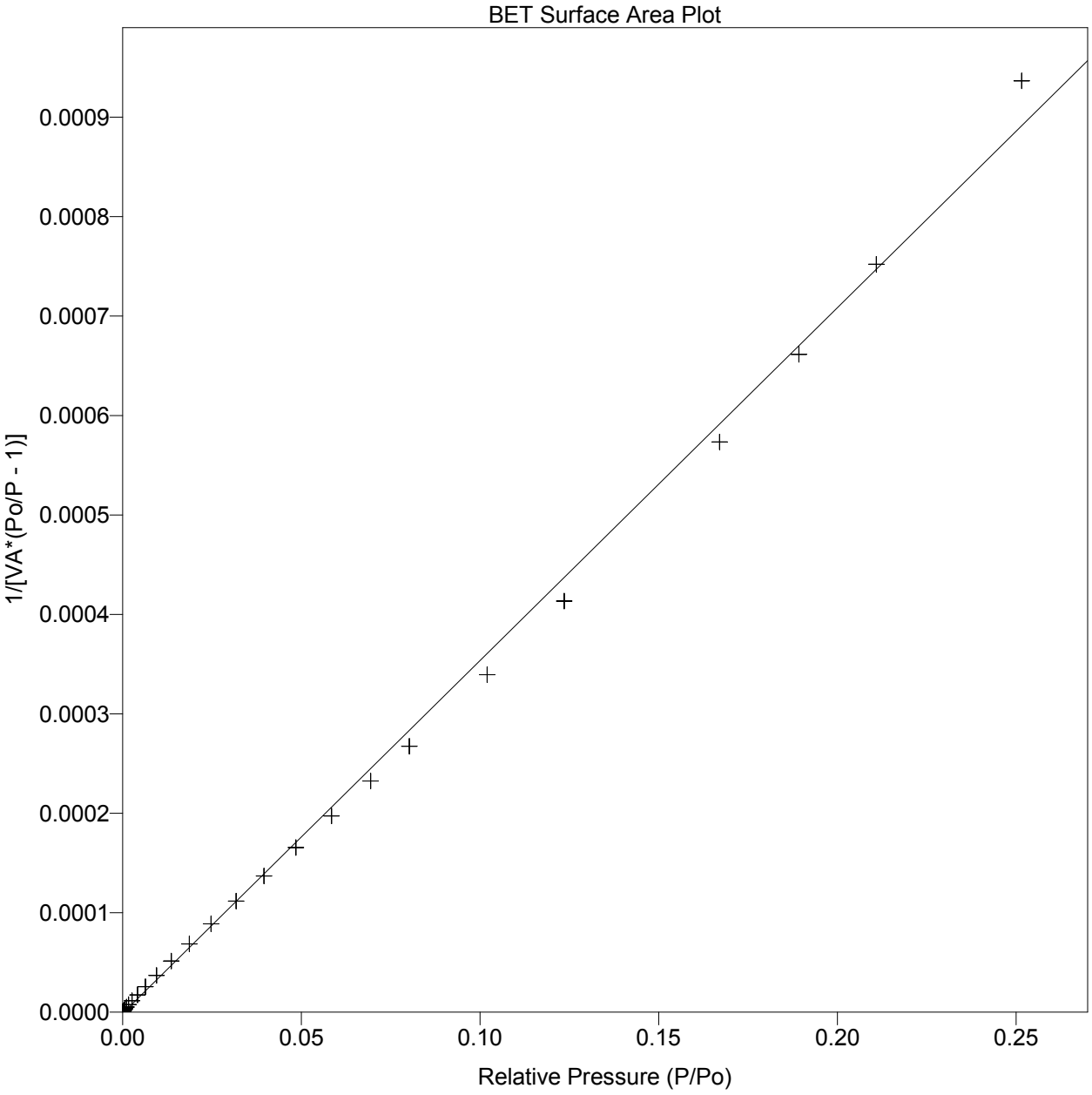

Sample: Rx3 EXTRA 570104
Operator: CSM
File Name: C:\...\BAXTER\001-379.SMP

Started: 12/7/2012 9:51:52AM Analysis Adsorptive: N2
Completed: 12/8/2012 11:44:07AM Analysis Bath: 77.35 K
Report Time: 12/10/2012 10:28:08AM Thermal Correction: No
Sample Weight: 0.2407 g Smoothed Pressures: No
Warm Freespace: 27.9527 cm³ MEASURED Cold Freespace: 92.4420 cm³
Equil. Interval: 25 secs Low Pressure Dose: 10.00 cm³/g STP

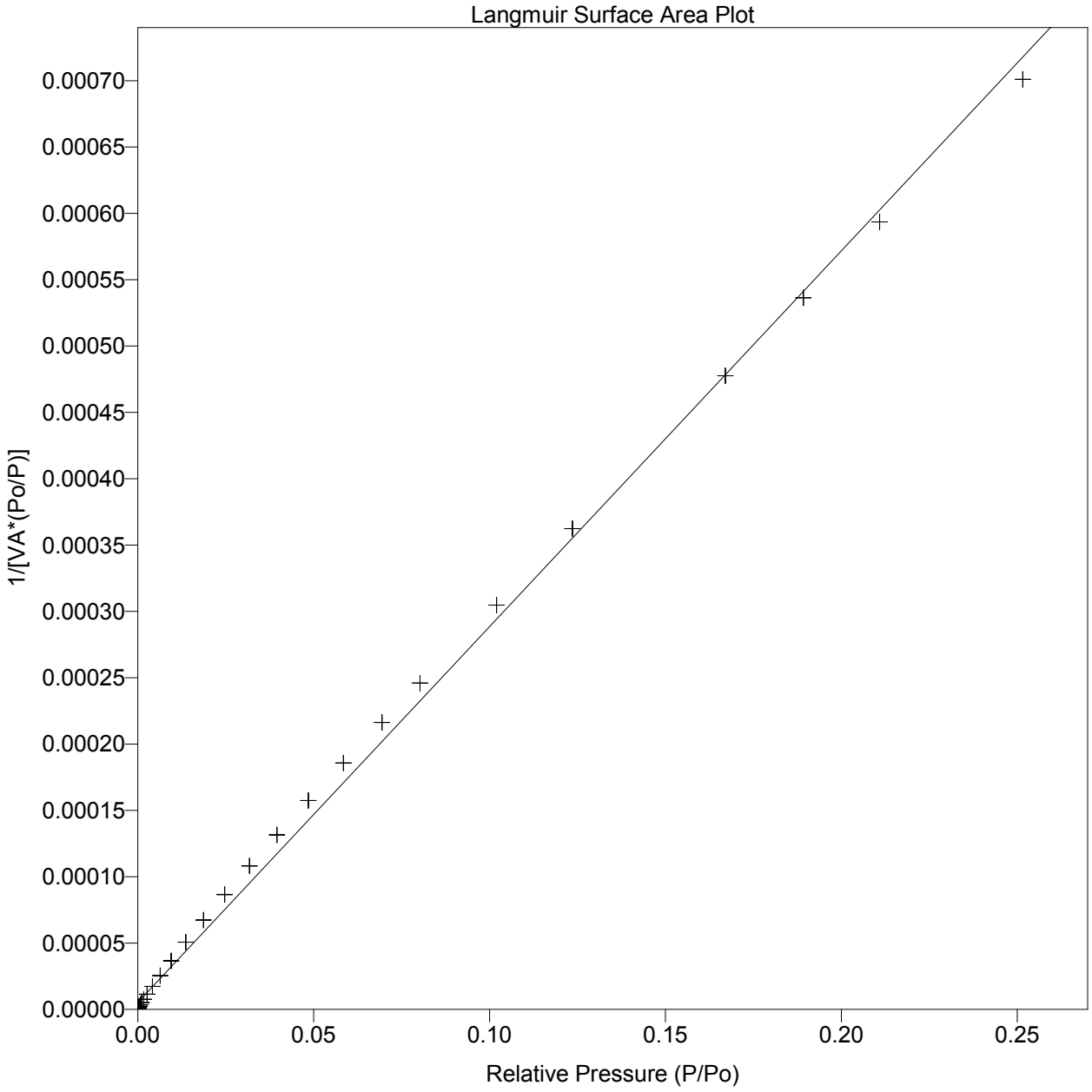

Sample: Rx3 EXTRA 570104
Operator: CSM
File Name: C:\...\BAXTER\001-379.SMP

Started: 12/7/2012 9:51:52AM Analysis Adsorptive: N2
Completed: 12/8/2012 11:44:07AM Analysis Bath: 77.35 K
Report Time: 12/10/2012 10:28:08AM Thermal Correction: No
Sample Weight: 0.2407 g Smoothed Pressures: No
Warm Freespace: 27.9527 cm³ MEASURED Cold Freespace: 92.4420 cm³
Equil. Interval: 25 secs Low Pressure Dose: 10.00 cm³/g STP

---

t-Plot Report

Micropore Volume: -0.091133 cm³/g
Micropore Area: -376.1682 m²/g
External Surface Area: 1603.1881 m²/g
Slope: 103.645465 ± 7.445548
Y-Intercept: -58.917222 ± 20.397440
Correlation Coefficient: 9.10439e-01
Thickness Range: 0.1500 to 0.5000 nm

t = [13.9900 / (0.0340 - log(P/Po))] 0.5000

Surface Area Correction Factor: 1.00
Density Conversion Factor: 0.001547
Total Surface Area (by BET): 1227.0198

Relative Pressure	Statistical Thickness (nm)	Vol Adsorbed (cm³/g)
0.000001463	0.1544	10.1282
0.000003065	0.1588	20.2559
0.000004154	0.1607	30.3842
0.000005067	0.1620	40.5126
0.000006100	0.1633	50.6407
0.000007563	0.1647	60.7691
0.000009801	0.1666	70.8971
0.000012840	0.1685	81.0250
0.000016906	0.1706	91.1527
0.000022442	0.1728	101.2797
0.000029928	0.1752	111.4061
0.000040179	0.1777	121.5304
0.000054725	0.1805	131.6525
0.000074905	0.1834	141.7725
0.000104125	0.1866	151.8888
0.000146131	0.1901	162.0009
0.000208259	0.1940	172.1053
0.000303955	0.1985	182.1968
0.000454317	0.2035	192.2668
0.000696213	0.2094	202.2999
0.001090485	0.2161	212.2705
0.001687986	0.2233	222.1648
0.002661139	0.2316	231.9221
0.004176815	0.2408	241.4623
0.006374951	0.2505	250.7119
0.009507148	0.2609	259.8734
0.013634377	0.2714	268.8491
0.018678863	0.2817	277.3633

Sample: Rx3 EXTRA 570104
Operator: CSM
File Name: C:\...\BAXTER\001-379.SMP

Started: 12/7/2012 9:51:52AM Analysis Adsorptive: N2
Completed: 12/8/2012 11:44:07AM Analysis Bath: 77.35 K
Report Time: 12/10/2012 10:28:08AM Thermal Correction: No
Sample Weight: 0.2407 g Smoothed Pressures: No
Warm Freespace: 27.9527 cm³ MEASURED Cold Freespace: 92.4420 cm³
Equil. Interval: 25 secs Low Pressure Dose: 10.00 cm³/g STP

---

t-Plot Report

Relative Pressure	Statistical Thickness (nm)	Vol Adsorbed (cm³/g)
0.024727956	0.2920	285.5991
0.031741508	0.3022	293.4643
0.039567451	0.3121	300.8338
0.048495453	0.3221	307.9396
0.058457509	0.3323	314.6617
0.069420786	0.3425	320.9274
0.080228588	0.3519	326.1805
0.101984368	0.3694	334.6262
0.123558661	0.3853	340.9676
0.167021423	0.4153	349.6824
0.189218457	0.4299	352.7908
0.210882416	0.4439	355.2878
0.251570069	0.4700	358.8836
0.280920126	0.4889	360.9528
0.306831035	0.5057	362.5235
0.328385394	0.5199	363.6918
0.351733681	0.5355	364.8635
0.398941648	0.5684	366.9566
0.424643986	0.5870	368.0053
0.449399573	0.6057	368.9684
0.499015728	0.6454	370.8287
0.524592691	0.6673	371.7801
0.549604264	0.6899	372.6890
0.598833938	0.7382	374.4685
0.624238167	0.7656	375.4186
0.649301150	0.7946	376.3338

Sample: Rx3 EXTRA 570104
Operator: CSM
File Name: C:\...\BAXTER\001-379.SMP

Started: 12/7/2012 9:51:52AM Analysis Adsorptive: N2
Completed: 12/8/2012 11:44:07AM Analysis Bath: 77.35 K
Report Time: 12/10/2012 10:28:08AM Thermal Correction: No
Sample Weight: 0.2407 g Smoothed Pressures: No
Warm Freespace: 27.9527 cm³ MEASURED Cold Freespace: 92.4420 cm³
Equil. Interval: 25 secs Low Pressure Dose: 10.00 cm³/g STP

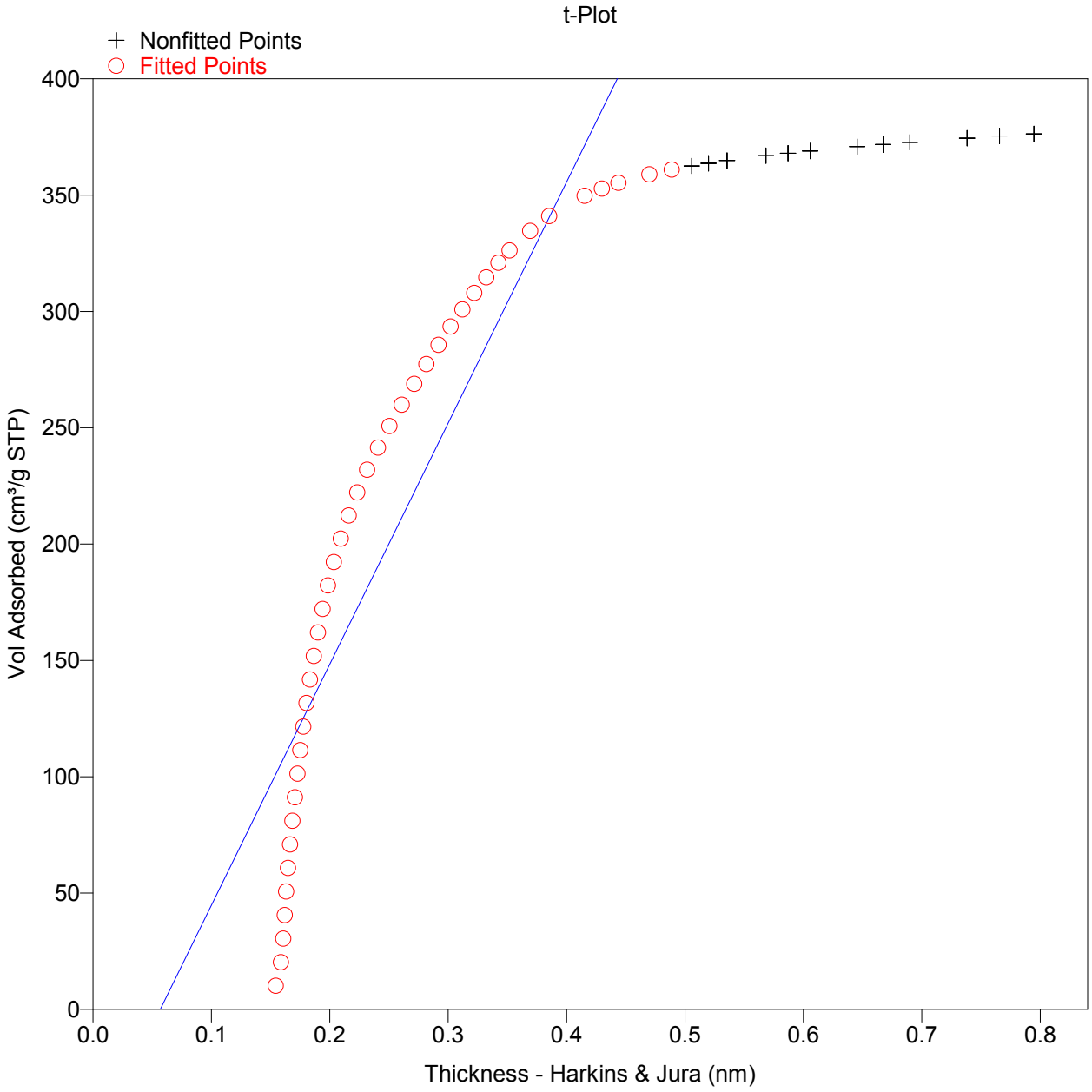

Sample: Rx3 EXTRA 570104
Operator: CSM
File Name: C:\...\BAXTER\001-379.SMP

Started: 12/7/2012 9:51:52AM Analysis Adsorptive: N2
Completed: 12/8/2012 11:44:07AM Analysis Bath: 77.35 K
Report Time: 12/10/2012 10:28:08AM Thermal Correction: No
Sample Weight: 0.2407 g Smoothed Pressures: No
Warm Freespace: 27.9527 cm³ MEASURED Cold Freespace: 92.4420 cm³
Equil. Interval: 25 secs Low Pressure Dose: 10.00 cm³/g STP

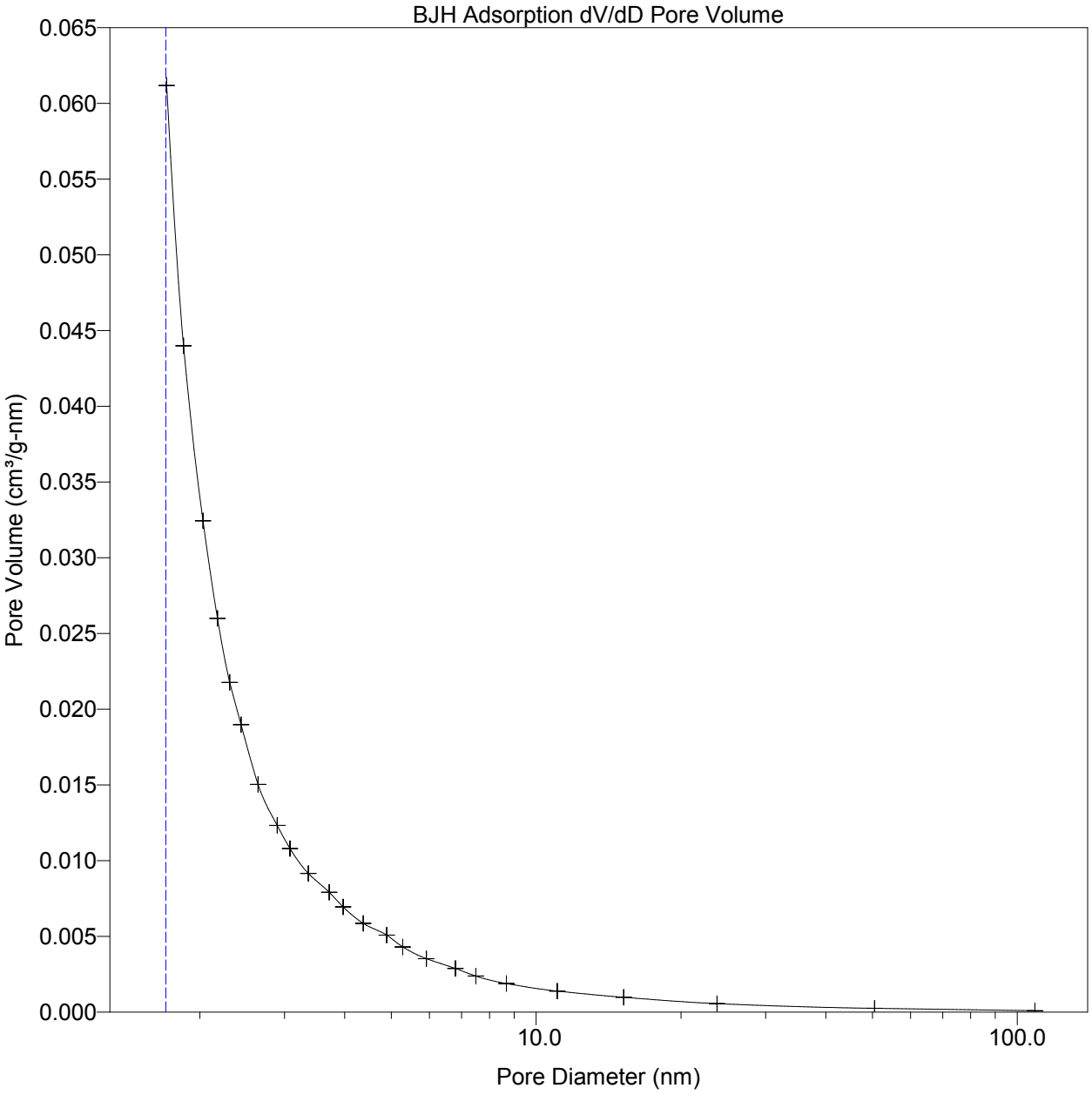

Sample: Rx3 EXTRA 570104
Operator: CSM
File Name: C:\...\BAXTER\001-379.SMP

Started: 12/7/2012 9:51:52AM Analysis Adsorptive: N2
Completed: 12/8/2012 11:44:07AM Analysis Bath: 77.35 K
Report Time: 12/10/2012 10:28:08AM Thermal Correction: No
Sample Weight: 0.2407 g Smoothed Pressures: No
Warm Freespace: 27.9527 cm³ MEASURED Cold Freespace: 92.4420 cm³
Equil. Interval: 25 secs Low Pressure Dose: 10.00 cm³/g STP

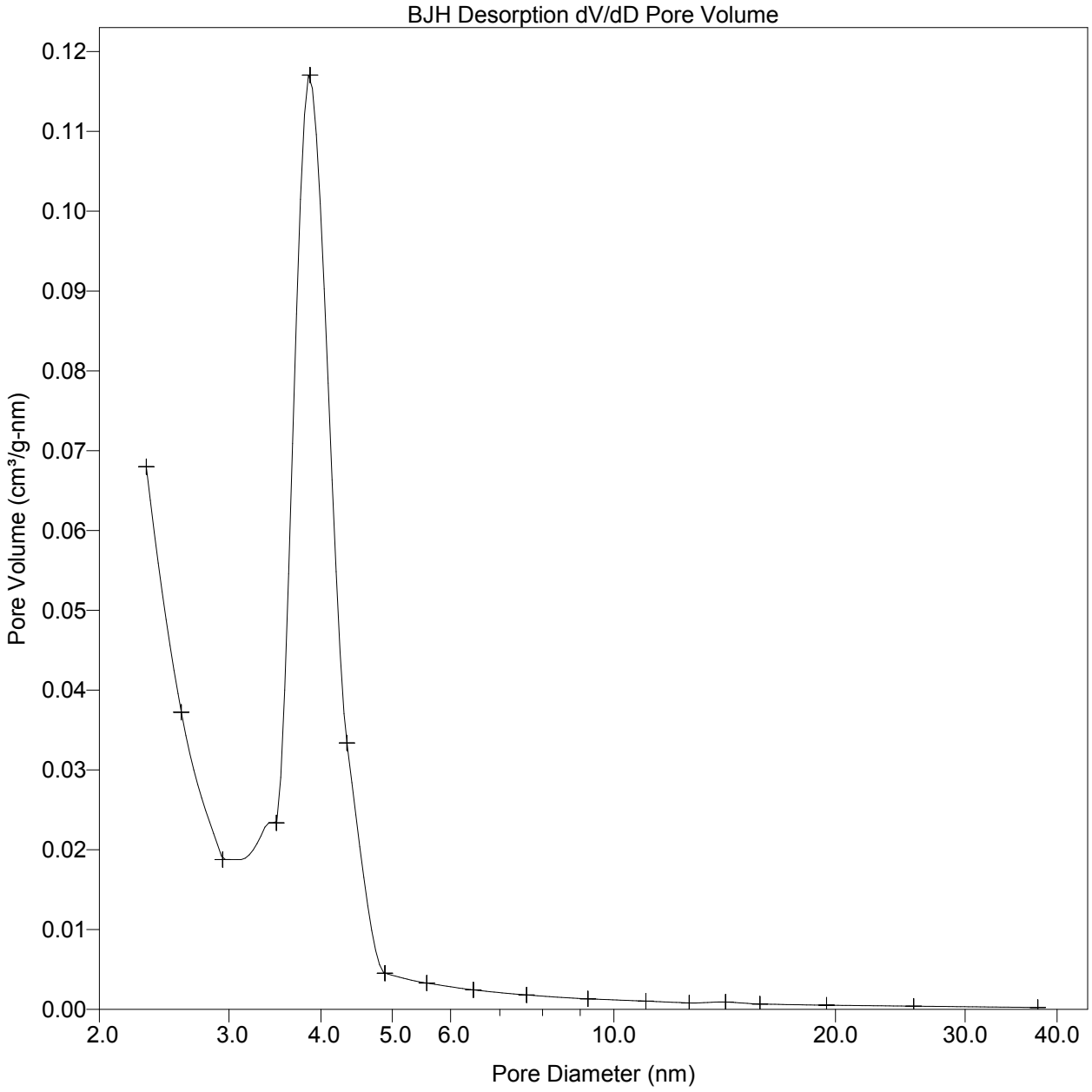

Sample: Rx3 EXTRA 570104
Operator: CSM
File Name: C:\...\BAXTER\001-379.SMP

Started: 12/7/2012 9:51:52AM Analysis Adsorptive: N2
Completed: 12/8/2012 11:44:07AM Analysis Bath: 77.35 K
Report Time: 12/10/2012 10:28:08AM Thermal Correction: No
Sample Weight: 0.2407 g Smoothed Pressures: No
Warm Freespace: 27.9527 cm³ MEASURED Cold Freespace: 92.4420 cm³
Equil. Interval: 25 secs Low Pressure Dose: 10.00 cm³/g STP

Horvath-Kawazoe Report
Cylinder Pore Geometry (Saito/Foley)

Maximum Pore Volume:		0.582113 cm³/g
at Relative Pressure:		0.649301150
Median Pore Diameter:		1.1 nm
Relative Pressure Range:	1.463005E-06 to	0.999999881
Diameter of Adsorptive Molecule:		0.3000 nm
Diameter of Sample Atom:		0.3400 nm
Interaction Parameter:		3.73e-43 ergs-cm4
Density Conversion Factor:		0.001547

Absolute Pressure (mmHg)	Relative Pressure	Volume Adsorbed (cm³/g STP)	Pore Diameter (nm)	Cumulative Pore Volume (cm³/g)	Differential Pore Volume (cm³/g-nm)
0.00110	0.000001463	10.1282	0.8	0.0157	0.0206
0.00231	0.000003065	20.2559	0.8	0.0313	0.4963
0.00313	0.000004154	30.3842	0.8	0.0470	1.1258
0.00382	0.000005067	40.5126	0.8	0.0627	1.6481
0.00460	0.000006100	50.6407	0.8	0.0783	1.7393
0.00570	0.000007563	60.7691	0.8	0.0940	1.4321
0.00739	0.000009801	70.8971	0.8	0.1097	1.1597
0.00968	0.000012840	81.0250	0.9	0.1253	1.0632
0.01276	0.000016906	91.1527	0.9	0.1410	1.0017
0.01694	0.000022442	101.2797	0.9	0.1567	0.9248
0.02260	0.000029928	111.4061	0.9	0.1723	0.8683
0.03035	0.000040179	121.5304	0.9	0.1880	0.8060
0.04135	0.000054725	131.6525	1.0	0.2036	0.7235
0.05661	0.000074905	141.7725	1.0	0.2193	0.6755
0.07872	0.000104125	151.8888	1.0	0.2349	0.6027
0.11051	0.000146131	162.0009	1.0	0.2506	0.5491
0.15755	0.000208259	172.1053	1.1	0.2662	0.4867
0.23001	0.000303955	182.1968	1.1	0.2818	0.4194
0.34389	0.000454317	192.2668	1.1	0.2974	0.3602
0.52715	0.000696213	202.2999	1.2	0.3129	0.3047
0.82594	0.001090485	212.2705	1.3	0.3283	0.2575
1.27888	0.001687986	222.1648	1.3	0.3436	0.2317
2.01683	0.002661139	231.9221	1.4	0.3587	0.1920
3.16669	0.004176815	241.4623	1.5	0.3735	0.1637
4.83541	0.006374951	250.7119	1.6	0.3878	0.1450
7.21247	0.009507148	259.8734	1.7	0.4020	0.1298
10.34473	0.013634377	268.8491	1.8	0.4159	0.1206
14.17372	0.018678863	277.3633	1.9	0.4290	0.1122
18.76599	0.024727956	285.5991	2.1	0.4418	0.1058

Sample: Rx3 EXTRA 570104
Operator: CSM
File Name: C:\...\BAXTER\001-379.SMP

Started: 12/7/2012 9:51:52AM Analysis Adsorptive: N2
Completed: 12/8/2012 11:44:07AM Analysis Bath: 77.35 K
Report Time: 12/10/2012 10:28:08AM Thermal Correction: No
Sample Weight: 0.2407 g Smoothed Pressures: No
Warm Freespace: 27.9527 cm^3 MEASURED Cold Freespace: 92.4420 cm^3
Equil. Interval: 25 secs Low Pressure Dose: 10.00 cm^3/g STP

Horvath-Kawazoe Report
Cylinder Pore Geometry (Saito/Foley)

Absolute Pressure (mmHg)	Relative Pressure	Volume Adsorbed (cm^3/g STP)	Pore Diameter (nm)	Cumulative Pore Volume (cm^3/g)	Differential Pore Volume (cm^3/g-nm)
24.09170	0.031741508	293.4643	2.2	0.4539	0.0980
30.03550	0.039567451	300.8338	2.3	0.4653	0.0914
36.81722	0.048495453	307.9396	2.4	0.4763	0.0839
44.38574	0.058457509	314.6617	2.6	0.4867	0.0766
52.71960	0.069420786	320.9274	2.7	0.4964	0.0680
60.93707	0.080228588	326.1805	2.8	0.5045	0.0606
77.47482	0.101984368	334.6262	3.1	0.5176	0.0500
93.88134	0.123558661	340.9676	3.4	0.5274	0.0390
126.92663	0.167021423	349.6824	3.9	0.5409	0.0268
143.81358	0.189218457	352.7908	4.1	0.5457	0.0179
160.29967	0.210882416	355.2878	4.4	0.5496	0.0144
191.25247	0.251570069	358.8836	4.9	0.5551	0.0103
213.58830	0.280920126	360.9528	5.4	0.5583	0.0075
233.33171	0.306831035	362.5235	5.8	0.5608	0.0058
249.75533	0.328385394	363.6918	6.2	0.5626	0.0048
267.54776	0.351733681	364.8635	6.6	0.5644	0.0042
303.50107	0.398941648	366.9566	7.6	0.5676	0.0033
323.09125	0.424643986	368.0053	8.1	0.5692	0.0029
341.96545	0.449399573	368.9684	8.7	0.5707	0.0025
379.77579	0.499015728	370.8287	9.9	0.5736	0.0024
399.28650	0.524592691	371.7801	10.6	0.5751	0.0023
418.37125	0.549604264	372.6890	11.2	0.5765	0.0021
455.90518	0.598833938	374.4685	12.6	0.5792	0.0020
475.29996	0.624238167	375.4186	13.3	0.5807	0.0020
494.43927	0.649301150	376.3338	14.1	0.5821	0.0018

Sample: Rx3 EXTRA 570104
Operator: CSM
File Name: C:\...\BAXTER\001-379.SMP

Started: 12/7/2012 9:51:52AM Analysis Adsorptive: N2
Completed: 12/8/2012 11:44:07AM Analysis Bath: 77.35 K
Report Time: 12/10/2012 10:28:08AM Thermal Correction: No
Sample Weight: 0.2407 g Smoothed Pressures: No
Warm Freespace: 27.9527 cm³ MEASURED Cold Freespace: 92.4420 cm³
Equil. Interval: 25 secs Low Pressure Dose: 10.00 cm³/g STP

Horvath-Kawazoe Differential Pore Volume Plot
Cylinder Pore Geometry (Saito/Foley)

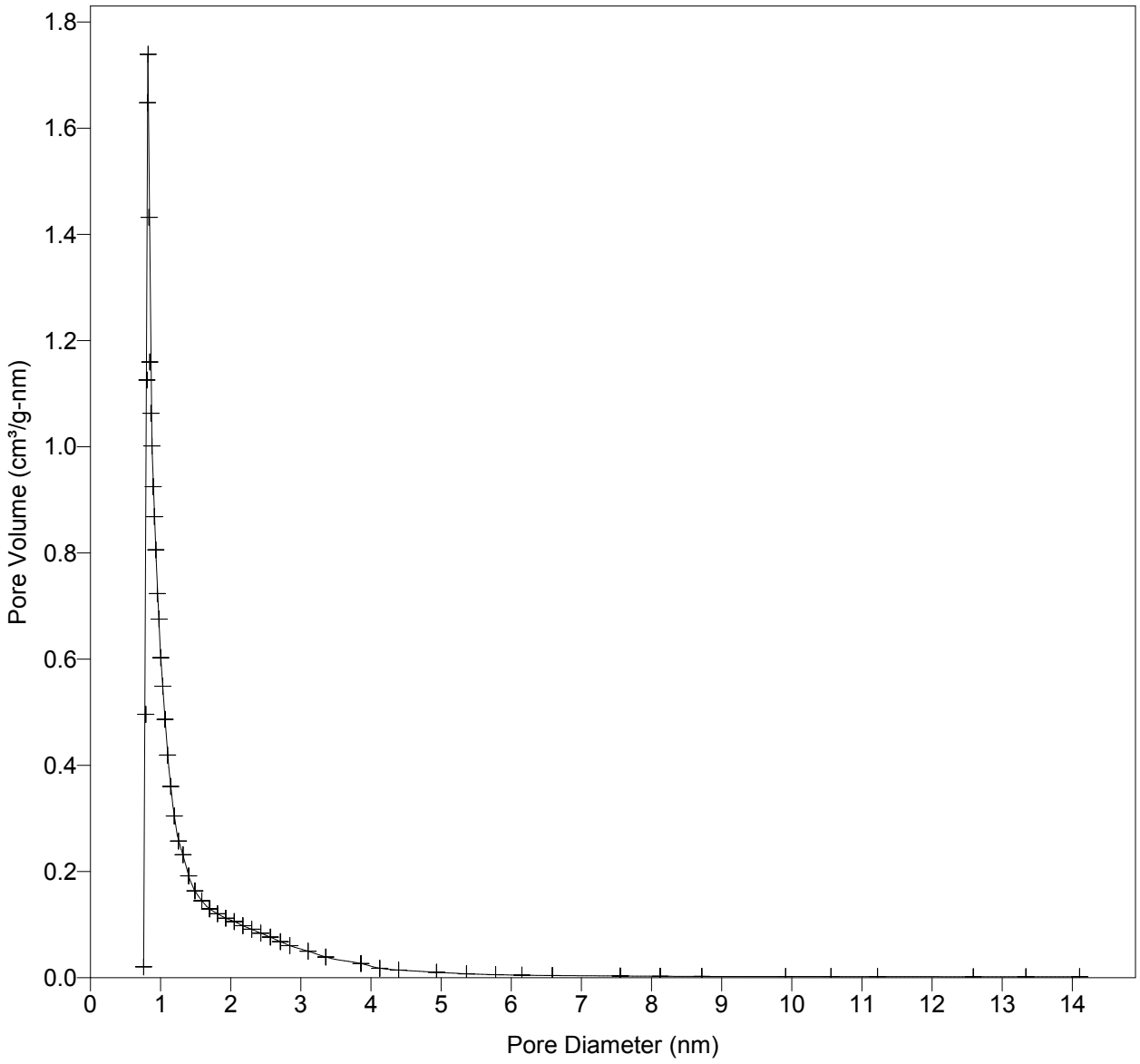

Sample: Rx3 EXTRA 570104
Operator: CSM
File Name: C:\...\BAXTER\001-379.SMP

Started: 12/7/2012 9:51:52AM Analysis Adsorptive: N2
Completed: 12/8/2012 11:44:07AM Analysis Bath: 77.35 K
Report Time: 12/10/2012 10:28:08AM Thermal Correction: No
Sample Weight: 0.2407 g Smoothed Pressures: No
Warm Freespace: 27.9527 cm^3 MEASURED Cold Freespace: 92.4420 cm^3
Equil. Interval: 25 secs Low Pressure Dose: 10.00 cm^3/g STP

Summary Report

Area

Single Point Surface Area at P/Po 0.25157007 :	1169.2660	m^2/g
BET Surface Area:	1227.0198	m^2/g
Langmuir Surface Area:	1536.8535	m^2/g
Micropore Area:	-376.1682	m^2/g
External Surface Area:	1603.1881	m^2/g
BJH Adsorption Cumulative Surface Area of pores between 1.700000 and 300.000000 nm Diameter:	99.2162	m^2/g
BJH Desorption Cumulative Surface Area of pores between 1.700000 and 300.000000 nm Diameter:	153.0733	m^2/g

Volume

Single Point Adsorption Total Pore Volume of pores less than 196.3985 nm Diameter at P/Po 0.99005964:	0.632735	cm^3/g
Micropore Volume:	-0.091133	cm^3/g
BJH Adsorption Cumulative Pore Volume of pores between 1.700000 and 300.000000 nm Diameter:	0.109894	cm^3/g
BJH Desorption Cumulative Pore Volume of pores between 1.700000 and 300.000000 nm Diameter:	0.148240	cm^3/g

Pore Size

Adsorption Average Pore Diameter (4V/A by BET):	2.0627	nm
BJH Adsorption Average Pore Diameter (4V/A):	4.4305	nm
BJH Desorption Average Pore Diameter (4V/A):	3.8737	nm

Horvath-Kawazoe

Sample: Rx3 EXTRA 570104
Operator: CSM
File Name: C:\...\BAXTER\001-379.SMP

Started: 12/7/2012 9:51:52AM Analysis Adsorptive: N2
Completed: 12/8/2012 11:44:07AM Analysis Bath: 77.35 K
Report Time: 12/10/2012 10:28:08AM Thermal Correction: No
Sample Weight: 0.2407 g Smoothed Pressures: No
Warm Freespace: 27.9527 cm^3 MEASURED Cold Freespace: 92.4420 cm^3
Equil. Interval: 25 secs Low Pressure Dose: 10.00 cm^3/g STP

Summary Report

Maximum Pore Volume at Relative Pressure 0.649301150:	0.582113 cm^3/g
Median Pore Diameter:	1.1273 nm